universität
wien

DISSERTATION

A PROTEOMIC STUDY ON OFF-TARGET EFFECTS OF THERAPEUTIC OLIGONUCLEOTIDES

angestrebter akademischer Grad

Doktorin der Naturwissenschaften (Dr. rer. nat.)

Verfasserin:	Mag. Martina Stessl
Matrikel-Nummer:	9912283
Dissertationsgebiet:	Pharmazie
Betreuer:	Univ.-Prof. Dipl.-Ing. Mag. Dr. Christian Noe

Wien, im April 2010

„Wahre Wissenschaft zeichnet sich aus durch Demut vor den Grenzen des Endlichen und durch Neugier auf das Unendliche hinter diesen Grenzen.“

Lisz Hirn

österr. Philosophin und Künstlerin

Danksagung

Diese Dissertation entstand am Department für Medizinisch/Pharmazeutische Chemie der Universität Wien. Besonders bedanken möchte ich mich bei Univ.-Prof. Dr. Christian Noe, der mir die Möglichkeit gegeben hat, die Arbeit in seinem Department zu schreiben, und mir durch die Anstellung als Assistentin auch eine finanzielle Basis dafür geboten hat. Er hat durch seine weitgefächerte Betrachtungsweise der Fragestellungen und seine vielfältigen Denkansätze viel positiven Einfluß auf die Arbeit genommen und ein sehr selbständiges Arbeiten gefördert.
Meinen Kollegen am Department für Medizinisch/Pharmazeutische Chemie bin ich für ihre Hilfsbereitschaft und für die angenehme Arbeitsathmosphäre dankbar - besonders Dr. Johannes Winkler, der mir mit seinen umfassenden Kenntnissen auf dem Gebiet der Antisense-Oligonukleotide und darüber hinaus stets mit Rat und Tat zur Seite gestanden ist, Dr. Bodo Lachmann, der in Bezug auf Validierung und Analytik ein sehr wichtiger Gesprächspartner war, sowie Dr. Bettina Germann, Dr. Winfried Neuhaus und Prof. Dr. Ernst Urban für ihre Unterstützung in vielerlei Hinsicht.

Ferner möchte ich mich bei Univ.-Prof. Dr. Allmaier vom Institut für Chemische Technologien und Analysen der TU Wien für die gute Zusammenarbeit und für seine kompetente und prompte Unterstützung auf dem Gebiet der Proteomik sehr herzlich bedanken. Mein Dank gilt hier besonders auch Univ.-Ass. Dr. Martina Marchetti-Deschmann, die mir mit ihrem profunden Fachwissen und ihrer unermüdlichen Energie sehr geholfen hat. Die konstruktive Zusammenarbeit, sowie die kritischen Anregungen und Diskussionen mit dieser Arbeitsgruppe, vor allem auch mit Dr. Wolfgang Winkler und Dr. Tom Grunert, haben nicht unerheblich zu dem erfolgreichen Abschluß der Dissertation beigetragen.

Herzlicher Dank gilt auch meiner Familie, auf deren uneingeschränkte Unterstützung ich in allen Zeiten meines Studiums zählen konnte. Für die intensiven Arbeitsphasen gilt meinen Eltern Dank für Ihre Babysitter-Dienste und für ihre unermüdliche Hilfe in vielen Dingen. Mein Sohn hat durch anfangs lange Schlafphasen einen unbewußten doch nicht unerheblichen Beitrag zu der Schreibarbeit geleistet. Ganz besonderer Dank gilt auch meinem Mann, Günter, der mir durch seine liebevolle Unterstützung und Geduld immer wieder Kraft und positive Energie gegeben hat.

Index

Abbreviations 1

Abstract 4

Summary / Zusammenfassung 5

Introduction 10

1. Nucleic-acid based therapy 11

    1.1. Antisense oligonucleotides (ASOs) 13

    1.2. RNA Interference (RNAi) 22

2. B-cell lymphoma 2 (Bcl-2) 27

    2.1. Bcl-2 and apoptosis 27

    2.2. Bcl-2 and cancer 32

Aim of the work 34

Materials and Methods 36

    Synthesis and purification of oligonucleotides 40

    Cell culture 44

    Oligonucleotide transfection and cell lysis 44

    Western blot analysis 45

    Caspase assay 45

    Annexin-V-FLUOS-staining 46

    Two-dimensional gel electrophoresis 47

    Software-based image analysis 50

    Protein identification by mass spectrometry 52

Results 54

1. Oligonucleotides 54

2. Influence on target protein expression 55

3. Apoptosis induction 59

4. Proteomic investigation 62

    4.1. Two-dimensional separation and staining conditions 62

    4.2. Establishment of a protein reference map of 607B cells 68

    4.3. Influence of image-analysis software on quantitation of 2-DE data 71

    4.4. DIGE-based off-target effect study 77

Discussion 93

References 109

Supplement A 123

    MALDI theory 123

    Mass spectra of reference proteins 128

Supplement B 152

    Mass spectra of differentially expressed proteins 152

Curriculum Vitae 185

Abbreviations

2-DE	two-dimensional gel electrophoresis
3-PGDH	D-3-phosphoglycerate dehydrogenase
ACTB	actin, cytoplasmatic 1
AHA-1	activator of 90kDa heat shock protein ATPase homolog 1
AIDS	acquired immune deficiency syndrome
ASO(s)	antisense oligonucleotide(s)
ATP	adenosine-5’-triphosphate
Bcl-2	B-cell lymphoma 2
bp	basepairs
BSA	bovine serum albumin
CBB	Coomassie Brilliant Blue
CD	circular dichroism
CID	collision-induced dissociation
COF-1	cofilin-1
CPG	controlled pore glass
CV	coefficient of variance
DCI	4,5-dicyanoimidazole
DEPC	diethyl-pyrocarbonate
DEVD-R110	Asp-Glu-Val-Asp-Rhodamine 110
DIGE	difference gel electrophoresis
DMT	4,4‘-dimethoxytriphenylmethyl-
dsRNA	double-stranded RNA
DTT	dithiothreitol
EDTA	ethylene diamine tetraacetic acid
EF-2	elongation factor 2
ENOA-1	alpha-enolase-1

ER	endoplasmic reticulum
ESI	electrospray ionization
FDA	Food and Drug Administration
GAPDH	glyceraldehyde-3-phosphate dehydrogenase
GRP-78	78kDa glucose-regulated protein
HRP	horse raddish peroxidase
HSP-60	heat shock protein 60
HSP-70	heat shock cognate 71kDa protein
HSP-90	heat shock protein HSP 90-alpha
IEF	isoelectric focusing
LDH	L-lactate dehydrogenase A chain
LEG-1	galectin-1
LNA	locked nucleic acid
MALDI	matrix-assisted laser desorption/ionisation
MD2L1	mitotic spindle assembly checkpoint protein MAD2A
MOMP	mitochondrial outer membrane permeability
MS	mass spectrometry
MW	molecular weight
NDK-A	nucleoside diphosphate kinase A
NL	non linear
NPM	nucleophosmin
nts	nucleotides
PDIA6	protein disulfide-isomerase A6
PDIA3	protein disulfide-isomerase A3
PDQ	PD-Quest
PGAM-1	phosphoglycerate mutase 1
PGK-1	phosphoglycerate kinase 1
p*I*	isoelectric point

PMF	peptide mass fingerprint
PPIA	peptidyl-prolyl cis-trans isomerase A
PRDX	peroxiredoxin
PSA-3	proteasome subunit alpha type-3
PSD	post source decay
PURH	bifunctional purine biosynthesis protein
RANG	ran-specific GTPase-activating protein
RNAi	RNA interference
ROS	reactive oxygen species
S-DNA	phosphorothioate
SDS-PAGE	sodium-dodecyl-sulfate polyacrylamide gel electrophoresis
siRNA	small interfering RNA
shRNA	short hairpin RNA
STIP-1	stress-induced-phosphoprotein 1
SYYC	tyrosyl-tRNA synthetase, cytoplasmic
TBAF	tetrabutyl-ammonium fluoride
TBDMS	tetrabutyl-dimethyl-silyl-
TBS	tris buffered saline
TCP β	t-complex protein 1 subunit beta
TCP ε	t-complex protein 1 subunit epsilon
TCP-1 zeta	t-complex protein 1 subunit zeta
TEAA	triethylammonium acetate
TETD	tetraethylthiuramdisulfide
TFA	trifluoroacetic acid
TOF/rTOF	time-of-flight/ reflectron time-of-flight
TPIS	triosephosphate isomerase
TRIS	tris(hydroxymethyl)-aminomethan
VDAC	voltage dependent anion channel

Abstract

Due to their capacity of silencing single genes sequence-specificly, antisense oligonucleotides (ASOs) and small interfering RNAs (siRNAs) represent two promising strategies in the development of urgently needed specific and safe therapies. Off-target effects, however, are among the major hurdles for their clinical success. A DIGE-based proteomic approach (two-dimensional gel electrophoresis in combination with mass spectrometry) comparing the phosphorothioate antisense oligonucleotide Oblimersen (Genasense, G3139) to a *bcl-2*-targeted siRNA sequence on human melanoma cells revealed significant off-target effects after phosphorothioate application that might contribute to the apoptotic effect of Oblimersen. Despite the effective down-regulation of Bcl-2 by both agents, only Oblimersen, but not the siRNA sequence, induced apoptosis in human melanoma cells, as determined by annexin staining and caspase assay. Phosphorothioate-treatment caused a reduction in the expression of several proteins linked to apoptosis and stress response (among those galectin-1, cofilin-1, GRP78, HSP60, nucleophosmin, and peroxiredoxins), whereas the siRNA sequence seemed to be highly target specific. Furthermore Oblimersen-treatment caused a down-regulation of four glycolytic enzymes (namely enolase-1, PGK-1, PGAM-1 and TPIS), what indicates a partial reversion of the cancer-related Warburg effect. The underlying mechanism for observed effects may be a blockage of the mitochondrial voltage dependent anion channel (VDAC) mediated by the phosphorothioate. Since similar effects have been obtained with control phosphorothioates, the observed reversal seems not to be caused by the Bcl-2 reduction alone, but rather by the phosphorothioate chemistry.

Summary

One focus of modern pharmaceutical research is the investigation of safe and efficacious ways of specifically silencing important targets that have been identified to play key roles in severe diseases. In this context gene silencing approaches, including antisense oligonucleotides (ASOs) and small interfering RNAs (siRNAs), have great potential as therapeutics. Despite this promising concept and the success of so far one approved product, the clinical development of antisense agents is challenged with issues regarding site-specific delivery, stability and off-target effects. Most antisense agents in late-stage clinical development belong to the group of phosphorothioates, such as Oblimersen (Genasense, G3139). The 18mer phosphorothioate is directed against Bcl-2, a key protein of the mitochondrial apoptotic pathway, and is clinically tested against a variety of different cancers including melanoma. The working mechanism of Oblimersen is poorly understood, since Bcl-2 silencing is supposed not to be the sole mechanism for chemosensitization in melanoma cells [Stein *et al.,* 2009].

The aim of this work was the establishment of a validated proteomic approach in order to monitor and compare potential off-target effects of the phosphorothioate Oblimersen and a *bcl-2*-targeted siRNA on the protein level. Required ASOs and siRNAs were synthesized and transfected to the human melanoma cell line 607B, which over-expressed the anti-apoptotic target protein Bcl-2. Although both sequences successfully down-regulated Bcl-2, only Oblimersen induced apoptosis in 607B cells after 48 hours of transfection as determined by annexin staining and caspase assay. Based on an equal target down-regulation of 75%, differently treated cell lysates were investigated by two-dimensional gel electrophoresis and subsequent software-based image analysis. Therefore optimization of two-

dimensional separation and staining conditions, as well as the validation of bioanalytical methods had to be performed in order to obtain reliable quantitative proteomic data. Since the used cell line had not been characterized on the protein level before, a protein reference map was established. The differential expression of 22 proteins after Oblimersen-treatment and of 2 proteins after siRNA-treatment, monitored by DIGE technology, suggested a higher target specificity for the used siRNA compared to the tested phosphorothioate. Changed proteins, which were unambiguously identified by *in-gel* digestion and subsequent MALDI-rTOF-MS, included cytoskeletal proteins, chaperons, transport proteins, glycolytic and other enzymes, proteins involved in Ca^{2+}-signaling and in redox-regulation as well as other proteins, such as galectin-1. Many of these proteins are linked to apoptosis or drug resistance. The most interesting result, however, was the observed reduction in the expression of glycolytic enzymes after Oblimersen treatment, indicating a partial reversal of the Warburg effect [Warburg *et al.,* 1930]. Using the same proteomic approach similar effects were obtained with control phosphorothioate-modified oligonucleotides targeted at genes not involved in apoptosis.

Presented findings support the theory that the Bcl-2 reduction is not the only essential molecular effect of Oblimersen. An unspecific apoptosis induction, possibly caused by a blockage of the voltage-dependent anion channel (VDAC) [Stein *et al.,* 2008] by the phosphorothioate, seems to play a further key role. Since the discussed partial reversal of the Warburg effect has been observed also with control sequences, it seems to be caused by the phosphorothioate chemistry and not exclusively by *bcl-2* targeted gene silencing.

Zusammenfassung

Ein Schwerpunkt der modernen pharmazeutischen Forschung liegt in der Erforschung sicherer und effizienter Methoden zur Hemmung bestimmter Gene im menschlichen Körper, die mit schwerwiegenden Krankheiten in Verbindung gebracht werden. In diesem Zusammenhang haben sogenannte „gene-silencing“ Therapeutika, also Substanzen, die spezifische Gensequenzen blockieren können, wie zum Beispiel Antisense-Oligonukleotide (ASOs) oder kleine hemmende RNA-Strukturen (siRNAs), großes Potential als potentielle neue Wirkstoffe. Trotz vielversprechender Ansätze und bisher einer Substanz dieser Klasse auf dem Markt, ist die erfolgreiche klinische Entwicklung dieser Therapeutika noch mit zahlreichen offenen Fragestellungen behaftet, wie etwa hinsichtlich der Stabilität, der Aufnahme in die entsprechenden kranken Zellen sowie unspezifischer Effekte mancher Substanzen. Die meisten Antisense-Oligonukleotide, die in höheren klinischen Studien getestet werden, gehören zur Gruppe der Phosphorthioate, wie zum Beispiel Oblimersen (Genasense, G3139), das gegen verschiedene Tumorarten, unter anderem gegen Melanome, getestet wird. Dieses 18 Basenpaar lange Oligonukleotid hemmt spezifisch ein Protein namens Bcl-2, das eine Schlüsselfunktion in der mitochondrialen Apoptose, also im programmierten Zelltod, spielt. Der genaue Wirkmechanismus von Oblimersen ist noch nicht völlig geklärt. Es wird aber davon ausgegangen, dass die Bcl-2 Hemmung nicht der einzige Mechanismus ist, mit dem Oblimersen eine (Re-)Sensibilisierung von Melanomzellen gegenüber Chemotherapie erreicht [Stein *et al*., 2009].

Das Hauptziel dieser Arbeit bestand darin, potentielle unspezifische Effekte am Proteom von Melanomzellen, verursacht durch Oblimersen und durch eine ebenfalls gegen Bcl-2 gerichtete siRNA, mit Hilfe einer validierten Proteomuntersuchung dar

zu stellen und zu vergleichen. Benötigte ASOs und siRNAs wurden synthetisiert. Anschließend wurde die humane Melanomzelllinie 607B, die das anti-apoptotische Zielprotein Bcl-2 über-exprimiert, damit transfiziert. Obwohl beide Sequenzen das Zielprotein effektiv herunter regulierten, konnte nach 48 Stunden Transfektion nur bei Oblimersen-behandelten Zellen eine Apoptoseinduktion festgestellt werden. Basierend auf derselben 75 prozentigen Bcl-2 Hemmung, wurden die unterschiedlich behandelten Zelllysate mittels zwei-dimensionaler Gelelektrophorese und anschließender Software-gestützter Bildanalyse untersucht. Dazu mußten im Vorfeld verschiedene Parameter, unter anderem die Auftrennungs- und Färbebedingungen, optimiert und die bioanalytischen Methoden validiert werden. Da die verwendete Zelllinie auf Proteinebene noch nicht charakterisiert worden war, wurde eine Referenzkarte des Proteommusters erstellt. Mit Hilfe der DIGE Technologie konnte eine Beeinflussung der Genexpression von 22 Proteinen nach der Behandlung mit Oblimersen und von 2 Proteinen nach der Behandlung mit der siRNA festgestellt werden. Dies deutet darauf hin, dass die verwendete siRNA target-spezifischer wirkt als das Phosphorthioate. Die in ihrer Expression beeinflußten Proteine wurden im Anschluß mittels „*in-gel*“ Verdau und MALDI-rTOF-MS eindeutig identifiziert. Unter ihnen befanden sich Zytoskelett-Proteine, Chaperone, Transportproteine, glykolytische und andere Enzyme, Proteine, die in die Ca^{2+}-Regulierung oder in die Redox-Regulierung der Zelle involviert waren, und auch andere Proteine, wie zum Beispiel Galectin-1. Viele dieser Proteine stehen mit Apoptose oder Therapie-Resistenzentwicklung in Verbindung. Das interessanteste Ergebnis der Studie war jedoch die beobachtete Expressionsreduktion glykolytischer Enzyme nach der Behandlung mit Oblimersen, welche auf eine teilweise Umkehr des sogenannten Warburg Effekts hinwies [Warburg *et al.,* 1930]. In derselben Proteomuntersuchung wurden ähnliche Ergebnisse mit Phosphorthioat-modifizierten Kontrollsequenzen erreicht, die gegen andere, nicht mit Apoptose in Zusammenhang stehende, Gene gerichtet waren.

Die präsentierten Ergebnisse unterstützen die Theorie, dass die bekannte Bcl-2 Reduktion nicht der einzige essentielle Wirkungsmechanismus von Oblimersen ist. Eine unspezifische Apoptoseinduktion, die wahrscheinlich durch eine Blockade des VDAC-Proteins („voltage-dependent anion channel“) [Stein *et al.,* 2008] durch das Phosphorthioat verursacht wird, dürfte eine weitere entscheidende Rolle spielen. Da die erwähnte teilweise Umkehr des Warburg Effektes auch mit den Kontrolloligonukleotiden beobachtet wurde, ist es sehr wahrscheinlich, dass diese durch die Phosphorthioatmodifikation und nicht nur durch die Bcl-2 Hemmung verursacht wird.

Introduction

The complexity of the human cell issues a challenge to modern drug discovery, which becomes even more important with the elucidation of new signaling cascades and protein interactions. The main problems of drug development have shifted from the elucidation of cellular targets to the monitoring of off-target and potential adverse effects on the whole genome, transcriptome, metabolome and proteome. These unspecific effects can be caused directly by the drugs or indirectly by the onset of alternative cellular pathways to circumvent treatments. In the best case the therapeutic effect of the drug is supported or in rare cases new therapeutic perspectives are opened up, in the worst case the therapeutic aim is opposed or even unexpected toxicity is caused by unspecific drug interactions [Stessl *et al.*, 2009]. In any way the elucidation of potential adverse effects of drugs in very early phases of drug development is an essential prerequisite for their effective clinical use.

Besides screening of drug candidates over a broad range of different targets, one way to contribute to this important question is the investigation of the unspecific drug influence on the protein level by a comprehensive proteomic approach, leading to a better understanding of intracellular interactions of biological molecules. Especially relevant are additional protein changes caused during or after the interaction of a drug on a specific cellular target. The specific and rational targeting of key genes, identified to play essential roles in various severe diseases, has led to the successful development of therapeutic antibodies, small molecules (such as polyamides [Dickinson *et al.*, 2004], isoxazolidines, which act as activator artificial transcription factors [Rowe *et al.*, 2007], or PARP-1 inhibitors [Tong *et al.,* 2009]) or nucleic acid based therapies, such as antisense oligonucleotides (ASOs). In contrast to therapeutic antibodies, which act at the protein level, gene regulation by so-called "antisense" oligonucleotides is mainly performed on the genetic level. Despite effective target gene down-regulation, antisense agents are confronted with reports about (un)desired (un)specific off-target effects, which represent a major safety issue with respect to their successful clinical development. Based on this background this thesis focused on the investigation of protein changes on human melanoma cells caused by the application of two different oligonucleotides, namely the phosphorothioate Oblimersen and a *bcl-2*-targeted small interfering RNA (siRNA).

1. Nucleic acid-based therapy

Nucleic acid-based therapeutics comprehend a variety of molecules with different rationales and mechanisms, including therapeutic nucleotides and nucleosides, oligo- and polynucleotides. Although therapeutic nucleotides and nucleosides interfering with nucleic acid metabolism and DNA polymerization have been successfully used as anticancer and antiviral drugs, they often produce toxic secondary effects related to dosage and continuous use [Alvarez-Salas, 2008]. Newer treatment strategies with high affinity to their biological targets, among others, include DNA vaccines, which are based on the activation of the human immune system by a plasmid DNA encoding for a foreign protein resulting in antibody production [Nemunaitis *et al.*, 2009; Tüting *et al.,* 2000], or ribozymes, catalytically active RNA molecules capable of site-specific cleavage of target mRNA [Bhindi *et al.,* 2007]. So far, the most promising nucleic acid-based strategies with regard to clinical development are aptamers and antisense oligonucleotides (ASOs), with two approved products for local administration at the eye (the antisense oligonucleotide fomivirsen (Vitravene; Isis Pharmaceuticals) and the aptamer pegaptanib (Macugen, Macuverse; NeXstar

Pharmaceuticals)). Aptamers are small single-stranded nucleic acids that fold into well-defined three-dimensional structures and bind their target with high affinity and specificity [Mayer, 2009]. Antisense oligonucleotides are small single-stranded DNA strands, the concept of which dates back to the work of Zamecnik and Stephenson [Zamecnik *et al.,* 1978] and is discussed below. Furthermore small interfering RNAs (siRNAs), which have been discovered about one decade ago [Fire *et al.,* 1998], represent a rapidly developing nucleic acid-based strategy, which is discussed in the next chapter.

Actual challenges for a successful clinical development of therapeutic oligonucleotides refer to partly understood pharmacokinetics, poor bioavailability, ineffective drug delivery and/or insufficient uptake into target cells, as well as the problem of specificity [Stein *et al.,* 1993]. The question of the interaction of different cellular pathways activated upon application of the drug strongly influences its therapeutic effect.

1.1 Antisense oligonucleotides (ASOs)

As well as any other gene-silencing strategy the antisense concept derives from an understanding of nucleic acid structure and function depending on Watson-Crick hybridization [Watson *et al.,* 1953]. Antisense oligonucleotides (ASOs), which are short single-stranded DNA sequences (10-30 nts [Opalinska *et al.,* 2002] or 13-35 nts [Mahato *et al.,* 2005], respectively), are designed to specifically modulate translation of a particular gene into a protein by hybridizing and disrupting the function of pre-mRNA and mRNA, thereby preventing the mRNA from being translated [Monia *et al.,* 2001]. Among several described gene expression inhibition mechanisms by ASOs [Noe *et al.,* 2000; Opalinska *et al.,* 2002; Bennett *et al.,* 2010] the most relevant is the degradation of the mRNA by RNase H activated at the site of ASO binding [Baker *et al.,* 1999]. RNase H is abundant in the cytoplasm and nucleus and functions as an endonuclease to recognize and cleave the RNA moiety of the formed RNA-DNA hybrid [Mahato *et al.,* 2005; Achenbach *et al.,* 2003]. The ASO is undamaged by the enzymatic attack and is free to hybridize with the next RNA molecule, thus functioning in a catalytic manner [Opalinska *et al.,* 2002]. The understanding of the ASO mechanism has led to the design of different chemical modifications of the phosphate backbone, the sugar components or the nucleobases in order to improve the most important features of ASOs, like binding affinity, base-pair specificity, nuclease resistance, support of endonucleolytic cleavage, chemical stability, lipophilicity, solubility and protein-binding as well as pharmacological properties [Cook, 2001; Noe *et al.,* 2000; Urban *et al.,* 2003; Winkler *et al.,* 2004].

Phosphorothioates, ASOs which contain a sulphur substitution in the backbone phosphate linkage, are referred to as first generation compounds and showed enhanced stability against tissue nucleases and improved plasma half-lifes [Eckstein, 2000]. Most of ASOs in late-stage clinical development, as well as the only launched compound, fomivirsen (Vitravene), are phosphorothioates (table 1).

Second generation antisense compounds are based on 2'-O-alkyl derivatives [Cotten *et al.,* 1991], which have exhibited superior *in vitro* characteristics. Prominent representatives are 2'-O-methoxyethyl (2'-MOE) derivatives showing increased resistance to plasma and tissue breakdown and improvements in the affinity with which they bind RNA [Monia *et al.,* 1993]. Subsequently more rigorous chemical modifications have been introduced in order to increase stability and target affinity, such as zwitterionic compounds [Noe *et al.,* 2005; Winkler *et al.,* 2004, 2007 and 2008], morpholino oligonucleotides [Summerton, 1999 and 2007] and locked nucleic acids (LNA) [Jepsen *et al.,* 2004; Simoes-Wüst *et al.,* 2004] as the most promising therapeutic derivatives (table 1).

Compound	Chemistry	Target	Clinical Status	Technologies	Indications
fomivirsen [Vitravene]	phosphorothioate	*IE2 of CMV virus*	launched	intravitreal	CMV retinitis
pegaptanib [Macugen, Macuverse]	aptamer	*VEGF165*	launched	iv., ophthalmic formul.	age related macular degeneration, retinal venous occlusion
aprinocarsen [Affinitak]	phosphorothioate	*PKC alpha*	discontinued (03/05)	iv.	solid tumor, NSCLC
oblimersen (G-3139) [Genasense]	phosphorothioate	*bcl-2*	phase III	iv., infusion	melanoma; chronic lymphocytic leukemia; multiple myeloma; non-small cell lung cancer; Non-Hodgkin lymphoma, B-cell lymphoma; breast, colorectal and prostate tumor
trabedersen (AP-12009)	phosphorothioate	*TGF beta 2*	phase III	intratumoral, iv	glioma, melanoma, solid tumors
aganirsen (GS-101)	phosphorothioate	*IRS-1*	phase III	ophthalmic formul.	retinopathy, glaucoma
mipomersen (ISIS-301012)	2'-methoxyethyl mod. phosphorothioate	*apoB-100*	phase III	sc.	hypercholesterolemia, cardiovascular disease
belagenpumatucel-L [Lucanix]	antisense-based cancer vaccine	*TGF beta*	phase III	intradermal	lung cancer, glioma
alicaforsen (ISIS-2302)	phosphorothioate	*ICAM-1*	phase III	iv., rectal	inflammatory disease, ulcerative colitis, asthma
bevasiranib (Cand5)	siRNA	*VEGF*	phase III	ophthalmic formul.	age related macular degeneration; diabetic macular edema
(AEG-35156)	phosphorothioate	*XIAP*	phase II	iv.	cancer (among leukemia, NSCLC, lymphoma)
(AGN-211745, AGN-745)	siRNA	*VEGFR-1*	phase II	intravitreal	age related macular degeneration
(ALN-RSV01)	siRNA	*respiratory syncytial virus N gene*	phase II	inhalant, nasal formul.	respiratory syncytial virus infection
(ASM-8, TPI-ASM-8)	combination of two ASOs	*IL-3 beta, IL-5, GM-CSF*	phase II	inhalant formulation	asthma
(AVI-4126) [Resten-NG/MP]		*c-myc*	phase II	iv, microparticle formul.	restenosis, renal disease, cancers
cenersen (EL-625) [Aezea]	phosphorothioate	*p53*	phase II	iv.	leukemias (AML, CLL), lymphoma
custirsen (OGX-011)	2'-methoxyethyl mod. phosphorothioate	*clusterin*	phase II	iv.	solid tumor
(DIMS-0150) [Kappaproct]		*NF-kappaB p65*	phase II	rectal	inflammatory disease, ulcerative colitis, cerebral edema

Table 1. Overview of therapeutical oligonucleotides in clinical phases II or III according to the IDdb3 (The Investigational Drugs database, www.iddb3.com), date august 2009. *Round brackets*: research code; *square brackets*: trade name. *Abbreviations: VEGF: vascular endothelial growth factor; PKC: protein kinase C; TGF: transforming growth factor; IRS-1: isulin receptor substrate 1; apoB-100: apolipoprotein B-100; ICAM: intercellular adhesion molecule; XIAP: X-linked inhibitor of apoptosis protein; GM-CSF: granulocyte-macrophage colony-stimulating factor.*

Compound	**Chemistry**	**Target**	**Clinical Status**	**Technologies**	**Indications**
(EHT-899)	DNA therapeutic	*HBV virus*	phase II	oral	Hepatitis B virus infection
(EZN-2968)	Locked Nucleic Acid	*HIF-1 alpha*	phase II	iv. formulation	cancer
(HGTV-43)	retrovirus-based stem cell therapy	*HIV virus*	phase II	iv.	HIV infection
(ISIS-113715)	2'-0-methoxyethyl modified ASO	*PTP-1B*	phase II	iv.	type 2 diabetes
(LOR-2040, GTI-2040)	phosphorothioate	*R2 ribonucleotide reductase*	phase II	iv.	cancer (among AML, renal tumor)
(LOR-2501)	phosphorothioate	*R1ribonucleotide reductase*	phase II	iv.	lymphoma, prostate cancer
(LY-2181308, ISIS-23722)		*survivin*	phase II	iv.	AML, prostate cancer
(PF-04523655, REDD-14-NP)	modified siRNA	*hypoxia-inducible gene RTP801*	phase II	iv., ophthalmic formulation	age related macular degeneration; diabetic macular edema
(QPI-1002)	siRNA	*p53*	phase II	iv.	kidney transplant rejection, renal injury
ranagengliotucel-T [Glionix]	antisense-based cancer vaccine	*TGF beta 2*	phase II		brain cancer
(RPI-4610) [Angiozyme]	ribozyme	*VEGFR-1*	phase II	sc.	colorectal tumor
(RX-0201) [Archexin]		*AKT protein kinase*	phase II	iv.	solid tumor (among renal cell carcinoma, pancreatic cancer)
(SPC-2996)	Locked Nucleic Acid	*bcl-2*	phase II	iv.	cancer (CLL)
(TV-1102, ISIS-107248)		*integrin alpha-4/beta-1 (CD49d)*	phase II	sc.	inflammatory disease, multiple sclerosis

Table 1 continuation. *Abbreviations: HIF-1: hypoxia-inducible factor 1; PTP-1B: Protein tyrosine phosphatase 1B; TGF: transforming growth factor; VEGFR: vascular endothelial growth factor receptor.*

In 2006 the voltage-dependent anion channel (VDAC) was first identified as a potential pharmacologic target of phosphorothioates in melanoma cells [Lai *et al.,* 2006; Tan *et al.,* 2007]. VDAC has been widely implicated in the initiation of the mitochondrially mediated intrinsic pathway of apoptosis maybe by a decrease in metabolic flux and subsequent permeabilization of the mitochondrial outer membrane to small proteins and cytochrome c, followed by an activation of caspase-dependent apoptosis [Stessl *et al.*, 2009]. Furthermore VDAC has been characterized as important component involved in mitochondrial membrane cholesterol distribution, which in turn might be related to a type of aerobic glycolysis for energy production present in most tumor types, widely known as Warburg effect [Campbell *et al.,* 2008]. Phosphorothioate oligonucleotides were found to be potent and specific inhibitors of this channel protein [Stein *et al.,* 2008].

Despite the steadily improving medicinal chemistry, the therapeutical efficiency of ASOs is often impeded by poor bioavailability, inefficient drug delivery and most important by off-target effects [Anderson *et al.,* 2006; Gjertsen *et al.,* 2007], leading to an obscurity of the antisense mode of action and, in some cases, causing cellular toxicity [Eckstein *et al*., 2000]. The best characterized classes of antisense drugs with respect to such toxicities are first-generation phosphorothioates and second-generation 2'-MOE modified antisense oligonucleotides [Bennett *et al.,* 2010]. Off-target effects of phosphorothioates can be generally caused by the actual reduction in target protein expression itself in a hybridization-dependent process, by antisense hybridization with related or nearly homologous sequences on nontarget mRNA and, most important, by nonspecific interactions with proteins [Levin *et al*., 2001]. Toxicities caused by exaggerated pharmacological effects (that means by excessive target down-regulation) and hybridization to nontarget RNAs can be avoided or minimized by proper selection of the target RNA and careful characterization of the pharmacology and toxicology of antisense inhibitors in preclinical models. Off-target hybridization-dependent effects can be minimized by performing careful bioinformatics analyses to identify targets with perfect mismatches or one to three mismatches [Bennett *et al.*, 2010]. The most prominent class-related toxicological effects observed in clinical studies after systemic administration are all related to nonspecific interactions with proteins and include complement activation, prolongation of clotting times (inhibition of the coagulation cascade), immune stimulation, pro-inflammatory action and reactions at the injection site [Levin *et al.,* 2001]. These effects are dose dependent and tend to occur at high doses of the oligonucleotides. They can be either sequence-dependent, such as interaction with Toll-like receptors, or sequence independent [Bennett *et al.,* 2010]. Toll-like receptor 9 has been identified to recognize specific CpG dinucleotide motifs of antisense oligonucleotides, leading to the rapid activation of cell signaling pathways, including mitogen-activated protein kinases and NF-*κ*B [Krieg *et al.,* 2003]. CpG-containing ASOs have been shown to trigger humoral immunity by inducing B-cell activation, proliferation and interleukin-6 and IgM secretion [Krieg *et al.*, 2003].

Besides the problem of specificity, a sufficient uptake of intact ASOs into the cell represents a significant challenge to the therapeutical use of these large molecules which usually harbour many solvent-exposed negative charges. The uptake appears to be an active, highly variable process dependent on cell type, time, concentration, energy, temperature, saturation, sequence and type of the oligonucleotide. From the application site ASOs need to be released from endosomes after endocytosis, travel to the cell surface, cross the plasma membrane and migrate to the cyto- or nucleoplasm in order to reach the target mRNA. Phosphorothioates have been described to be taken up by receptor-mediated endocytosis at lower concentrations, but via fluid-phase endocytosis at higher concentrations [Mahato *et al.,* 2005]. Typically oligonucleotides are administered by intravenous injection and infusion. Routes of administration, however, have been expanded over the last decades including also topical application to the skin, enema, inhalation and subcutaneous injection. Research efforts are rapidly advancing even oral formulations (across the gut wall) of oligonucleotides toward the clinic [Akhtar, 2009]. Oligonucleotides have been modified by appending lipophilic substituents, ligands for cell surface receptors, or cell-penetrating peptides to enhance their delivery to the cytoplasm, [Bennett *et al.,* 2010].

The therapeutical spectrum of antisense agents actually tested in the clinic is wide (table 1), including cardiovascular disease, inflammation, infection and, above all, cancer [Crooke, 2004]. Diseases that are characterized by over-expression or inappropriate expression of specific genes, or genes that are expressed by invading microorganisms, are candidates for this therapeutic approach. Malignant diseases, in particular, are attractive candidates, since conventional cancer therapies are highly toxic and affect also normal cells [Opalinska *et al.,* 2002]. Nevertheless many clinical studies in the field of oncology failed to reach their end points and so far the antisense concept could not fulfill all expectations. The best example is the 18mer phosphorothioate Oblimersen (G-3139, Genasense, Genta Inc., Berkeley Heights, NL, USA), which is directed against the first six codons of the anti-apoptotic *bcl-2*. Oblimersen selectively reduces *bcl-2* mRNA and subsequently decreases the expression of the protein Bcl-2, which plays a key role in preventing programmed cell death (*id est* apoptosis) [Willis *et al.,* 2003]. The effective knock-down of this protein is critical to tumor cell survival and positively influences the resistance of human malignancies towards standard chemotherapy [Wacheck *et al.,* 2002].

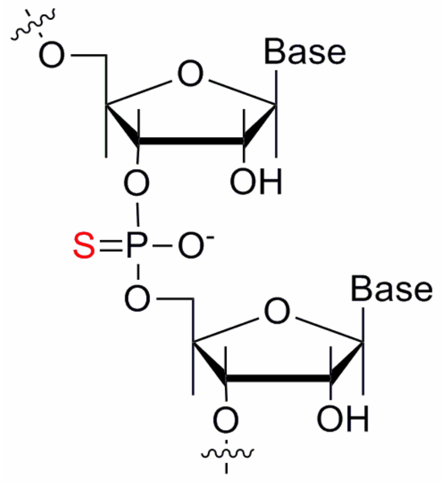

Figure 1. Phosphorothioate structure.

Multiple phase I, II and III clinical trials of Oblimersen alone or in combination with other anticancer agents have been conducted or are still going on in various cancer types (table 1) including advanced melanoma [Tarhini *et al.,* 2007]. As chemotherapy resistance in melanoma has been related to anti-apoptotic effects mediated by Bcl-2 [Jansen *et al.,* 2000], it was tested whether Bcl-2 inhibition by Oblimersen would improve the efficacy of standard chemotherapy [Bedikian *et al.,* 2006]. After the largest study ever conducted for advanced melanoma using a combination of Oblimersen and dacarbazine compared to dacarbazine monotreatment, overall survival, set as the primary end point, failed to reach the statistical significance level of $p<0.05$ [Bedikian *et al.,* 2006]. Although results of this trial showed increased secondary end points, including progression free survival and response rates, the results were not enough for FDA approval ultimately. Closer examination of the results confirmed serum lactate dehydrogenase (LDH) as a potent prognostic biomarker for malignant melanoma, since patients with normal LDH levels were more likely to benefit from the Oblimersen-dacarbazine regimen including statistically significant prolongation of overall survival [Agarwala *et al.,* 2009]. Consequently, Genta Inc. has decided to conduct a new phase III trial recruiting only patients with a maximum of 80% of normal LDH serum levels [Agarwala *et al.,* 2009]. Observed adverse events of the Oblimersen treatment have included fatigue, myelosuppression, transient thrombocytopenia, leukopenia, anemia and lymphopenia. Dose-related, reversible changes in liver function tests (aspartate aminotransferase, alanine aminotransferase, bilirubin and/or alkaline phosphatase) have been observed after prolonged infusion (14 days or longer), but these and other side effects are uncommon with shorter infusions [Tarhini *et al.,* 2007].

The exact molecular mechanism of action of Oblimersen and its impact on non-target proteins has not been clarified up to now. The success of antisense therapy and the effective use of phosphorothioates in the clinic will be strongly dependent on the identification of involved cellular signaling pathways and intracellular interactions with proteins playing key roles in malignant processes such as proliferation, angiogenesis and apoptosis.

1.2 RNA interference (RNAi)

RNA interference is a naturally occurring biological process in which small 21-23 [Mahato *et al.,* 2005] or 21-28 [Rao *et al.,* 2005] nucleotide duplexes (small interfering RNAs, siRNAs), respectively, silence a target gene by binding to its complementary mRNA thereby triggering its elimination [Mahato *et al.,* 2005]. The silencing process by siRNA occurs post-transcriptionally in the cytoplasm [Zeng *et al.,* 2002] and it is an ATP-dependent event. It was first discovered in *Caenorhabditis elegans* [Fire *et al.,* 1998] and has most likely evolved as a mechanism for cells to eliminate unwanted foreign genes. The physiological functions of RNAi are described to be a defense against viral infections, cell fate specification, transposon silencing and the regulation of developmental pathways [Rao *et al.,* 2005; Milhavet *et al.,* 2003].

The discovery of RNAi has revolutionized the field of gene silencing strategies and has prompted intensive research efforts in the last decade [Mello *et al.,* 2004; Grimm, 2009], thereby benefitting very much from earlier acquired knowledge about ASO structures and functions. In essence, long stretches of double stranded RNA (dsRNA) undergo processing by an enzyme referred to as Dicer, which cuts long stretches into duplexes with 19 paired nucleotides and two nucleotide overhangs at both 3'-ends [Elbashir *et al.,* 2001]. These double-stranded siRNAs then associate with the RNA-induced silencing complex (RISC), a large (approximately 160 kDa) protein complex comprising Argonaute proteins as the catalytic core [Tang, 2005]. Argonaute proteins are higly basic proteins which contain two common domains, PAZ and PIWI. The PIWI domain is essential for interaction with Dicer and contains the nuclease activity that cleaves off target mRNAs [Sioud, 2007]. Within RISC the siRNA is unwound and the sense strand is removed for degradation by cellular nucleases. The antisense strand of the siRNA directs RISC to the target mRNA sequence, where it anneals complementarily by Watson-Crick base pairing. Finally the target mRNA is degraded by RISC endonuclease activity [Cejka *et al.,* 2006]. In 2001, Tuschl and co-workers provided the first evidence that siRNAs can mediate sequence-specific gene silencing in mammalian cells bypassing the Dicer step by direct transfection of siRNA molecules into cells [Elbashir *et al.,* 2001], which opened up the way towards a use as tool and potential therapeutic.

The leading application for RNAi technology to date is the *in vitro* study of gene knockdown, because RNAi represents a fast and reliable tool for the characterization and influence of gene knockdown phenotypes [Cejka *et al.,* 2006]. As they have benefitted very much from the antisense experiences made before, the first siRNA candidates have rapidly entered the clinic (table 1), with bevasiranib (Cand5), an anti-VEGF-siRNA, being actually tested in phase III against age related macular degeneration. Main therapeutic applications include viral infections, neurological disease, oncology, ocular disease as well as inflammation and apoptosis [Uprichard, 2005]. The high sequence specificity of RNA interference may provide a means of inhibiting even the expression of single alleles, while the essential wild type allele is not inhibited. This is of great interest for neurodegenerative disorders that results from dominant mutations in a single allele, such as Parkinson`s disease, Huntington’s disease or amyothrophic lateral sclerosis [Uprichard, 2005]. RNAi might also complement chemotherapy in the treatment of patients that have developed multidrug resistance. 30% of all cancers develop resistance to standard chemotherapy due to an elevated expression of the multidrug resistance gene (MDR-1) [Tsuruo *et al*., 2003]. RNAi-mediated suppression of MDR-1 has been shown to re-sensitize cells to chemotherapy [Nieth *et al.,* 2003].

The developmental progress has required 10-15 years for ASOs but only 2-4 years for RNAi, since both strategies – apart from fundamental differences in the mode of action - have many similarities (table 2) [Corey, 2007]. RNAi effectors can be delivered to cells using either synthetic siRNAs or DNA, which encode for short hairpin RNA (shRNA) expression cassettes which are processed into active siRNAs by the host cells [Uprichard, 2005]. Actual clinical trials use intravenous and ophthalmic formulations of siRNAs, since RNAi technology is facing similar *in vivo* challenges compared to ASOs, such as limited stability, the problem of delivery as well as safety issues including off-target and nonspecific effects. siRNAs have been assumed to be higly specific and small enough to evade the immune system, but up to now several off-target effects, among them immunostimulatory effects, have been observed even in low nanomolar concentrations [Sioud *et al.*, 2003]. siRNAs have activated the interferon-regulated double-stranded RNA-dependent protein kinase (PKR) and endosomal Toll-like receptors (TLRs), a family of transmembrane proteins, which play a crucial role in microbe recognition and activation of innate and adaptive immunity [Sioud *et al.*, 2007]. Certain sequences have stimulated monocytes via TLR-8 or dendritic cells via TLR-7 to produce proinflammatory cytokines and large amounts of interferon α, respectively. Immunostimulatory siRNA effects are sequence dependent and can occur with double- and single-stranded siRNAs. Although GU dinucleotides have been found to trigger TLR-7 and TLR-8 activation, the absolute requirement in siRNA activation of innate immunity is still not clear [Sioud *et al.*, 2007]. Furthermore, interactions with undesired target mRNAs leading to the destruction of genes unrelated to target silencing have been observed [Jackson *et al.,* 2003; Scacheri *et al.*, 2004]. 2′-uridine modifications of siRNAs, however, have been reported to evade immune activation and to reduce mentioned off-target effects [Cekaite *et al.*, 2007]. With regard to an improvement of stability and cellular uptake of therapeutically relevant siRNAs, many of the precedent antisense modification concepts are used, including direct chemical alterations of nucleic acids and various methods of packaging the effector into protective particles [Uprichard, 2005].

Similarities and differences between antisense oligonucleotides (ASOs) and siRNA

Similarities
Short (~20 bases) nucleic acids
Common methods for delivery to cultured cells
Induce post-transcriptional gene silencing by targeting mRNA
siRNA and many ASOs cause mRNA cleavage
Properties can be altered by introducing modified bases
Similar biodistribution profiles

Differences
Two strands for siRNA, one strand for ASOs
Unmodified duplex RNA is more stable than unmodified single-stranded RNA or DNA
In cultured cells, chemical modifications are much less necessary for siRNA than for ASOs
Effects of siRNA mediated by the RISC complex
ASOs act by activation of RNAse H or steric inhibition
Rapid and widespread adoption of siRNA among biomedical researchers

Table 2. Adapted from Paroo and Corey, 2004.

The theoretical discussion, which of the two described antisense strategies is superior can only be solved by clinical development. Antisense oligonucleotides have the advantages that they are half the molecular weight and do not require a hybridization step, thus simplifying large-scale preparation of drugs. Furthermore the introduction of a synthetic RNA may perturb the native machinery resulting in *in vivo* toxicities, since endogenous duplex RNAs control important physiologic processes [Corey, 2007]. These potential advances are balanced against high potencies of siRNAs. In various *in vitro* models siRNAs have shown to be effective in already very low nanomolar concentrations (5-100nM compared to 50-400nM of ASOs) [Cejka *et al.,* 2006]. Most likely ASOs may have chemical and biological properties that might be superior for some tissues and gene targets, whereas siRNAs may be superior for others [Corey, 2007].

2. B-cell lymphoma 2 (Bcl-2)

2.1 Bcl-2 and apoptosis

Apoptosis is a programmed cell death mechanism involving two distinct but converging pathways and is generally characterized by sequential activation of cysteine proteases of the caspase family (figure 2) [Adams, 2003; Sun *et al.,* 2001]. The core of the intrinsic apoptotic machineries, which are mainly regulated by proteins of the B-cell lymphoma 2 (Bcl-2) family, is built by mitochondria. Additionally, the extrinsic pathway is driven by cell surface receptors of the tumor necrosis factor receptor gene superfamily (including TNFR-1, Fas/CD95 and TRAIL [Ashkenazi, 2002]), which activate Caspase-8 (and Caspase-10 in humans) when their ligand-mediated trimerization on the plasma membrane recruits the adaptor protein FADD (Fas-associated death domain protein) and the caspase into multi-protein complexes [Adams *et al.,* 2007]. In many cell types, however, death receptor-mediated apoptotic signaling induces a mitochondrial death amplification loop via proteolytic activation of the BH3-only protein Bid [Gul *et al.,* 2008]. The intrinsic pathway (also termed as ‘mitochondrial’ or ‘stress’ pathway), which has been extensively reviewed (Adams *et al.,* 2003 and 2007; Danial *et al.,* 2004), activates Caspase-9 on the scaffold protein Apaf-1 when cytochrome c is released from damaged mitochondria in response to diverse stresses, including cytokine deprivation and DNA damage. These initiator caspases can cleave and activate the effector caspases (Caspase-3, Caspase-6, and Caspase-7) that mediate cellular demolition by cleaving multiple critical cellular proteins [Adams *et al.,* 2007].

Defects in apoptotic signaling can be a cause or contributing factor in a variety of diseases, including cancer (resistance to chemotherapy, defective tumor surveillance by the immune system), autoimmunity (accumulation of autoreactive lymphocytes) and infection (accumulation of infected cells), as well as neurodegeneration (excessive apoptosis in e.g. Alzheimer's disease, Parkinson's disease or amyotrophic lateral sclerosis), AIDS (excessive depletion of T cells) or ischaemia (stroke, myocardial infarction) [Reed, 2002; Fischer *et al.,* 2005].

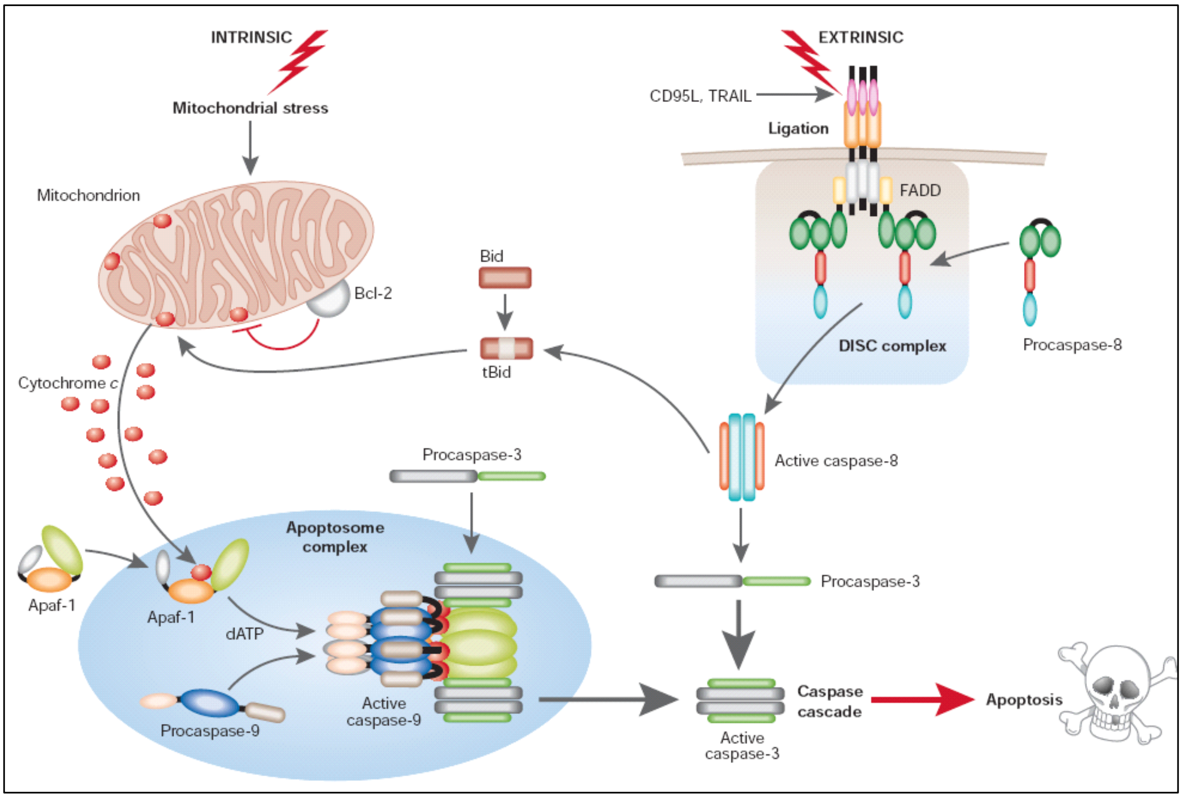
INTRINSIC
Mitochondrial stress
Mitochondrion
Bcl-2
Cytochrome c
Apaf-1
Apaf-1
dATP
Apoptosome complex
Procaspase-9
Active caspase-9
Procaspase-3
Bid
tBid
EXTRINSIC
CD95L, TRAIL
Ligation
FADD
DISC complex
Procaspase-8
Active caspase-8
Procaspase-3
Active caspase-3
Caspase cascade
Apoptosis

Figure 2. Illustration of the two major apoptotic pathways (picture taken from MacFarlane *et al.,* 2004).

The *bcl-2* gene and protein product were originally described following the identification of the t(14;18) chromosome translocation in follicular B-cell non-Hodgkin lymphoma cells [Tsujimoto *et al.,* 1984 and 1987]. The protein Bcl-2 itself is referred to as the prototypic anti-apoptotic protein belonging to a superfamily of proteins (n=24 in humans [Reed, 2003]), which includes pro-survival representatives (among others Bcl-2, Bcl-x_L, Bcl-w, A1 and Mcl-1) as well as pro-apoptotic members (the Bax-subfamily including Bax, Bak and Bok, and the BH3-only proteins, including Bad, Bik, Bid, Bim, Bmf, BNIP3, Noxa and Puma) [Cory *et al.,* 2002]. Most Bcl-2 family members, apoptosis agonists and antagonists, have Bcl-2 homologous (BH) regions, designated as BH1-BH4 (figure 3), which determine their capacity to interact with other Bcl-2 proteins and with the mitochondrial membrane [Tolcher, 2005].

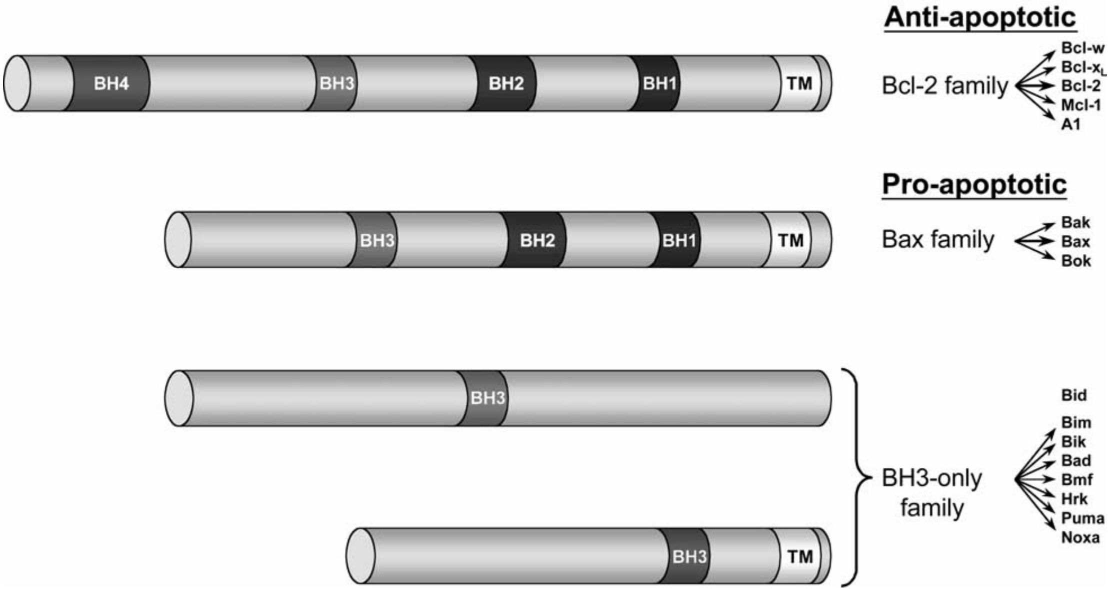
Anti-apoptotic
BH4
BH3
BH2
BH1
TM
Bcl-2 family
Bcl-w
Bcl-x$_L$
Bcl-2
Mcl-1
A1
Pro-apoptotic
BH3
BH2
BH1
TM
Bax family
Bak
Bax
Bok
BH3
BH3
TM
BH3-only family
Bid
Bim
Bik
Bad
Bmf
Hrk
Puma
Noxa

Figure 3. Scheme of Bcl-2 family members. BH – Bcl-2 homology domain; TM – transmembrane domain; picture taken from Bush *et al.,* 2003.

One of the key events in cell death is an increase of the mitochondrial membrane permeability leading to a loss of ΔΨ (mitochondrial inner transmembrane potential), mitochondrial swelling, and rupture of the outer mitochondrial membrane [Tsujimoto *et al.,* 2007]. As a result pro-apoptotic molecules are released to the cytosol (including cytochrome c, apoptosis-inducing factor AIF, endonuclease G, Smac/Diablo and Htr/Omi [Gul *et al.,* 2008]) which trigger the further activation of the caspase cascade. Whether apoptosis or cell survival is favored is controlled by Bcl-2 proteins through the competitive dimerization between selective pairs of death antagonists and agonists of this family [Coultas *et al.,* 2003]. Upon cell death stimuli, the pro-apoptotic proteins Bax and Bak are activated, inserted into the outer mitochondrial membrane and oligomerized, thereby facilitating mitochondrial outer membrane permeability (MOMP) either by forming channels by themselves [Antonsson *et al.,* 2000] or by interacting with components of the so-called permeability transition pore (PTP). This pore putatively consists of the voltage-dependent anion channel (VDAC), the adenine nucleotide translocator (ANT), cyclophilin D (Cyp D: a mitochondrial peptidyl prolyl-cis, trans-isomerase) and other molecules [Tsujimoto *et al.,* 2007].

Anti-apoptotic Bcl-2 proteins act as gatekeepers of MOMP through binding and sequestering pro-apoptotic Bax and Bak (figure 4). Activated BH3-only proteins, which differ in their potency among each other (Bim, Puma and truncated Bid (tBid) can bind all pro-survival proteins, whereas the selective proteins Noxa and Bad can only sequester Bcl-2 and Bcl-x_L) play another important role in the apoptosis cascade. They trigger apoptosis either by directly sequestering Bax and Bak as activators and by inhibiting pro-survival proteins Bcl-2 and Bcl-xL (figure 4a, direct activation model) or by binding only to their pro-survival relatives (figure 4b, indirect activation model). In the first model, the remaining BH3-only proteins, termed sensitizers, function by binding to the pro-survival proteins, thereby freeing any bound Bim or tBid to directly activate Bax and Bak. In the second, according to the author more probable indirect activation model, BH3-only proteins trigger apoptosis solely by binding to their pro-survival relatives, thereby preventing those guardians of cell survival from inhibiting Bax and Bak [Gul *et al.,* 2008; Adams *et al.,* 2007].

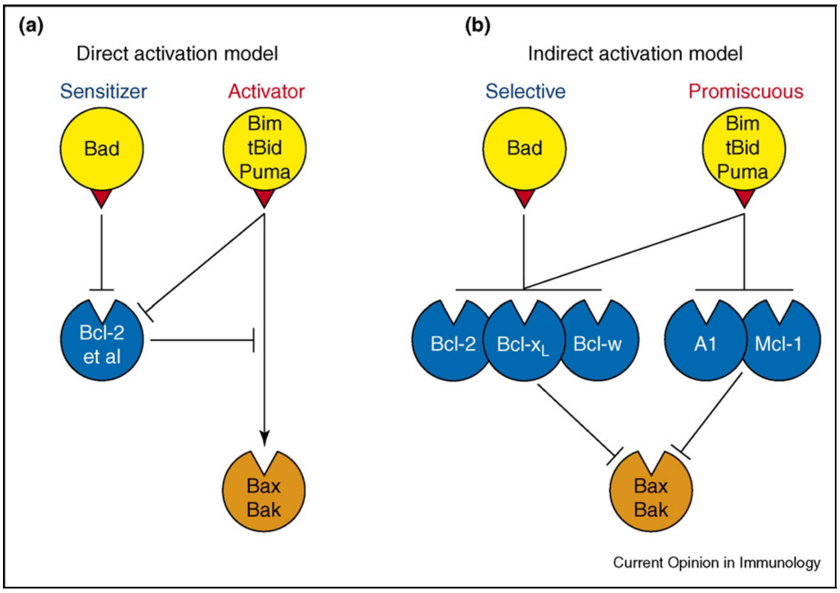
(a)
Direct activation model
Sensitizer
Activator
Bad
Bim
tBid
Puma
Bcl-2
et al
Bax
Bak
(b)
Indirect activation model
Selective
Promiscuous
Bad
Bim
tBid
Puma
Bcl-2
Bcl-x$_L$
Bcl-w
A1
Mcl-1
Bax
Bak
Current Opinion in Immunology

Figure 4. Actually discussed models of the roles of Bcl-2 family proteins in the apoptosis cascade. Picture taken from Adams *et al.,* 2007.

Mitochondrial membrane permeability transition is Ca$^{(2+)}$-dependent [Tsujimoto, 2007] and is linked to increased generation of reactive oxygen species (ROS) [Kroemer *et al.,* 2000].

2.2 Bcl-2 and cancer

In many cancer types such as melanoma [Jansen *et al.,* 2000], ovarian carcinoma [Williams *et al.,* 2005] or leukemia [Bachmann *et al.,* 2007] over-expression of anti-apoptotic Bcl-2 proteins has been associated with cell survival and increased resistance to chemotherapy (including most cytotoxic anticancer drugs [Reed, 2003]). Supposedly high levels of Bcl-2 inhibit apoptosis, among others by suppressing the generation of ROS, stabilizing $\Delta\Psi$ or preventing membrane permeability transition and consequently blocking the release of cytochrome c [Reed, 1998]. In melanoma, for instance, the expression of Bcl-2 protein has been shown in some studies with high frequency (90-100% of tumor biopsies). Moreover, Bcl-2 has been found in normal melanocytes, and the loss of Bcl-2 function in Bcl-2 knockout mice leads to accelerated disappearance of melanocytes. Depleting Bcl-2 simultaneously with the administration of chemotherapy may amplify apoptotic activity and improve clinical outcome of therapy, what has been demonstrated in preclinical studies with Bcl-2 antisense therapy having shown down-regulation of Bcl-2 protein and apoptosis induction in numerous solid and hematologic malignancies, including metastatic melanoma [Tarhini *et al.,* 2007].

Various therapeutical concepts have been established targeting key components of the apoptotic machinery. Up to now, most of the key players in cellular apoptosis regulation are identified and can be targeted by developed therapies. These include death receptors triggering apoptosis from the cell surface, Bcl-2 proteins as the gatekeepers of the mitochondrial pathway, caspases as the executioner enzymes or endogenous caspase inhibitors [Fischer *et al.,* 2005]. Attempts to overcome the cytoprotective effects of Bcl-2 and Bcl-x_L in cancer include three strategies: (1) shutting off gene transcription, (2) inducing mRNA degradation with antisense oligonucleotides (Genasense; ISIS 22783) and (3) directly attacking the proteins with small-molecule drugs (Bcl-2 blockers; Tetrocarcin A; Antimycin A derivatives) [Reed, 2003; Fischer *et al.,* 2005].

It is assumed that cancer cells depend more on apoptosis suppression than normal healthy cells, due to aberrations in proto-oncogene activity and/or cell cycle checkpoint control. Exploiting this differential dependence on apoptosis-suppressing mechanisms will contribute to an improved understanding of cell death pathways and will hopefully lead to improved clinical outcomes. It is of great importance, however, to determine to what extend toxicity and off-target effects to normal tissues limits application of apoptosis-based therapies for cancer treatment [Reed, 2003].

Aim of the work

The sucessful clinical development of therapeutically relevant oligonucleotides, such as phosphorothioates or small interfering RNAs, is challenged with unspecific drug effects. These off-target effects can be caused directly or indirectly by the onset of alternative cellular pathways, supporting or opposing the therapeutic aim or even causing unexpected toxicity.

The background of this work is based on the controversial question of specificity of oligonucleotides, which are therapeutically used or tested in late-stage clinical development, and leads to the main aims of this thesis. Is it possible to monitor any off-target effects of therapeutically relevant oligonucleotides, *id est* effects in addition to the known influence on the target sequence, on the cytosolic proteome? If yes, will these potential off-target effects differ among the application of distinct types of oligonucleotides, namely phosphorothioates and small interfering RNAs, which show the same pharmacodynamic effect on the target protein? In case of a successful identification of additionally changed proteins: Would these proteins be of importance to the metabolic networks of respective oligonucleotides?

Potential off-target effects of the phosphorothioate Oblimersen (Genasense, G3139) and a *bcl-2*-targeted siRNA on the proteome of the human melanoma cell line 607B have to be compared by the establishment of a validated proteomic approach. To ensure reliable results, special emphasis has to be put on the optimization of the used methods including two-dimensional separation conditions, gel staining protocols and software-based image analysis. Since the used cell line has not been characterized on the protein level before, a protein reference map of 607B melanoma cells has to be set up. Differentially expressed proteins have to be unambiguously identified by tryptic *in-gel* digestion and subsequent matrix-assisted laser desorption/ionization reflectron time-of-flight mass spectrometry (MALDI-rTOF-MS). If any effect on the proteome will be found, the roles of these particular proteins have to be investigated whether their abundancy changes are due to secondary effects in response to Bcl-2 depletion or indication of off-target effects. The first should be observed regardless of the oligonucleotide structure (antisense or siRNA), while the latter would likely result only after treatment with either compound.

The results of this thesis contribute to the elucidation of the molecular impact of therapeutically relevant oligonucleotides on the protein level.

Materials and Methods

Materials

DNA and RNA synthesis and purification

Standard β-cyanoethylphosphoramidites for RNA and DNA synthesis [SAFC, Proligo Biochemie, Hamburg, Germany]:

Standard liquid reagents for DNA and RNA synthesis [SAFC, Proligo Biochemie, Hamburg, Germany]:

Tetraethylthiuram disulfide, recrystallized from ethanol, 0.5M in acetonitrile [Sigma-Aldrich, St. Louis, MO, USA]

Diethyl-pyrocarbonate (DEPC) [Sigma-Aldrich, St. Louis, MO, USA]

Equipment

CD quartz cuvette (100-QS) [Hellma, Müllheim, Germany]

10 column DNA-synthesizer [Polygen™, Langen, Germany]

Jasco J-810 CD spectropolarimeter [Jasco, Gross-Umstadt, Germany]

Rotilabo® filter for syringes, 0.45µm [Carl Roth, Karlsruhe, Germany]

SepPak® Plus C_{18} cartridges [Waters, Framingham, MA, USA]

Spectrophotometer, PharmaSpec UV-1700 [Shimadzu Europe, Duisburg, Germany]

Suprasil® UV-cuvette, QS 284 [Hellma, Müllheim, Germany]

Cell culture

Amphotericin B [Sigma-Aldrich, St. Louis, MO, USA]

Annexin-V-FLUOS Staining Kit [Roche Diagnostics, Mannheim, Germany]

Dulbecco’s Modified Eagle Medium [Gibco™, Invitrogen, Carlsbad, CA, USA]

Dulbecco’s Phosphate Buffered Saline [Gibco™, Invitrogen, Carlsbad, CA, USA]

Fetal bovine serum, heat inactivated [Gibco™, Invitrogen, Carlsbad, CA, USA]

Hank’s Balanced Salt Solution [Sigma-Aldrich, St. Louis, MO, USA]

HEPES [Gibco™, Invitrogen, Carlsbad, CA, USA]

Homogenous Caspase Assay, fluorimetric [Roche Diagnostics, Mannheim, Germany]

Lipofectamine™ 2000 [Invitrogen, Carlsbad, CA, USA]

L-Glutamine [Gibco™, Invitrogen, Carlsbad, CA, USA]

OptiMem® [Gibco™, Invitrogen, Carlsbad, CA, USA]

Penicillin/Streptomycin [Gibco™, Invitrogen, Carlsbad, CA, USA]

Protease Inhibitor Cocktail, P8340 [Sigma-Aldrich, St. Louis, MO, USA]

Sodium Bicarbonate [Gibco™, Invitrogen, Carlsbad, CA, USA]

Trypsin/EDTA [Gibco™, Invitrogen, Carlsbad, CA, USA]

Equipment

6-well plates [Falcon™, BD Biosciences, San Jose, CA, USA]

24-well plates [Iwaki, Tokyo, Japan]

96-well plates [Greiner Bio-One, Kremsmünster, Austria]

Cell culture flasks [Greiner Bio-One, Kremsmünster, Austria]

Coverslips [Menzel-Gläser, Braunschweig, Germany]

Fluorescence microscope, Nikon Eclipse 50i [Nikon Instruments Inc., Europe]

Microplate reader, PolarStar Galaxy [BMG LABTECH, Offenburg, Germany]

Thoma® cell counting chamber [Hawksley, Lancing, UK]

Gel electrophoresis and Western Blotting

Coomassie® Brilliant Blue G-250 [Serva Electrophoresis, Heidelberg, Germany]

Dithiothreitol [Serva Electrophoresis, Heidelberg, Germany]

ECL Plus Western blotting detection reagent [GE Healthcare, Freiburg, Germany]

Immobiline™ DryStrip Gels, 18cm [GE Healthcare, Freiburg, Germany]

Iodoacetamide [Serva Electrophoresis, Heidelberg, Germany]

IPG buffers [GE Healthcare, Freiburg, Germany]

Precision Plus Protein™ Standard, All Blue and Unstained [Bio-Rad Laboratories, München, Germany]

PVDF blotting membrane, Immun-Blot® [Bio-Rad Laboratories, München, Germany]

Silver nitrate, p.a. [ACROS Organics, Geel, Belgium]

SYPRO® Ruby Protein Gel Stain [Bio-Rad Laboratories, München, Germany]

Primary antibodies

Actin, (A 2066) [Sigma-Aldrich, St. Louis, MO, USA]

Bcl-2, monoclonal (13-8800) [Zymed® Laboratories, Invitrogen, Carlsbad, CA, USA]

Secondary antibodies

Goat anti-mouse IgG HRP, (sc-2005) [Santa Cruz Biotechnology Inc., Santa Cruz, CA, USA]

Goat anti-rabbit IgG HRP, (sc-2004) [Santa Cruz Biotechnology Inc., Santa Cruz, CA, USA]

Equipment

1D-gel electrophoresis devices, Mini-Protean® 3 [Bio-Rad Laboratories, München, Germany]

2D-gel electrophoresis devices, Protean® II xi [Bio-Rad Laboratories, München, Germany]

DeCyder™ 2D differential analysis software, version 6.5 [GE Healthcare, Freiburg, Germany]

Ettan™ IPGphor™ isoelectric focussing unit [GE Healthcare, Freiburg, Germany]

Imaging Densitometer GS-710 [Bio-Rad Laboratories, München, Germany]

Molecular Imager ChemiDoc™ XRS System [Bio-Rad Laboratories, München, Germany]

PD-Quest™ Advanced 2D analysis software, version 8.0 [Bio-Rad Laboratories, München, Germany]

Quantity One® 1D analysis software, version 4.6 [Bio-Rad Laboratories, München, Germany]

Trans-Blot® SD Semi-Dry Transfer Cell [Bio-Rad Laboratories, München, Germany]

Typhoon™ Variable Mode Imager 9400 [GE Healthcare, Freiburg, Germany]

Protein identification

α-Cyano-4-hydroxy cinnamic acid [Sigma-Aldrich, St. Louis, MO, USA]

Acetonitrile, p.a. [Merck, Darmstadt, Germany]

Ammonium hydrogen carbonate [Fluka, Sigma-Aldrich, St. Louis, MO, USA]

Ditihiothreitol [Fluka, Sigma-Aldrich, St. Louis, MO, USA]

Formaldehyde, p.a. [Fluka, Sigma-Aldrich, St. Louis, MO, USA]

Iodoacetamide [Fluka, Sigma-Aldrich, St. Louis, MO, USA]

Potassium hexacyanoferrate(III), p.a. [Fluka, Sigma-Aldrich, St. Louis, MO, USA]

Sodium thiosulfate, anhydrous, p.a. [Fluka, Sigma-Aldrich, St. Louis, MO, USA]

Trifluoroacetic acid [Riedel-de-Haen, Fluka, Sigma-Aldrich, St. Louis, MO, USA]

Trypsin from bovine pancreas, modified, sequencing grade [Roche Diagnostics, Mannheim, Germany]

ZipTip® C_{18} Pipette Tips [Millipore, Bedford, MA, USA]

Equipment

MALDI TOF/RTOF (AXIMA Tof$^{2\text{TM}}$ and CFR™) [Shimadzu Biotech Kratos Analytical, Manchester, UK]

Methods

Synthesis of oligonucleotides

The used anti-*bcl-2*-siRNA was bought from MWG Biotech [Germany], all other used anti-Bcl-2 DNA and RNA oligonucleotide sequences were synthesized on a DNA synthesizer according to the phosphoramidite method, which is described in the thesis of Winkler [Winkler, 2003]. In brief, the synthesis cycle consists of four repeating steps, detritylation (A), coupling (B), capping (C) and oxidation (D), and the oligonucleotide is built up from the 3'-end to the 5'-end. Controlled Pore Glass (CPG) is used as solid phase. (A) The DMT group of the first CPG-bound nucleotide is split off by 3% trichloroacetic acid in dichloromethane (the absorption of the cation is measured at 495nm and is used as in-process control in most synthesizers). (B) The coupling of the second phosphoramidite is improved by the use of 1H-tetrazole as catalyst. (C) Since coupling rates lie between 95 and 100%, an acetylation of remaining free 5'-hydroxy-groups is necessary to avoid a further reaction of shorter nucleotides. This capping step is done in acetic anhydride in tetrahydrofuran using the catalysts N-methylimidazole and 2,6-lutidine. Cap A and Cap B reagents are mixed *in situ*. (D) The oxidation step is performed in iodine/water/pyridine to oxidize P(III) to the stable P(V). (E) At the end of the synthesis the solid phase, cyanoethylphosphate protecting groups and organic base protecting groups are split off by heating the product in concentrated ammonia at 55°C for 16 hours. RNA sequences harbor an additional protecting group (t-butyltrimethylsilylester) at the 2'-end (figure 5), which is stable in concentrated ammonia, but can be removed by fluoride ions.

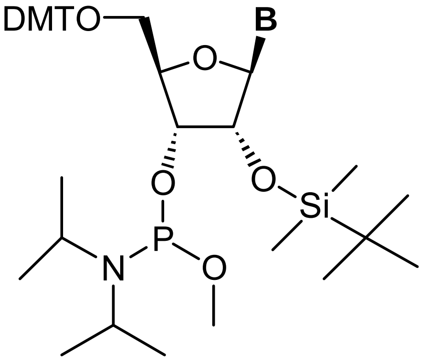

Figure 5. RNA phosphoramidite.

Synthesis of phosphorothioates (S-DNA) was performed using tetraethylthiuramdisulfide (TETD) as sulfurization reagent, which was recrystallized in ethanol before use, and 4,5-dicyanoimidazole (DCI) as activator. Resulting phosphorothioates were used as diastereomers, like most of the clinically tested S-DNAs. Phosporamidites were dissolved 0.05M in water-free acetonitrile and DNA oligonucleotides were synthesized in DMT-on mode according to the standard procedure described above. RNA sequences were synthesized lacking the last DMT group (DMT-off) and heated in a solution of concentrated ammonia and 96% ethanol (3:1) at 55°C for 15 minutes. In order to remove the 2`-O-TBDMS-protecting group RNA sequences were subsequently stored in tetrabutylammonium fluoride solution over night.

Purification of oligonucleotides

Purification of raw products was performed with SepPak® C_{18} cartridges. All aqueous solutions for DNA purification were prepared with double distilled water (*aqua purificata)*. Ammonia solutions containing dissolved S-DNA strands were filtered, solvents were evaporated at 40°C and oligonucleotides were resolved in 1M TEAA. Cartridges were activated with acetonitrile and equilibrated with 1M TEAA.

Subsequently oligonucleotides were repeatedly applied onto the cartridge and impurities were washed out with 5% ammonium hydroxide solution and water. After detritylation of S-DNA with 2% trifluoroacetic acid (TFA) and removal of remaining TFA with water, the pure oligonucleotide was eluated with 30% acetonitrile. Again liquids were evaporated and purification was completed by ammonium acetate precipitation (20-50µl water, 50µl 7.5M ammonium acetate and ethanol *ad* 1200µl, stored at –20°C for at least 24 hours). Resulting precipitates were centrifuged with 15000rpm at 4°C for 10min and pellets were resolved in water. Concentrations of purified oligonucleotides were determined by UV measurement at 260nm. Molar extinction coefficients were calculated as the sum of nucleotides (A, 15400; G, 11700; C, 7300; T, 8800; U, 9950). 1mM stock solutions were prepared and stored at –20°C until used.

For the purification of RNA sequences RNase-free equipment (heat sterilization of used glass ware at 120°C for at least 12hours) and solutions (prepared with RNase-free water) were used. Distilled water containing 0.1% DEPC was stirred over night and subsequently autoclaved to prepare RNase-free water. The elimination of the 2`-protecting group with TBAF was stopped by addition of the same amount of 1M TEAA. Subsequently solvents were evaporated. RNA strands (DMT-off) were resolved in 1M TEAA and subsequently desalted with SepPak® C_{18} cartridges. Cartridges were activated with 100% acetonitrile and equilibrated with 1M TEAA. RNA oligonucleotides were repeatedly applied to the column, salts were washed out with RNase-free water and desalted oligonucleotides were eluated with 30% acetonitrile. Ammonium acetate precipitation and concentration determinations were performed as described above. 1mM stock solutions were stored at –20°C until used.

Quality control of oligonucleotides

Quality of purified oligonucleotides was controlled by gel electrophoresis and circular dichroism.

Gel electrophoresis:

RNA and DNA strands were monitored on denaturing 20% polyacrylamide gels containing 8M urea. Nucleic acids were mixed with formamide sample buffer (90% formamide, 2% 0.5M EDTA, 8% water) and denatured (3min at 95°C, immediately cooled on ice). After a pre-run of 30 min in electrophoresis buffer (89mM Tris, 89mM boric acid, 4% 0.5mM EDTA) at 200V, samples (1 nM) were run on gels for 90 min at the same constant voltage. A mixture of Bromphenol Blue (corresponding to a length of 10bp) and Xylene Cyanole (corresponding to a length of 18bp) was used as size standard. Oligonucleotide bands were stained with methylene blue (0.1% in sodium-acetate solution, pH 5.2) for 20min and gel backgrounds were destained with water. Pure samples contained only one clearly visible band without shorter or larger impurities.

Circular dichroism (CD):

Oligonucleotide solutions (9µM) were measured in CD buffer (0.15M NaCl, 0.01M Tris, pH 7.1) as single and double strands in a quartz cuvette with a pathlength of 1mm. In the latter case the two complementary single strands were incubated 15 min at room temperature before measurement. Instrument parameters were chosen as follows: sensitivity: high, scan start: 320nm, scan stop: 200nm, scanning speed: 20nm/min, data pitch: 0.5nm, band width: 1nm, response: 16sec, accumulation: 3, temperature: 20°C. Pure RNA sequences resembled typical A-DNA CD-spectra (C_3'-endo ribose conformation, which is characterized by a distinct positive band with a maximum at ~270nm and weaker negative bands at ~235nm and 210nm), whereas pure DNA sequences displayed typical B-DNA spectra (C_2'-endo conformation, which is characterized by a smaller positive maximum at ~280nm and a stronger negative band with a minimum between 245-250nm). For details on CD of nucleic acids see Johnson W.C. in: Berova *et al*., 2000.

Cell culture

The human melanoma cell line 607B [Thallinger *et al.*, 2007; Jansen *et al.*, 1999] was a kind gift from Dr. Wacheck (Medical University of Vienna) and was cultured in Dulbecco's modified Eagle medium supplemented with 10% (v/v) fetal calf serum, 100U/ml penicillin, 100µg/ml streptomycin, 6mM L-glutamine and 0.25µg/ml amphotericin B.

Oligonucleotide transfections and cell lysis

For oligonucleotide transfections cells were grown on six-well plates (6×10^5 cells/well, uncoated plates) until cells had reached 80% confluence (24 hours after seeding). Oligonucleotides were pre-complexed with Lipofectamin2000™ in serum-free OptiMem® and transfected to 607B cells 24 and 48 hours after seeding. Four hours after each application of oligonucleotide-lipid complexes, serum was added to the cells to reach the normal growth media serum concentration. After a total of 72 hours the media was removed, cells were washed twice with D-PBS and harvested by addition of ice-cold lysis buffer (8M urea, 2M thiourea, 0.5% (v/v) Triton X-100, 2% (w/v) CHAPS, 5mM EDTA, 32mM DTT and 1% (v/v) protease inhibitor cocktail). After centrifugation (15 000 rpm, 10min, 4°C) to remove cell debris, supernatants were collected and total protein concentrations were determined according to Bradford [Bradford, 1976].

For the Bradford assay samples were mixed with Bradford reagent (0.01% (w/v) Coomassie brilliant blue G250, 5% (v/v) ethanol, 10% (v/v) phosphoric acid), incubated for 5min at room temperature and measured by spectrophotometry at 595nm. The protein amount of the samples was calculated by means of a calibration curve based on standard bovine serum albumin concentrations (2.5-10µg/ml).

Western blot analysis

Aliquots of cell lysates containing 20µg of total protein and molecular weight marker were resolved by 12.5% SDS-PAGE according to Laemmli [Laemmli, 1970] in 250mM Tris, 8% (w/v) SDS, 20% (v/v) glycerol, 0.02% (w/v) Bromphenol blue, 6.2mg/mL DTT after heating the samples for 10min at 95°C. Samples were blotted onto PVDF membranes in a semi-dry blotter and unspecific binding was blocked over night at 4°C with 1% (w/v) milk powder in TBS buffer containing 0.1% Tween®20 (0.1% TBST). After four washing cycles with 0.1% TBST à 10min membranes were incubated with primary antibodies recognizing either Bcl-2 (1 µg/ml) or actin (0.6 µg/ml) for 45min at room temperature. Blots were washed again four times à 10min with 0.1% TBST and subsequently incubated with HRP-conjugated secondary antibodies for one hour at room temperature in the dark. Detection was performed using chemiluminescence (ECL Plus). Relative quantification of protein bands was done with software–based analysis (Quantity One™ version 4.6.3) after digitalization of X-ray films.

Caspase Assay

Apoptosis is accompanied by a series of characteristic morphological changes. One of these intracellular biochemical events is the activation of specific cysteinyl-aspartic-acid-proteases or short caspases, which play a key role in the further processing of the programmed cell death. Therefore a high caspase activity is related to increased apoptosis.

1×10^4 607B cells per well were seeded in 96-well fluorescence plates and transfected with oligo-lipoplexes as described above. Caspase-3 activity was measured after 24 hours in a fluorescence plate reader after incubation with DEVD-R110 substrate for one hour at 37°C (excitation filter 470-550nm and emission filter 500-560nm).

Annexin-V-FLUOS staining

Annexin-V is a calcium-dependent phospholipid-binding protein with high affinity to phosphatidylserine and is therefore suitable for the detection of apoptotic cells. The simultaneous application of Propidium iodide (red), which stains DNA of leaky necrotic cells only, allows the discrimination of necrotic cells from the Annexin-V (green) positively stained cell clusters [van Engeland *et al.,* 1996].

1.6×10^5 607B cells per well were seeded on coverslips in 24-well plates. Cells were transfected with oligonucleotide-Lipofectamin2000™ complexes as described above and control samples were treated with lipofectamine 2000 alone. After a total of 72 hours medium was removed, samples were washed one time with D-PBS and incubated for 15min at room temperature with Annexin-V-FLUOS labeling solution as recommended by the manufacturer. Coverslips were embedded with FluorSave™ reagent and analyzed in a Nikon Eclipse 50i microscope equipped with an EXFO X-Cite 120 fluorescence illumination system.

Excitation and emission filter blocks were at 465-495/515-555 for green fluorescence and at 510-560/>590 for red fluorescence. Pictures were acquired at 20x and 40x magnification, respectively, using Lucia Gv5.0 software for image evaluation.

Two dimensional gel electrophoresis (2-DE)

For DIGE gels pH values of cell lysates of treated and untreated samples were adjusted to 8.5 using 50mM sodium hydroxide and labeled with CyDye™ Fluor minimal dyes according to the manufacturer’s instructions (8pmol dye per µg protein). The experimental setup of the DIGE approach is shown in table 3.

Gel number	Cy2	Cy3	Cy5
1	Pooled standard	control 1	siRNA 1
2	Pooled standard	OBL 1	control 1
3	Pooled standard	control 2	OBL 1
4	Pooled standard	siRNA 1	control 2
5	Pooled standard	siRNA 2	OBL 2
6	Pooled standard	OBL 2	siRNA 2
7	Pooled standard	OBL 3	control 3
8	Pooled standard	siRNA 3	OBL 3
9	Pooled standard	control 3	siRNA 3

Table 3. Experimental design of the comparison of two antisense agents on the protein level using DIGE technology.

In order to compare Oblimersen-treated, siRNA-treated and untreated cells a total of nine gels was prepared. Each triplicate corresponded to another biological replicate. For the internal standard equal amounts of all samples were pooled and labeled with Cy2. Samples were labeled with Cy3 and Cy5. 25µg of labeled samples (Cy3 labeled), 25µg of labeled samples (Cy5 labeled) and 25µg of internal standard (Cy2 labeled) were diluted to 350µl with rehydration buffer (8M urea, 4% (w/v) CHAPS, 13mM DTT and 1% (v/v) pharmalyte 3-11) and applied to 18cm non linear IPG strips. Rehydration of the strip/sample application was performed for 12 hours at 20°C. Isoelectric focusing was carried out to a total of 80kVhr on an IPGphor unit. The focused IPG strips were reduced 15min (1% DTT (w/v)) and alkylated 15min (2.5% iodoacetamide) in equilibration buffer (50mM Tris-HCl, 6M urea, 30% (v/v) glycerol, 2% (w/v) SDS, a few grains of Bromphenol blue, pH 8.8). The second dimension was performed on homogenous 12.5% polyacrylamide gels (20x22cm) applying constant 50mA per gel. All gels were scanned at 100µm resolution on a Typhoon 9400 imager and analyzed with DeCyder software version 6.5.

2-DE experiments for silver, Coomassie and Sypro Ruby staining were carried out as described above lacking the labeling process (rehydration solution: 8M urea, 2M thiourea, 4% (w/v) CHAPS, 0.5% (v/v) Triton X-100, 0.005% Bromphenol blue, 32mM DTT and 0.5% pharmalyte; equilibration solution: 50mM Tris-HCl, pH 8.8, 6M urea, 30% (v/v) glycerol, 2% (w/v) SDS and a few grains of Bromphenol blue).

Instrument parameters for isoelectric focusing with IPG strips of different p*I* are summarized in table 4.

p*I*	**3-11**	**4-7**	**6-9**
	rehydration 12hours 20°C	rehydration 12hours 20°C	rehydration 12hours 20°C
Step 1	gradient 500V, 300Vhr	gradient 500V, 300Vhr	step 500V, 500Vhr
Step 2	gradient 1000V, 750Vhr	gradient 1000V, 750Vhr	gradient 1000V, 800Vhr
Step 3	gradient 2000V, 1500Vhr	gradient 2000V, 1500Vhr	gradient 10 000V, 16 500Vhr
Step 4	gradient 4000V, 2000Vhr	gradient 4000V, 2000Vhr	step-n-hold 10 000V, 50 000Vhr
Step 5	gradient 8000V, 6000Vhr	gradient 8000V, 6000Vhr	step-n-hold 5000V, 5h
Step 6	step-n-hold 8000V, 73200Vhr	step-n-hold 8000V, 73200Vhr	
Step 7	step-n-hold 2000V, 5 h	step-n-hold 2000V, 5 h	

Table 4. Summary of isoelectric focusing parameters.

2-DE gels were post-stained with Coomassie R-250 or silver according to Blum or Shevchenko, respectively [Blum, 1987; Shevchenko, 1996]. Briefly, silver staining according to Blum included a fixation step (over night in 10% (v/v) acetic acid, 40% (v/v) methanol), two washing steps à 20min with 30% (v/v) ethanol and one with water, followed by a sensitization step (1min in 200mg/l sodium thiosulfate), the incubation in silver solution (30min in 0.02% (v/v) formaldehyde, 2g/l silver nitrate) and a developing step (30g/l sodium carbonate, 5mg/l sodium thiosulfate, 0.05% formaldehyde). Staining was stopped by addition of a glycine solution (5g/l glycine). The second silver staining method, which was better compatible with subsequent MS experiments, started with a fixation step (20min in 50% (v/v) methanol, 5% (v/v) acetic acid), a washing step in 50% (v/v) methanol and one in water, followed by a sensitization step (1min in 200mg/l sodium thiosulfate), two short washing steps in water, the incubation in silver solution (1g/l silver nitrate), a short washing step in water and the developing step (20g/l sodium carbonate, 0.04% (v/v) formaldehyde). Staining was stopped with a solution containing 5% (v/v) acetic acid and gel backgrounds were washed with water. Wet gels were digitized at 85µm resolution using the densitometer GS-710.

For Coomassie R-250 standard staining gels were fixed for one hour in a fixing solution (45% (v/v) methanol, 5% (v/v) acetic acid), washed two times with water and incubated with the staining solution (0.025% (v/v) Coomassie Brilliant Blue R-250, 40% (v/v) methanol, 7% (v/v) acetic acid) until blue protein bands were visible. Subsequently gel backgrounds were destained in two steps: 30min destaining solution I (40% (v/v) methanol, 7% (v/v) acetic acid), ~1 hour destaining solution II (7% (v/v) acetic acid, 5% (v/v) methanol) until backgrounds were clear. Coomassie-stained gels were digitized using the densitometer GS-710, using the integrated Coomassie Blue filter.

SYPRO® Ruby post-staining included a fixation step (30min, 10% (v/v) methanol, 7% (v/v) acetic acid), the light-protected incubation with SYPRO® Ruby (over night at room temperature using 250ml for 2 gels) and a background-destaining step (30min, 10% (v/v) methanol, 7% (v/v) acetic acid) as well as two washing steps in water afterwards. Wet gels were imaged with a CCD-based ChemiDoc XRS imager at a resolution of ~150µm using the integrated filter for fluorescence imaging.

Software-based image analysis

Silver-, Coomassie and Sypro Ruby-stained 2-DE gels were analyzed with the software tool PD-Quest (Bio-Rad; version 6.1 and 8.0, respectively), whereas DIGE gels were evaluated using the software package DeCyder (GE Healthcare, version 6.5). The image analysis process with PD-Quest was performed using the spot detection wizard provided by the software and is described in Stessl *et al*., 2009. In brief, raw gel files were cropped and classified into replicate groups. A parameter set including sensitivity, size scale and minimal peak height was chosen according to the appearance of respectively stained gels. Speckle and streak filters were applied and all gels were warped before analysis. Spot detection was performed automatically excluding all saturated spots from further evaluation. Spot matching was performed either on the basis of the selection of landmark spots (version 6.1) or automatically (version 8.0). In both cases all matched spots were subjected to a careful manual control with regard to spot positions and match quality. In order to compensate for non-expression-related variations in spot intensities, normalization was performed using the recommended standard procedures by the respective software version ("total density on gel" version 6.1; "local regression model", version 8.0). For further quantitative and statistical analyses only appropriately matched spots with a satisfying spot quality (a parameter including accuracy of Gaussian fitting, horizontal and vertical streaking, spot overlap and linearity) were included (for silver stained gels the minimum spot quality was assumed with 60 according to Schlags *et al*., 2005).

DIGE image evaluation with DeCyder included two major steps of cropped raw images (DIA: differential analysis module, BVA: biological variation module) and was based on volume ratios (sample spot volume divided by the corresponding internal standard spot volume). Since differences between Cy3- and Cy5-labeled proteins have been reported [Tonge et al., 2001] only Cy3-labeled samples and Cy2-labeled internal standards were taken into consideration for further quantitative analyses. The following DIA module parameters were chosen: number of estimated spots: 2500, exclusion filter (volume<75000 and slope>1.7), whereupon all excluded spots were manually controlled for eventual false exclusions. Remaining spots were normalized [for details on the automatic normalization process performed by DeCyder see Winkler W et al., 2008], grouped and exported to the BVA module, where the matching process was performed. ~75 well resolved spots from different gel regions (corresponding to 8.5% of all included spots), which were present in all gel maps, were defined as landmark proteins to facilitate the matching process. After manual control and matching confirmation, proteins of interest were defined, including only spots passing the following criteria: average ratio ±1.5, Student's t-test ($p \leq 0.05$), 1-way ANOVA ($p \geq 0$ and ≤ 0.05), appearance in at least 16 of 18 spot maps and match quality <6. The match quality is a value calculated by the software from the surface profiles of each internal standard on each gel matched to the master spot maps, ranging from 0 (very good) to 15 (very bad). The raw data of interesting spots were exported to Microsoft Excel 97 using the DeCyder XML tool. Afterwards gels were post-stained with silver nitrate according to Shevchenko [Shevchenko, 1996] and stored in water at room temperature until protein identification.

Protein identification by mass spectrometry

The theory about the used mass spectrometric method (matrix-assisted laser desorption/ionization reflectron time-of-flight mass spectrometry (MALDI-rTOF-MS)) is summarized in supplement A of this thesis. Identification of proteins was performed as described in [Stessl et al., 2009]. Spots of interest were cut out manually from 2-DE gels and subjected to in-gel digestion using trypsin. Desalted and purified samples (ZipTip C18) were measured in positive reflectron mode by MALDI-rTOF MS (MALDI Tof^2 and CFR± instrument, respectively) using α-cyano-4-hydroxycinnamic acid as matrix. Both thin layer and dried droplet sample preparation techniques [Vorm et al., 1994] were used. External calibration was performed using singly charged monoisotopic m/z values of standard peptides (bradykinin fragment 1-7, human angiotensin II, angiotensin I, glu-1-fibrinogen peptide, N-acetyl renin substrate and ACTH fragments). Unsmoothed PMF were manually reviewed using the Shimadzu Biotech Kratos Analytical software (Launchpad, version 2.7.1) and monoisotopic m/z values were listed excluding peaks belonging to tryptic auto-digestion, keratins [Mattow et al., 2004] or matrix ion-clusters [Smirnov et al., 2004]. The publicly available search engines MASCOT (Revision 2.1.0) [Perkins et al., 1999] and ProFound [Zhang et al., 2000] were used to search different databases: SwissProt (MSDB (version 50.6 of 2006-09-05 to 54.5 of 2007-11-04) and the non redundant NCBI (Sequence Release 19 of 2006-09-10 to 26 of 2007-11-13) databases. Search criteria: fixed modification (carbamidomethylation of cysteins), variable modification (oxidation of methionins), taxonomy (H. sapiens), missed tryptic cleavages (1), m/z tolerance (±50 mDa), molecular weights (±20Da, ProFound only) and isoelectric points estimated from 2-D gels (±2, ProFound only). Protein identification was further confirmed by post source decay (PSD) and MS/MS experiments of selected peptides on the above mentioned instruments. The fragment ion m/z values were exported from smoothed spectra (Savitsky Golay algorithm [Savitzky et al., 1964]). MS/MS database search was performed using average peptide fragment ion masses with the same restrictions as for PMF, additionally a product ion tolerance of ±1 Da was defined. A hit was considered to be significant, if the scores obtained for PMF and MS/MS data clearly exceeded each algorithm's significance threshold ($p<0.05$).

Protein accession numbers mentioned in the text and tables can be found in the publicly available database SwissProt at www.expasy.org.

Results

1. Oligonucleotides

One main focus of this work was the investigation of specific and unspecific effects of the 18-mer phosphorothioate (S-DNA) Oblimersen (Genasense, G-3139), which is directed against the first six codons of the human *bcl-2* mRNA. The following control sequences for cell culture experiments were used: (1) the antiparallel, complementary sense sequence, (2) a scrambled sequence (containing the same number of organic bases as the original antisense sequence but in randomly chosen order) and (3) a mismatch sequence harboring thymidine instead of guanine at position eight. Similar control sequences were prepared for respective anti-*bcl-2* siRNA sequences. An overview of the DNA and RNA oligonucleotide sequences for the present work is given in table 5.

	Sequence (5‘-3‘)	Target	Reference
S-DNA:			
Oblimersen (G 3139) antisense	TCT-CCC-AGC-GTG-CGC-CAT	*bcl-2*	Tarhini *et al* (2007)
Oblimersen sense	ATG-GCG-CAC-GCT-GGG-AGA		
Oblimersen scrambled (control)	GAG-TCT-ACC-GTC-CCT-GCC		
Oblimersen 1base mm (control)	TCT-CCC-ATC-GTG-CGC-CAT		
si RNA			
Anti-Bcl-2-siRNA antisense	UGU-GGA-UGA-CUG-AGU-ACC-UAG-dTdT	*bcl-2*	Wacheck *et al* (2003)
sense	UCA-GGU-ACU-CAG-UCA-UCC-ACA-dTdT		
Anti-Bcl-2-siRNA scrambled (control)	AUU-CGC-ACU-CGC-ACU-CGA-AUA-dTdT		
Anti-Bcl-2-siRNA 3 base mm (control)	UGU-AGA-UGA-CUU-AGU-ACG-UGA-dTdT		

Table 5. Summary of synthesized DNA and RNA oligonucleotide sequences. Sequences were taken from denoted references.

2. Influence on target protein expression

The human melanoma cell line 607B was used for performed cell culture experiments. 607B cells over-express the target protein Bcl-2 [Thallinger *et al.*, 2007; Jansen *et al.*, 1999]. Preliminary experiments were performed to optimize oligonucleotide transfection conditions. Working concentrations leading to the same level of target protein inhibition were determined. Inhibitions of Bcl-2 expression levels are shown in table 6 and figure 6 and 7.

Sequence [nM]	**Bcl-2 inhibition [%] ***
Obl 50	46 ± 5.81
Obl 100	**75 ± 4.89**
Obl 150	65 ± 4.89
Obl 200	59
siRNA 5	78 ± 2.98
siRNA 10	80 ± 2.48
siRNA 15	80
siRNA 25	82 ± 4.29
siRNA 50	**75 ± 5.70**
siRNA 100	80 ± 1.49

Table 6. % Bcl-2 inhibition achieved with different concentrations of Oblimersen (Obl) and anti-*bcl-2*-siRNA (siRNA). * Values were calculated with QuantityOne® software as means of triplicates. Treated samples were referred to untreated controls (100% target protein) and normalized on the expression of actin as loading control.

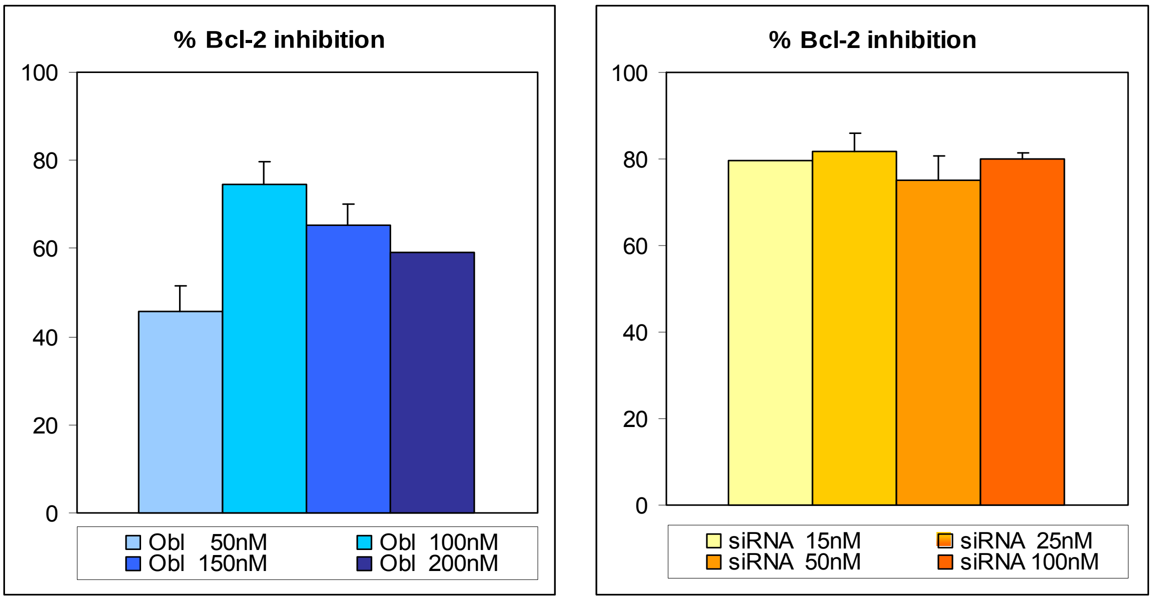

Figure 6. Illustrations of target inhibition by four different concentrations of Oblimersen (Obl; left) and anti-*bcl-2*-siRNA (siRNA; right). Values were referred to untreated controls and normalized on expression levels of actin.

In accordance with literature the phosphorothioate had to be applied in higher concentrations than the respective siRNA to monitor any influence on target protein expression [Anderson *et al*., 2006; Wacheck *et al*., 2003]. For Oblimersen a minimum concentration of 50 nM was necessary to achieve 46% of down-regulation – below that, no significant regulation could be observed. The maximum Bcl-2 expression inhibition of 75% could be achieved at 100 nM. This concentration was therefore chosen as Oblimersen working concentration. Higher phosphorothioate concentrations (150 nM, 200 nM) again resulted in lower inhibition levels of 65% and 59%, respectively.

The chosen siRNA sequence was more effective in target protein down-regulation than the phosphorothioate - even in very low concentrations of 5 nM or 10 nM Bcl-2 expression levels could be reduced for ~80%. Since a concentration of 50 nM achieved the same 75% of target protein inhibition compared to Oblimersen, this concentration was chosen as corresponding siRNA working concentration.

Denoted control sequences (scrambled and mismatch-containing sequences) did not show any target protein knockdown under the same experimental conditions. As shown in table 7 the combination of the two antisense agents did not lead to a significant increase of protein knockdown compared to siRNA alone.

Combinations	Bcl-2 inhibition [%]
Obl 50nM + siRNA 25nM	73
Obl 50nM + siRNA 50nM	79
Obl 100nM + siRNA 10nM	68
Obl 100nM + siRNA 50nM	85

Table 7. Bcl-2 inhibition levels achieved by combinations of Oblimersen (Obl) and anti-Bcl-2 siRNA (siRNA). Standard deviations are not available (n.a.) since these transfections were only performed once.

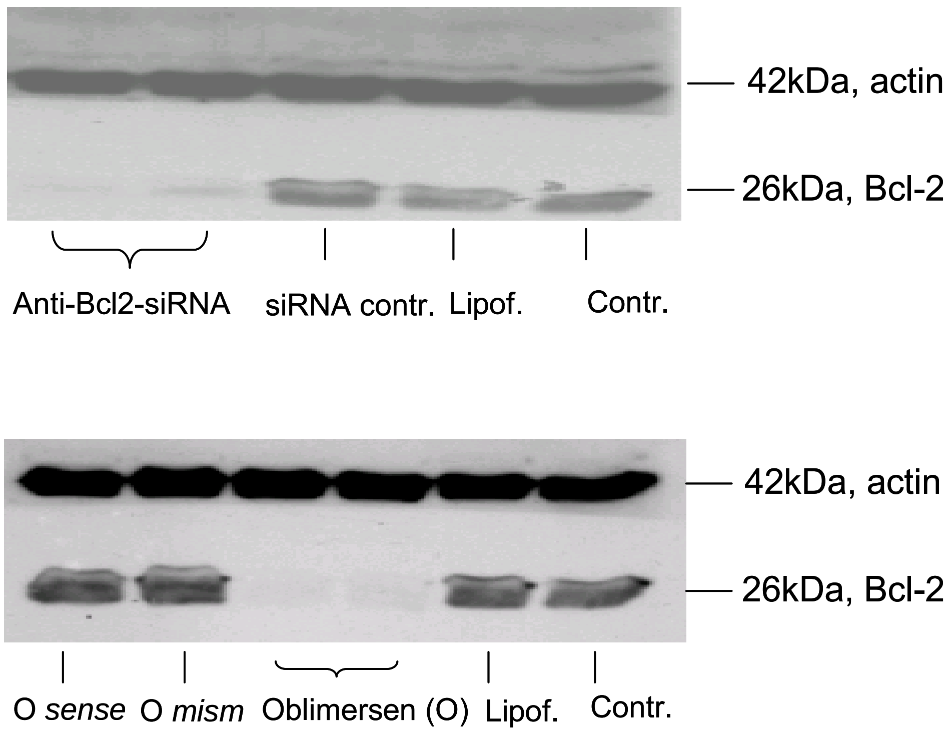
42kDa, actin
26kDa, Bcl-2
Anti-Bcl2-siRNA
siRNA contr.
Lipof.
Contr.
42kDa, actin
26kDa, Bcl-2
O *sense*
O *mism*
Oblimersen (O)
Lipof.
Contr.

Figure 7. Western blot analyses demonstrating effective Bcl-2 down-regulation by antisense (Oblimersen) and anti-Bcl-2-siRNA. Total proteins were extracted after 72 h and protein levels were assessed by Western blotting using protein specific antibodies. *Lipof.*, unloaded lipofectamine2000, *Oblimersen or O,* Oblimersen [100 nM] transfected with lipofectamine2000 (representative duplicate), *siRNA*, anti-Bcl-2-siRNA [50 nM] transfected with lipofectamine2000 (representative duplicate), *O mism.*, Oblimersen with 3 mismatches, *siRNA contr.*, scrambled siRNA sequence, *Contr.*, untreated cells. Equal gel loading was controlled by actin expression.

3. Apoptosis induction

For oligonucleotide transfections 607B cells were seeded in 6-well plates and grown to nearly confluent monolayers. After 48 hours Oblimersen-treated 607B cells showed a significant loss of adhesion from cell culture plates, indicating a high level of cell death. Cell layers transfected with siRNA, however, did not show any significant differences from untreated cells and cell layers were still intact (figure 8).

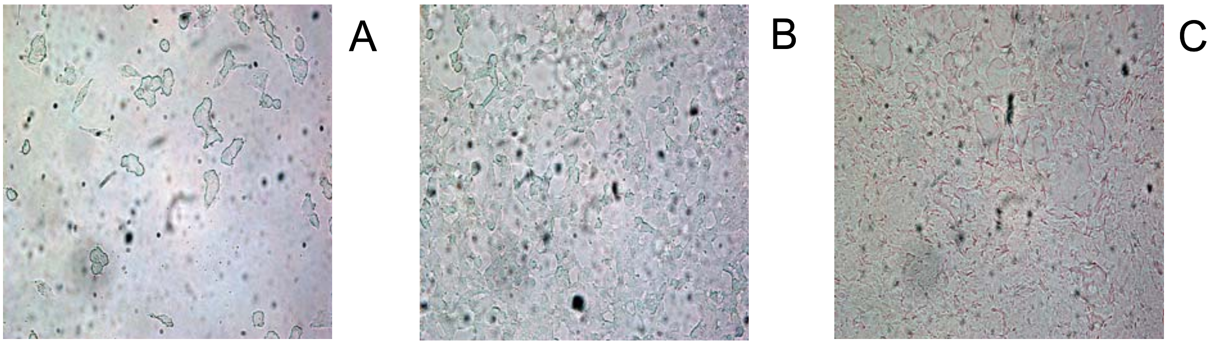

Figure 8. 607B cell layers after respective oligonucleotide transfections. 6×10^5 cells/well were seeded in 6-well plates and monitored in the light microscope after 48 hours. **A**: Obl-treated cells, **B**: siRNA-treated cells, **C**: untreated cells.

It has been previously described that Oblimersen and *bcl-2*-targeted siRNAs are not equivalent as apoptotic/cytostatic agents and that they induce disparate phenotypes in PC3 and LNCaP prostate cancer cells [Anderson *et al*., 2006]. Therefore, the levels of oligonucleotide-induced apoptosis were investigated on 607B melanoma cells. Based on an equal Bcl-2 protein down-regulation of 75%, apoptotic state and caspase-3 activity after phosphorothioate and siRNA treatment were monitored with respective assays (figure 9 and 10).

After Oblimersen treatment a significantly higher number of apoptotic cells (green, Annexin-V-Fluorescein-stained) could be detected compared to anti-*bcl-2*-siRNA-treated and untreated cells (figure 9). Therefore it can be stated that Oblimersen treatment clearly induced apoptosis in 607B melanoma cells, whereas no significant increase in Annexin-V-stained apoptotic cells could be detected in siRNA-treated and control cells. None of both treatments did induce necrosis, since no significant number of necrotic cells (red, Probidium iodide-stained) could be detected.

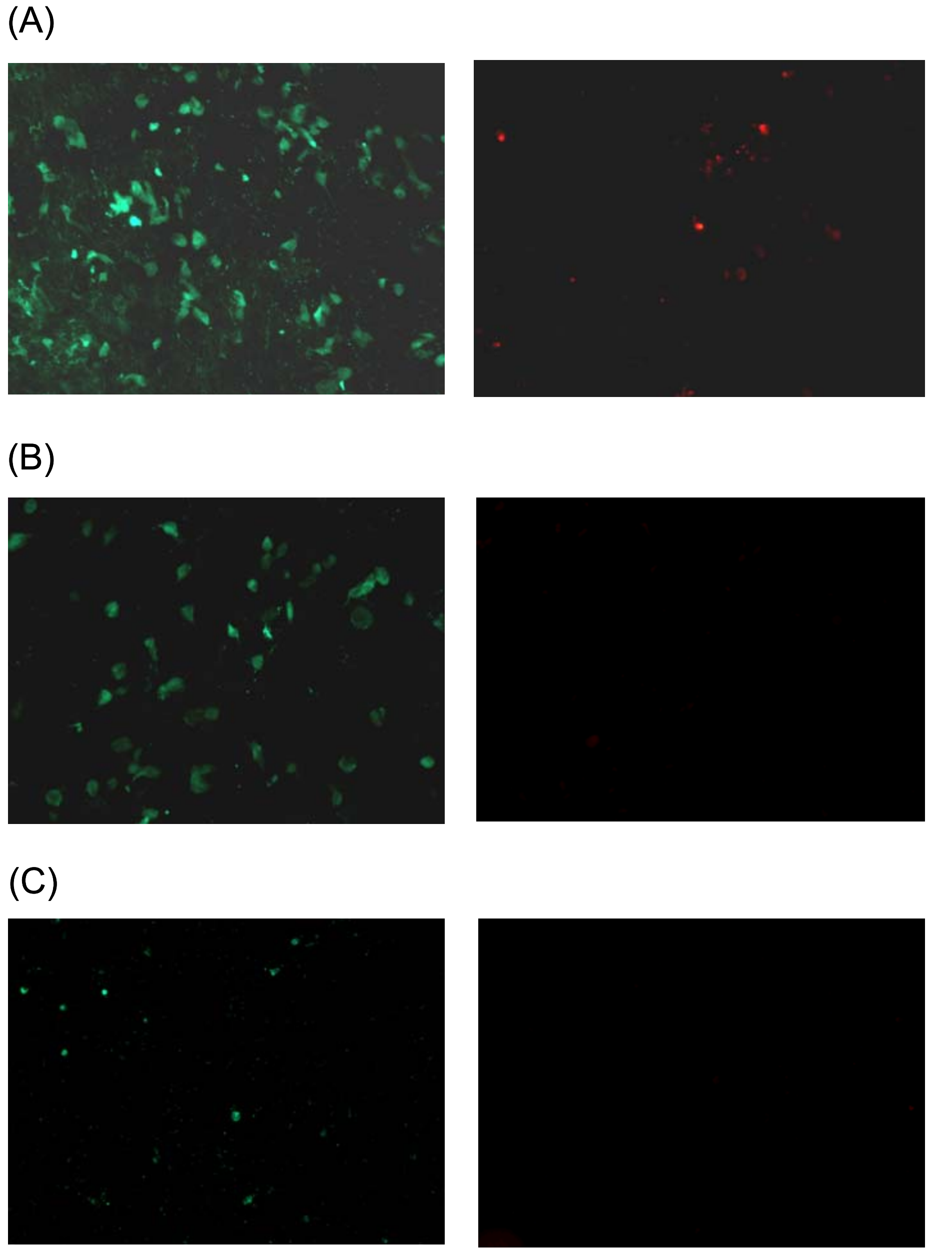

Figure 9. Fluorescence images of melanoma cells show apoptosis induction in Oblimersen-treated **(A)** but not in siRNA-treated **(B)** or control cells **(C)**. Apoptotic cells were detected with annexin-V-fluorescein (left panel) and necrotic cells are stained with Probidium iodide (right panel).

Additionally a higher level of caspase-3 activity was detected in 607B cells after Oblimersen treatment (+30%) compared to siRNA application and control (figure 10).

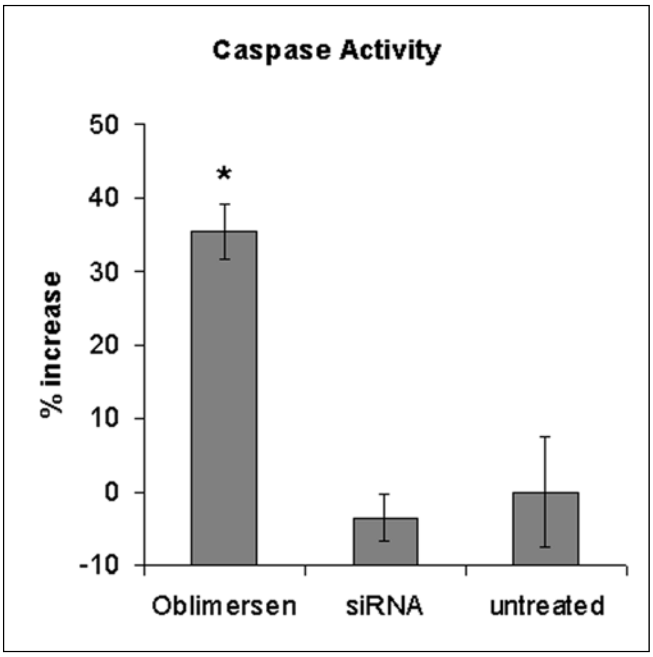

Figure 10. Evaluation of apoptosis induction reflected by increase of caspase-3 activity induced by respective treatments. The untreated control was set to 0%.
*: $p<0.05$ compared to untreated control.

Gene profiling studies of Oblimersen and Bcl-2-targeting siRNAs [Anderson *et al*., 2006] revealed an additional involvement of various genes in the mechanism of action of Oblimersen. Since the effects on the genome and the proteome are not necessarily the same and even siRNA-sequences have been reported to have varying off-target effects [Jackson *et al.,* 2003], the present study focused on the quantitative elucidation of off-target effects of Oblimersen and the anti-Bcl-2 siRNA on the proteome using DIGE technology.

4. Proteomic investigation

4.1 Two-dimensional separation and staining conditions

The measurement of quantitative changes in protein expression upon a special treatment deserves a careful selection of the appropriate method providing reliable and significant information. Two-dimensional spot patterns can be visualized in different ways, including staining after the separation with dyes such as silver nitrate [Shevchenko *et al.,* 1996], Coomassie Brilliant Blue [Fievet *et al.*, 2004], Sypro Ruby [Smejkal *et al*., 2004] or by pre-labeling of samples prior to separation with fluorescence [Ünlü *et al*., 1997; Minden, 2007]. For various biological questions and sample types, however, used two-dimensional gel electrophoresis (2-DE) [O'Farrell, 1975] conditions and analytical parameters have to be carefully optimized in terms of sensitivity, linear dynamic range, reproducibility, compatibility with mass spectrometry and easiness of handling.

For the separation of 607B cell lysates Immobiline^{TM} DryStrip gels ranging from p*I* 3-11 NL and an acrylamide concentration of 12.5% were chosen. Under these prerequisites an optimal resolution could be achieved and the highest number of protein spots (averagely 2500-3000) could be monitored on one gel.

Figures 11-14 demonstrate two-dimensional gels of untreated melanoma cell lysates stained with Coomassie Brilliant Blue R-250 (figure 11), silver nitrate (figure 12), SYPRO® Ruby (figure 13) and CyDyes™ (figure 14).

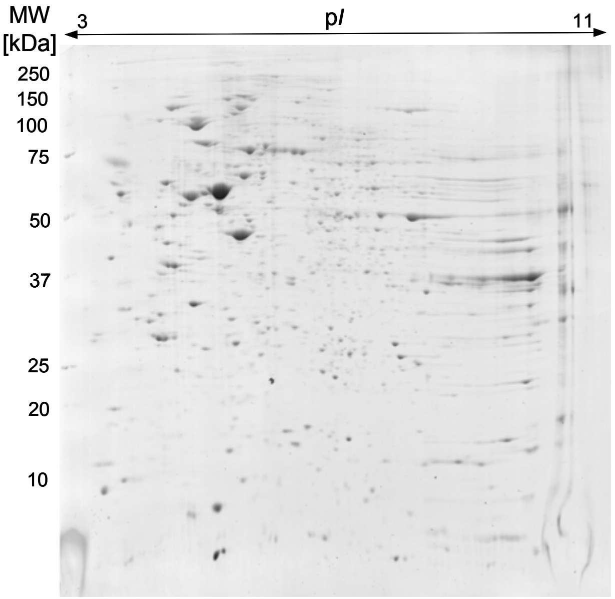
MW
[kDa]
3
p*I*
11
250
150
100
75
50
37
25
20
10

Figure 11. Two-dimensional gel image of 607B cell lysate, 75µg of total protein, p*I* 3-11 NL, stained with Coomassie Brilliant Blue R-250.

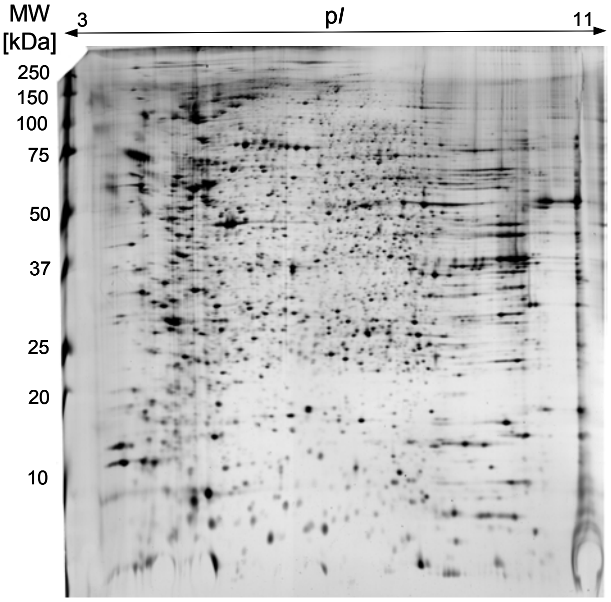
MW
[kDa]
3
p*I*
11
250
150
100
75
50
37
25
20
10

Figure 12. Two-dimensional gel image of 607B cell lysate, 75µg of total protein, p*I* 3-11 NL, stained with silver nitrate according to Blum [Blum *et al*., 1987].

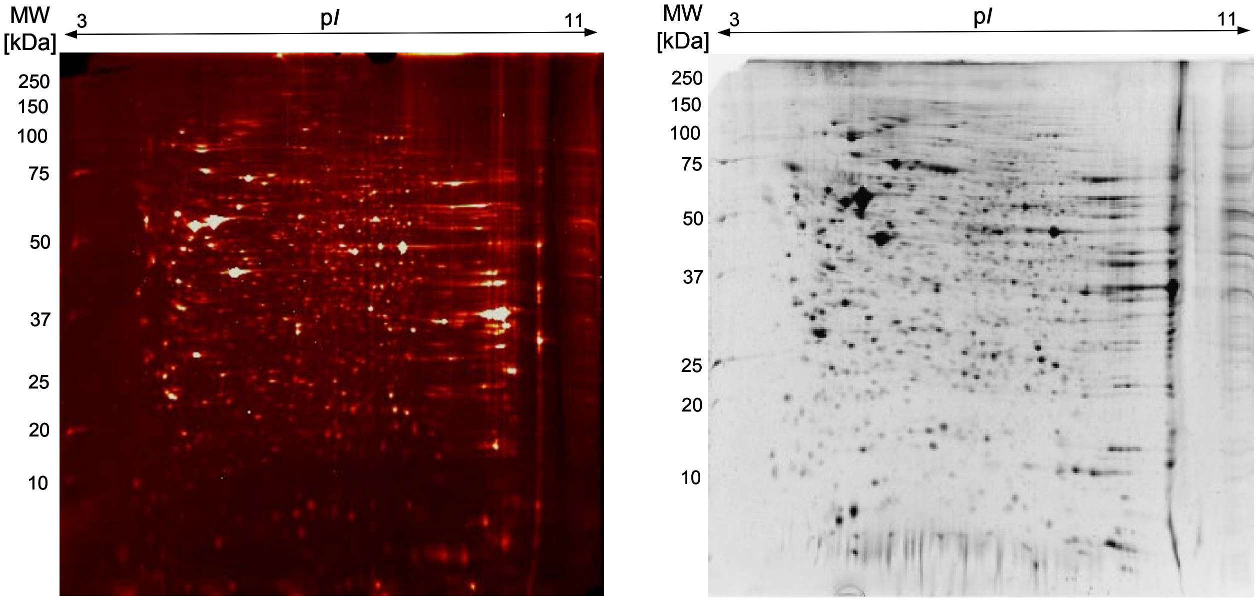
MW
[kDa]
3
p*I*
11
250
150
100
75
50
37
25
20
10
MW
[kDa]
3
p*I*
11
250
150
100
75
50
37
25
20
10

Figure 13. Two-dimensional gel image of 607B cell lysate, 75µg of total protein, p*I* 3-11 NL, stained with SYPRO® Ruby (left panel: original image; right panel: inverted data).

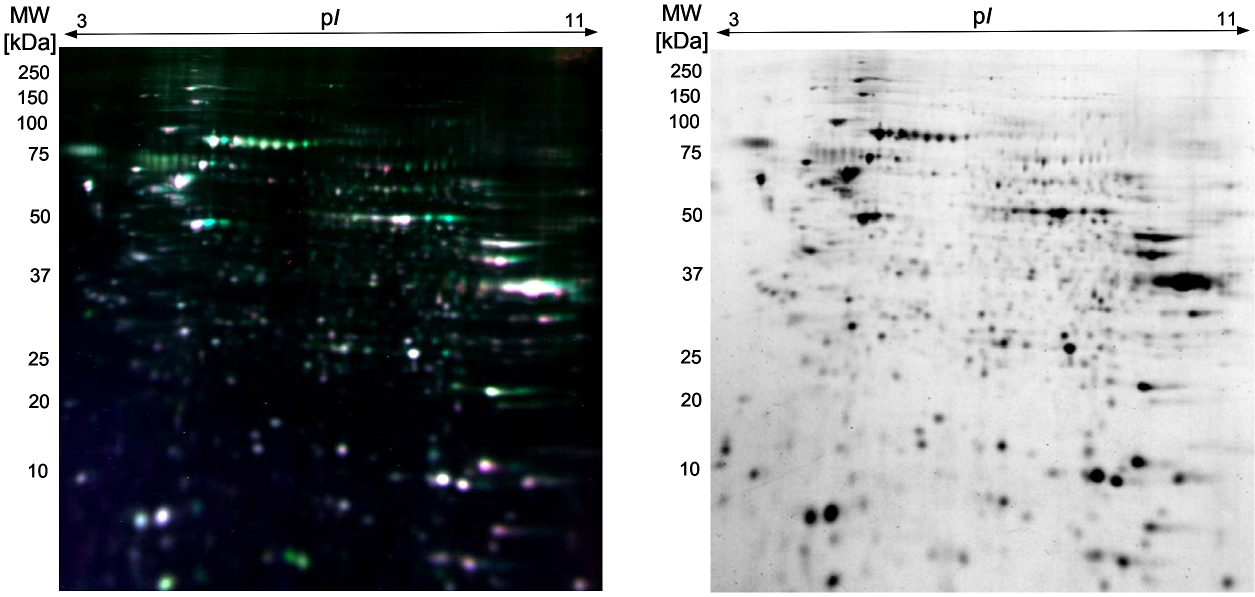
MW
[kDa]
3
p*I*
11
250
150
100
75
50
37
25
20
10
MW
[kDa]
3
p*I*
11
250
150
100
75
50
37
25
20
10

Figure 14. DIGE image of 607B cell lysate (overlay of all three channels), 75µg of total protein, p*I* 3-11 NL (left panel: original image; right panel: inverted data).

Coomassie Brilliant Blue (CBB) R-250 staining was easy to perform and excised protein spots could be directly used for subsequent *in-gel* digestion and mass spectrometry (MS) measurements. Approximately only two third of the overall number of protein spots, however, could be detected with CBB compared to the other staining protocols used. CBB-stained two-dimensional gels were therefore only used for preliminary MS experiments.

On silver stained gels an average number of 2700 spots could be detected, which was approximately one third more than on CBB stained gels. The four-step protocol consisting of fixation, sensitization, silver impregnation and development is relatively easy to perform, but - even if staining times and conditions were exactly kept – high inter-gel variations were observed. During software-based image analysis many saturated spots were detected, which had to be excluded from quantitative analysis. For subsequent *in-gel* digestion and MS experiments, excised protein spots had to be destained [50:50 aqueous solution of 100 mM sodium thiosulfate and 30 mM potassium hexacyanoferrate[III] according to Blum, 1987] in order to get pure MS spectra. Due to the low dynamic and linear range of silver staining [Westermeier *et al.,* 2005] this method is not reliable for quantification. Taking advantage of the high sensitivity, silver staining was only used for qualitative gels.

With the fluorescent dye SYPRO® Ruby a similar sensitivity compared to silver staining protocols was achieved - on average 2500-2700 spots could be detected for separated 607B cell lysates. Gel backgrounds were clear and the handling was rather easy. The wide linear and dynamic range (over four orders of magnitude) [Miller *et al.*, 2006] made it very suitable for subsequent image analysis. Since the staining with fluorescent dyes is an endpoint method [Miller *et al.,* 2006], no over-staining or saturation of protein spots was observed. SYPRO® Ruby stained proteins could be directly subjected to *in-gel* digestion and MS measurements. In brief, this staining method represented the best of all used post-staining protocols.

The method of choice for the quantitative comparison of treated and untreated 607B cell lysates was given by the Difference Gel Electrophoresis (DIGE) technology [Ünlü *et al.*, 1997; Sitek *et al.*, 2006]. Treated and untreated samples were labeled with different CyDyes™ prior to electrophoresis and an internal standard was included into the approach according to the scheme in figure 15. Since these dyes are structurally similar but spectrally quite distinct, the method allows multiplexing, that means the separation of two to three complex protein samples – each labeled with another dye – on the very same gel.

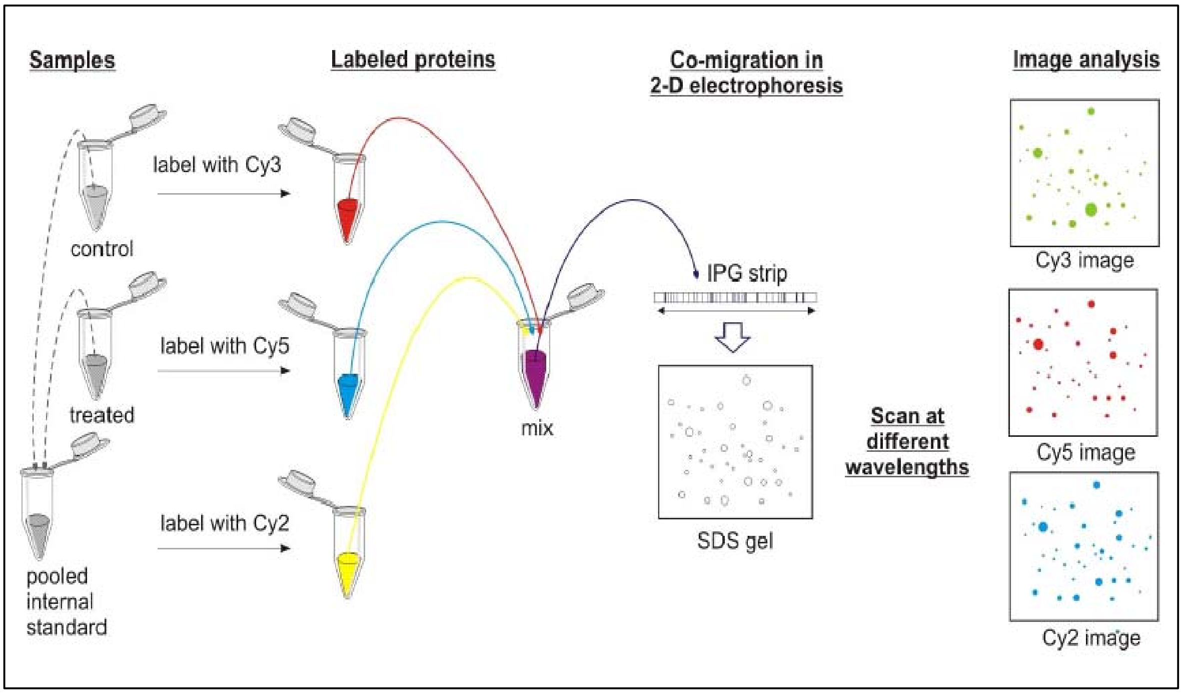
Samples
Labeled proteins
Co-migration in 2-D electrophoresis
Image analysis
label with Cy3
control
label with Cy5
treated
label with Cy2
pooled internal standard
mix
IPG strip
SDS gel
Scan at different wavelengths
Cy3 image
Cy5 image
Cy2 image

Figure 15. Schematic representation of a DIGE workflow [picture taken from Westermeier *et al*., 2005].

Gels were scanned at three different wavelengths corresponding to the dyes used – so on one gel three samples could be run and fewer gels had to be done compared to post-staining techniques. Inter-gel variations resulting from experimental handling could be excluded leading to highly reliable quantitative data. With the help of the protein pattern created by the internal standard, other sample patterns could be more easily matched and each sample spot volume could be normalized to the standard spot volume. Consequently, protein expression changes of ±1.5 fold were considered to be relevant. Although the received sensitivity was lower compared to silver staining – on average ~2000 spots could be detected -, most of the spots were better resolved and fewer "shine-spots", *id est* speckles and impurities, were detected. Therefore fewer spots had to be excluded from statistical analysis. For the used "minimal labeling" the dye/protein ratio is kept at average 3/100 - so it is ensured that only one single lysine residue in each protein is labeled. Since the dyes are charge-matched, the p*I* of investigated proteins is supposed to stay constant upon labeling. The molecular mass of the labeled protein slightly differs from the unlabeled protein (about 0.5kDa, equal for each dye [Alban *et al.*, 2003]) and so does the p*I*. Therefore all gels had to be post-stained with silver for subsequent *in-gel* digestion and MS measurements.

4.2 Establishment of a protein reference map of 607B cells

For all proteomic investigations cells from the same batch were used (ranging from passage 90 to passage 180). As a first step the used cell line 607B was characterized on the protein level by the establishment of a protein reference map. Most abundant spots as well as spots from varying p*I* and molecular weight sections of the gel were identified. Figure 16 gives an overview of identified reference proteins.

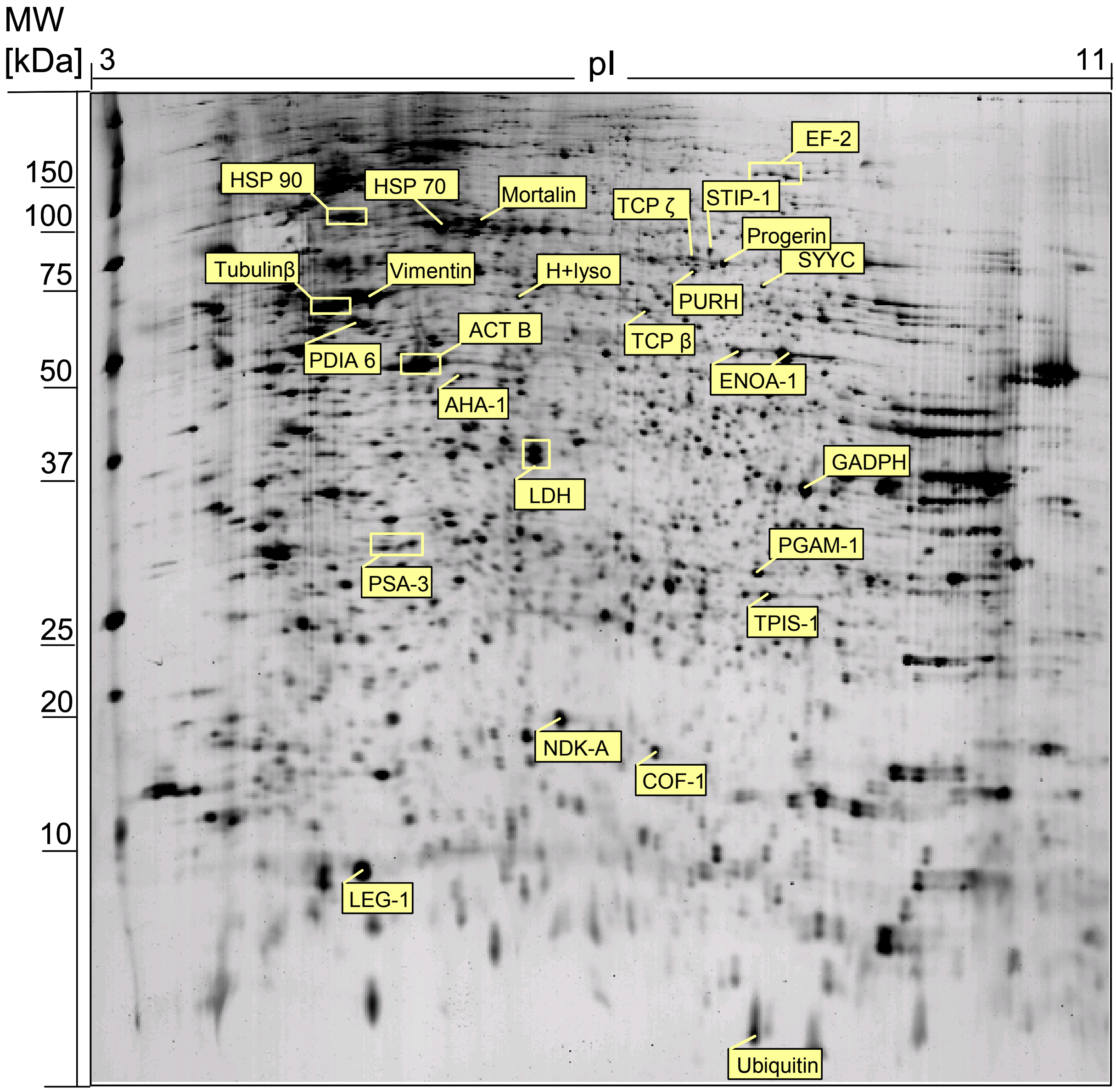
MW
[kDa]
3
pI
11
150
100
75
50
37
25
20
10
EF-2
HSP 90
HSP 70
Mortalin
TCP ζ
STIP-1
Progerin
SYYC
Tubulinβ
Vimentin
H+lyso
PURH
ACT B
TCP β
PDIA 6
ENOA-1
AHA-1
GADPH
LDH
PGAM-1
PSA-3
TPIS-1
NDK-A
COF-1
LEG-1
Ubiquitin

Figure 16. Established protein reference map of 607B cells. Positions of identified reference proteins are indicated with yellow boxes.

Mass spectrometric data of reference proteins

All proteins were subjected to tryptic *in-gel* digestion and unambiguously identified by subsequent matrix-assisted laser desorption/ionization reflectron time-of-flight mass spectrometry (MALDI-rTOF-MS) (peptide mass fingerprinting (PMF) in combination with post source decay (PSD) experiments for selected tryptic peptides) as described under Materials and Methods. Representative PMF spectra with m/z value lists and MS/MS graphs are presented in supplement A (figure A-S). Detailed information about identified reference proteins are summarized in table 8, including PMF and PSD scores, sequence coverage, the number of matched peptides, p*I*, molecular weight and peptide sequences of precursor ions used for PSD. Data for the proteins actin (ACTB), cofilin-1 (COF-1), enolase-1 (ENOA-1), galectin-1 (LEG-1), phosphoglycerate mutase (PGAM) and triosephosphatisomerase (TPIS) are presented in supplement B, since they have been found to be differentially expressed after Oblimersen treatment.

For *in-gel* digestion trypsin from bovine pancreas [Roche] was used. The following monoisotopic m/z values resulting from tryptic auto-digestion were experimentally obtained: 659.55, 805.60, 906.67, 1153.77, 2163.22, 2273.93 and 2611.96. These m/z values were used to check calibration for accuracy.

Table 8. Identified landmark protein species present in 607B melanoma cells.

Protein name	Acc. number	pI theor.	MW [kDa]	PMF Score*	Sequ. Cov [%]	Matching peptides**	PSD	Peptide sequences	Score***
AHA-1	O95433	5.4	38.27	126	30	12 (18)	1484.6; 1714.7	ETFLTSPEELYR; ADATNVNNWHWTER	187 (38)
TCP zeta	P40227	6.25	58.31	124	33	17 (29)	758.0; 938.5; 1499.5	EGIVALR; GLVLDHGAR; QADLYISEGLHPR	175 (39)
EF-2	P13639	6.42	96.12	104	16	16 (22)	970.0	GGGQIIPTAR	22 (39)
GADPH	P04406	8.58	36.05	68	21	8 (15)	1764.3	LISWYDNEFGYSNR	87 (38)
H+ATPase lyso	P15313	5.57	56.82	100	22	15 (23)	1309.8	NFIAQGPYENR	90 (39)
HSP-70	P11142	5.28	70.90	194	36	23 (32)	1200.3	DAGTIAGLNVLR	57 (36)
HSP-90	P07900	4.94	84.88	102	19	17 (25)	730.8; 1195.6	LSELLR; IDIIPNPQER	69 (40)
LDH	P00338	5.71	36.90	52	14	5 (9)	743.0; 914.5	LNLVQR; IVVVTAGVR	50 (39)
Mortalin	P38646	5.87	73.68	106	24	16 (26)	1362.5	AQFEGIVTDLIR	73 (36)
NDK A	P15531	5.42	19.87	70	38	7 (10)	1052.5; 1345.4	GDFCIQVGR; TFIAIKPDGVQR	85 (39)
PDIA6	Q15084	4.95	48.12	145	35	13 (18)	1528.7	LAAVDATVNQVLASR	42 (38)
Progerin	Q6UYC3	6.22	69.49	96	21	15 (25)	-	-	-
PSA-3	P25788	5.19	28.51	101	33	9 (15)	1579.3	SLADIAREEASNFR	24 (38)
PURH	P31939	6.39	64.94	128	25	14 (19)	-	-	-
STIP-1	P31948	7.81	68.67	55	13	12 (26)	1465.8;	LDPHNHVLYSNR	62 (38)
SYYC	P54577	6.61	59.49	132	25	16 (21)	1059.7; 1206.7	EYTLDVYR; VDAQFGGIDQR	68 (40)
Tubulin β	P07437	4.71	49.67	222	66		1039.4; 1131.61; 2799.8	YLTVAAVFR; FPGQLNADLR; SGPFGQIFRPDNFVFGQSGAGNNWAK	135 (38)
Ubiquitin	P62988	5.73	8.12	189	97	11 (16)	1039.4	EGIPPDQQR	22 (39)
Vimentin	P08670	5.06	53.65	242	46	26 (32)	1295.6; 1571.7	MALDIEIATYR; ISLPLPNFSSLNLR	118 (38)

* Protein scores greater than 64 are significant ($p<0.05$). ** Number of unmatched peaks is given in brackets. *** Ion scores greater than the number given in brackets are significant ($p<0.05$). *AHA, activator of 90 kDa ATPase homolog, EF, elongation factor, GADPH, glyceraldehyde-3-phosphate dehydrogenase, LDH, L-lactate dehydrogenase, NDK, nucleoside diphosphate kinase, PSA, proteasome subunit alpha, PURH, bifunctional purine biosynthesis protein, STIP, stress-induced-phosphoprotein, SYYC, tyrosyl-tRNA synthetase.*

4.3 Influence of image-analysis software on quantitation of 2-DE data

During this thesis the available image analysis software PD-Quest™ version 6.1 [Bio-Rad Laboratories] of the laboratory was equipped with the update version 8.0 and the question arose whether a different software or software version, respectively, would lead to different quantitative results for the same 2D-gel set. Two replicate gel groups (Oblimersen-treated versus untreated) were prepared, cropped (p*I* ~4-8) to simplify the process and independently analysed with PD-Quest™ version 6.1, PD-Quest™ version 8.0 and Delta 2D [Decodon] version 6.5 [Stessl *et al.*, 2009].

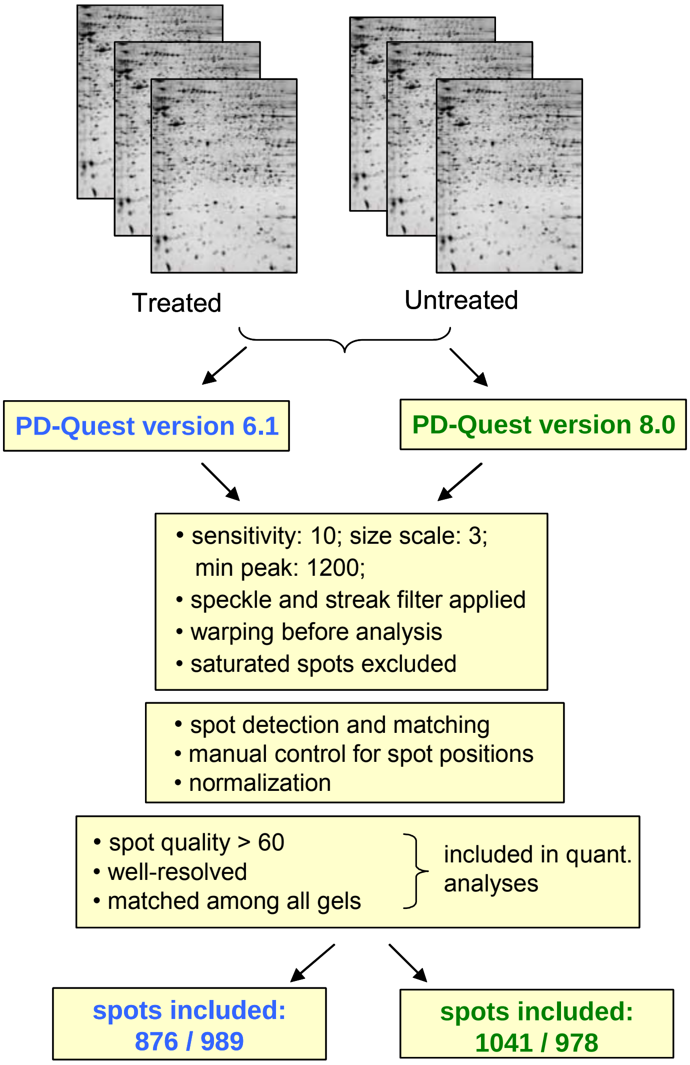
Treated
Untreated
PD-Quest version 6.1
PD-Quest version 8.0
• sensitivity: 10; size scale: 3; min peak: 1200;
• speckle and streak filter applied
• warping before analysis
• saturated spots excluded
• spot detection and matching
• manual control for spot positions
• normalization
• spot quality > 60
• well-resolved
• matched among all gels
included in quant. analyses
spots included: 876 / 989
spots included: 1041 / 978

Figure 17. Scheme outlining the PD-Quest based 2-DE image analysis process. For a detailed description of image analysis with PD-Quest see Marengo *et al.*, 2005.

Figure 17 represents a simplified scheme of the image-analysis process with the two mentioned versions of PD-Quest. The analysis with Delta 2D was performed externally by Markus Kolbe [Decodon].

Using a defined parameter set and the same two-dimensional gel set, 876 (control group) and 989 (treated group) protein spots, respectively, remained in the data set with version 6.1. 1041 (control group) and 978 (treated group) protein spots, respectively, passed the criteria for being included in quantitative analyses with version 8.0 (table 9 A). The number of detected spots was reproducible with both versions.

Matching capabilities of image-analysis software are strongly influenced by gel and spot quality. Therefore used gels were critically reviewed for their reproducibility. Table 9 B shows spot qualities and CV values calculated among biological replicates of ten randomly selected spots from different p*I* and MW areas. According to Schlags [Schlags *et al.,* 2005] the quantitative repeatability for silver-stained replicates is given if RSD values (relative standard deviation or coefficient of variance [CV]) are below 30% and the spot quality of included spots (optical density, defined as [INT*mm^2]) is beyond a value of 60.

A

Replicate group	version 6.1			version 8.0		
	Mean	SD	CV(%)	Mean	SD	CV(%)
Control	876	137	15.6	1041	204	19.6
Treated	989	89	9.0	978	47	4.8

B

Spot number	CV [%] treated	CV [%] untreated	Spot quality
1	24.93	23.52	82
2	13.19	19.13	86
3	16.63	1.61	93
4	16.86	13.31	89
5	20.27	11.88	70
6	1.10	12.12	97
7	15.02	26.46	80
8	4.84	9.05	74
9	11.62	7.12	90
10	8.76	0.79	93

Table 9 A. The total number of detected spots is reproducible with both software versions. **B.** Spot qualities (mean of triplicates) and CV values calculated among biological replicates of ten randomly chosen spots are presented. If CV values are below 30%, spots are considered as reproducible.

In version 6.1 the matching process is based on the selection of reference spots, therefore ten well-resolved spots (table 9 B) were chosen as landmarks. Version 8.0 provides automatic matching. Nevertheless, in both cases all matched spots were subjected to a careful manual control with regard to spot positions. Only semiautomatic tools (“delete, add, manual match and unmatch”) were used to minimize the operator’s influence on the study. Thereby the newly introduced group consensus tool of version 8.0 was very helpful to find spot matching errors among replicates.

Differentially expressed proteins were determined by their differences in the corresponding gel-spot volumes between control and treated sample. Generally this difference is determined by a volume ratio, whereupon a factor of 2 corresponds to 100% variation. The chosen threshold level is based on the quality of the gel, reflected by the total variance among replicates and the staining method used for spot visualization. The treshold represents a sensitive variable ruling over in- or exclusion of spots in a quantitative analysis set. In this study, spots showing a fold-change of at least 2 meeting the criteria of a statistical Student's *t*-test (significance level of 90%) were considered as differentially expressed. Volume ratios of ten spots (figure 18) were calculated using the mean values of exported normalized spot volumes provided by the respective software (table 10).

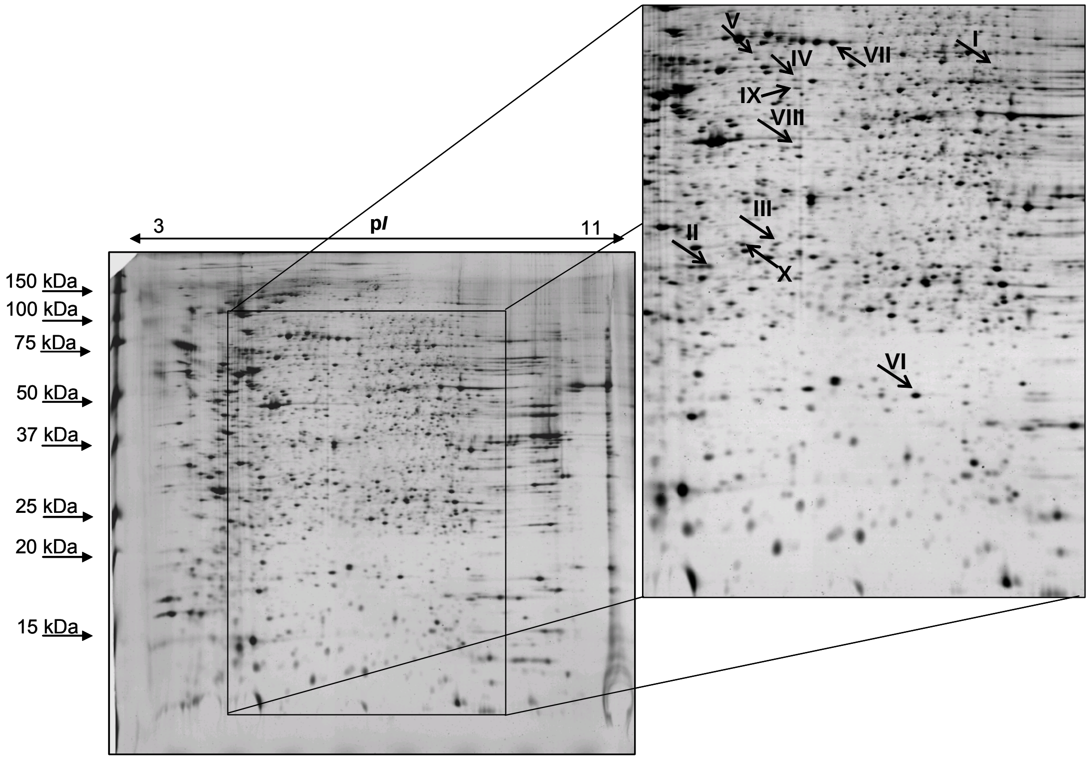

Figure 18. 75µg of total protein were separated on a 3-11 NL IPG strip, 12.5% SDS-PAGE, silver-stained. The zoomed area shows the gel part that was taken for image analysis. Arrows and numbers indicate the ten spots, which were investigated for their volume ratios.

Spot number	PDQ version 6.1	PDQ version 8.0	Delta 2D version 3.6
I	1.46	1.91	1.30
II	2.18	1.64	1.14
III	2.56	1.81	1.02
IV	1.68	1.92	1.36
V	1.42	1.98	1.49
VI	1.82	2.00	1.48
VII	2.97	2.45	2.29
VIII	2.40	2.21	1.32
IX	2.31	2.10	1.27
X	1.87	1.96	1.29

Table 10. Calculated factors reflecting the volume ratios of treated versus untreated or vice versa, respectively, based on normalized spot volumes exported from the different software packages.

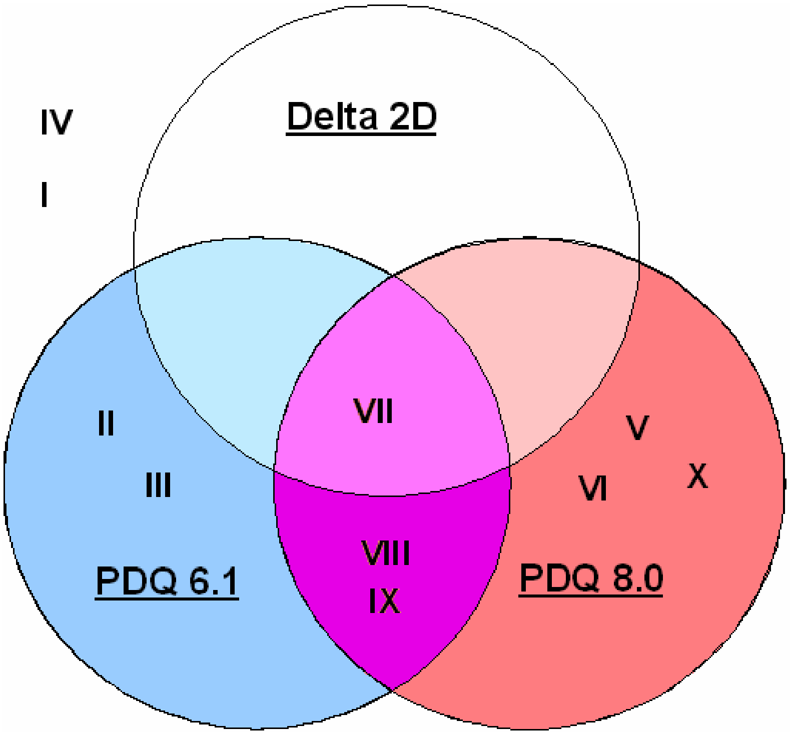

Figure 19. Venn diagram illustrating the detection of differentially expressed (± 2 fold-changes) spots from table 10 by respective software packages. Factors 1.98 and 1.96 (spots V and X) were included.

A Venn diagram (figure 19) visualizes differences and overlaps for the chosen gel spots. Under the chosen quantitative conditions (fold-change of at least ±2 AND meeting a Student's *t*-test $p<0.10$) only one spot (VII) was detected as differentially expressed with all three software packages (figure 19) and is therefore placed in overlapping circles. Spot VII is also the only spot showing a fold change of >2 after analysis with Delta 2D. Two additional spots (VIII and IX) met the criteria with both PD-Quest versions, but not with Delta 2D. All other spots were only detected as differentially expressed by one of the three software packages. Spot II and III were found to be significantly changed with PDQ version 6.1, but were not part of a quantitative analysis set after evaluation with PDQ 8.0 and Delta 2D. Spot VI (and V), however, is (were) found as changed with PDQ 8.0, but no significant difference could be detected with PDQ 6.1 or Delta 2D. No general tendency of in- or decreasing volume ratios was observed during the comparison of volume ratios with the three tools, each spot had to be controlled individually. Since the same digital images were included in all three evaluations and important analysis parameters were kept constant (figure 17), obtained results point out that - beside the variance introduced by experimental procedures - software-related variations are another important reason why 2-DE data are not directly comparable to each other [Stessl *et al.*, 2009].

4.4 DIGE-based off-target effect study

The DIGE-based proteomic approach for the comparison of off-target effects of the phosphorothioate Oblimersen and a *bcl-2*-targeted siRNA-sequence on the protein level was applied based on cell lysates with an equal bcl-2 down-regulation of 75% (chapter 1). Lysates of all treatments (Oblimersen-, siRNA- and control cells) and an internal standard, a mixture of all samples, were labeled with Cy3 and Cy2, respectively (experimental setup see Materials and Methods). Protein mixtures labeled with these fluorescence dyes can be separated on the same 2-DE gel, resulting in a reliable quantitative method to monitor subtle changes in protein abundances with high statistical confidence since most technical variation is eliminated [Friedman, 2007]. Each cell treatment was performed in triplicates.

Although the transfection reagent lipofectamine 2000 is described as cytotoxic in higher concentrations, 607B cells did not show increased apoptosis or Bcl-2 down-regulation after treatment with the transfection reagent alone (chapter 3). In addition, no significant change in the proteomic pattern compared to untreated cells could be detected upon treatment with unloaded lipofectamine 2000. Consequently, liopfectamine only treated cells were used as control group for 2D-DIGE experiments comparing antisense and siRNA oligonucleotides.

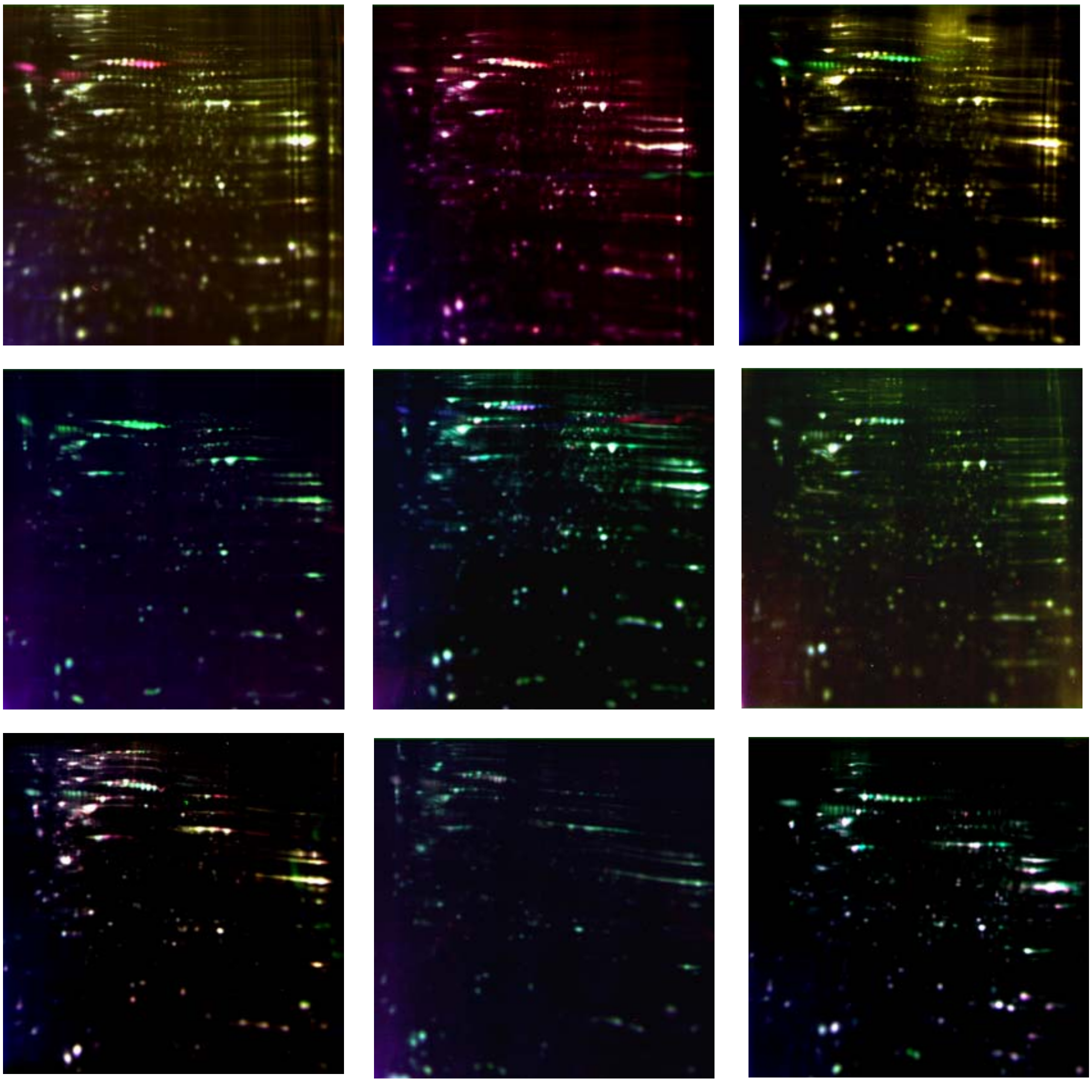

Figure 20. Original DIGE gel images of differentially treated 607B melanoma cell lysates.

Image analysis was performed with the software DeCyder [GE Healthcare, version 6.5]. Obtained protein statistics are summarized in table 11 and 12. According to gel and spot quality criteria for differentially expressed proteins were chosen as follows: average ratio ±1.5, Student's *t*-test ($p \leq 0.05$), 1-way ANOVA ($p \geq 0$ and ≤ 0.05), appearance in at least 16 out of 18 spot maps and match quality <6. Relevant 78 (Oblimersen) and 8 (siRNA) spots, respectively, were subjected to a careful manual control,

Average ratio	no T-Test AND no ANOVA	no T-Test BUT ANOVA (p = 0 AND = 0.05)	ANOVA AND T-Test (p<0.5)	(p<0.2)	(p<0.1)	(p<0.05)
± 1.1	1351	237	199	191	175	130
± 1.2	1168	229	194	188	174	129
± 1.3	995	214	184	180	167	126
± 1.4	836	193	165	161	151	115
± 1.5	674	156	131	128	119	**78**
± 1.6	571	128	105	102	95	78
± 1.7	471	98	76	73	68	53
± 1.8	405	79	61	59	55	42
± 1.9	348	61	47	45	42	31
± 2.0	301	50	36	35	32	24
± 2.5	181	24	15	15	15	9
± 3.0	144	17	10	10	10	7
± 3.5	109	11	4	4	4	3
± 4.0	84	7	2	2	2	2
± 4.5	67	4	1	1	1	1

Table 11. Protein statistics of Oblimersen-treatment; number of spots passing different protein filters are listed. 78 spots met the criteria for being considered as differentially expressed (1.5-fold change and p<0.05) before manual control.

Average ratio	no T-Test AND no ANOVA	no T-Test BUT ANOVA (p = 0 AND = 0.05)	ANOVA AND T-Test (p<0.5)	(p<0.2)	(p<0.1)	(p<0.05)
± 1.1	934	156	118	76	48	33
± 1.2	653	85	64	51	34	24
± 1.3	493	56	40	34	26	17
± 1.4	373	38	24	21	18	14
± 1.5	282	25	14	12	10	**8**
± 1.6	210	18	9	8	7	5
± 1.7	178	13	8	8	7	5
± 1.8	150	11	6	6	5	3
± 1.9	125	10	6	6	5	3
± 2.0	104	9	5	5	5	5
± 2.5	44	4	3	3	3	2
± 3.0	18	1	1	1	1	1

Table 12. Protein statistics of siRNA-treatment; number of spots passing different protein filters are listed. 8 spots met the criteria for being considered as differentially expressed (1.5-fold change and p<0.05) before manual control.

In a second evaluation step all remaining spots were checked for quality (exclusion of speckles and unclear, small spots with high background noise) and possible medium origin (e.g. BSA). Despite many washing steps during cell lysis some persistent cell culture components could be detected on 2-DE gels. This contamination is often observed when cell lysates are separated by 2-DE [Miller *et al.,* 2006]. It can be reduced to a minimum but in most cases it can not be completely avoided. Figure 21 represents high abundant components of 607B cell culture medium separated on a 2-DE gel in a concentration about ten times higher than present in used cell lysates.

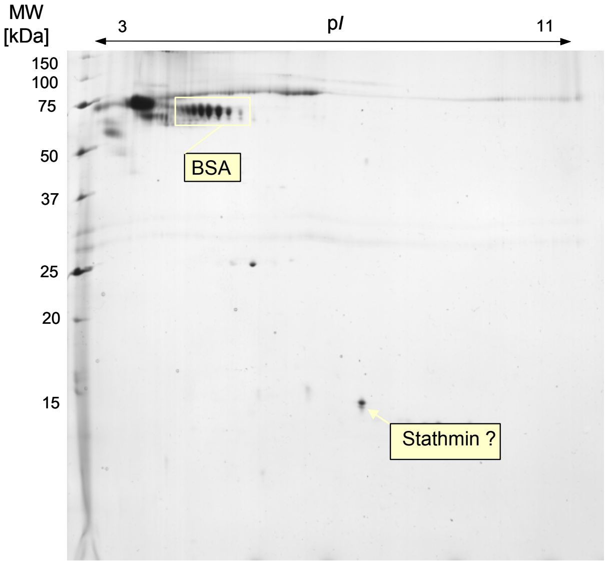

Figure 21. 2-DE gel of 607B cell culture medium. 10µg of total protein, silver stained. Identified spots are indicated with boxes. Stathmin has been identified by direct *in-gel* digestion from DIGE gels, therefore its position on the silver-stained gel in is provided with a question mark.

High abundant spots have been identified as serum albumin spots of bovine origin (P02769; 71.19kDa, p*I* 5.88) by MS (representative spectrum see figure 22). The following peaks belonging to BSA have been found: 689.46, 712.51, 733.51, 789.59, 927.62, 1138.63, 1163.77, 1283.83, 1419.80, 1439.95, 1480.45, 1537.93, 1568.64, 1881.10, 1908.06, 2045.24, 2301.53 and 2587.65. Comparing these 17 of 23 peptides to protein databases (see Materials and Methods) resulted in a PMF score of 121 and a sequence coverage of 27%. With PSD spectra of peptides at m/z 1480.45 and 1568.64 a PSD score of 130 was achieved. Other spots (~25kDa and ~9kDa) have been repeatedly subjected to MALDI measurements after excision from silver-stained gels, but no results were obtained.

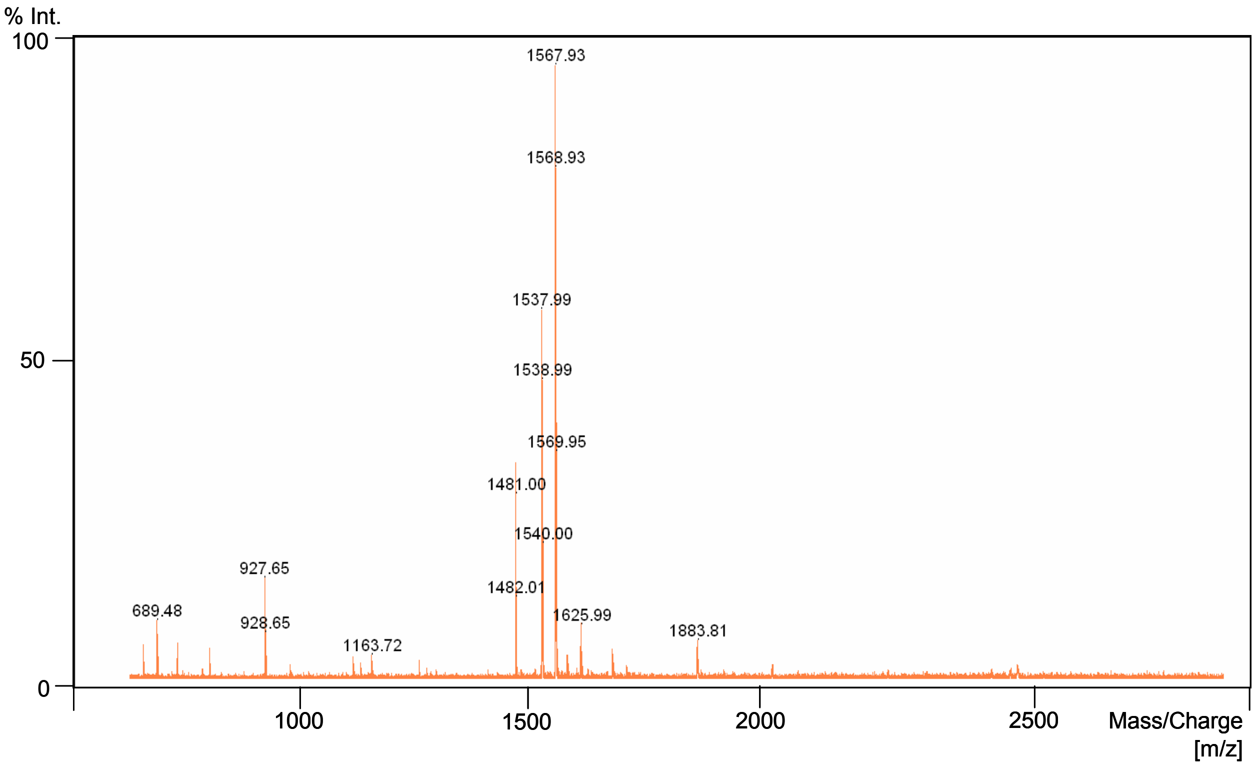

Figure 22. Representative peptide mass fingerprint of BSA.

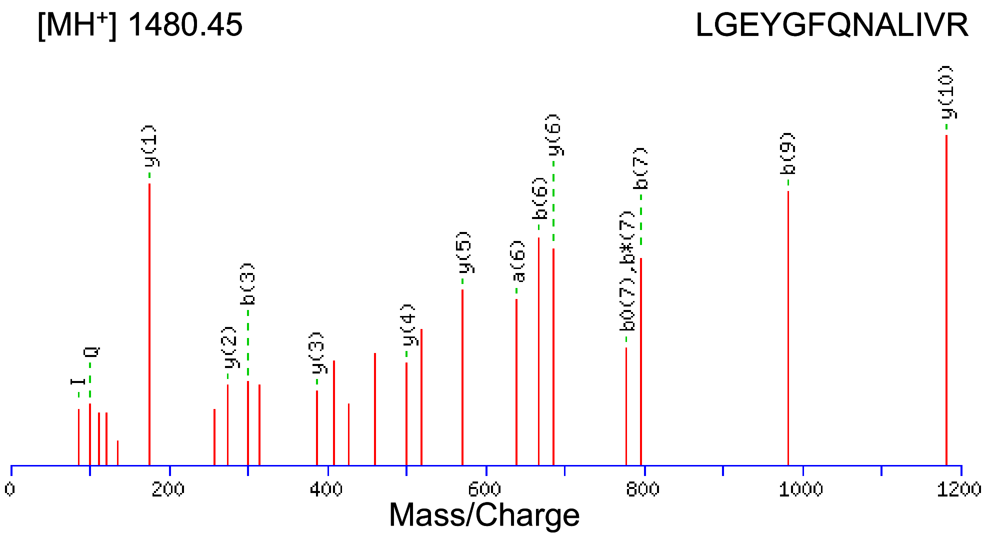

Figure 22 A. Mascot result graph of the MALDI-TOF-PSD mass spectrum of the precursor ion m/z = 1480.45 with different ion species indicated.

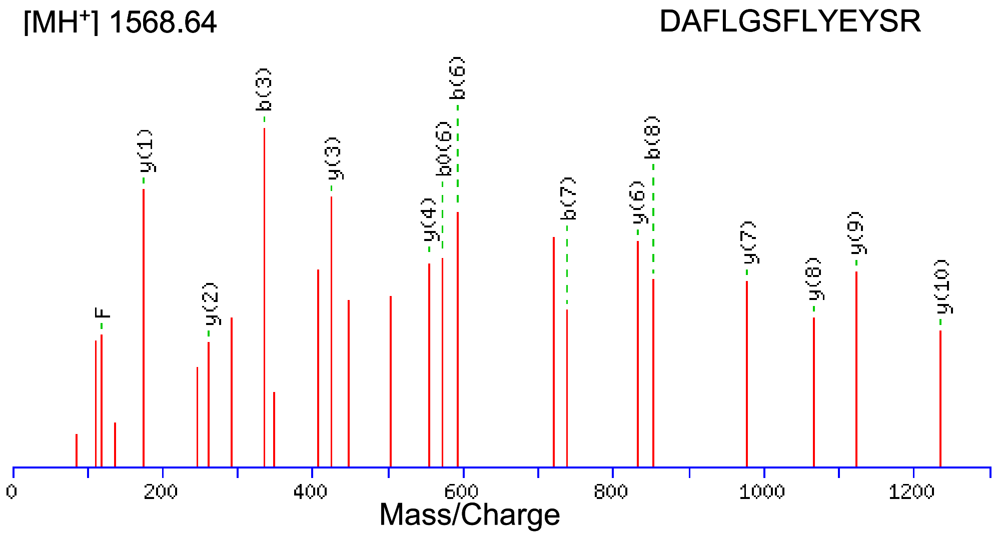

Figure 22 B. Mascot result graph of the MALDI-TOF-PSD mass spectrum of the precursor ion m/z = 1568.64 with different ion species indicated.

Furthermore bovine stathmin (Q3T0C7; 17.3kDa, p*I* 5.8) was identified by MALDI-rTOF-MS (figure 23). The following stathmin peptides were detected: 782.20, 973.31, 1139.28, 1326.39, 1388.46 and 1604.35, resulting in a score of 61 and 34% sequence coverage. PSD experiments of the precursor ion 1388.46 achieved a protein identification score of 75. Respective spectra are shown in figure 24. Depending on the staining method used, proteins can show a varying protein pattern on a 2-DE gel and protein identification by MS may be difficult in some cases, especially for silver-stained gels. Stathmin has been identified by direct *in-gel* digestion from DIGE gels. Unfortunately no respective spots on silver-stained gels were obtained. So its position on the silver-stained medium gel in figure 21 is provided with a question mark. But, considering the theoretical molecular weight and p*I*, stathmin can be attributed to the ~15kDa spot.

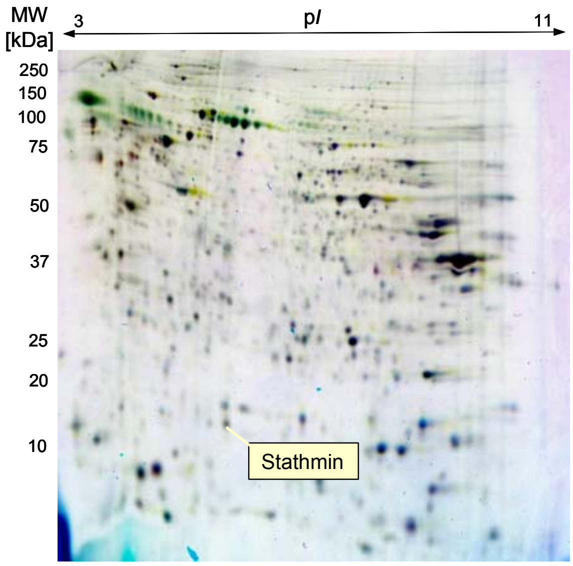
MW
[kDa]
3
p*I*
11
250
150
100
75
50
37
25
20
10
Stathmin

Figure 23. Inverted DIGE gel of 607B cell lysate indicating the position of bovine stathmin, which has been identified by MALDI/MS.

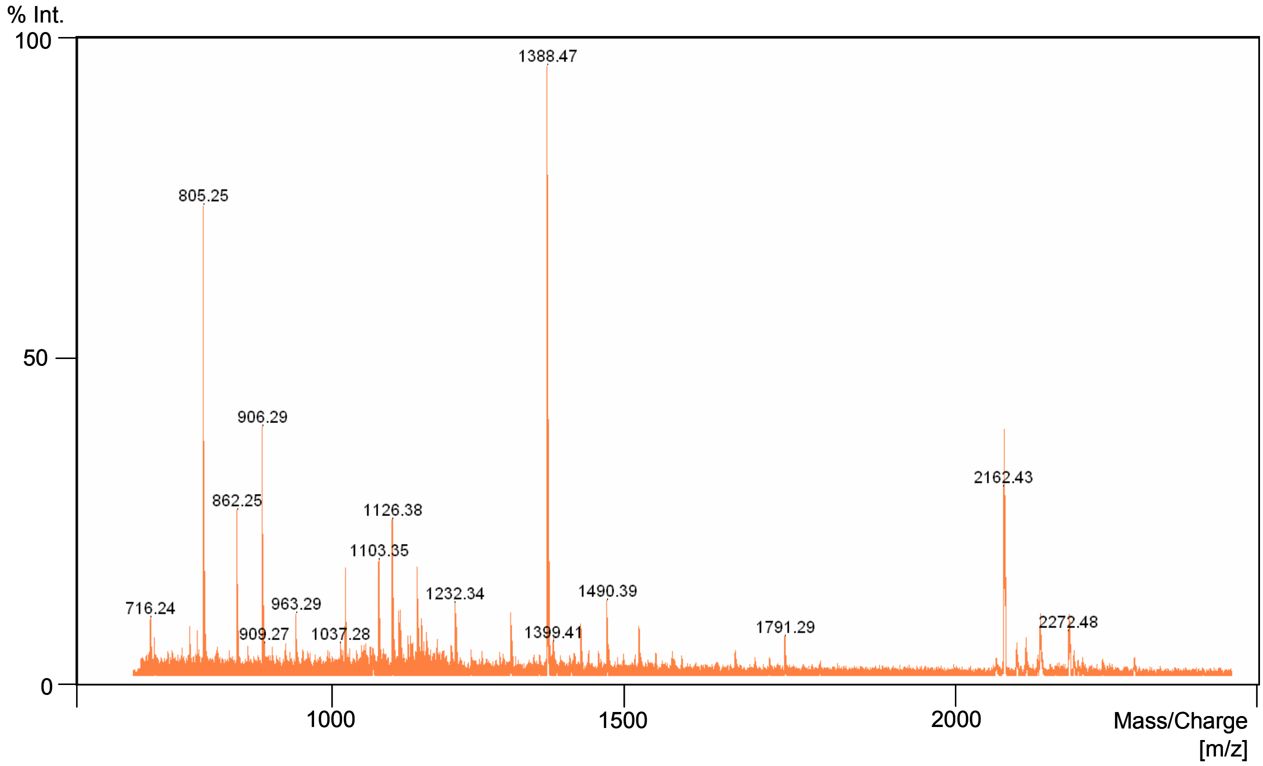

Figure 24. Representative peptide mass fingerprint of bovine stathmin.

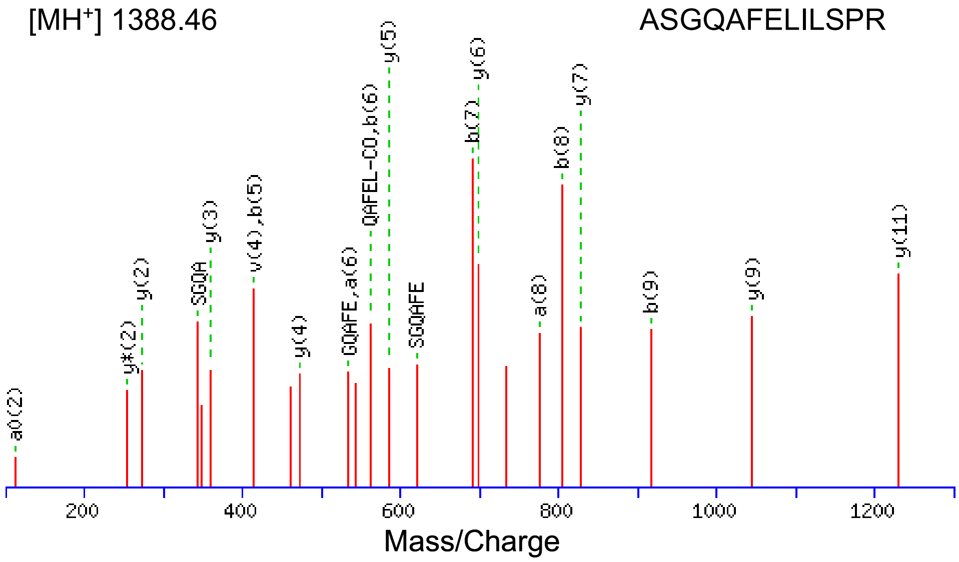

Figure 24 A. Mascot result graph of the MALDI-TOF-PSD mass spectrum of the precursor ion m/z = 1388.46 with different ion species indicated.

As a results of this evaluation (taking a closer look on inherent spots originating from the cell medium) only two significantly changed protein spots (master gel number 1202 and 252) remained in the siRNA group, whereas 46 spots (master gel number 17, 150, 154, 252, 255, 259, 276, 318, 342, 359, 364, 480, 486, 493, 517, 546, 584, 588, 627, 632, 701, 731, 743, 790, 795, 806, 856, 862, 925, 972, 1029, 1032, 1054, 1067, 1121, 1134, 1202, 1306, 1355, 1457, 1466, 1593, 1668, 1701, 1811, 1833) remained in the Oblimersen group.

The three-dimensional resolution of spots was chosen as a further quality criterium. Figure 25 shows three-dimensional views of selected spots, which were exported from DeCyder.

Spot 17

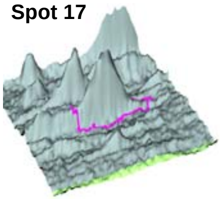

Spot 150+154

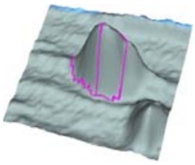

Spot 252

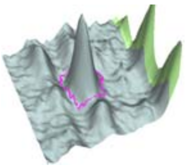

Spot 255

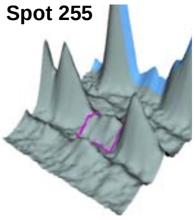

Spot 259

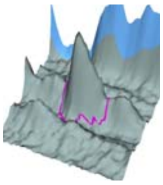

Spot 276

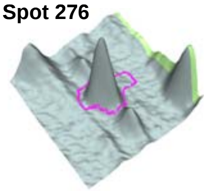

Spot 318

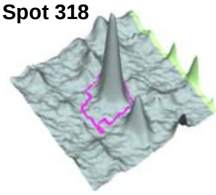

Spot 342+364

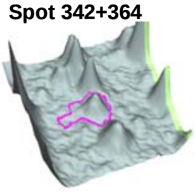

Spot 359

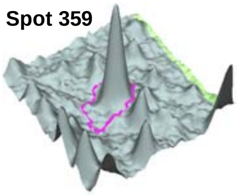

Spot 480

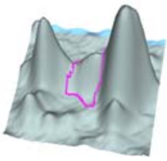

Spot 486

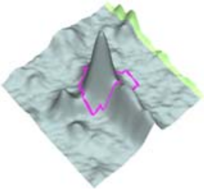

Spot 493+517

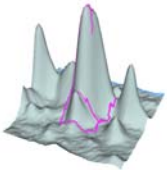

Spot 546

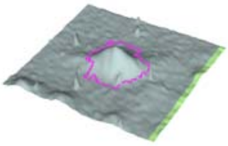

Spot 584

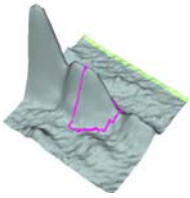

Spot 588

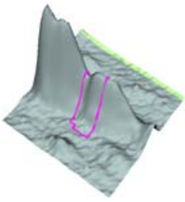

Spot 627

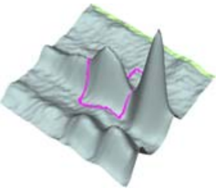

Spot 632

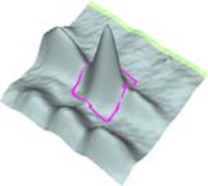

Spot 701

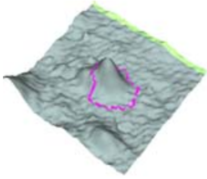

Spot 731

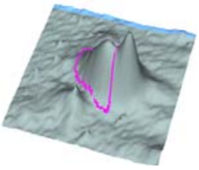

Spot 743

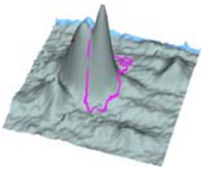

Spot 790

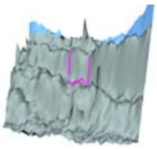

Spot 795

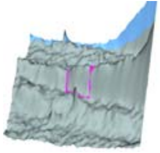

Spot 806

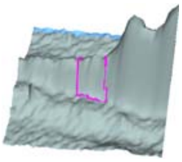

Spot 856

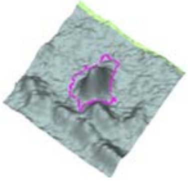

Spot 862

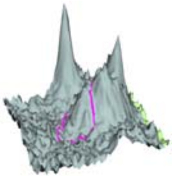

Spot 925

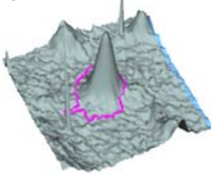

Spot 972

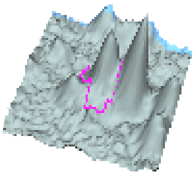

Spot 1029

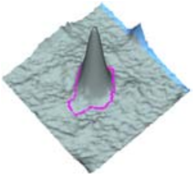

Spot 1032

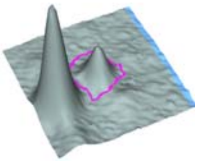

Spot 1054

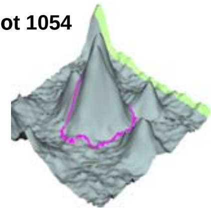

Spot 1067

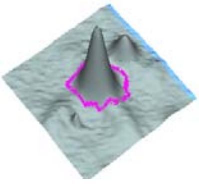

Spot 1121

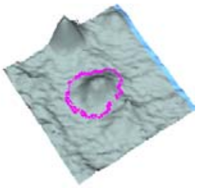

Spot 1134

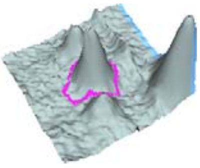

Spot 1202

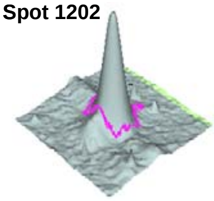

Spot 1306

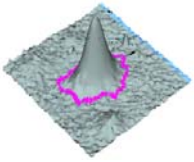

Spot 1355

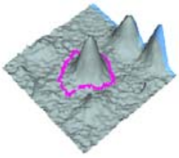

Spot 1457

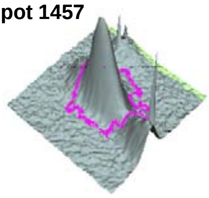

Spot 1466

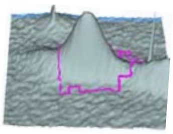

Spot 1593

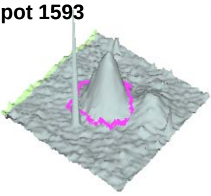

Spot 1688

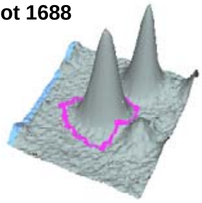

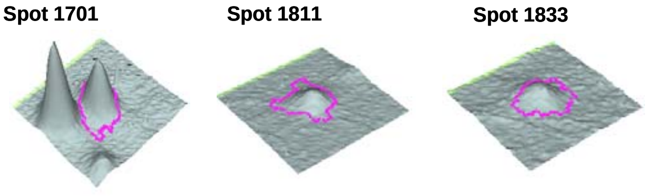

Figure 25. Three-dimensional views of selected protein spots exported from DeCyder. Spot area boundaries are indicated in magenta. Spots 150 and 154, spots 342 and 364 as well as spots 493 and 517 have been detected as a single spot by the software during analysis.

Spots 790, 795 and 806 were excluded from the group of differentially expressed proteins due to their inadequate three-dimensional structure (figure 25). These spots were part of badly resolved protein mixtures at alkaline pH during isoelectric focusing. For a proper analysis a different p*I* range would have been necessary.

The very small spots 701 and 856, as well as spots 1593, 1701, 1811 and 1833 could not be identified, since repeated extraction from gels (and pooling of protein material from up to five gels) did not lead to successful identification by MALDI-MS.

Remaining 37 spots have been unambiguously identified after tryptic *in-gel* digestion and subsequent mass spectrometry using peptide mass fingerprinting in combination with peptide sequence tag determination. Since some spots were identified as protein isoforms, in total 22 proteins were found to be differentially expressed after Oblimersen application, whereas only two protein spots meeting the same criteria were detected after siRNA application. Representative MALDI PMF and PSD spectra for all of these proteins and experimentally found m/z values are presented in supplement B (figure A-V). Table 13 contains a summary of relevant MS data, including accession number of SwissProt, p*I*, molecular weight, fold change after treatment, statistical data (Student’s t-Test and ANOVA), PMF score, sequence coverage and number of matched peptides. Continuation of table 13 contains additional MS/MS data including PSD score and sequences of peptides used for MS/MS.

Table 13. List of identified differentially expressed protein species after oblimersen (A) and siRNA (B) treatment.

Table 13 A.

Spot number	Protein name	Accession number	pI theor.	MW [kDa]	Change	T-Test	ANOVA	PMF Score*	Sequ. Cov [%]	Matching peptides**
Apoptosis-related										
546	CALU	O43852	4.47	37.19	-	*0.0022*	*0.0013*	93	26	10 (21)
1668	LEG-1	P09382	5.34	14.72	-	*0.0029*	*0.00032*	121	53	9 (17)
17/150/ 154	GRP 78	P11021	5.1	72.29	-	*0.018*	*0.0027*	94	20	13 (23)
276	HSP-60	P10809	5.7	61.06	-	*0.0011*	*0.00012*	126	34	15 (25)
731/ 743	NPM	P06748	4.64	32.73	-	*0.021*	*0.0027*	83	39	8 (12)
1202	PRDX-1	Q06830	8.3	22.11	-	*0.029*	*0.0011*	98	29	7 (10)
1054	PRDX-6	P30041	6.02	25.02	-	*0.023*	*0.0051*	88	39	9 (18)
359	TCP β	P78371	6.0	57.70	-	*0.01*	*0.002*	92	36	12 (21)
252/ 259/ 255	TCP ε	P48643	5.4	60.11	--	*0.0052*	*0.00047*	77	20	10 (16)
Cytoskeleton										
584/ 588	ACT B	P60709	5.5	41.74	---	*0.0059*	*0.00051*	130	31	12 (18)
1306	COF-1	P23528	8.26	18.59	-	*0.032*	*0.005*	101	61	10 (20)
925	Tropomyosin α	Q5VU72	4.76	28.89	-	*0.0063*	*0.0012*	94	29	10 (20)
972	Tropomyosin β	P07951	4.7	32.95	-	*0.015*	*0.014*	77	36	11 (21)
Glycolysis										
480/ 486/ 493/ 517	ENOA-1	P06733	6.99	47.17	-	*0.022*	*0.0047*	129	21	10 (17)
1032	PGAM-1	P18669	6.75	28.80	-	*0.018*	*0.004*	152	59	13 (20)
627/632	PGK1	P00558	8.6	45.85	-	*0.016*	*0.0038*	82	33	9 (15)
1067	TPIS	P60174	6.51	26.81	-	*0.018*	*0.003*	129	54	12 (24)
Miscellaneous:										
1121	MD2L1	Q13257	5.02	23.66	-	*0.0043*	*0.00034*	83	35	7 (15)
318	PDIA-3	P30101	6.10	57.04	--	*0.027*	*0.018*	99	27	13 (25)
342/ 364	3-PGDH	O43175	6.31	57.23	--	*0.035*	*0.0072*	145	34	14 (20)
1457/ 1466	PPIA	P62937	7.7	18.01	-	*0.036*	*0.0075*	130	51	9 (13)
1029	RANG	P43487	5.19	23.40	-	*0.049*	*0.023*	101	49	8 (14)

Table 13 B.

Spot number	Protein name	Accession number	pI theor.	MW [kDa]	Change	T-Test	ANOVA	PMF Score*	Sequ. Cov [%]	Matching peptides**
252	TCP ε	P48643	5.4	60.11	+	*0.0052*	*0.00047*	77	20	10 (20)
1202	PRDX-1	Q06830	8.3	22.11	++	*0.029*	*0.0011*	98	29	7 (10)

* Protein scores greater than 64 are significant ($p<0.05$). ** Number of unmatched peaks is given in brackets. Proteins of interest are presented with theoretical pI and MW, calculated statistically relevant parameters and accession numbers of the protein database. Fold changes are indicated; - / + ranges from ±1.5 to ±2.0, -- / ++ from ±2.01 to ±3.0 and --- / +++ from ±3.01 to ±4.0. *(CALU, calumenin, LEG-1, galectin-1, GRP 78, 78kDa glucose-regulated protein, HSP, heat shock protein, NPM, nucleophosmin, PRDX, peroxiredoxin, TCP, T-complex protein 1, ACTB, actin beta, COF-1, cofilin-1, ENOA-1, enolase-1, PGAM, phosphoglycerate mutase, PGK, phosphoglycerate kinase, TPIS, triosephosphatisomerase, MD2L1, mitotic-spindel-assembly-checkpoint protein MAD2A, PDIA, protein disulfide-isomerase, 3-PGDH, D-3-phosphoglycerate dehydrogenase, PPIA, peptidyl-prolyl cis-trans isomerase A, RANG, Ran-specific GTPase-activating protein)*

Table 13 continuation. PSD and MS/MS data of identified differentially expressed protein species after oblimersen (A) and siRNA (B) treatment.

Table 13 A.

Spot number	Protein name	Accession number	Precursor ion [m/z]	Peptide sequences	Score***
Apoptosis-related					
546	CALU	O43852	955.6; 1110.6; 1581.0	EQFVEFR; WIYEDVER; TFDQLTPEESKER	203 (39)
1668	LEG-1	P09382	1076.6; 1487.5	DGGAWGTEQR; DSNNLCLHFNPR	186 (39)
17/150/ 154	GRP 78	P11021	1568.1; 1817.0	ITPSYVAFTPEGER; IINEPTAAAIAYGLDKR	113 (38)
276	HSP-60	P10809	1685.6; 2561.8	AAVEEGIVLGGGCALLR; LVQDVANNTNEEAGDGTTTATVLAR	294 (37)
731/ 743	NPM	P06748	1569.7; 1821.0; 2228.6	VDNDENEHQLSLR; MTDQEAIQDLWQWR; MSVQPTVSLGGFEITPPVVLR	282 (38)
1202	PRDX-1	Q06830	1212.8; 1360.7; 1984.0	QITVNDLPVGR; GLFIIDDKGILR; TIAQDYGVLKADEGISFR	213 (38)
1054	PRDX-6	P30041	1086.5	LPFPIIDDR	79 (39)
359	TCP β	P78371	1331.8; 1584.3	GATQQILDEAER; QVLLSAAEAAEVILR	121 (38)
252/ 259/ 255	TCP ε	P48643	1094.8; 1739.8	IADGYEQAAR; WVGGPEIELIAIATGGR	140 (38)
Cytoskeleton					
584/ 588	ACT B	P60709	977.0; 1199.4; 1791.9	AGFAGDDAPR; AVFPSIVGRPR; SYELPDGQVITIGNER	121 (36)
1306	COF-1	P23528	1337.0; 1341.7	YALYDATYETK; LGGSAVISLEGKPL	113 (39)
925	Tropomyosin α	Q5VU72	1400.7; 1729.2	RIQLVEEELDR; IQLVEEELDRAQER	86 (40)
972	Tropomyosin β	P07951	1539.1	TIDDLEDEVYAQK	44 (38)
Glycolysis					
480/ 486/ 493/ 517	ENOA-1	P06733	1541.7; 1908.9	VVIGMDVAASEFFR; LAMQEFMILPVGAANFR	160 (38)
1032	PGAM-1	P18669	613.3; 2137.4	LVLIR; FSGWYDADLSPAGHEEAKR	137 (38)
627/632	PGK1	P00558	1636.9; 1769.8	LGDVYVNDAFGTAHR; ALESPERPFLAILGGAK	150 (39)
1067	TPIS	P60174	1587.3; 2193.2	DCGATWVVLGHSER; VPADTEVVCAPPTAYIDFAR	284 (39)
Miscellaneous					
1121	MD2L1	Q13257	-		
318	PDIA-3	P30101	1173.5; 1759.9	FVMQEEFSR; QAGPASVPLRTEEEFK	48 (39)
342/ 364	3-PGDH	O43175	987.5	DLPLLLFR	62 (41)
1457/ 1466	PPIA	P62937	1379.7	VSFELFADKVPK	27 (39)
1029	RANG	P43487	1621.7; 2740.6	FASENDLPEWKER; AWVWNTHADFADECPKPELLAIR	122 (37)

Table 13 B.

Spot number	Protein name	Accession number	Precursor ion [m/z]	Peptide sequences	Score***
252	TCP ε	P48643	1094.8; 1739.8	IADGYEQAAR; WVGGPEIELIAIATGGR	140 (38)
1202	PRDX-1	Q06830	1212.8; 1360.7; 1984.0	QITVNDLPVGR; GLFIIDDKGILR; TIAQDYGVLKADEGISFR	213 (38)

***Ion scores greater than the number given in brackets idicate identity or extensive homology ($p<0.05$). *(CALU, calumenin, LEG-1, galectin-1, GRP 78, glucose-regulated protein, HSP, heat shock protein, NPM, nucleophosmin, PRDX, peroxiredoxin, TCP, T-complex protein 1, ACTB, actin beta, COF-1, cofilin-1, ENOA-1, enolase-1, PGAM, phosphoglycerate mutase, PGK, phosphoglycerate kinase, TPIS, triosephosphatisomerase, MD2L1, mitotic-spindel-assembly-checkpoint protein MAD2A, PDIA, protein disulfide-isomerase, 3-PGDH, D-3-phosphoglycerate dehydrogenase, PPIA, peptidyl-prolyl cis-trans isomerase A, RANG, Ran-specific GTPase-activating protein)*

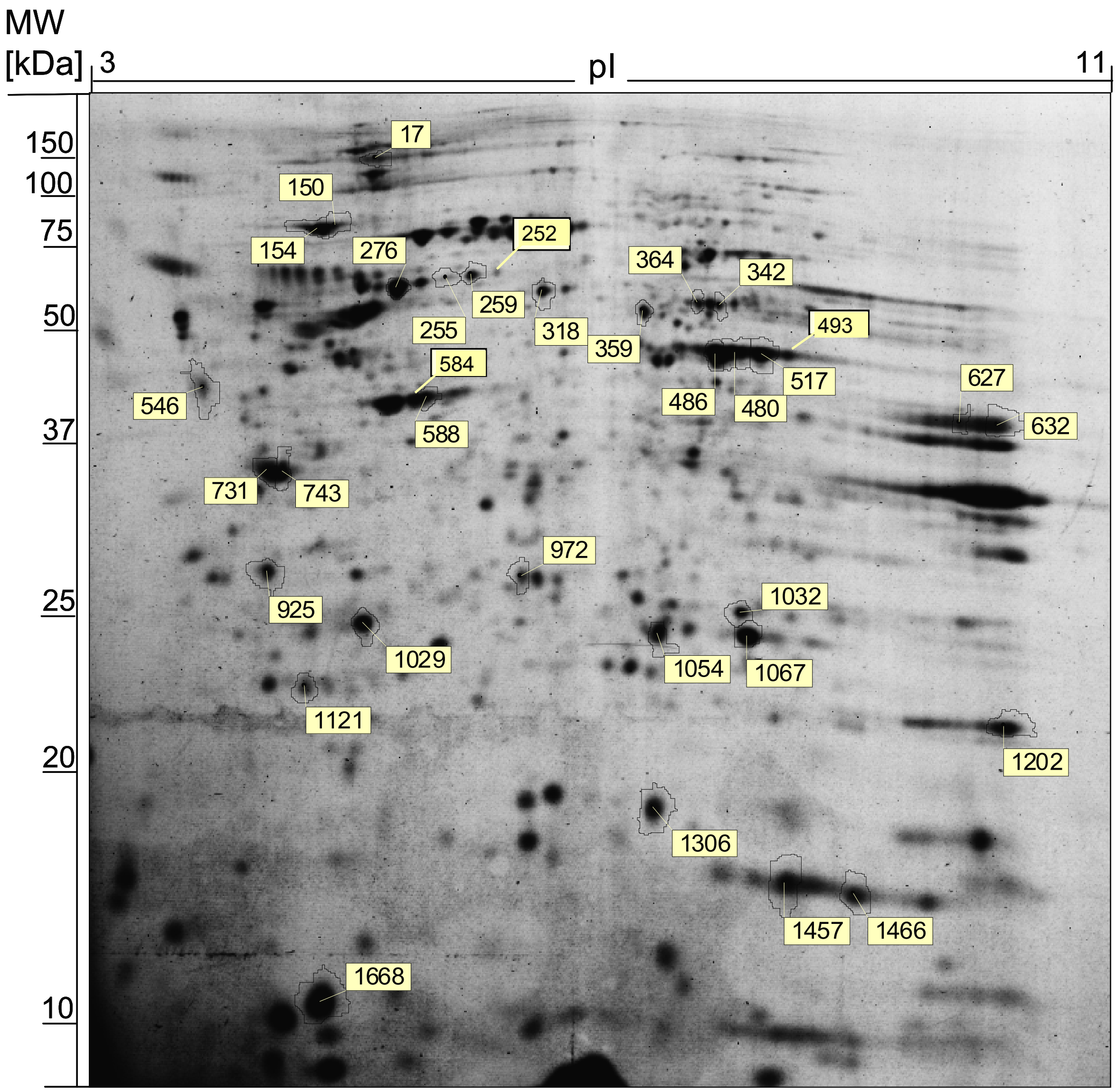
MW
[kDa]
3
pI
11
150
100
75
50
37
25
20
10
17
150
154
276
252
364
342
259
255
318
359
493
584
517
627
546
486
480
632
588
731
743
972
1032
925
1029
1054
1067
1121
1202
1306
1457
1466
1668

Figure 26. DIGE image with positions of differentially expressed protein spots indicated.

All proteins with significant alterations in protein expression after antisense treatment were found to be down-regulated. Actin and TCP ε were down-regulated more than two-fold, all other proteins showed a down-regulation between 1.5 and 2 (table 13). TCP ε and peroxiredoxin-1, both down-regulated by Oblimersen, were the only proteins changed by siRNA treatment. Both proteins were up-regulated, TCP ε by more than 1.5 fold, and peroxiredoxin two-fold [Stessl *et al.,* 2009].

Many of the differentially expressed proteins can be linked to mitochondrial apoptosis and drug resistance, and have been found to be up-regulated in clinical cancer samples or cancer cell lines. Among them are calumenin, a protein involved in the calcium metabolism, heat-shock protein 60, the galactose binding lectin galectin-1, which is up-regulated in cancer cells and activates h-ras, growth-related protein 78, which is implicated in mitochondrial protein import and assembly, nucleophosmin, a transport protein for nucleus-cytoplasm trafficking, and peroxiredoxins, which are involved in the redox-regulation of the cell. The cytoskeleton proteins actin, cofilin-1, which is also an important player in cancer cell metastasis and invasion, and tropomyosin were also significantly down-regulated. In addition, the expression of several enzymes was reduced after Oblimersen treatment. Surprisingly, four enzymes of the glycolytic pathway, enolase-1, phosphoglycerate kinase-1, triosephosphate isomerase, and phosphoglycerate mutase were found to be reduced in their expression, possibly indicating a reduction of anaerobic glucose consumption. Other identified enzymes include D-3-phosphoglycerate dehydrogenase, important for serine biosynthesis, peptidyl-prolyl cis-trans isomerase, often found to be up-regulated in proteomic studies of cancer, and the protein disulfide isomerase, which rearranges protein disulfide bonds. Finally, the mitotic spindle assembly checkpoint protein MAD2A and the ran-specific GTPase-activating protein were also reduced after Oblimersen treatment. Figure 27 shows a schematic classification of all identified proteins of interest with regard to their basic cellular functions [Stessl *et al.,* 2009].

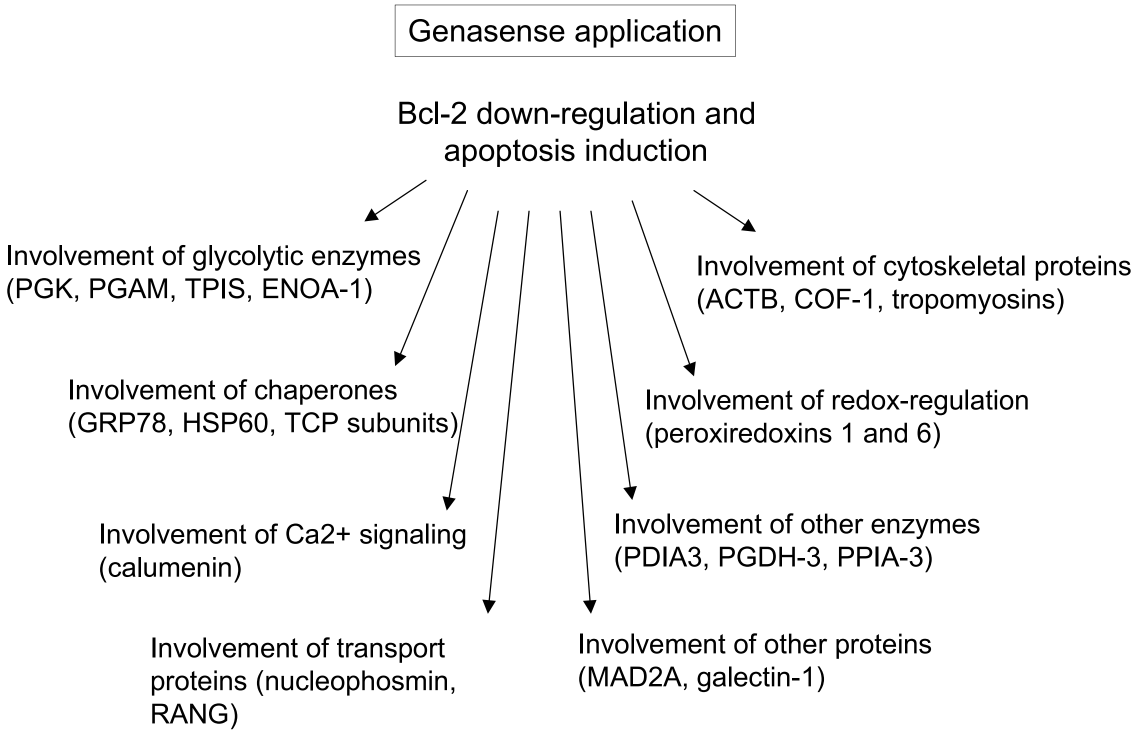
Genasense application
Bcl-2 down-regulation and apoptosis induction
Involvement of glycolytic enzymes (PGK, PGAM, TPIS, ENOA-1)
Involvement of cytoskeletal proteins (ACTB, COF-1, tropomyosins)
Involvement of chaperones (GRP78, HSP60, TCP subunits)
Involvement of redox-regulation (peroxiredoxins 1 and 6)
Involvement of Ca2+ signaling (calumenin)
Involvement of other enzymes (PDIA3, PGDH-3, PPIA-3)
Involvement of transport proteins (nucleophosmin, RANG)
Involvement of other proteins (MAD2A, galectin-1)

Figure 27. Schematic classification of differentially expressed proteins. Picture taken from Stessl *et al.,* 2009.

Discussion

Gene-targeted approaches have great potential for the treatment of many severe and debilitating diseases [Mahato *et al.*, 2005] but for an establishment as therapeutics still many difficulties, such as effective drug delivery, cellular uptake or the question of specificity have to be solved. Antisense oligonucleotides (ASOs) and small interfering RNAs (siRNAs) are two powerful tools that influence gene expression at the post-transcriptional level. siRNAs use the RISC-associated RNAi pathway to mediate gene-knockdown, which can be achieved in cell culture experiments even in low nanomolar concentrations, whereas phosphorothioates act via a less characterized mechanism usually requiring higher concentrations for efficient target protein knockdown. Apart from the only antisense agent on the market (fomivirsen, Vitravene) the ASO representative with the highest clinical relevance is the 18mer phosphorothioate Oblimersen (Genasense, G3139, Genta [Moreira *et al.,* 2006]), which is directed against the first six codons of the open-reading frame of *bcl-2*. The anti-apoptotic protein Bcl-2 is a potent regulator of programmed cell death and its over-expression has been associated with decreased apoptosis and increased resistance against chemotherapy [Reed, 1995 and 2008]. The *bcl-2*-targeted antisense molecule Oblimersen has been tested in clinical trials against various cancer types, both alone and in combination with other anticancer agents. The rationale for testing Oblimersen is based on data supporting a relevant role for Bcl-2 in cell survival and enhanced tumor response when it is combined with chemotherapy. Beyond the sequence-specific Bcl-2 down-regulation, phosphorothioates have been reported to have unspecific effects – studies have shown that several effects are caused by the CpG motifs [Gekeler *et al.,* 2006] or the phosphorothioate chemistry [Stein *et al.*, 2008]. The question of specificity and the elucidation of the exact mechanism of action, however, still remain major safety issues for the therapeutical development of antisense agents. In this thesis a proteomic approach was applied in order to monitor and compare qualitative and quantitative off-target effects of the phosphorothioate antisense oligonucleotide Oblimersen and a *bcl-2*-targeted siRNA on the protein level with the aim to contribute to a better understanding of the molecular network of this compound class.

In accordance with published results [Herbst *et al.,* 2004; Benimetskaya *et al.,* 2005; Wacheck *et al.,* 2001; Jansen *et al.,* 2000] it was found that Oblimersen down-regulates Bcl-2 (figure 6 and 7) and induces cell death in the human melanoma cell line 607B (figure 9 and 10). The highest level of target protein down-regulation on human melanoma cells (75% compared to untreated controls) was achieved with a concentration of 100 nM, whereas other phosphorothioate concentrations (50 nM, 150 nM and 200 nM, respectively) resulted in lower protein down-regulation (table 6). The used anti-*bcl-2*-siRNA was more effective, since even very low concentrations, 5 nM and 10 nM, were enough to decrease target protein levels for ~80%. With a concentration of 50 nM the same Bcl-2 expression inhibition was achieved (75%), therefore this concentration was further chosen as siRNA working concentration. The same level of *bcl-2* knockdown caused by the anti-*bcl-2*-siRNA failed to increase apoptosis as determined by Annexin staining and caspase activity measurement (figure 9 and 10). It has been previously described that Oblimersen and *bcl-2*-targeted siRNAs are not equivalent as apoptotic/cytostatic agents and that they induce disparate phenotypes in PC3 and LNCaP prostate cancer cells [Anderson *et al.*, 2006]. Together with the higher number of proteins found to be differentially regulated after treatment with Oblimersen compared to the siRNA treated samples (table 13), it is demonstrated that an additional effect other than Bcl-2 down-regulation is involved in the phosphorothioate mechanism. Since the effects on the genome and proteome level are not the same and even siRNA-sequences have been reported to have varying off-target effects [Jackson *et al.,* 2003] the present study focused on the quantitative elucidation of off-target effects of Oblimersen and the anti-*bcl-2* siRNA on the proteome using DIGE technology.

Considering the different efficiencies in this study human melanoma cells were treated with 100 nM Oblimersen and 50 nM siRNA lipoplexes and after 48 hours subjected to lysis. *In vitro* applications of antisense agents are usually supported by transfection reagents (e.g. cationic lipids such as cholesterol derivatives) [Meidan *et al.,* 2006] which facilitate their delivery and uptake into the cell. In this study all oligonucleotides were complexed with lipofectamine 2000. Although lipofectamine 2000 is described as cytotoxic in higher concentrations, 607B cells did not show increased apoptosis or *bcl-2* down-regulation after treatment with the transfection reagent alone (figures 6, 9 and 10). In addition, no significant change in the proteomic pattern compared to untreated cells could be detected upon treatment with unloaded lipofectamine 2000. Consequently, lipofectamine 2000 only treated cells were used as control group for DIGE experiments comparing antisense and siRNA oligonucleotides effects on the proteome level.

The comparison of effects of different cell treatments on the basis of two-dimensional gel electrophoresis deserves a careful characterization of the used cell line, an optimization of separation and staining conditions for the biological question, as well as a validation of used bioanalytical methods in order to minimize potential bias.

As a first step the human melanoma cell line 607B was characterized by the establishment of a protein reference map (figure 16), since 607B cells have not been characterized on the protein level yet. Table 8 summarizes all reference proteins that have been unambiguously identified by *in-gel* digestion and subsequent MALDI-rTOF-MS. In that context also two proteins of bovine origin were identified, namely bovine serum albumin (BSA) and bovine stathmin. BSA is a major component of the fetal calf serum, which was added to the 607B cell culture medium and stathmin, a protein involved in proliferation and differentiation of immortalized cells [Tamura *et al.,* 2007], was most likely introduced by cell culture medium too, even though cells were repeatedly washed before lysis. High abundant proteins of this medium can be seen in figure 21. According to Miller [Miller *et al.,* 2006] the presence of cell culture additives in cell lysates is a commonly observed contamination, which can be reduced to a minimum but cannot be completely avoided in most cases. Since the DIGE approach was followed by unambiguous identification of proteins by mass spectrometry, bovine proteins could be easily distinguished from human ones.

For the two-dimensional separation of 607B lysates non linear IPG strips ranging from p*I* 3-11 and an acrylamide concentration of 12.5% were chosen. Under these prerequisites a high resolution could be achieved and the highest number of protein spots (averagely 2500-3000) could be monitored on one gel. Although the highest number of spots could be detected with silver staining according to Blum [Blum *et al.,* 1987], DIGE technology was chosen for the quantitative evaluation. It is a pre-labeling technique with CyDyes™, which offers the high linear and dynamic range of fluorescent dyes, a low limit of detection and the possibility to introduce an internal standard providing reliable quantitative data. The disadvantage of this method is the need for a post-staining with silver nitrate or fluorescent dyes, since CyDyes™, once linked to sample proteins, introduce a small shift in p*I* and molecular weight of proteins [Alban *et al.,* 2003]. For subsequent MS analysis it is necessary to extract as much protein material as possible from 2-DE gels, therefore a post-staining is inevitable. Although all used methods have resulted in similar a protein pattern with high abundant spots present in all gels (figures 11-14), spot assignment among differently stained gels has been a critical issue. Physico-chemical properties of proteins and staining chemistry give variations which have to be taken into consideration as a prominent source for incorrect protein spot assignment.

Beside experimental sources of variance (such as insufficient IPG strip rehydration prior to IEF, incomplete protein transfer from the first (IEF) to the second dimension (SDS-PAGE) or inhomogeneity in staining procedures [repeatedly addressed by Barry *et al.,* 2003; Schlags *et al.,* 2005; Schröder *et al.,* 2008]), which can be widely avoided by the use of DIGE technology, a trained operator and respective equipment, variance caused by computer-assisted post-experimental processes is rarely considered and only a limited number of publications deal with the influence of the image analysis process on obtained 2-DE data [Wheelock *et al.,* 2005 and 2006; Clark *et al.,* 2008; Karp *et al.,* 2008]. A lot of different software packages in the field of 2-DE image analysis are commercially available (for a detailed review see Marengo *et al.,* 2005 or Berth *et al.,* 2007). Along with high-quality technical devices and improved visualization methods for 2-DE gels, these packages become increasingly sophisticated with regard to spot detection algorithms, spot normalization, quantification and performance of analysis. Due to a lack of publicly available information regarding the algorithms used, the information about their performance is limited to practical evaluation [Wheelock *et al.,* 2006]. During the validation of bioanalytical methods for this thesis the question arose whether an analysis with the update version (8.0) of the software PD-Quest (Bio-Rad), which was introduced in the laboratory, would lead to different 2-DE data than an analysis with the original version (6.1) or with the software package Delta 2D (Decodon), respectively, making data comparison with older data critical or even impossible. A gel set of six gels was independently analyzed with the three mentioned software packages keeping important parameters constant (figure 17) and gained fold changes of selected spots were exported and compared to each other (table 10 and figure 19). Fold changes were represented as factors, whereupon a factor of 2 corresponded to 100% variation in the spot volume. A spot with a factor of 2 was considered as differentially expressed protein. Under these prerequisites only one out of ten spots (VII) was detected as significantly changed with all three software packages, two additional spots (VIII and IX) met the criteria with both PD-Quest versions, but not with Delta 2D. All other spots were only detected as differentially expressed by one of the three software packages. Despite the inclusion of the same gel set and constant parameters, obtained 2-DE data differed significantly from each other when analysed with different software packages. During image analysis quantitative variation can be introduced by a lot of parameters, such as image acquisition, background subtraction, smoothing filters/algorithms or normalization methods [Wheelock *et al.,* 2006]. The latter have to be applied in order to compensate for small deviations introduced by experimental procedures to improve software performance [Stessl *et al.,* 2009]. For silver stained gels the total gel density (the raw quantity of each spot in a member gel is divided by the total intensity value of all the pixels in the image) is used for normalization to compensate for inconsistent gel backgrounds [Zahn *et al.,* 2003]. In the analysis with PDQ version 6.1 this method was considered as the most suitable one, whereas in version 8.0 the newly introduced local regression model was used, since it is recommended as a more sophisticated method. According to the manufacturer it is based upon a loess regression [Cleveland *et al*., 1988; Hua *et al.*, 2008] and less susceptible to outliers than a simple linear regression [Stessl *et al.,* 2009]. Since other mentioned parameters were kept constant, the study underlines the effect of the normalization process on obtained data. In the analysis with Delta 2D spots were normalized on the total quantity of spots per gel. Available information about the different algorithms underlying the software packages and versions is limited. Nevertheless, they highly influence parameters on spot quantitation [Stessl *et al.,* 2009].

The software comparison of the three packages did not lead to a general judgement about the packages in terms of being “best in all cases”. The decision which software to use depends on several factors, including number of replicates, biological questions or applied staining methods. The study, however, clearly shows that quantitative data obtained with different software packages – even with different versions of the same software – differ significantly and are not directly comparable. One aim of the study was to draw the attention of the user to the fact that image-analysis parameters chosen by the operator, the normalization processes as well as software algorithms can have a strong influence on the quantitative outcome.

Taking these critical points of potential bias into consideration the off-target effect study comparing Oblimersen and a *bcl-2* targeted siRNA on the basis of equal target protein down-regulation of 75% was performed using DIGE technology. 22 proteins were found to be differentially expressed after Oblimersen treatment, whereas only 2 proteins were significantly changed after siRNA application on human melanoma cells (table 13, figure 26 and 27). Beta-actin, cofilin-1, glucose-regulated protein 78, HSP60, nucleophosmin, phosphoglycerate mutase, protein disulfide isomerase, T-complex proteins, and tropomyosins were also found to be differentially regulated in a comprehensive proteomic profiling of apoptotic cells [Thiede *et al.,* 2004], indicating their significance for apoptosis. Some of these proteins (peroxiredoxins, enolase-1, triose phsophate isomerase, actin, TCP-1, and peptidyl-prolyl cis-trans isomerase) belong to a group of proteins described in a meta-analysis as repeatedly altered throughout many 2-DE experiments regardless of tissue or treatment [Perkins *et al.,* 1999]. While this may be a consequence of a technical bias, it seems more likely that the expression of these proteins easily fluctuates in response to a particular treatment or a changing environment. In any case, the significance of a differentially regulated protein of this “hit list” should not be over-interpreted. The reduction of the expression of some of the proteins, namely peptidyl-prolyl cis trans isomerse, beta-actin, RANG, proteins involved in calcium metabolism and some cytoskeletal proteins, are in good agreement to a gene profiling study [Anderson *et al.,* 2006] which detected several differentially regulated mRNAs to be involved in the phosphorothioate action mechanism [Stessl *et al.*, 2009].

Peroxiredoxins are a family of multifunctional proteins that are involved in the cellular protection against oxidative stress, modulation of intracellular signaling, and regulation of cell proliferation [Immenschuh *et al.,* 2005]. The context among peroxiredoxins, oxidative stress and apoptosis has been described [Chu *et al.,* 2003] and it has been stated that high levels of peroxiredoxins inhibit apoptosis and induce cell proliferation. The down-regulation of peroxiredoxin-1 after Oblimersen application and its converse up-regulation after siRNA-treatment are in very good accordance to these findings [Stessl *et al.*, 2009].

Calcium ions play an important role in the complex interplay that allows signals to be decoded into activation of cell death [Giorgi *et al.,* 2008]. The cytosolic Ca2+-concentration is tightly controlled by interactions among transporters, pumps, ion channels and binding proteins. Calumenin (crocalbin) belongs to a family of calcium-binding proteins, participates in Ca2+-regulated activities [Honore *et al.,* 2000] and is found to be modulated in studies of apoptosis [Thiede *et al.,* 2004] or drug resistance [Castagna *et al.,* 2004; Smaili *et al.,* 2000; Stessl *et al.*, 2009].

Galectin-1 and nucleophosmin were also described to be involved in apoptosis regulation. A knockdown of galectin-1 sensitizes mouse melanoma cells to temozolomide [Mathieu *et al.,* 2007] and furthermore it was found that it induces growth inhibition and apoptosis in the prostate cancer cell line LNCaP [Ellerhorst *et al.,* 1999]. The multifunctional and nearly ubiquitous phosphoprotein nucleophosmin is dysregulated in many human malignancies leading to apoptotic resistance and inhibition of differentiation [Qi *et al.,* 2008]. A specific knockdown of NPM by RNAi was described to attenuate apoptosis [Kerr *et al.,* 2007; Stessl *et al*., 2009].

The cytoskeleton proteins actin and cofilin-1 are important in metastatic cancer cells for cell migration, metastasis and invasion, and the activity of cofilin-1 is mainly expression-regulated [Wang *et al.,* 2007]. Cofilin-1 is over-expressed in many highly invasive cancer cell lines and in clinical tumor samples. Considering the depletion of other cancer markers mentioned above, the reduction of these cytoskeleton proteins further supports the total apoptosis-inducing and growth inhibiting effect of Oblimersen [Stessl *et al.*, 2009].

Besides the proteins with a connection to apoptosis or drug resistance, several enzymes of the glycolytic pathway were found to be down-regulated after Oblimersen treatment. Enolase-1 plays important additional roles in various processes. It was reported to be a hypoxic stress protein as well as a heat shock protein and to be involved in cellular energy metabolism and proliferation. Several studies have identified enolase-1 as an alternatively translated 37kDa tumor suppressor c-myc promotor binding protein (MBP-1) and ectopic MBP-1 expression was described to induce cell death and growth suppression [Kim *et al*., 2005; Subramanian *et al.,* 2000; Kondoh *et al*., 2007]. Enolase-1 is frequently found as differentially up- or down-regulated in 2D gel electrophoresis based proteomics experiments, underlining its abundance and fragility [Petrak *et al*., 2008]. Phosphoglycerate mutase was found to be up-regulated in cancer cell lines or clinical tumour samples [Turhani *et al.,* 2006]. The reduction in the expression of these glycolytic enzymes suggests that the energy metabolism of the melanoma cells changes upon Oblimersen influence [Stessl *et al*., 2009]. Most of the pyruvic acid in healthy animal and human tissues is obtained by normal glycolysis, *id est* the convertion of glucose to pyruvate. The pyruvate enters the mitochondria where it is oxidized to carbon dioxide (CO_2) and water [Harris, 2006] under the formation of adenosine-5'-triphosphate (ATP) via the so-called "ATP synthasome" [Chen *et al.,* 2004]. In the early part of the 20th century the German biochemist Otto Warburg showed that cancerous tumors develop a modified sugar (glucose) metabolism whereby a significant portion of the blood sugar consumed by the tumor is converted one step beyond pyruvate, *id est* to lactic acid, even in the presence of sufficient oxygen [Warburg *et al.,* 1930]. That means that even if tumor mitochondria have sufficient oxygen to metabolize all the pyruvate formed from the blood glucose to carbon dioxide and water, the tumor assumes a significant role in energy (ATP) production via the conversion of glucose to lactic acid [Pedersen, 2007]. The benefits of the Warburg effect to cancer lie (a) in an additional source for carbon precursors needed for the usually rapid growth of tumor cells, (b) in an increased protection of the tumor against the immune system caused by the low pH of produced lactic acid, and (c) in a kind of precaution assuring longer tumor survival for limited oxygen situations. The genes coding for the enzymes catalyzing the high glycolytic rates of tumor cells are activated under hypoxic or anoxic conditions [Pedersen, 2007]. Summarizing, the “Warburg effect” refers to increased utilization of the glycolytic pathway for energy (ATP) production (and likely other needs) even though sufficient oxygen is present to support mitochondrial functions of cancerous tumors [Pedersen, 2007]. The findings presented in this thesis may indicate that the Warburg effect is partially reversed after treatment with the phosphorothioate antisense oligonucleotide [Stessl *et al.,* 2009].

As pivotal proteins involved in the Warburg effect of cancer cells hexokinase-2 and its receptor on the outer mitochondrial membrane, the voltage dependent anion channel protein (VDAC), have been identified [Bustamante *et a*l., 1977 and 1981]. Hexokinase-2 bound to VDAC has preferred access to ATP synthesized in the inner membrane and thus facilitates the increased glycolysis of cancer cells. Furthermore hexokinase-2 has been reported to play a very important role in cell growth and/or apoptosis suppression, since its mitochondrial binding inhibits Bax-induced cytochrome c release and apoptosis [Pastorino *et al.,* 2008]. VDAC has been described to be essential in the apoptosis-triggering change of the mitochondrial outer membrane permeabilization and subsequent release of cytochrome c into the cytoplasm [Campbell *et al.,* 2008; Thinnes, 2009]. It is discussed as a potential cellular target of anti-cancer agents [Simamura *et al.,* 2008] and has been identified as a potential cellular target of phosphorothioates. The effect of Oblimersen and other phosphorothioates was described to be different from a general polyanion effect and phosphodiesters failed to increase the mitochondrial membrane permeability. The concentrations that effectively cause a VDAC block on isolated mitochondria are in the micromolar range. Upon applying a lipofectamine-oligonucleotide mixture of 100 nM Oblimersen, the intracellular concentration was estimated to be up to 2 to 3 µM [Lai *et al.,* 2006]. Furthermore VDAC was found to be the binding partner for hexokinase-2 and therefore it represents a key player in the Warburg effect. Binding to VDAC increases hexokinase-2's affinity for ATP, providing it with preferred access to ATP, effectively jump starting the glycolytic pathway [Stessl *et al.*, 2009].

The over-expression of VDAC in cancer cells and its role in the activation of the mitochondrial apoptosis pathway and enhanced glycolysis support its potential as a cancer drug target [Shoshan-Barmatz *et al.,* 2008]. Phosphorothioates have been shown to cause a potent specific VDAC block followed by the induction of apoptosis [Stein *et al.,* 2008]. The blockage of the mitochondrial anion channel does not only explain the differential regulations of proteins linked to apoptosis, but also the down-regulation of enzymes involved in the glycolytic pathway. Presented reduction in glycolysis on the protein level after treatment with a phosphorothioate antisense oligonucleotide is shown for the first time. These findings, although undesired for a specific gene silencing agent, might represent an interesting new therapeutic field for non-targeted phosphorothioate oligonucleotides or other compounds selectively inhibiting the VDAC. While the VDAC block is not dependent on oligonucleotide sequence [Stein *et al.,* 2008], the apoptotic effect of Oblimersen is higher than that of an untargeted control phosphorothioate, indicating that the *bcl-2* down-regulation possibly along with other, yet unknown molecular targets are also contributing to its effect [Stessl *et al.*, 2009].

Control phosphorothioate oligonucleotides targeted at different proteins, not involved in apoptosis, (including an untargeted and an ICAM-1 targeting phosphorothioate, a second generation antisense oligonucleotide (2'-O-methyl gapmer), as well as an unmodified and a phosphorothioate backbone modified siRNA sequence) showed similar results compared to Oblimersen [Winkler *et al.,* 2010]. Most proteins, namely glucose-related protein 78 (GRP78), galectin-1 (GAL-1), calumenin (CALU), protein-disulfide isomerase (PDIA-3), heat-shock protein 60 (HSP60), nucleophosmin (NPM), cofilin-1 (COF-1), tropomyosin β, T-complex protein 1 subunit beta (TCP β), as well as the glycolytic enzymes triosephosphate isomerase (TPIS), glycerate aldehyde dehydrogenase (GAPDH), phosphoglycerate mutase (PGAM) and D-3-phosphoglycerate dehydrogenase (PHGDH) were significantly depleted after treatment with control phosphorothioates or similarly modified double stranded siRNA. Therefore the discussed partial reversal of the Warburg effect observed after Oblimersen treatment seems not to be exclusively caused by *bcl-2* targeted gene silencing and hence resulting apoptosis induction. Only Oblimersen and the random control antisense agent, but not an siRNA or a second generation antisense oligonucleotide resulted in reduced *L*-lactate production when normalized to glucose consumption. These results further indicate that the effect on glycolysis is not Oblimersen specific, but rather a characteristic of the phosphorothioate backbone modification [Winkler *et al.*, 2010].

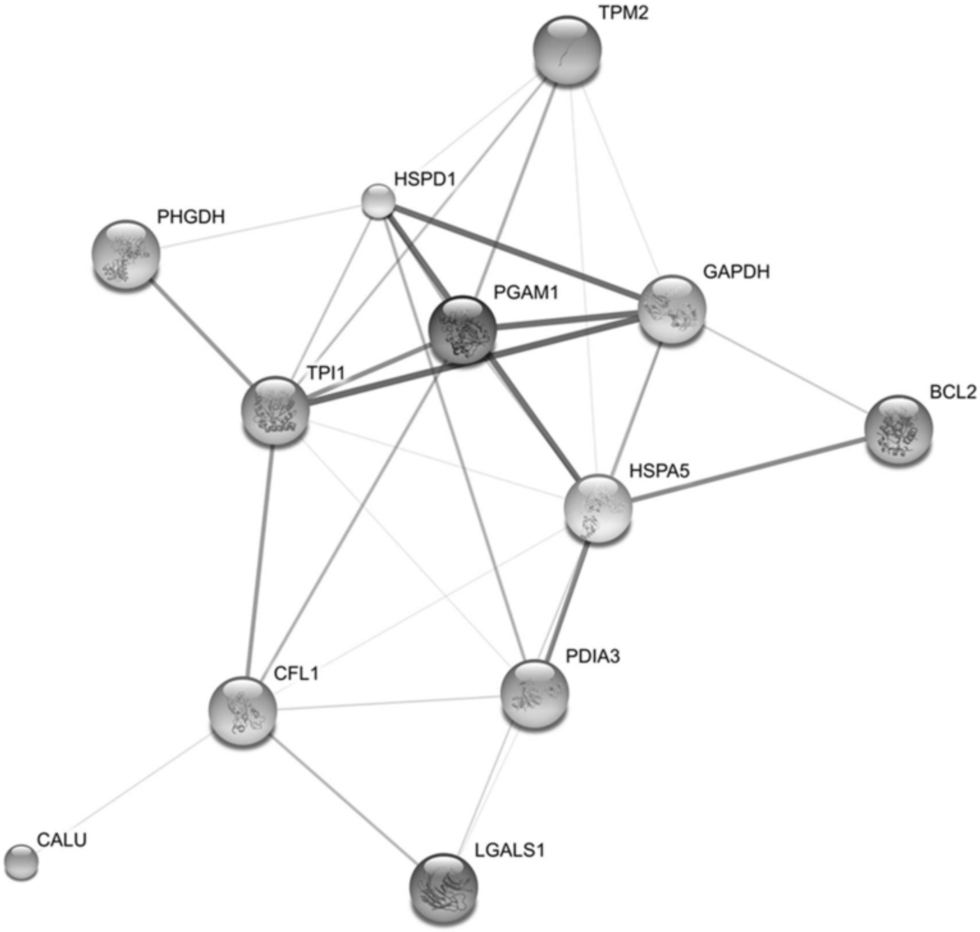

Figure 28. Visualized associations of proteins down-regulated by phosphorothioate treatment computed by the STRING database [Jensen *et al.*, 2009]. These associations, reflecting experimental interactions, co-occurrences or co-expression of genes, as well as co-mentioning in Medline abstracts, show the network of the changed proteins with the glycolytic machinery as the central complex [Winkler *et al*., 2010]. *LGALS1, galectin-1, GAPDH, glyceraldehyde-3-phosphate dehydrogenase, PDIA3, protein disulfideisomerase A3 (58kDa glucose regulated protein), HSPA5 78 kDa glucose-regulated protein, BCL2, apoptosis regulator bcl-2, HSPD1, 60 kDa heat shock protein, CALU, calumenin, PHGDH, D-3-phosphoglycerate dehydrogenase, PGAM1, phosphoglycerate mutase 1, TPM2 tropomyosin beta chain, TPI1, triosephosphate isomerase, CFL1, cofilin-1.*

Of course, the *in vivo* significance of these results found *in vitro* remains to be proven. In clinical trials, Oblimersen is applied without cationic lipids. Consequently, the intracellular concentrations in the organism are unknown, and may be much lower than those achieved in cultured cells. These data, however, demonstrate the possibility of clinically relevant off-target effects in oligonucleotide drug candidates and the need for careful pharmacologic and pharmacokinetic analysis at the preclinical stage of antisense or siRNA oligonucleotides.

Conclusion

The present study represents the first attempt to compare two different therapeutic gene silencing strategies with the same effect on the target in terms of their off-target effects on the protein level. A siRNA mediated target protein knockdown is much more specific and reveals hardly any off-target effects. The phosphorothioate antisense oligonucleotide, on the other hand, clearly shows significant unspecific effects on the cellular proteome, resulting in differential regulation of 22 proteins other than the targeted one. Identified proteins play a role in the mitochondrial apoptotic network, endoplasmatic reticulum stress and glycolysis. Many show an increased expression in cancer cell lines and clinical cancer samples, indicating that Oblimersen has an apoptosis inducing and resistance reversing effect. This study supports the theory that the Bcl-2 reduction is not the only essential molecular effect of Oblimersen, but that an unspecific apoptosis-induction, possibly caused by a phosphorothioate mediated VDAC block, also plays a key role. Furthermore the first evidence of a phosphorothioate oligonucleotide-mediated reduction of the expression of glycolytic enzymes is presented. On the one hand the findings may point to a potential new interesting therapeutic field for phosphorothioate oligonucleotides in cancer, taking advantage of their unspecific rather than their specific effects or applying metabolic network based strategies. On the other hand the results underline the importance of the critical use of phosphorothioates in the clinic until their unspecific effects are fully understood.

References

Achenbach, T., Brunner, B., Heermeier, K. (2003) Oligonucleotide-based knockdown technologies: antisense versus RNA interference. *Chembiochem*, **4**(10), 928-935.

Adams, J.M. (2003) Ways of dying: multiple pathways to apoptosis. *Genes Dev*, **17**, 2481-2495.

Adams, J.M., Cory, S. (2007) Bcl-2-regulated apoptosis: mechanism and therapeutic potential. *Curr Opin Immunol*, **19**, 488–496.

Agarwala, S.S., Keilholz, U., Gilles, E., Bedikian, A.Y., Wu, J., Kay, R., Stein, C.A., Itri, L.M., Suciu, S., Eggermont. A.M. (2009) LDH correlation with survival in advanced melanoma from two large, randomised trials (Oblimersen GM301 and EORTC 18951). *Eur J Cancer*., **45**(10), 1807-1814.

Akhtar, S. (2009) Oral delivery of siRNA and antisense oligonucleotides. *J Drug Target*., **17**(7), 491-495.

Alban, A., David, S.O., Bjorkesten, L., Andersson, C., Sloge, E., Lewis, S., Currie, I. (2003) A novel experimental design for comparative two-dimensional gel analysis: two-dimensional difference gel electrophoresis incorporating a pooled internal standard. *Proteomics*, **3**(1), 36-44.

Alvarez-Salas, L.M. (2008) Nucleic acids as therapeutic agents. *Curr Top Med Chem*., **8**(15), 1379-1404.

Anderson, E.M., Miller, P., Ilsley, D., Marshall, W., Khvorova, A., Stein, C.A., Benimetskaya, L. (2006) Gene profiling study of G3139- and Bcl-2-targeting siRNAs identifies a unique G3139 molecular signature. *Cancer Gene Ther*, **13**, 406-414.

Antonsson, B., Montessuit, S., Lauper, S., Eskes, R., Martinou, J.C. (2000) Bax oligomerization is required for channel-forming activity in liposomes and to trigger cytochrome c release from mitochondria. *Biochem J*, **345**(2), 271-278.

Ashkenazi, A. (2002) Targeting death and decoy receptors of the tumour-necrosis factor superfamily. *Nat Rev Cancer*, **2**(6), 420-430.

Bachmann, P.S., Gorman, R., Papa, R.A., Bardell, J.E., Ford, J., Kees, U.R., Marshall, G.M., Lock, R.B. (2007) Divergent mechanisms of glucocorticoid resistance in experimental models of pediatric acute lymphoblastic leukemia. *Cancer Res*., **67**(9), 4482-4490.

Baker, B.F., Monia, B.P. (1999) Novel mechanisms for antisense-mediated regulation of gene expression. *Biochim Biophys Acta*., **1489**(1), 3-18.

Barry, R.C., Alsaker, B.L., Robison-Cox, J.F., Dratz, E.A. (2003) Quantitative evaluation of sample application methods for semipreparative separations of basic proteins by two-dimensional gel electrophoresis. *Electrophoresis*, **24**, 3390-3404.

Bedikian, A.Y., Millward, M., Pehamberger, H., Conry, R., Gore, M., Trefzer, U., Pavlick, A.C., DeConti, R., Hersh, E.M., Hersey, P., Kirkwood, J.M., Haluska, F.G. (2006) Bcl-2 Antisense (oblimersen sodium) Plus Dacarbazine in Patients With Advanced Melanoma: The Oblimersen Melanoma Study Group. *J. Clin. Oncol*., **24**, 4738-4745.

Benimetskaya, L., Lai, J.C., Khvorova, A., Wu, S., Miller, P., Stein, C.A. (2005) Induction of apoptosis by G3139 in melanoma cells. *Ann. N Y Acad. Sci*., **1058**, 235-245.

Bennett, C.F., Swayze, E.E. (2010) RNA Targeting Therapeutics: Molecular Mechanisms of Antisense Oligonucleotides as a Therapeutic Platform. *Annu. Rev. Pharmacol. Toxicol.,* **50**, 259-293.

Berth, M., Moser, F.M., Kolbe, M., Bernhardt, J. (2007) The state of the art in the analysis of two-dimensional gel electrophoresis images. *Appl Microbiol Biotechnol*, **76**(6), 1223-43.

Bhindi, R., Fahmy, R.G., Lowe, H.C., Chesterman, C.N., Dass, C.R., Cairns, M.J., Saravolac, E.G., Sun, L.Q., Khachigian, L.M. (2007) Brothers in arms: DNA enzymes, short interfering RNA, and the emerging wave of small-molecule nucleic acid-based gene-silencing strategies. *Am J Pathol.*, **171**(4), 1079-1088.

Blum, H., Beier, H., Gross, H.J. (1987) Improved silver staining of plant proteins, RNA and DNA in polyacrylamide gels. *Electrophoresis*, **8**, 93-99.

Bradford, M.M. (1976) A rapid and sensitive method for the quantitation of microgram quantities of protein utilizing the principle of protein-dye binding. *Anal Biochem*, **72**, 248-254.

Bush, J.A., Li, G. (2003) The role of Bcl-2 family members in the progression of cutaneous melanoma. *Clin Exp Metastasis*, **20**(6), 531-539.

Bustamante, E., Pedersen, P.L. (1977) High aerobic glycolysis of rat hepatoma cells in culture: role of mitochondrial hexokinase. *Proc Natl Acad Sci USA*., **74**(9), 3735-3739.

Bustamante, E., Morris, H.P., Pedersen, P.L. (1981) Energy metabolism of tumor cells. Requirement for a form of hexokinase with a propensity for mitochondrial binding. *JBC*, **256**(16), 8699-8704.

Campbell, A.M., Chan, S.H. (2008) Mitochondrial membrane cholesterol, the voltage dependent anion channel (VDAC), and the Warburg effect. *J. Bioenerg. Biomembr*., **40**(3), 193-197.

Castagna, A., Antonioli, P., Astner, H., Hamdan, M., Righetti, S.C., Perego, P., Zunino, F., Righetti, P.G. (2004) A proteomic approach to cisplatin resistance in the cervix squamous cell carcinoma cell line A431. *Proteomics*, **4**(10), 3246-3267.

Cejka, D., Losert, D., Wacheck, V. (2006) Short interfering RNA (siRNA): tool or therapeutic? *Clin Sci (London)*, **110**(1), 47-58.

Cekaite, L., Furset, G., Hovig, E., Sioud, M. (2007) Gene expression analysis in blood cells in response to unmodified and 2′-modified ss siRNAs reveals TLR-dependent and independent effects. *J. Mol. Biol*., **365**, 90–108.

Chen, C., Ko, Y., Delannoy, M., Ludtke, S.J., Chiu, W., Pedersen, P.L. (2004) Mitochondrial ATP synthasome: three-dimensional structure by electron microscopy of the ATP synthase in complex formation with carriers for Pi and ADP/ATP. *J Biol Chem*., **279**(30), 31761-8.

Chu, S.H., Lee-Kang, J., Lee, K.H., Lee, K. (2003) Roles of reactive cxygen species, NF-kappaB and peroxiredoxins in glycochenodeoxycholic acid-induced rat hepatocytes death. *Pharmacology*, **69**(1), 12-19.

Clark, B.N., Gutstein, H.B. (2008) The myth of automated, high-throughput two-dimensional gel analysis. *Proteomics*, **8**, 1197-1203.

Cleveland, W.S., Devlin, S.J. (1988) Locally Weighted Regression: An Approach to Regression Analysis by Local Fitting. *J Amer Stat Assoc*, **83**(403), 596-610.

Cook, P.D. in: Crooke, S.T. (Ed.) *Antisense Drug Technology: Principles, Strategies and Applications*, Marcel Dekker Inc., New York 2001, pp 29-56.

Corey, D.R. (2007) RNA learns from antisense. *Nature Chem. Biol*., **3**(1), 8-11.

Cory, S., Adams., J.M. (2002) The Bcl2 family: regulators of the cellular life-or-death switch. *Nat Rev Cancer*, **2**(9), 647-656.

Cotten, M., Oberhauser, B., Brunar, H., Holzner, A., Issakides, G., Noe, C.R., Schaffner, G., Wagner, E., Birnstiel, M.L. (1991) 2'-O-methyl, 2'-O-ethyl oligoribonucleotides and phosphorothioate oligodeoxyribonucleotides as inhibitors of the in vitro U7 snRNP-dependent mRNA processing event. *Nucleic Acids Res*., **19**(10), 2629-2635.

Coultas, L., Strasser, A. (2003) The role of the Bcl-2 protein family in cancer. *Sem Cancer Biol.*, **13**, 115.123.

Crooke, S.T. (2004) Progress in antisense technology. *Annu Rev Med*, **55**, 61–95.

Danial, N.N., Korsmeyer, S.J. (2004) Cell death: critical control points. *Cell*; **116**(2), 205-219.

Dickinson, L., Burnett, R., Melander, C., Edelson, B.S., Arora, P.S., Dervan, P., Gottesfeld, J.M. (2004) Arresting Cancer Proliferation by Small-Molecule Gene Regulation. *Chem Biol*., **11**, 1583–1594. Erratum in: *Chem Biol*, 2006, **13**, 339.

Eckstein, F. (2000) Phosphorothioate oligodeoxynucleotides: what is their origin and what is unique about them? *Antisense Nucleic Acid Drug Dev*., **10**(2), 117-121.

Elbashir, S.M., Harborth, J., Lendeckel, W., Yalcin, A., Weber, K., Tuschl, T. (2001) Duplexes of 21-nucleotide RNAs mediate RNA interference in cultured mammalian cells. *Nature*, **411**(6836), 494-498.

Elbashir, S.M., Lendeckel, W., Tuschl, T. (2001) RNA interference is mediated by 21- and 22-nucleotide RNAs. *Genes Dev*., **15**, 188-200.

Ellerhorst, J., Nguyen, T., Cooper, D.N., Estrov, Y., Lotan, D., Lotan, R. (1999) Induction of differentiation and apoptosis in the prostate cancer cell line LNCaP by sodium butyrate and galectin-1. *J. Oncol*., **14**(2), 225-232.

Fievet, J., Dillmann, C., Lagniel, G., Davanture, M., Negroni, L., Labarre, J., de Vienne, D. (2004) Assessing factors for reliable quantitative proteomics based on two-dimensional gel electrophoresis. *Proteomics*, **4**(7), 1939-49.

Fire A, Xu S, Montgomery MK, Kostas SA, Driver SE, Mello CC. (1998) Potent and specific genetic interference by double-stranded RNA in Caenorhabditis elegans. *Nature*, **391**(6669), 806-811.

Fischer, U., Schulze-Osthoff, K. (2005) Apoptosis-based therapies and drug targets. *Cell Death Differ*., **12**(Suppl 1), 942-961.

Friedman, D.B. in: Matthiesen, R. (Ed.) *Methods in Molecular Biology, Vol.367: Mass Spectrometry Data Analysis in Proteomics*, Humana Press, 2007, pp 219-239.

Gekeler, V., Gimmnich, P., Hofmann, H.P., Grebe, C., Römmele, M., Leja, A., Baudler, M., Benimetskaya, L., Gonser, B., Pieles, U., Maier, T., Wagner, T., Sanders, K., Beck, J.F., Hanauer, G., Stein, C.A. (2006) G3139 and other CpG-containing immunostimulatory phosphorothioate oligodeoxynucleotides are potent suppressors of the growth of human tumor xenografts in nude mice. *Oligonucleotides*, **16**(1), 83-93.

Giorgi, C., Romagnoli, A., Pinton, P., Rizzuto, R. (2008) Ca2+ signaling, mitochondria and cell death. *Curr. Mol. Med*., **8**(2). 119-130.

Gjertsen, B.T., Bredholt, T., Anensen, N., Vintermyr, O.K. (2007) Bcl-2 antisense in the treatment of human malignancies: a delusion in targeted therapy. *Curr Pharm Biotechnol*., **8**(6), 373-381.

Glish, G.L., Vachet, R.W. (2003) The basics of mass spectronomy in the twenty-first century. *Nature Rev Drug Discov*, **2**, 140-150.

Grimm, D. (2009) Small silencing RNAs: state-of-the-art. *Adv Drug Deliv Rev*., **61**(9), 672-703.

Gul, O., Basaga, H., Kutuk, O. (2008) Apoptotic blocks and chemotherapy resistance: strategies to identify Bcl-2 protein signatures. *Brief Funct Genomic Proteomic*, **7**(1), 27-34.

Harris, R.A. in Devlin, T.M. (Ed.): *Textbook of Biochemistry with Clinical Correlations*, Wiley-Liss, 2006 (6th edition), New York, USA, pp 582-608.

Herbst, R.S., Frankel, S.R. (2004) Oblimersen sodium (Genasense bcl-2 antisense oligonucleotide): a rational therapeutic to enhance apoptosis in therapy of lung cancer. *Clin. Cancer Res.*, **10**(12), 4245-4248.

Hillenkamp, F., Karas, M. in: Hillenkamp, F., Peter-Katalinic, J. (Eds.) *MALDI MS. A practical guide to instrumentation, methods and applications*, Wiley-VCH, Weinheim 2007, pp 1-28.

Hjerno, K., Jensen, O.N. in: Hillenkamp, F., Peter-Katalinic, J. (Eds.) *MALDI MS. A practical guide to instrumentation, methods and applications*, Wiley-VCH, Weinheim 2007, pp 83-108.

Honore, B., Vorum, H. (2000) The CREC family, a novel family of mutiple EF-hand, low-affinity Ca2+-binding proteins localised to the secretory pathway of mammalian cells. *FEBS Lett.*, **466**(1), 11-18.

Hua, Y.J., Tu, K., Tang, Z.Y., Li, Y.X., Xiao, H.S. (2008) Comparison of normalization methods with microRNA microarray. *Genomics*, **92**(2), 122-128.

Immenschuh, S., Baumgart-Vogt, E. (2005) Peroxiredoxins, oxidative stress and cell proliferation. *Antioxid. Redox Signal*, **7**(5-6), 768-777.

Jackson, A.L., Bartz, S.R., Schelter, J., Kobayashi, S.V., Burchard, J., Mao, M., Li, B., Cavet, G., Linsley, P.S. (2003) Expression profiling reveals off-target gene regulation by RNAi. *Nat Biotechnol*, **21**, 635-637.

Jansen, B., Schlagbauer-Wadl, H., Kahr, H., Heere-Ress, E., Mayer, B.X., Eichler, H., Pehamberger, H., Gana-Weisz, M., Ben-David, E., Kloog, Y., Wolff, K. (1999) Novel Ras antagonist blocks human melanoma growth. *Proc Natl Acad Sci USA*, **96**(24), 14019-24.

Jansen, B., Wacheck, V., Heere-Ress, E., Schlagbauer-Wadl, H., Hoeller, C., Lucas, T., Hoermann, M., Hollenstein, U., Wolff, K., Pehamberger, H. (2000) Chemosensitisation of malignant melanoma by BCL2 antisense therapy. *Lancet,* **356**(9243), 1728-1733.

Jensen, L. J., Kuhn, M., Stark, M., Chaffron, S., Creevey, C., Muller, J., Doerks, T., Julien, P., Roth, A., Simonovic, M., Bork, P., von Mering, C. (2009) STRING 8--a global view on proteins and their functional interactions in 630 organisms. *Nucleic Acids Res.*, 37, D412-416.

Jepsen, J.S., Wengel, J. (2004) LNA-antisense rivals siRNA for gene silencing. *Curr Opin Drug Discov Devel.*, **7**(2), 188-194.

Johnson, R.S., Martin, S.A., Biemann, K. (1988) Collision-induced fragmentation of $(M + H)^+$ ions of peptides. Side chain specific sequence ions. *Int J Mass Spectrom Ion Process*, **86**, 137-154.

Johnson, W.C., in: Berova, N., Nakanishi, K., Woody, R.W. (Eds.) *Circular Dichroism: Principles and Applications,* 2nd edition, Wiley-VCH, New York 2000, p. 703-718.

Karas, M., Bachmann, D., Hillenkamp, F. (1985) Influence of the wavelength in high-irradiance ultraviolet laser desorption mass spectrometry of organic molecules. *Anal. Chem*., **57**, 2935-2939.

Karp, N.A., Feret, R., Rubtsov, D.V., Lilley, K.S. (2008) Comparison of DIGE and post-stained gel electrophoresis with both traditional and SameSpots analysis for quantitative proteomics. *Proteomics*, **8**, 948-960.

Kerr, L.E., Birse-Archbold, J.L., Short, D.M., McGregor, A.L., Heron, I., Macdonald, D.C., Thompson, J., Carlson, G.J., Kelly, J.S., McCulloch, J., Sharkey, J. (2007) Nucleophosmin is a novel Bax chaperone that regulates apoptotic cell death. *Oncogene*, **26**(18), 2554-2562.

Kim, J., Dang, C.V. (2005) Multifaceted roles of glycolytic enzymes. *Trends Biochem. Sci*., **30**(3), 142-150.

Kondoh, H., Lleonart, M.E., Bernard, D., Gil, J. (2007) Protection from oxidative stress by enhanced glycolysis; a possible mechanism of cellular immortalization. *Histol. Histopathol.*, **22**(1), 85-90.

Krieg, A.M., Guga, P., Stec, W. (2003) P-chirality-dependent immune activation by phosphorothioate CpG oligodeoxynucleotides. *Oligonucleotides*., **13**(6), 491-499.

Kroemer, G., Reed, J.C. (2000) Mitochondrial control of cell death. *Nat Med*, **6**(5), 513-519.

Laemmli, U.K. (1970) Cleavage of structural proteins during the assembly of the head of bacteriophage T4. *Nature*, **227**, 680-685.

Lai, J.C., Tan, W., Benimetskaya, L., Miller, P., Colombini, M., Stein, C.A. (2006) A pharmacologic target of G3139 in melanoma cells may be the mitochondrial VDAC. *Proc. Natl. Acad. Sci. USA*, **103**(19), 7494-7499.

Levin, A.A., Henry, S.P., Monteith, D., Templin, M.V. in: Crooke, S.T. (Ed.) *Antisense Drug Technology: Principles, Strategies and Applications,* Marcel Dekker Inc., New York 2001, pp 201-267.

MacFarlane, M., Williams, A.C. (2004) Apoptosis and disease: a life or death decision. *EMBO Rep*, **5**(7), 674-678.

Mahato, R.I., Cheng, K., Guntaka, R.V. (2005) Modulation of gene expression by antisense and antigene oligodeoxynucleotides and small interfering RNA. *Expert Opin. Drug Deliv.,* **2**(1), 3-28.

Marchetti, M., Hirschmann, J., Förster-Waldl, E., Allmaier G. in: Vekey, K., Telekes, A., Vertes, A. (Eds.) *Medical Applications of Mass Spectrometry*, Elsevier, 2008, pp 449-475.

Marengo, E., Robotti, E., Antonucci, F., Cecconi, D., Campostrini, N., Righetti, P.G. (2005) Numerical approaches for quantitative analysis of two-dimensional maps: a review of commercial software and home-made systems. *Proteomics*, **5**, 654-666.

Mathieu, V., LeMercier, M., DeNeve, N., Sauvage, S., Gras, T., Roland, I., Lefranc, F., Kiss, R. (2007) Galectin-1 knockdown increases sensitivity to temozolomide in a B16F10 mouse metastatic melanoma model. *J. Invest. Dermatol*., **127**(10), 2399-2410.

Mattow, J., Schmidt, F., Höhenwarter, W., Siejak, F., Schaible, U.E., and Kaufmann, S.H. (2004) Protein identification and tracking in two-dimensional electrophoretic gels by minimal protein identifiers. *Proteomics*, **4**, 2927-2941.

Mayer, G. (2009) The chemical biology of aptamers. *Angew Chem Int Ed Engl*., **48**(15), 2672-2689.

Meidan, V.M., Glezer, J., Salomon, S., Sidi, Y., Barenholz, Y., Cohen, J.S., Lilling, G. (2006) Specific lipoplex-mediated antisense against Bcl-2 in breast cancer cells: a comparison between different formulations. *J Liposome Res*, **16**(1), 27-43.

Mello, C.C., Conte, D. (2004) Revealing the world of RNA interference. *Nature* (London), **431**, 338-342.

Milhavet, O., Gary, D.S., Mattson, M.P. (2003) RNA interference in biology and medicine. *Pharmacol Rev*., **55**(4), 629-648.

Miller, I., Crawford, J., Gianazza, E. (2006) Protein stains for proteomic applications: Which, when, why? *Proteomics*, **6**, 5385-5408.

Miller, I., Radwan, M., Strobl, B., Müller, M., Gemeiner, M. (2006) Contribution of cell culture additives to the two-dimensional protein pattern of mouse macrophages. *Electrophoresis,* **27**, 1626-1629.

Minden, J. (2007) Comparative proteomics and difference gel electrophoresis. *Biotechniques*, **43**, 739-743.

Monia, B.P., Lesnik, E.A., Gonzalez, C., Lima, W.F., McGee, D., Guinosso, C.J., Kawasaki, A.M., Cook, P.D., Freier, S.M. (1993) Evaluation of 2'-modified oligonucleotides containing 2'-deoxy gaps as antisense inhibitors of gene expression. *J Biol Chem*., **268**(19), 14514-14522.

Monia, B.P., Koller, E., Gaarde, W.A. in: Crooke, S.T. (Ed.) *Antisense Drug Technology: Principles, Strategies and Applications,* Marcel Dekker Inc., New York 2001, pp 83-105.

Moreira JN, Santos A, Simões S. (2006) Bcl-2-targeted antisense therapy (Oblimersen sodium): towards clinical reality. *Rev. Recent Clin. Trials*, **1**(3), 217-235.

Nemunaitis, J., Nemunaitis, M., Senzer, N., Snitz, P., Bedell, C., Kumar, P., Pappen, B., Maples, P.B., Shawler, D., Fakhrai, H. (2009) Phase II trial of Belagenpumatucel-L, a TGF-beta2 antisense gene modified allogeneic tumor vaccine in advanced non small cell lung cancer (NSCLC) patients. *Cancer Gene Ther*., 16(8), 620-624.

Nieth, C., Priebsch, A., Stege, A., Lage, H. (2003) Modulation of the classical multidrug resistance (MDR) phenotype by RNA interference (RNAi). *FEBS Lett*., **545**(2-3), 144-150.

Noe, C.R., Kaufhold, L. in: Gualtieri, F. (Ed.): *New Trends in Synthetic Medicinal Chemistry: Chemistry of Antisense Oligonucleotides,* Wiley-VCH, New York 2000, pp 261-347.

Noe, C.R., Winkler, J., Urban, E., Gilbert, M., Haberhauer, G., Brunar, H. (2005) Zwitterionic oligonucleotides: a study on binding properties of 2'-O-aminohexyl modifications. *Nucleosides Nucleotides Nucleic Acids*., **24**(8), 1167-1185.

O'Connor, P.B., Hillenkamp, F. in: Hillenkamp, F., Peter-Katalinic, J. (Eds.) *MALDI MS. A practical guide to instrumentation, methods and applications*, Wiley-VCH, Weinheim 2007, pp 29-82.

O'Farrell, P.H. (1975) High resolution two-dimensional electrophoresis of proteins. *J Biol Chem,* **250**, 4007-4021.

Opalinska, J.B., Gewirtz, A.M. (2002) Nucleic-acid therapeutics: Basic principles and recent applications. *Nature Rev Drug Discov*, 1, 503-514.

Paroo, Z., Corey, D.R. (2004) Challenges for RNAi in vivo. *TRENDS Biotechnol*., **22**(8), 390-394.

Pastorino, J.G., Hoek, J.B. (2008) Regulation of hexokinase binding to VDAC. *J Bioenerg Biomembr.,* **40**(3), 171-182.

Pedersen, P.L. (2007) Warburg, me and Hexokinase 2: Multiple discoveries of key molecular events underlying one of cancers' most common phenotypes, the "Warburg Effect", i.e., elevated glycolysis in the presence of oxygen. *J. Bioenerg. Biomembr*., **39**(3), 211-222.

Perkins, D.N., Pappin, D.J., Creasy, D.M., and Cottrell, J.S. (1999) Probability-based protein identification by searching sequence databases using mass spectrometry data. *Electrophoresis*, **20**, 3551-3567.

Petrak, J., Ivanek, R., Toman, O., Cmejla, R., Cmejlova, J., Vyoral, D., Zivny, J., Vulpe, C.D. (2008) Déjà vu in proteomics. A hit parade of repeatedly identified differentially expressed proteins. *Proteomics*, **8**(9), 1744-1749.

Qi, W., Shakalya, K., Stejskal, A., Goldman, A., Beeck, S., Cooke, L., Mahadevan, D. (2008) NSC348884, a nucleophosmin inhibitor disrupts oligomer formation and induces apoptosis in human cencer cells. *Oncogene*, **27**(30), 4210-4220.

Rao, M., Sockanathan, S. (2005) Molecular Mechanisms of RNAi: Implications for Development and Disease. *Birth Defects Res*., **75**, 28-42.

Reed J.C. (1995) Bcl-2 family proteins: regulators of chemoresistance in cancer. *Toxicol. Lett.*, **82-83**, 155-158.

Reed, J.C. (1998) Bcl-2 family proteins. *Oncogene*, **17**(25), 3225-3236.

Reed, J.C. (2002) Apoptosis-based therapies. *Nat Rev Drug Discov*., **1**(2), 111-121.

Reed, J.C. (2003) Apoptosis-targeted therapies for cancer. *Cancer Cell*, **3**, 17-22.

Reed JC. (2008) Bcl-2–family proteins and hematologic malignancies: history and future prospects. *Blood,* **111**(7), 3322-3330.

Roepstorff, P., Fohlman, J. (1984) Proposal for a common nomenclature for sequence ions in mass-spectra of peptides. *Biomed Mass Spectrom*, **11**(11), 601.

Rowe, S.P., Casey, R.J., Brennan, B.B., Buhrlage, S.J., Mapp, A.K. (2007) Transcriptional up-regulation in cells mediated by a small molecule. *J Am Chem Soc*., **129**(35), 10654-10655.

Savitzky, A., Golay, M. (1964) Smoothing and differentiation of data by simplified least squares. *Anal Chem*, **36**, 1627-1639.

Scacheri, P.C., Rozenblatt-Rosen, O., Caplen, N.J., Wolfsberg, T.G., Umayam, L., Lee, J.C., Hughes, C.M., Shanmugam, K.S., Bhattacharjee, A., Meyerson, M., Collins, F.S. (2004) Short interfering RNAs can induce unexpected and divergent changes in the levels of untargeted proteins in mammalian cells. *Proc Natl Acad Sci USA*, **101**(7), 1892-1897.

Schlags, W., Walther, M., Masree, M., Kratzel, M., Noe, C.R., Lachmann, B. (2005) Towards validating a method for two-dimensional electrophoresis/silver staining. *Electrophoresis,* **26**, 2461-2469.

Schröder, S., Zhang, H., Yeung, E.S., Jänsch, L., Zabel, C., Wätzig, H. (2008) Quantitative gel electrophoresis: sources of variation. *J Proteome Research*, **7**, 1226-1234.

Shevchenko, A., Wilm, M., Vorm, O., Mann, M. (1996) Mass spectrometric sequencing of proteins silver-stained polyacrylamide gels. *Anal Chem*, **68**, 850-858.

Shoshan-Barmatz, V., Keinan, N., Zaid, H. (2008) Uncovering the role of VDAC in the regulation of cell life and death. *J. Bioenerg. Biomembr*., **40**(3), 183-191.

Simamura, E., Shimada, H., Hatta, T., Hirai, K. (2008) Mitochondrial voltage-dependent anion channels (VDACs) as novel pharmacological targets for anti-cancer agents. *J Bioenerg Biomembr*., **40**(3), 213-217.

Simoes-Wüst, A.P., Hopkins-Donaldson, S., Sigrist, B., Belyanskaya, L., Stahel, R.A., Zangemeister-Wittke, U. (2004) A functionally improved locked nucleic acid antisense oligonucleotide inhibits Bcl-2 and Bcl-xL expression and facilitates tumor cell apoptosis. *Oligonucleotides*., **14**(3), 199-209.

Sioud, M., Sørensen, D.R. (2003) Cationic liposome-mediated delivery of siRNAs in adult mice. *Biochem. Biophys. Res. Commun*., **312**, 1220–1225.

Sioud, M. (2007) RNA interference and innate immunity. *Adv Drug Deliv Rev*, **59**, 153–163.

Sitek, B., Scheibe, B., Jung, K., Schramm, A., Stuehler, K., in: Marcus, K., Stuehler, K., van Hall, A., Hamacher, M. *et al*. (Eds.), *Proteomics in Drug Research*, Wiley-VCH, Weinheim 2006, pp. 33-55.

Smaili, S.S., Hsu, Y.T., Youle, R.J., Russell, J.T. (2000) Mitochondria in Ca2+ Signaling and Apoptosis. *J. Bioener. Biomembr*., **32**(1), 35-46.

Smejkal, G.B., Robinson, M.H., Lazarev, A. (2004) Comparison of fluorescent stains: relative photostability and differential staining of proteins in two-dimensional gels. *Electrophoresis*, **25**, 2511-2519.

Smirnov, I. P., Zhu, X., Taylor, T., Huang, Y., Ross, P., Papayanopoulos, I.A., Martin, S.A., and Pappin, D.J. (2004) Suppression of alpha-cyano-4-hydroxycinnamic acid matrix clusters and reduction of chemical noise in MALDI-TOF mass spectrometry. *Anal Chem*, **76**, 2958-2965.

Stein, C.A., Cheng, Y.C. (1993) Antisense oligonucleotides as therapeutic agents--is the bullet really magical? *Science*, **261**, 1004-1012.

Stein, C.A., Colombini, M. (2008) Specific VDAC inhibitors: phosphorothioate oligonucleotides. *J Bioenerg Biomembr*., **40**(3), 157-62.

Stein, C.A., Wu, S., Voskresenskiy, A.M., Zhou, J.F., Shin, J., Miller, P., Souleimanian, N., Benimetskaya, L. (2009) G3139, an anti-Bcl-2 antisense oligomer that binds heparin-binding growth factors and collagen I, alters in vitro endothelial cell growth and tubular morphogenesis. *Clin Cancer Res*, **15**(8), 2797-2807.

Stessl, M., Noe, C.R., Lachmann, B. (2009) Influence of image-analysis software on quantitation of two-dimensional gel electrophoresis data. *Electrophoresis*, **30**(2), 325-328.

Stessl, M., Marchetti-Deschmann, M., Winkler, J., Lachmann, B., Allmaier, G., Noe, C.R. (2009) A proteomic study reveals unspecific apoptosis induction and reduction of glycolytic enzymes by the phosphorothioate antisense oligonucleotide oblimersen in human melanoma cells. *J Proteomics*, **72**(6), 1019-1030.

Subramanian, A., Miller, D.M. (2000) Structural analysis of alpha-enolase. Mapping the functional domains involved in down-regulation of the c-myc protooncogene. *J. Biol. Chem*., **275**(5), 5958-5965.

Summerton, J. (1999) Morpholino antisense oligomers: the case for an RNase H-independent structural type. *Biochim Biophys Acta*., **1489**(1), 141-158.

Summerton, J.E. (2007) Morpholino, siRNA, and S-DNA compared: impact of structure and mechanism of action on off-target effects and sequence specificity. *Curr Top Med Chem.*, **7**(7), 651-60.

Sun, S.Y., Yue, P., Zhou, J.Y., Wang, Y., Choi Kim, H.R., Lotan, R., Wu, G.S. (2001) Overexpression of BCL2 blocks TNF-related apoptosis-inducing ligand (TRAIL)-induced apoptosis in human lung cancer cells. *Biochem Biophys Res Commun*., **280**(3), 788-797.

Tamura, K., Yoshie, M., Hara, T., Isaka, K., Kogo, H. (2007) Involvement of stathmin in proliferation and differentiation of immortalized human endometrial stromal cells. *J Reprod Dev.*, **53**(3), 525-33.

Tan, W., Lai, J.C., Miller, P., Stein, C.A., Colombini, M. (2007) Phosphorothioate oligonucleotides reduce mitochondrial outer membrane permeability to ADP. *Am. J. Physiol. Cell Physiol.*, **292**(4); 1388-1397.

Tang, G. (2005) siRNA and miRNA: an insight into RISCs. *TRENDS Biochem Sciences*, **30**(2), 106-114.

Tarhini, A.A., Kirkwood, J.M. (2007) Oblimersen in the treatment of metastatic melanoma. *Future Oncol*, **3**(3), 263-271

Thallinger, C., Werzowa, J., Poeppl, W., Kovar, F.M., Pratscher, B., Valent, P., Quehenberger, P., Joukhadar, C. (2007) Comparison of a treatment strategy combining CCI-779 plus DTIC versus DTIC monotreatment in human melanoma in SCID mice. *J Invest Dermatol*, **127**(10), 2411-7.

Thiede, B., Rudel, T. (2004) Proteome analysis of apoptotic cells. *Mass Spec. Rev.*, **23**(5), 333-349.

Thinnes, F.P. (2009) Neuroendocrine differentiation of LNCaP cells suggests: VDAC in the cell membrane is involved in the extrinsic apoptotic pathway. *Mol Genet Metab*., **97**(4), 241-243.

Tolcher, A.W. (2005) Targeting Bcl-2 protein expression in solid tumors and hematologic malignancies with antisense oligonucleotides. *Clin Adv Hematol Oncol*, **3**(8), 635-642, 662.

Tong, Y., Bouska, J.J., Ellis, P.A., Johnson, E.F., Leverson, J., Liu, X., Marcotte, P.A., Olson, A.M., Osterling, D.J., Przytulinska, M., Rodriguez, L.E., Shi, Y., Soni, N., Stavropoulos, J., Thomas, S., Donawho, C.K., Frost, D.J., Luo, Y., Giranda, V.L., Penning, T.D. (2009) Synthesis and evaluation of a new generation of orally efficacious benzimidazole-based poly(ADP-ribose) polymerase-1 (PARP-1) inhibitors as anticancer agents. *J Med Chem*, **52**(21), 6803-6813.

Tonge, R., Shaw, J., Middleton, B., Rowlinson, R., Rayner, S., Young, J., Pognan, F., Hawkins, E., Currie, I., Davison, M. (2001) Validation and development of fluorescence two-dimensional differential gel electrophoresis proteomics technology. *Proteomics*; **1**(3), 377-396.

Tsujimoto, Y., Finger, L.R., Yunis, J., Nowell, P.C., Croce, C.M. (1984) Cloning of the chromosome breakpoint of neoplastic B cells with the t(14;18) chromosome translocation. *Science*, **226,** 1097-1099.

Tsujimoto, Y., Ikegaki, N., Croce, C.M. (1987) Characterization of the protein product of bcl-2, the gene involved in human follicular lymphoma. *Oncogene*, **2**(1), 3-7.

Tsujimoto, Y., Shimizu, S. (2007) Role of the mitochondrial membrane permeability transition in cell death. *Apoptosis*, **12**(5), 835-840.

Tsuruo, T., Naito, M., Tomida, A., Fujita, N., Mashima, T., Sakamoto, H., Haga, N. (2003) Molecular targeting therapy of cancer: drug resistance, apoptosis and survival signal. *Cancer Sci*., **94**(1), 15-21.

Turhani, D., Krapfenbauer, K., Thurnher, D., Langen, H., Fountoulakis, M. (2006) Identification of differentially expressed, tumor-associated proteins in oral squamous cell carcinoma by proteomic analysis. *Electrophoresis*, **27**(7), 1417-1423.

Tüting, T., Austyn, J., Storkus, W.J., Falo, L.D. in: Lowrie, D.B., Whalen, R.G. (Eds): *Methods in Molecular Medicine, vol. 29, DNA vaccines: Methods and Protocols*. Humana Press Inc. 2000, New Jersey, USA.

Ünlü, M., Morgan, M.E., Minden, J. (1997) Difference gel electrophoresis: a single gel method for detecting changes in protein extracts. *Electrophoresis*, **18**, 2071-2077.

Uprichard, S.L. (2005) The therapeutic potential of RNA interference. *FEBS Letters*, **579**, 5996-6007.

Urban, E., Noe, C.R. (2003) Structural modifications of antisense oligonucleotides. *Farmaco*, **58** (3), 243-258.

Van Engeland, M., Ramaekers, F.C., Schutte, B., Reutelingsperger, C.P. (1996) A novel assay to measure loss of plasma membrane asymmetry during apoptosis of adherent cells in culture. *Cytometry*, **24**(2), 131-9.

Vorm, O., Roepstorff, P., Mann, M. (1994) Improved resolution and very high sensitivity in MALDI TOF of matrix surfaces made by fast evaporation. *Anal Chem*, **66**, 3281-3287.

Wacheck, V., Heere-Ress, E., Halaschek-Wiener, J., Lucas, T., Meyer, H., Eichler, H.G., Jansen, B. (2001) Bcl-2 antisense oligonucleotides chemosensitize human gastric cancer in a SCID mouse xenotransplantation model. *J. Mol. Med*., **79**(10), 587-593.

Wacheck, V., Krepler, C., Strommer, S., Heere-Ress, E., Klem, R., Pehamberger, H., Eichler, H.G., Jansen, B. (2002) Antitumor effect of G3139 Bcl-2 antisense oligonucleotide is independent of its immune stimulation by CpG motifs in SCID mice. *Antisense Nucleic Acid Drug Dev.*, **12**(6), 359-367.

Wacheck, V., Losert, D., Günsberg, P., Vornlocher, H.P., Hadwiger, P., Geick, A., Pehamberger, H., Müler, M., Jansen, B. (2003) Small interfering RNA targeting Bcl-2 sensitizes malignant melanoma. *Oligonucleotides*, **13**, 393-400.

Walker, T., Wendel, H.P., Tetzloff, L., Heidenreich, O., Ziemer, G. (2005) Suppression of ICAM-1 in human venous endothelial cells by small interfering RNAs. *Eur J Cardiothorac Surg,* **28**(6), 816-20.

Wang, W., Eddy, R., Condeelis, J. (2007) The cofilin pathway in breast cancer invasion and metastasis. *Nat. Rev. Cancer*, **7**(6), 429-440.

Warburg, O., Wind., F., Negelein, E. (1930) Ueber den Stoffwechsel von Tumoren im Körper. *J Mol Med*., **5**(19), 1432-1440.

Watson, J., Crick, F. (1953) Molecular structure of nucleic acids: a structure for deoxyribose nucleic acid. *Nature*, **171**, 737-8.

Westermeier, R., Marouga, R. (2005) Protein detection methods in proteomics research. *Bioscience Reports*, **25**, 19-32.

Wheelock, A.M., Buckpitt, A.R. (2005) Software-induced variance in two-dimensional gel electrophoresis image analysis. *Electrophoresis*, **26**, 4508-4520.

Wheelock, A.M., Goto, S. (2006) Effects of post-electrophoretic analysis on variance in gel-based proteomics. *Expert Rev Proteomics*, **3**, 129-142.

Williams, J., Lucas, P.C., Griffith, K.A., Choi, M., Fogoros, S., Hu, Y.Y., Liu, J.R. (2005) Expression of Bcl-xL in ovarian carcinoma is associated with chemoresistance and recurrent disease. *Gynecol Oncol*, **96**(2), 287-295.

Willis, S., Day, C.L., Hinds, M.G., Huang, D.C. (2003) The Bcl-2-regulated apoptotic pathway. *J Cell Sci*., **116**(Pt 20), 4053-4056.

Winkler, J. *Rückgratmodifizierte Antisense Oligonukleotide und Konjugate mit 2‘-Aminomodifikationen.* Vienna 2003, University of Vienna, Austria.

Winkler, J., Urban, E., Losert, D., Wacheck, V., Pehamberger, H., Noe, C.R. (2004) A novel concept for ligand attachment to oligonucleotides via a 2'-succinyl linker. *Nucleic Acids Res.*, 32(2), 710-718.

Winkler, J., Noe, C.R. (2007) Oligonucleotide charge reversal: 2'-O-lysylaminohexyl modified oligonucleotides. *Nucleosides Nucleotides Nucleic Acids*., **26**(8-9), 939-942.

Winkler, J., Gilbert, M., Kocourková, A., Stessl, M., Noe, C.R. (2008) 2'-O-Lysylaminohexyl Oligonucleotides: Modifications for Antisense and siRNA. *ChemMedChem*, **3**(1), 102-110.

Winkler, J., Stessl, M., Amartey, J., Noe, C.R. (2010) Off-target effects related to phosphorothioate modification of nucleic acids. *Manuscript submitted to ChemMedChem, Feb., 2010 (DOI: 10.1002/cmdc.200).*

Winkler, W., Zellner, M., Diestinger, M., Babeluk, R., Marchetti, M., Goll, A., Zehetmayer, S., Bauer, P., Rappold, E., Miller, I., Roth, E., Allmaier, G., Oehler, R. (2008) Biological variation of the platelet proteome in the elderly population and its implication for biomarker research. *Mol Cell Proteomics*, **7**(1), 193-203.

Zahn, X., Desiderio, D.M. (2003) Spot volume vs. amount of protein loaded onto a gel: a detailed, statistical comparison of two gel electrophoresis systems. *Electrophoresis*, **24**, 1818-1833.

Zamecnik, P.C., Stephenson, M.L. (1978) Inhibition of Rous sarcoma virus replication and cell transformation by a specific oligodeoxynucleotide. *Proc. Natl. Acad. Sci. USA*, **75**(1), 280-284.

Zeng, Y., Cullen, B.R. (2002) RNA interference in human cells is restricted to the cytoplasm. *RNA*, **8**(7), 855-860.

Zha, H., Aimé-Sempé, C., Sato, T., Reed, J.C. (1996) Proapoptotic protein Bax heterodimerizes with Bcl-2 and homodimerizes with Bax via a novel domain (BH3) distinct from BH1 and BH2. *J Biol Chem*., **271**(13), 7440-7444.

Zhang, W., Chait, B. T. (2000) ProFound: an expert system for protein identification using mass spectrometric peptide mapping information. *Anal Chem*, **72**, 2482-2489.

“Ich habe mich bemüht, sämtliche Inhaber der Bildrechte ausfindig zu machen und ihre Zustimmung zur Verwendung der Bilder in dieser Arbeit eingeholt. Sollte dennoch eine Urheberrechtsverletzung bekannt werden, ersuche ich um Meldung bei mir.“

Martina Stessl

Supplement A

Matrix-assisted laser desorption/ionization (MALDI)

Today, mass spectrometry (MS) is the most useful analytical technique for protein and proteome analysis, as it provides a relatively robust platform for the determination of molecular masses and the characterization of biological molecules [Hjerno *et al.,* 2007]. Depending on the desired information and the complexity of the samples, different strategies have evolved. For proteomics analysis and the analysis of large protein complexes, MS must be combined with protein or peptide separation techniques, which are typically one- or two-dimensional gel electrophoresis or liquid chromatography approaches. The individual proteins/peptides are then identified by searching of the obtained MS-data (m/z values) against *in-silico*-digested proteins from databases, known or predicted sequences. Correlations between the experimental and theoretical data are used for a statistical scoring of the probability for a certain protein identification [Hjerno *et al.,* 2007]. Today, the two main techniques used to generate peptide and protein ions for MS analysis are matrix-assisted laser desorption/ionization (MALDI) and electrospray ionization (ESI), which allow the sensitive detection of large, non-volatile and labile molecules, particularly proteins [Marchetti *et al.*, 2008]. Unlike ESI, in which analyte ions are produced continuously, ions in MALDI are produced by pulsed-laser irradiation of the sample. The technique was first described in 1985 [Karas *et al.,* 1985] and has evolved to an indispensable tool in life sciences and polymer analysis [Hillenkamp *et al.,* 2007]. The sample is co-crystallized with a solid matrix that can absorb the wavelength of emitted light by the laser. In a typical UV-MALDI sample preparation small volumes of an analyte solution (about 10^{-6}M) and a near saturated (ca. 0.1M) matrix solution are mixed, the solvent is evaporated and the matrix crystallizes to form a homogenous bed of small crystals the size of which ranges from a few to a few hundred micrometers, depending on the matrix and preparation technique [Hillenkamp *et al.,* 2007]. The mixture of sample and matrix on a probe is inserted into the vacuum system of the MALDI instrument and after irradiation the gas-phase ions that are formed are directed towards the analyser [Glish *et al.,* 2003].

MALDI technique has several favourable attributes, such as very high levels of sensitivity, often providing data from sub-femtomole ($<1\times10^{-15}$ moles) amounts of sample loading. In addition, the formation of usually singly-protonated analytes and the relatively high tolerance to salts and buffers facilitate further analyses [Glish *et al.,* 2003]. On the one side the fact that most MALDI lasers are of pulsed nature is reported to be an advantage, since ions are formed in discrete events and very little sample is wasted, if mass analysis is coupled with ion fragmentation. On the other hand the pulsed nature of this technique does not allow the coupling of all available mass analysers. Furthermore the presence of matrix, which facilitates ionization, causes a large degree of chemical noise – especially at m/z ratios below 500 Da. As a result, low molecular weight proteins are difficult to analyse with MALDI [Glish *et al.,* 2003].

Matrix-assisted laser desorption/ionization time-of-flight (MALDI-TOF)

The most commonly used mass analyser in MALDI is the time-of-flight (TOF) mass spectrometer, which separates ions according to their velocity. Using MALDI-TOF m/z ratios of up to several hundred thousand can be analysed. Theoretically all ions are formed at the same time and space, are then accelerated (fixed potential of 1-20 kV) towards a TOF drift tube and finally reach the detector, whereupon lower m/z ions achieve higher velocities and consequently arrive earlier at the detector. Thus, by measuring the time it takes to reach the detector after ion formation, m/z ratios of the ions can be determined [Glish *et al.,* 2003]. Better mass resolution, that is the ability to resolve two adjacent peaks going along with better precision (in contrast to mass accuracy, which provides information how close the measured mass is to the theoretical/true mass given in decimal points), can be gained with reflectron TOF instruments. In a reflectron TOF, after travelling through the first flight tube, the ions enter an electrostatic mirror (reflectron) which turns the ions around and directs them towards a second flight distance to the detector. The function of the reflectron is to compensate for small differences in ion velocities with the same m/z ratio, leading to a better resolution [Glish *et al.,* 2003].

Matrix-assisted laser desorption/ionization reflectron time-of-flight mass spectrometry (MALDI-rTOF-MS)

Tandem mass spectrometry (often termed as MS/MS) involves two stages of MS. In the first stage ions of desired m/z (mass-to charge) ratios are isolated from the bulk of ions emanating from the ion source. These so-called parent ions or precursor ions are then induced to undergo a collision induced dissociation that changes (m) and/or (z). These ion products are then analysed in the second stage of the experiment, providing more detailed information about the ion structure [Glish *et al.,* 2003; O'Connor *et al.,* 2007]. Because of the high energy transfer during ionization the MALDI process generally produces metastable ions, allowing a “pseudo-MS/MS” technique. Selected parent ions decay either already in the ionization source, “in-source” decay, or while passing the flight tube, “post-source” decay (PSD), and the fragment ions are then refocused in the reflectron. These fragment ions can be used for structural characterization, provided that the sample is homogenous [O'Connor *et al.,* 2007].

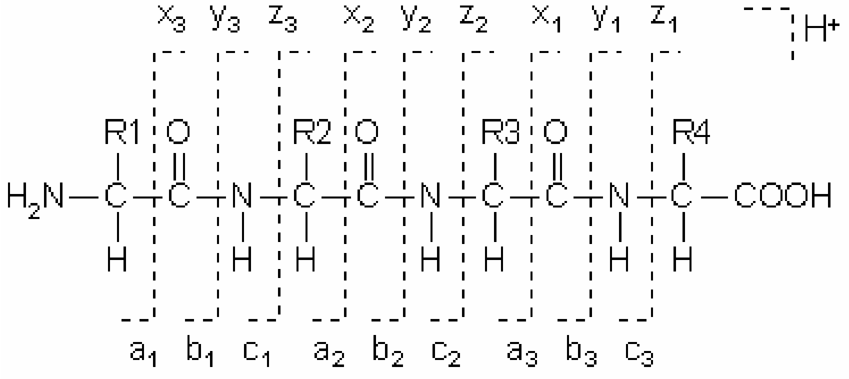
x3 y3 z3 x2 y2 z2 x1 y1 z1
H+
R1 O R2 O R3 O R4
H2N—C—C—N—C—C—N—C—C—N—C—COOH
H H H H H H H
a1 b1 c1 a2 b2 c2 a3 b3 c3

Figure I. Nomenclature for peptide sequencing according to Roepstorff and Fohlman (picture taken from O'Connor *et al.,* 2007). Cleavage at the amide bond is most frequently observed in MALDI MS/MS resulting in y- and b-ions. If the charge is retained on the C-terminal fragment, ions are called y_n-ions. If the charge remains on the N-terminal part, ions are called b_n-ions, where *n* is the number of residues in the fragment.

For peptides, metastable decay predominantly leads to b-and y-fragments (following the Roepstorff nomenclature, figure 1 [Roepstorff *et al.*, 1984]). Larger ions, and proteins in particular, typically lose small neutrals such as water or ammonia, which are not useful for structure elucidation. The yield of fragments from metastable decay can be increased either by choosing a "hot" matrix, such as alpha-cyano-4-cinnamic acid, or by prompt ion extraction in TOF mass spectrometers. Often, the yield of structurally relevant fragments from metastable decay is not sufficient. In this case the ion energy must be increased by external heating. The most common method for this collisional activation of the molecules is the use of inert gas in collision cell, which is termed collision-induced dissociation (CID). The mean collisional energy of individual collisions can be either only a few eV/charge (low-energy CID) or >100eV (high-energy CID). The latter generates additional types of fragments that carry specific structrual information such as the side-chain structure in peptides (d-, w- and z-ions; figure 1 and 2, respectively).

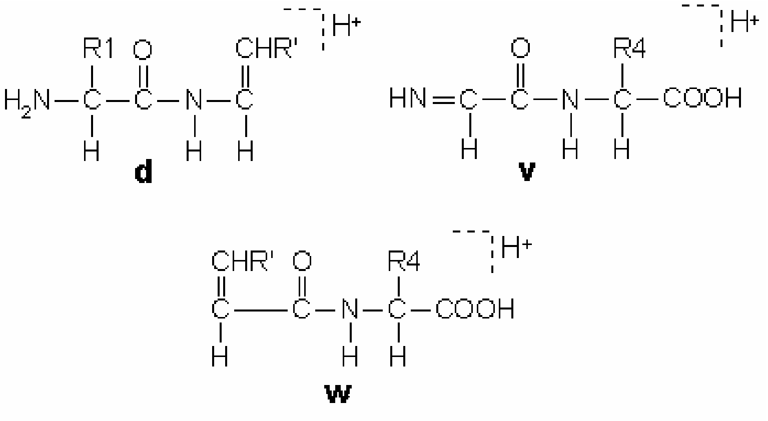

Figure II. Additional ion types generated by high-energy CID (picture taken from Johnson, 1988) at the beta carbon following the loss of the gamma carbon by side chain cleavage. R' is the substituent, if any. Isoleucine and threonine are doubly substituted at the beta carbon, so that side chain loss can give rise to two different ion structures. These pairs are designated d and d' or w and w'.

Mass spectra of reference proteins

Activator of 90kDa heat shock protein ATPase homolog 1 (AHA-1)

The following monoisotopic m/z values were experimentally obtained: 674.40, 816.42, 831.45, 899.47, 906.52, 919.50, 955.59, 997.54, 1088.57, 1484.71, 1713.72 and 2717.90.

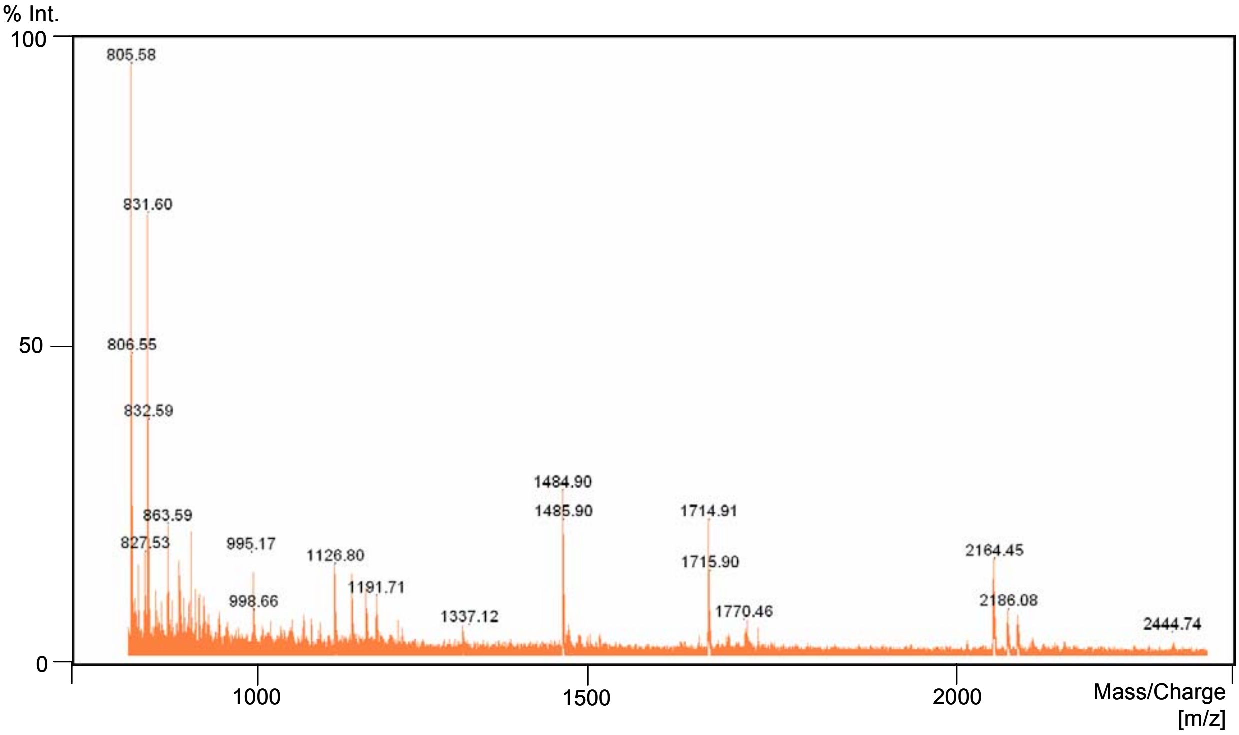

Figure A. Representative peptide mass fingerprint of AHA-1.

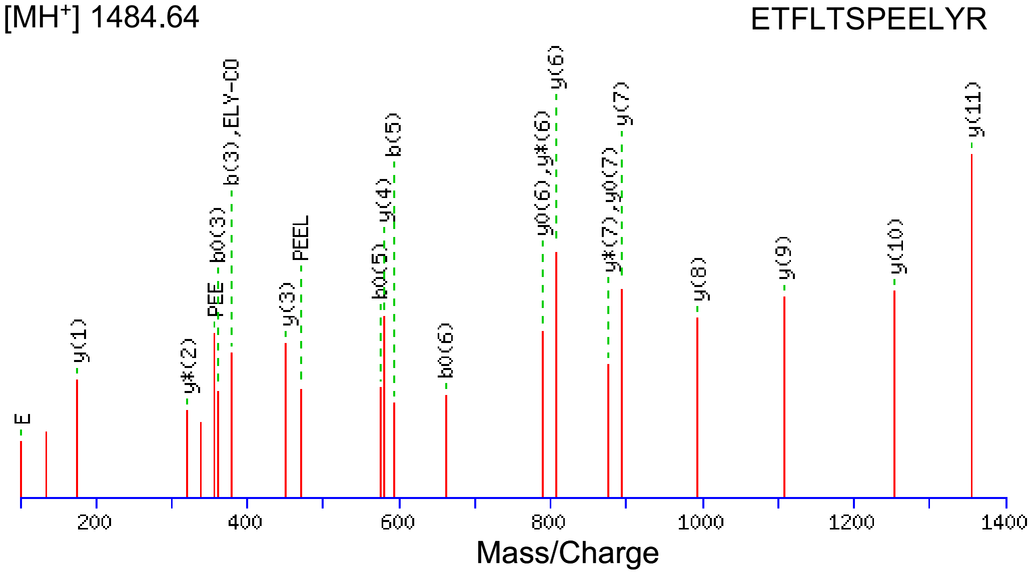

Figure A.a. Mascot result graph of the MALDI-TOF-PSD mass spectrum of the precursor ion m/z = 1484.6 with different ion species indicated.

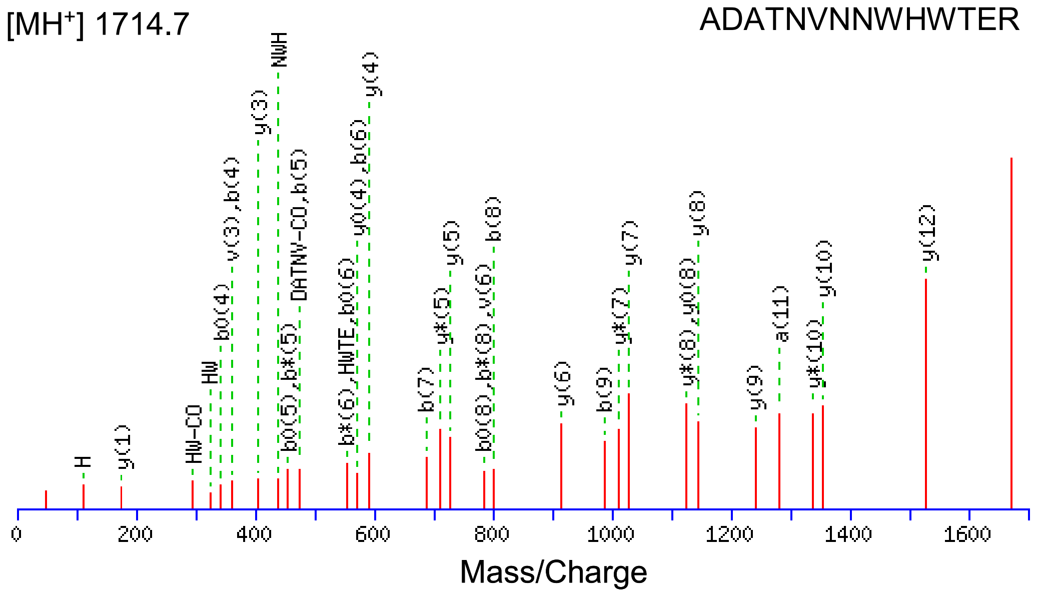

Figure A.b. Mascot result graph of the MALDI-TOF-PSD mass spectrum of the precursor ion m/z = 1714.7 with different ion species indicated.

T-complex protein 1 subunit zeta (TCP-1 zeta)

The following monoisotopic m/z values were experimentally obtained: 572.56, 615.56, 750.64, 757.60, 800.61, 906.56, 916.61, 937.62, 1021.72, 1076.80, 1078.76, 1191.63, 1255.91, 1498.94, 1762.06, 2202.20 and 2544.47.

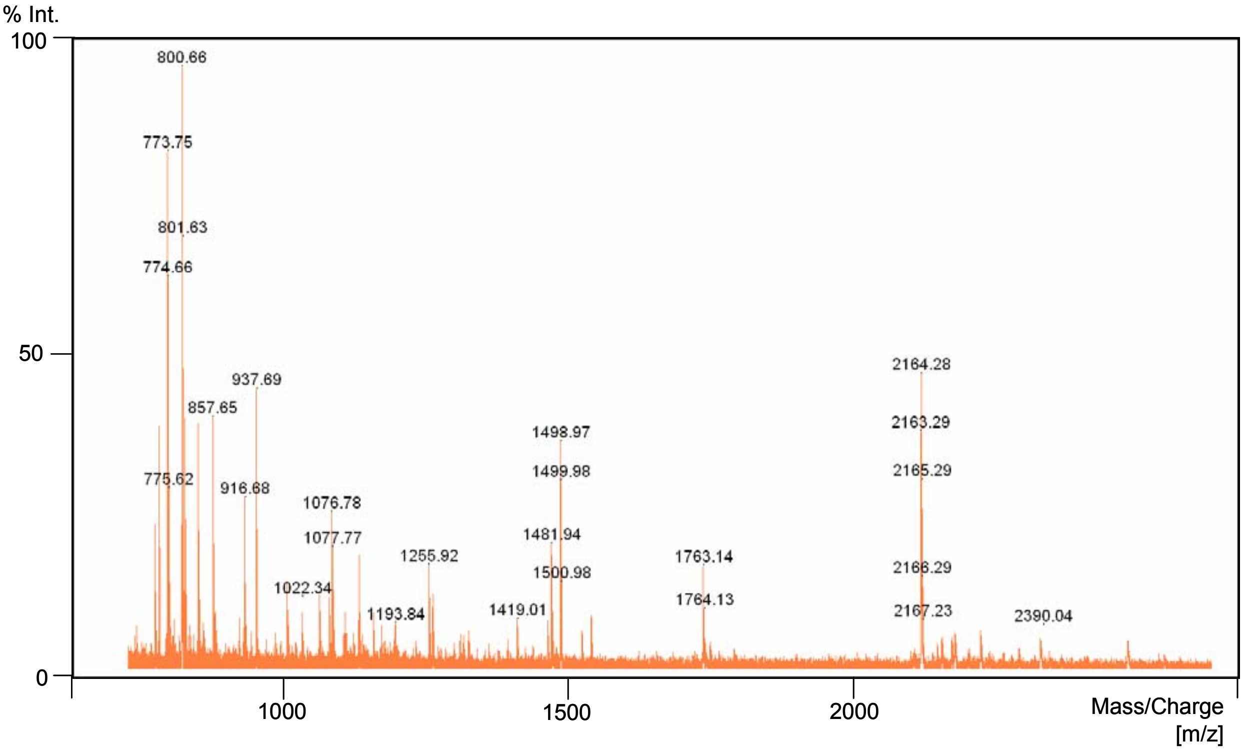

Figure B. Representative peptide mass fingerprint of TCP-1 zeta.

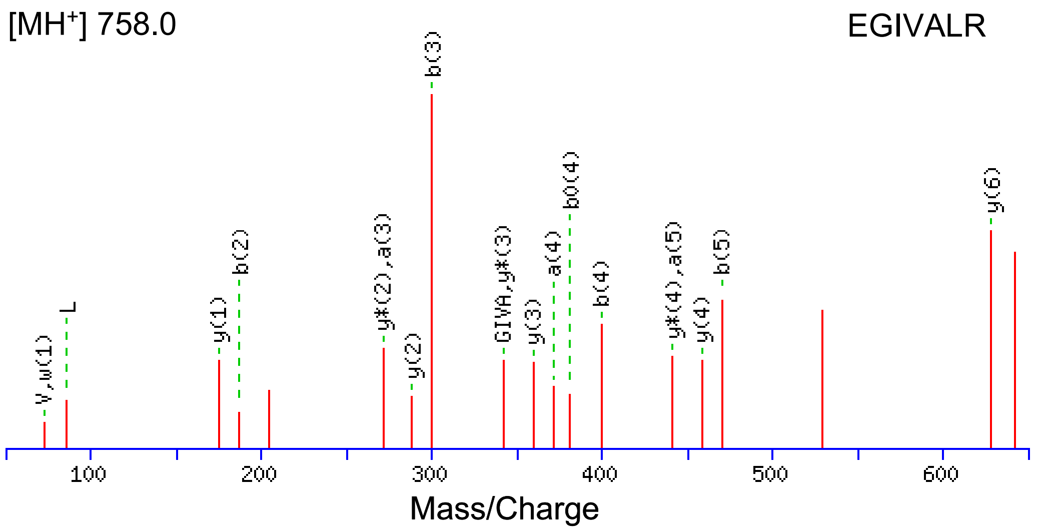

Figure B.a. Mascot result graph of the MALDI-TOF-PSD mass spectrum of the precursor ion m/z = 758.0 with different ion species indicated.

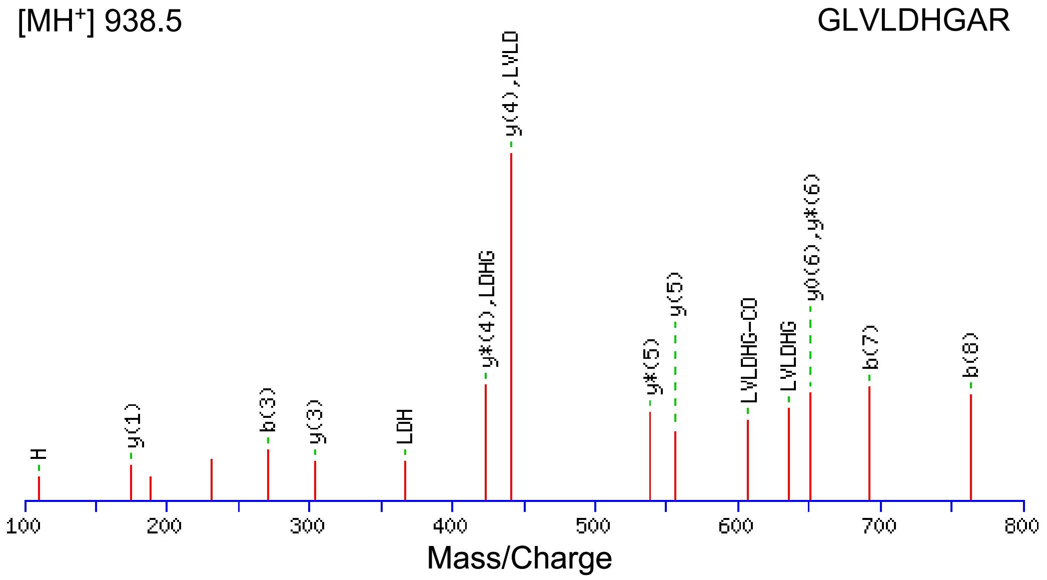

Figure B.b. Mascot result graph of the MALDI-TOF-PSD mass spectrum of the precursor ion m/z = 938.5 with different ion species indicated.

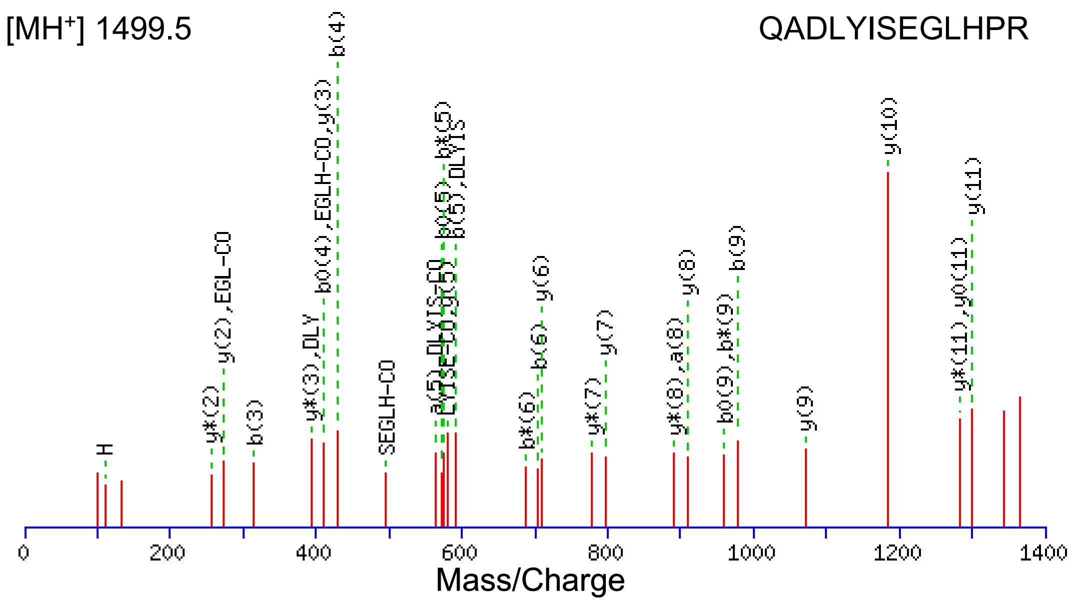

Figure B.c. Mascot result graph of the MALDI-TOF-PSD mass spectrum of the precursor ion m/z = 1499.5 with different ion species indicated.

Elongation factor 2 (EF-2)

The following monoisotopic m/z values were experimentally obtained: 687.54, 752.69, 754.00, 758.68, 760.60, 821.66, 837.61, 890.73, 922.68, 969.78, 1013.73, 1091.81, 1378.97, 1743.07, 1800.15 and 2220.24.

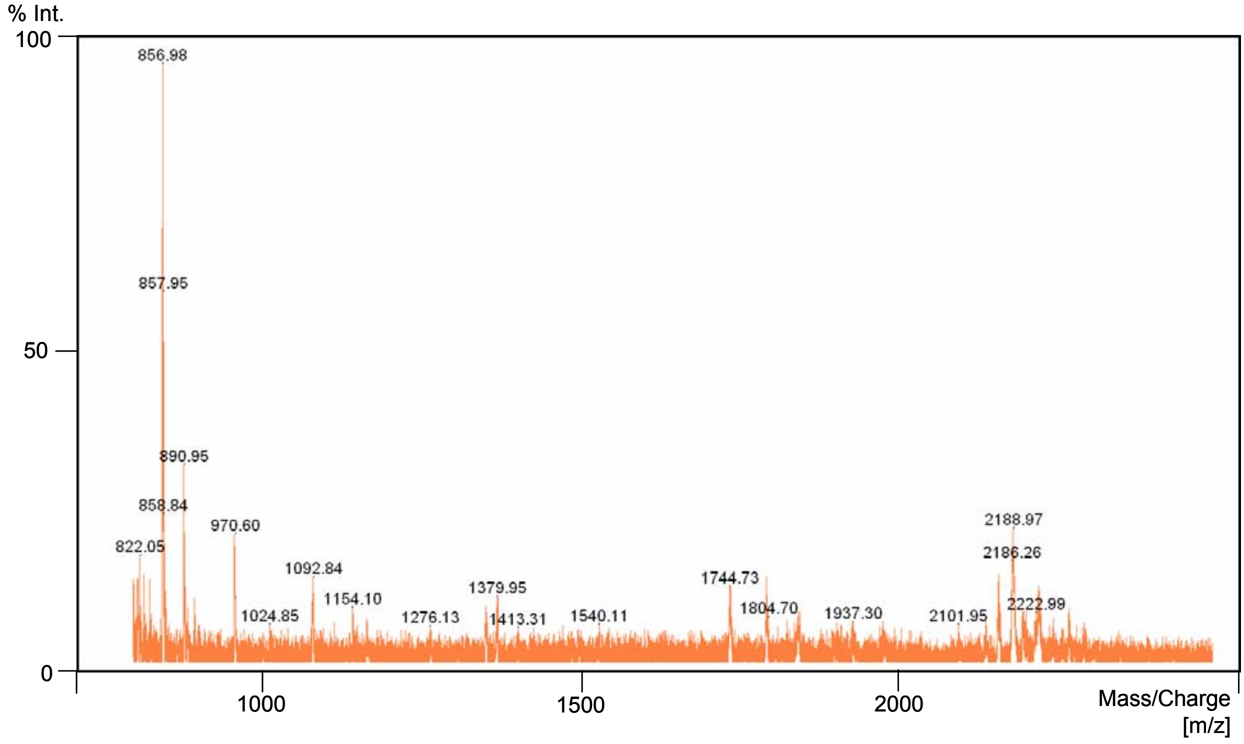

Figure C. Representative peptide mass fingerprint of EF-2.

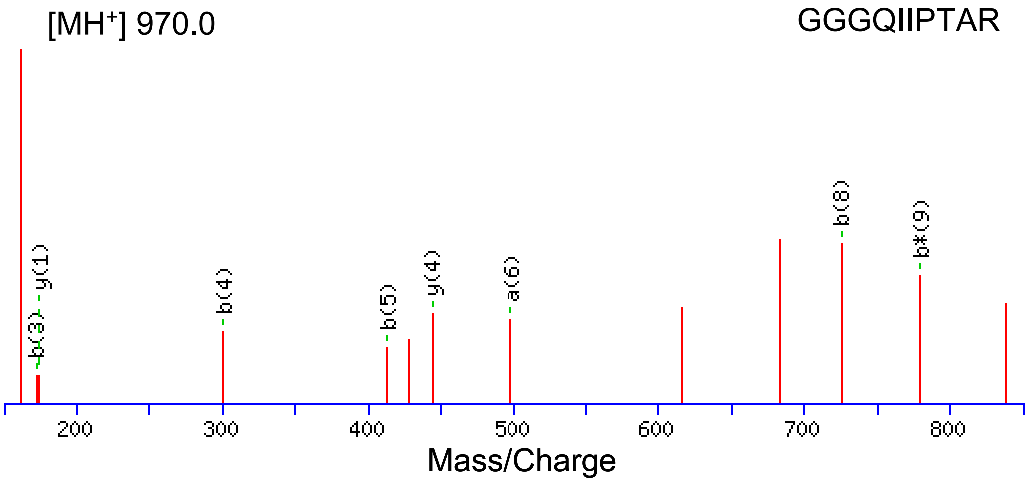

Figure C.a. Mascot result graph of the MALDI-TOF-PSD mass spectrum of the precursor ion m/z = 970.0 with different ion species indicated.

Glyceraldehyde-3-phosphate dehydrogenase (GAPDH)

The following monoisotopic m/z values were experimentally obtained: 685.51, 688.45, 795.52, 811.52, 909.61, 1411.88, 1530.83 and 1763.76.

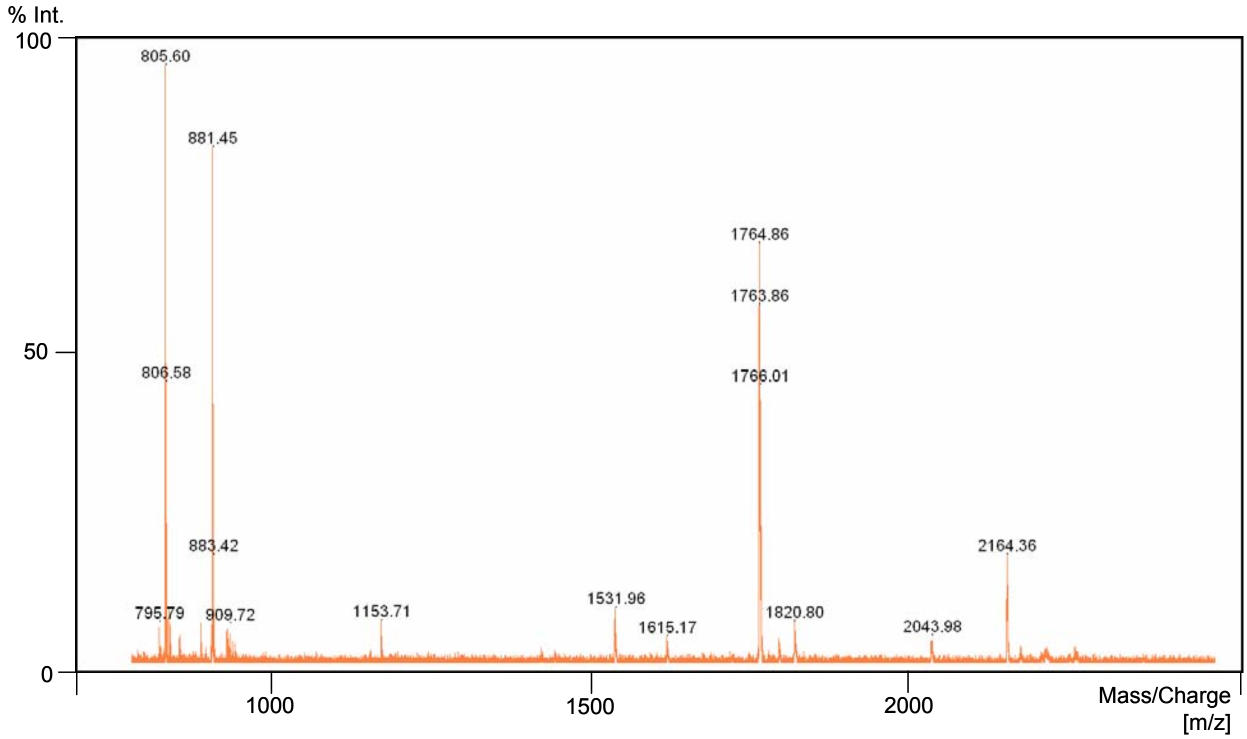

Figure D. Representative peptide mass fingerprint of GAPDH.

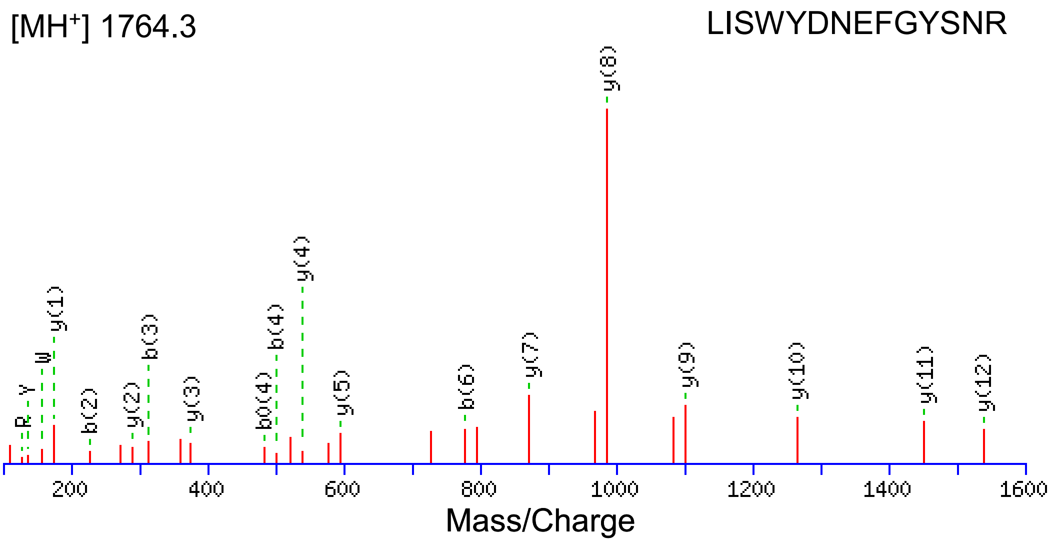

Figure D.a. Mascot result graph of the MALDI-TOF-PSD mass spectrum of the precursor ion m/z = 1764.3 with different ion species indicated.

H$^+$ATPase lysosomal (V-type proton ATPase subunit B)

The following monoisotopic m/z values were experimentally obtained: 524.29, 599.46, 632.22, 743.62, 873.62, 877.59, 1104.77, 1308.79, 1437.89, 1594.01, 1597.06, 1758.02 and 1896.96.

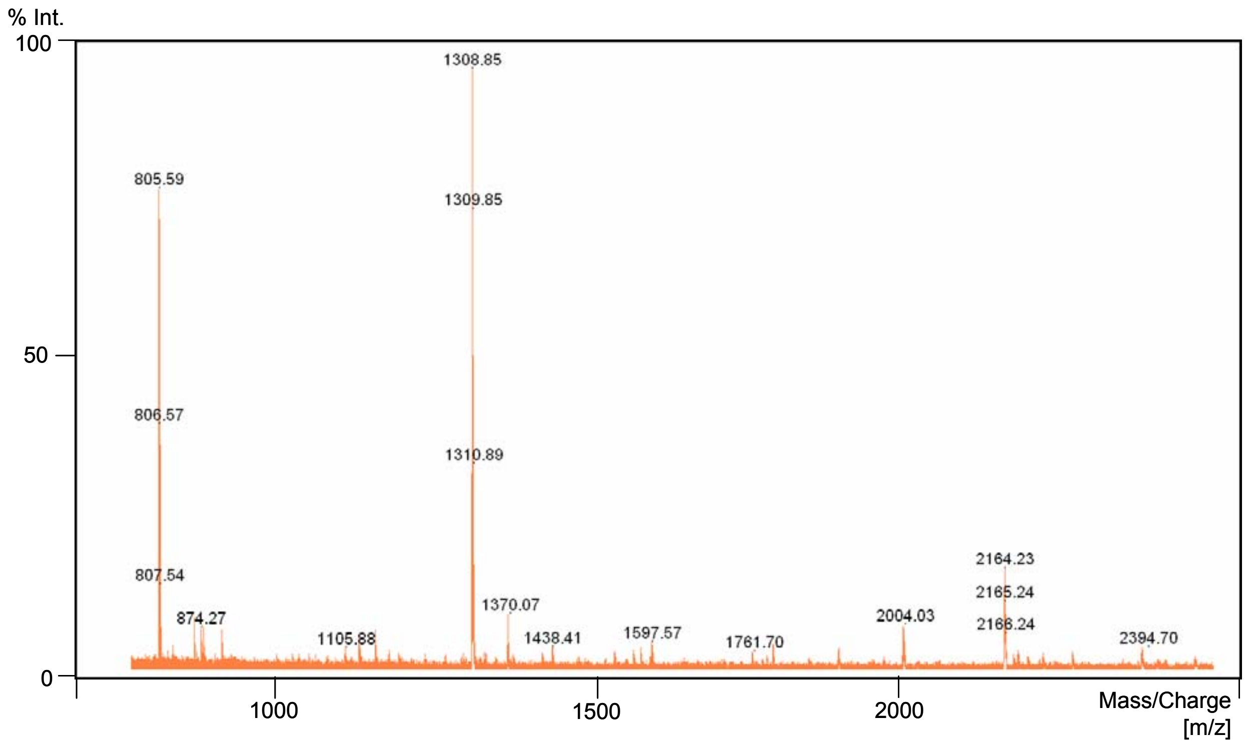

Figure E. Representative peptide mass fingerprint of H$^+$ATPase lysosomal.

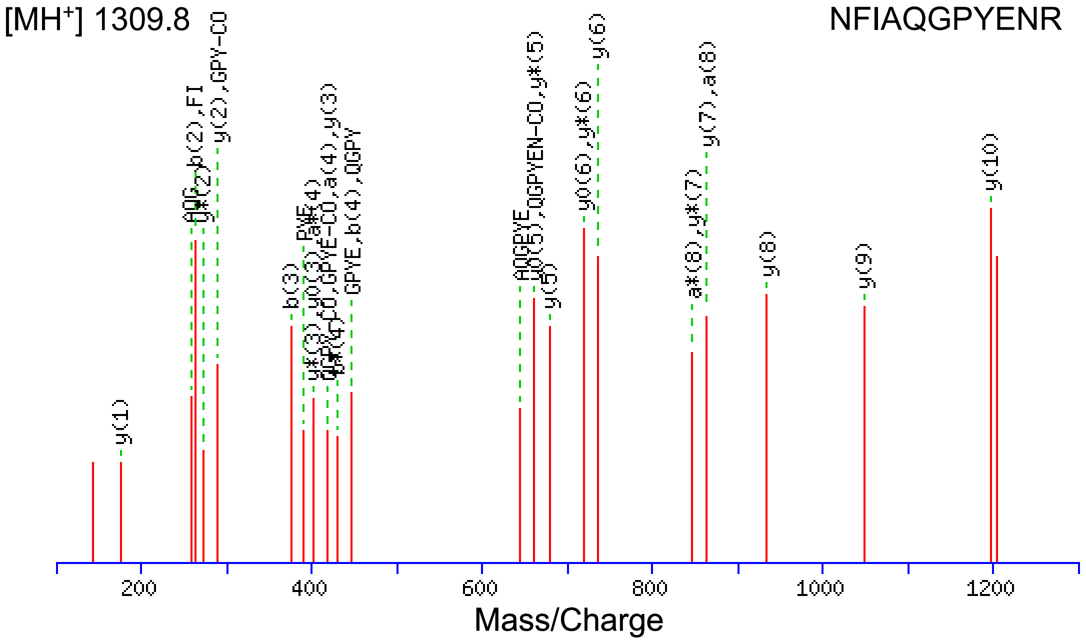

Figure E.a. Mascot result graph of the MALDI-TOF-PSD mass spectrum of the precursor ion m/z = 1309.8 with different ion species indicated.

Heat shock cognate 71kDa protein (HSP 70)

The following monoisotopic m/z values were experimentally obtained: 614.47; 687.49, 765.50, 774.54, 858.56, 861.54, 905.49, 930.65, 944.57, 989.61, 1017.65, 1081.70, 1199.80, 1228.73, 1235.75, 1253.76, 1410.79, 1480.83, 1487.78, 1691.83, 1982.10, 2774.30 and 2997.56.

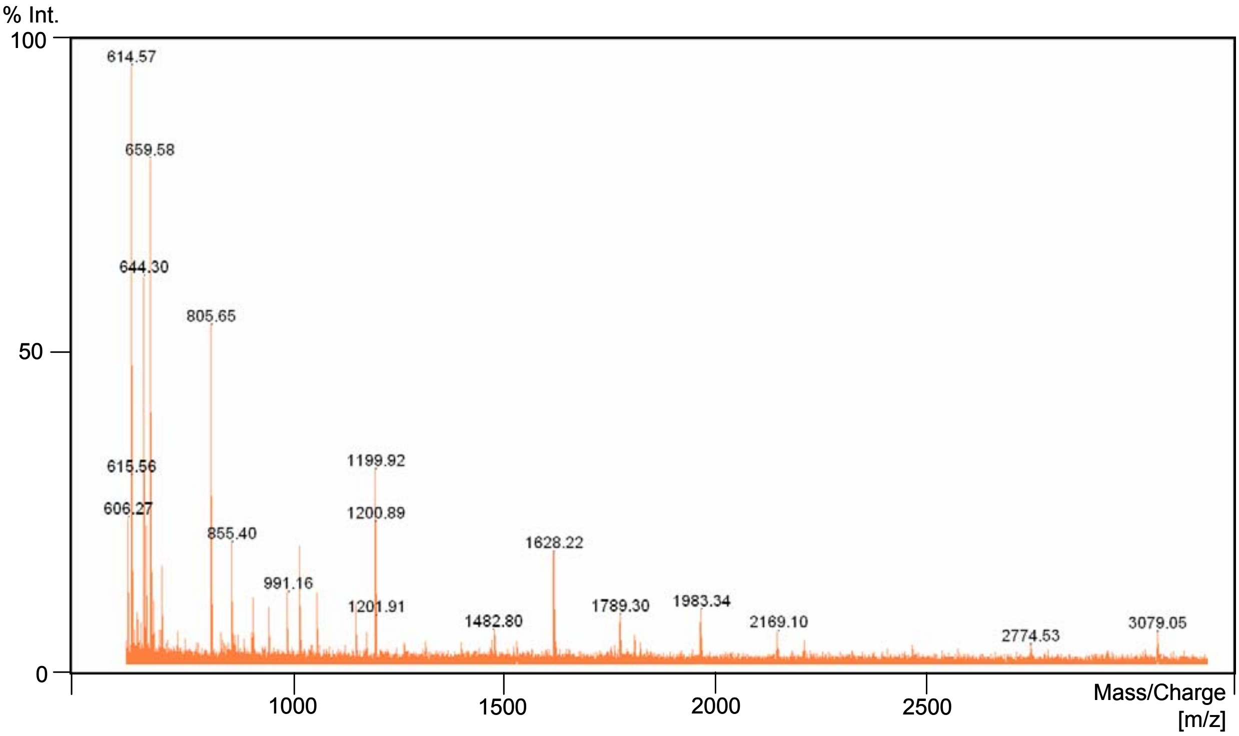

Figure F. Representative peptide mass fingerprint of HSP-70.

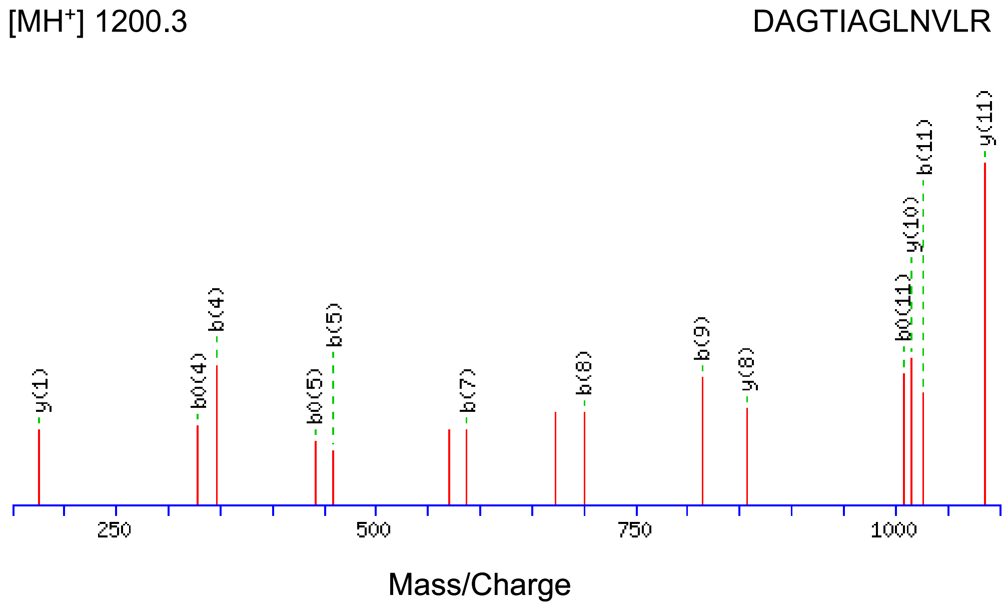

Figure F.a. Mascot result graph of the MALDI-TOF-PSD mass spectrum of the precursor ion m/z = 1200.3 with different ion species indicated.

Heat shock protein HSP 90-alpha (HSP-90)

The following monoisotopic m/z values were experimentally obtained: 673.53, 677.50, 681.49, 706.56, 722.56, 730.58, 815.65, 858.69, 901.77, 1168.79, 1236.84, 1242.89, 1265.83, 1349.91, 1513.93, 1560.96 and 1590.00.

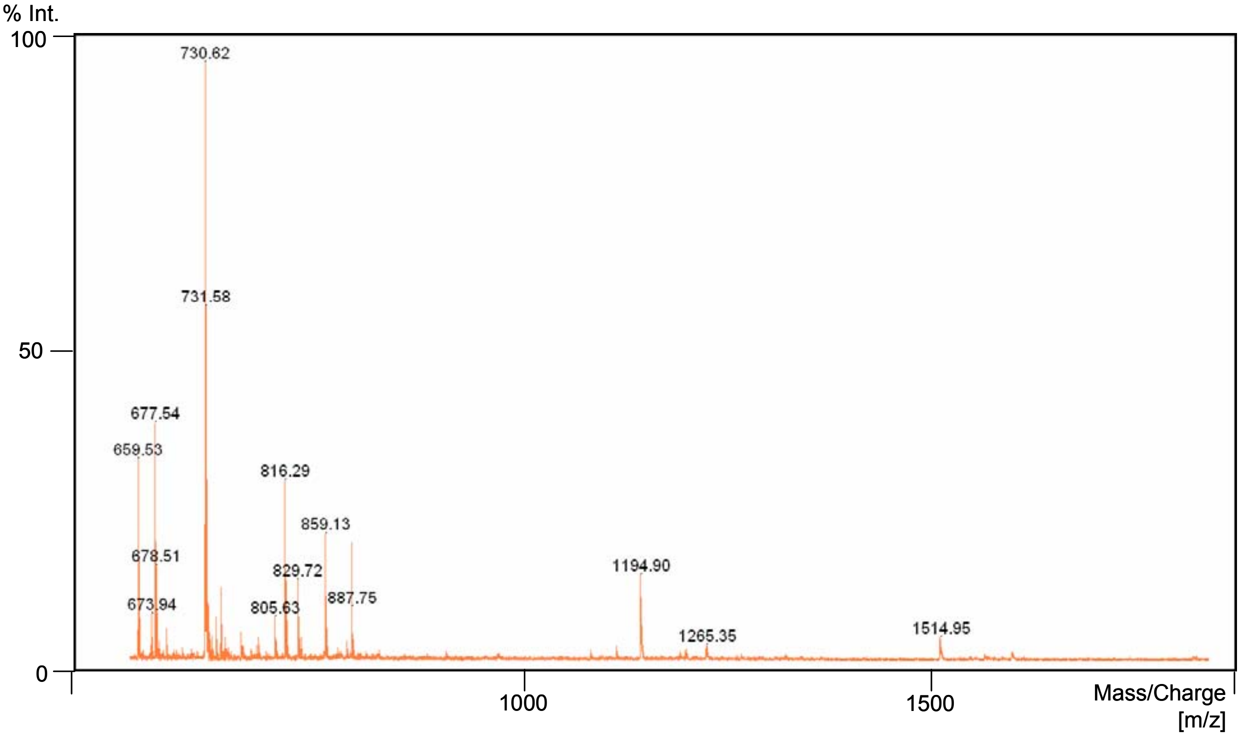

Figure G. Representative peptide mass fingerprint of HSP-90.

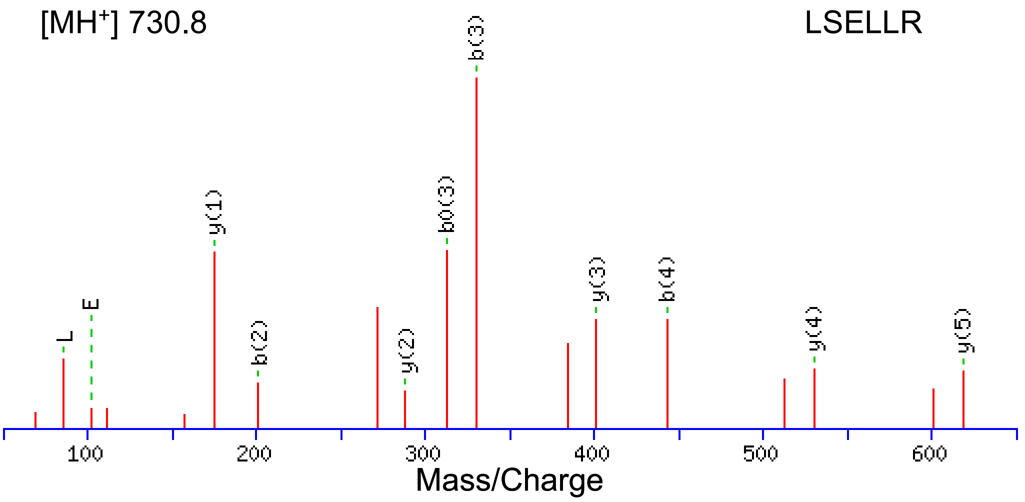

Figure G.a. Mascot result graph of the MALDI-TOF-PSD mass spectrum of the precursor ion m/z = 730.8 with different ion species indicated.

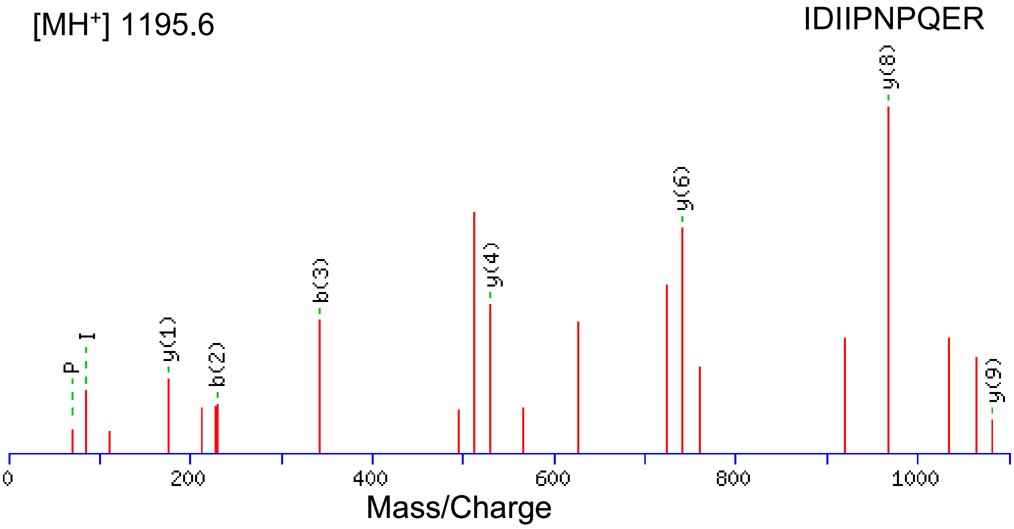

Figure G.b. Mascot result graph of the MALDI-TOF-PSD mass spectrum of the precursor ion m/z = 1195.6 with different ion species indicated.

L-lactate dehydrogenase A chain (LDH)

The following monoisotopic m/z values were experimentally obtained: 742.58, 913.78, 959.71, 1248.84 and 1267.96.

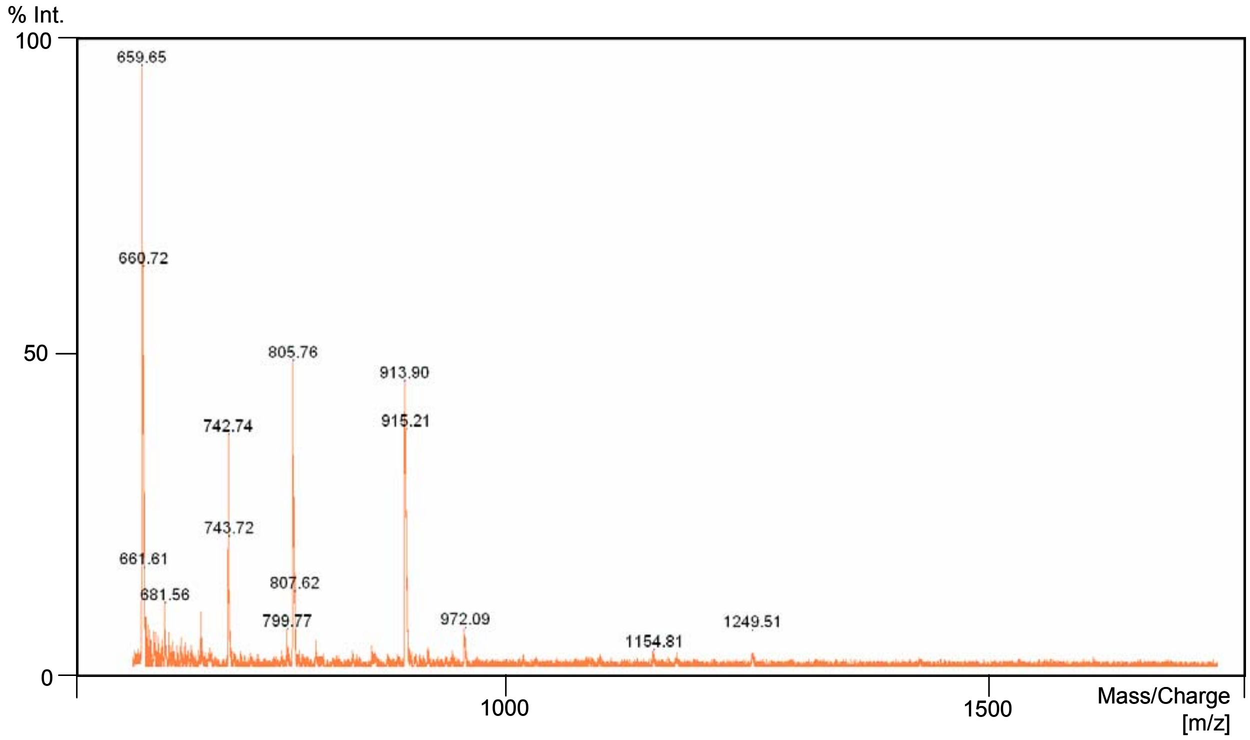

Figure H. Representative peptide mass fingerprint of LDH.

[MH$^+$] 743.0 LNLVQR

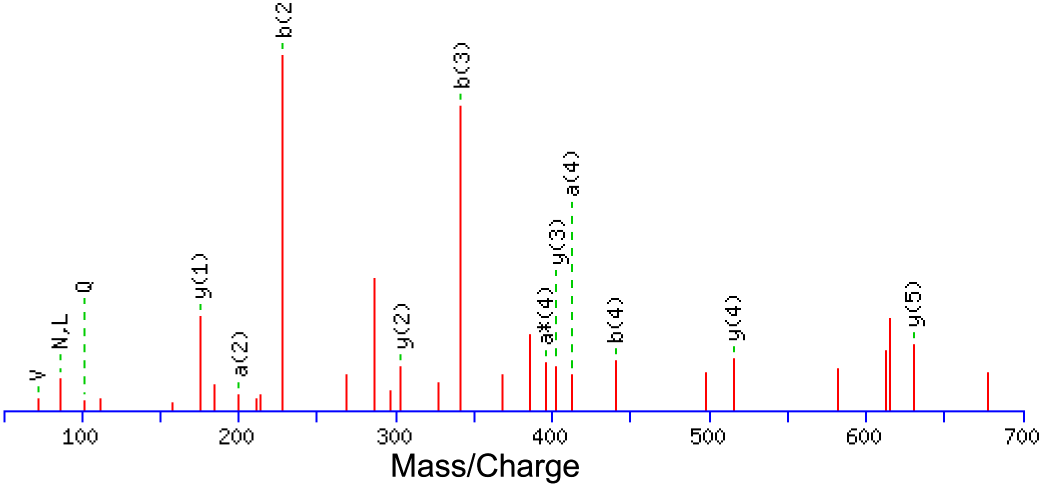

Figure H.a. Mascot result graph of the MALDI-TOF-PSD mass spectrum of the precursor ion m/z = 743.0 with different ion species indicated.

[MH$^+$] 914.5 IVVVTAGVR

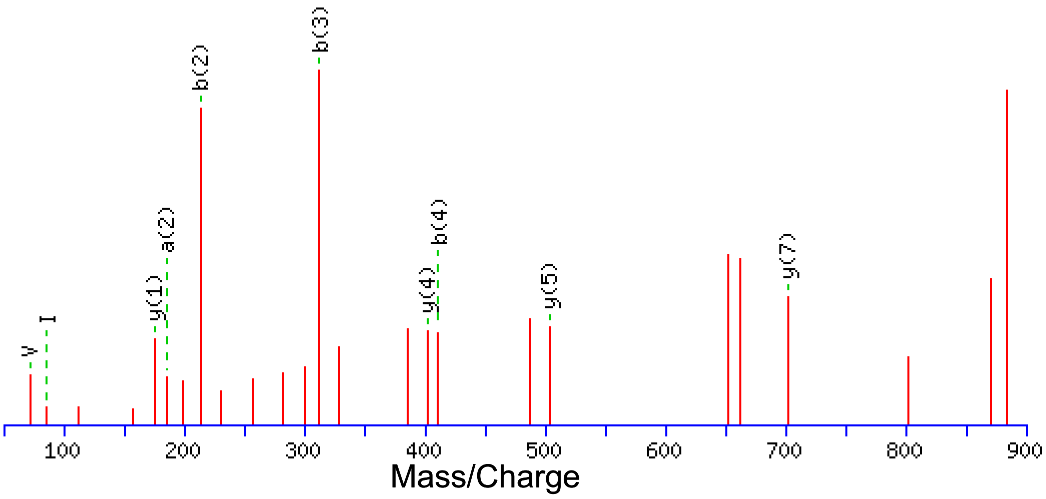

Figure H.b. Mascot result graph of the MALDI-TOF-PSD mass spectrum of the precursor ion m/z = 914.5 with different ion species indicated.

Stress-70 protein, mitochondrial (Mortalin)

The following monoisotopic m/z values were experimentally obtained: 715.54, 774.69, 862.60, 958.75, 994.27, 1242.79, 1333.18, 1361.92, 1405.66, 1446.85, 1462.29, 1518.00, 1569.93, 1593.10, 1695.02 and 2056.10.

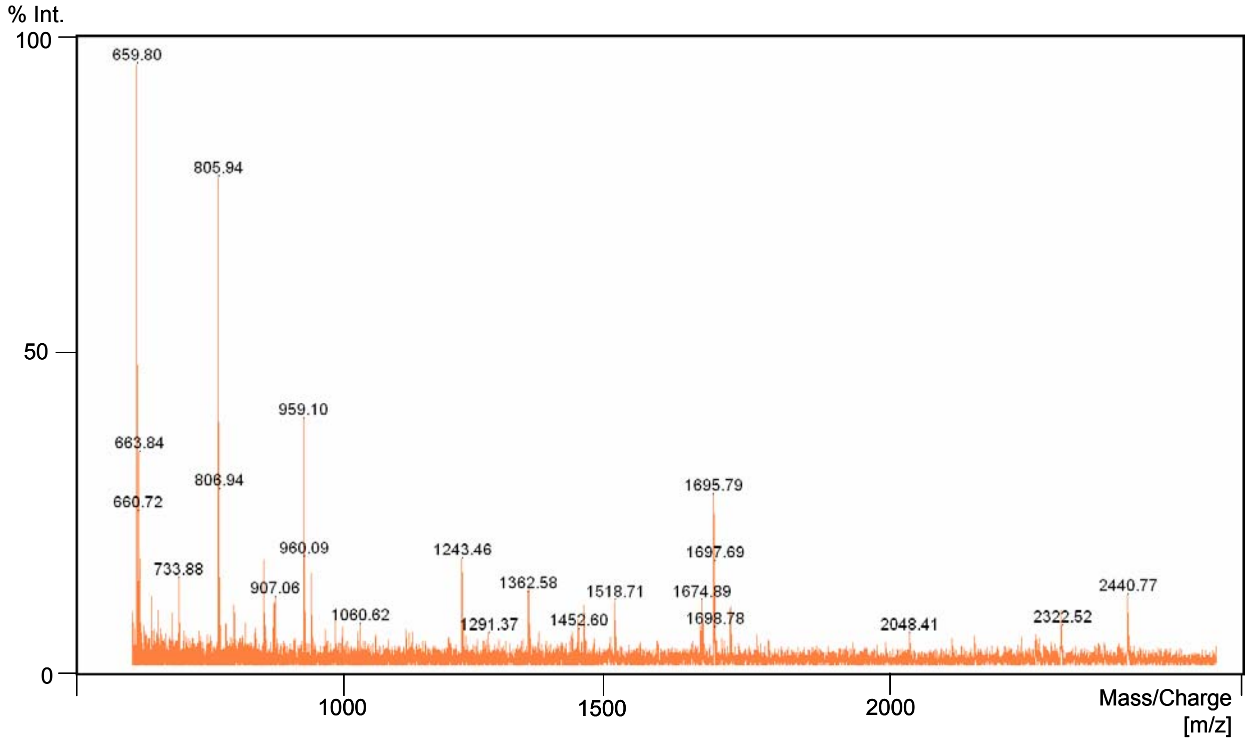

Figure I. Representative peptide mass fingerprint of Mortalin.

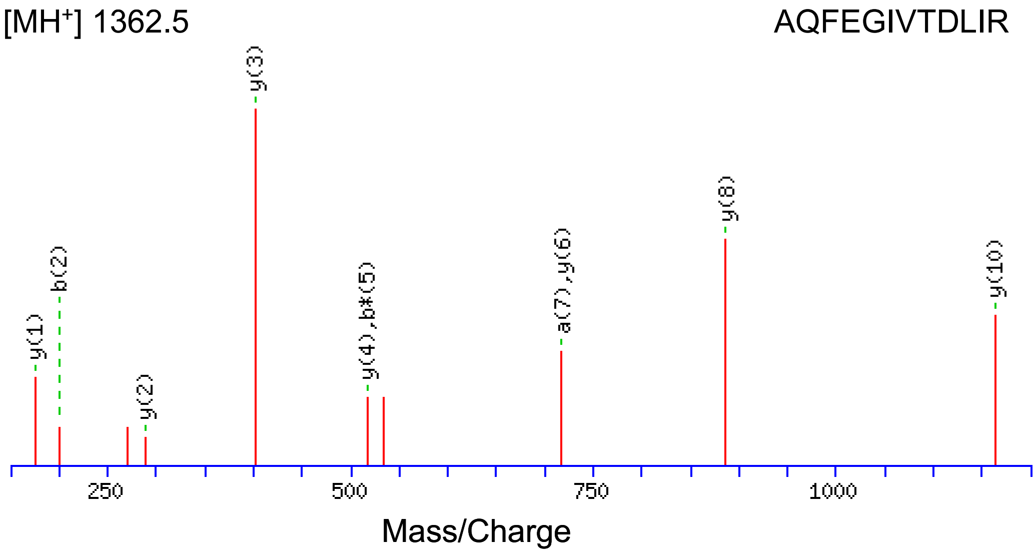

Figure I.a. Mascot result graph of the MALDI-TOF-PSD mass spectrum of the precursor ion m/z = 1362.5 with different ion species indicated.

Nucleoside diphosphate kinase A (NDK-A)

The following monoisotopic m/z values were experimentally obtained: 707.35, 828.33, 984.46, 1051.34, 1149.44, 1344.53 and 1785.63.

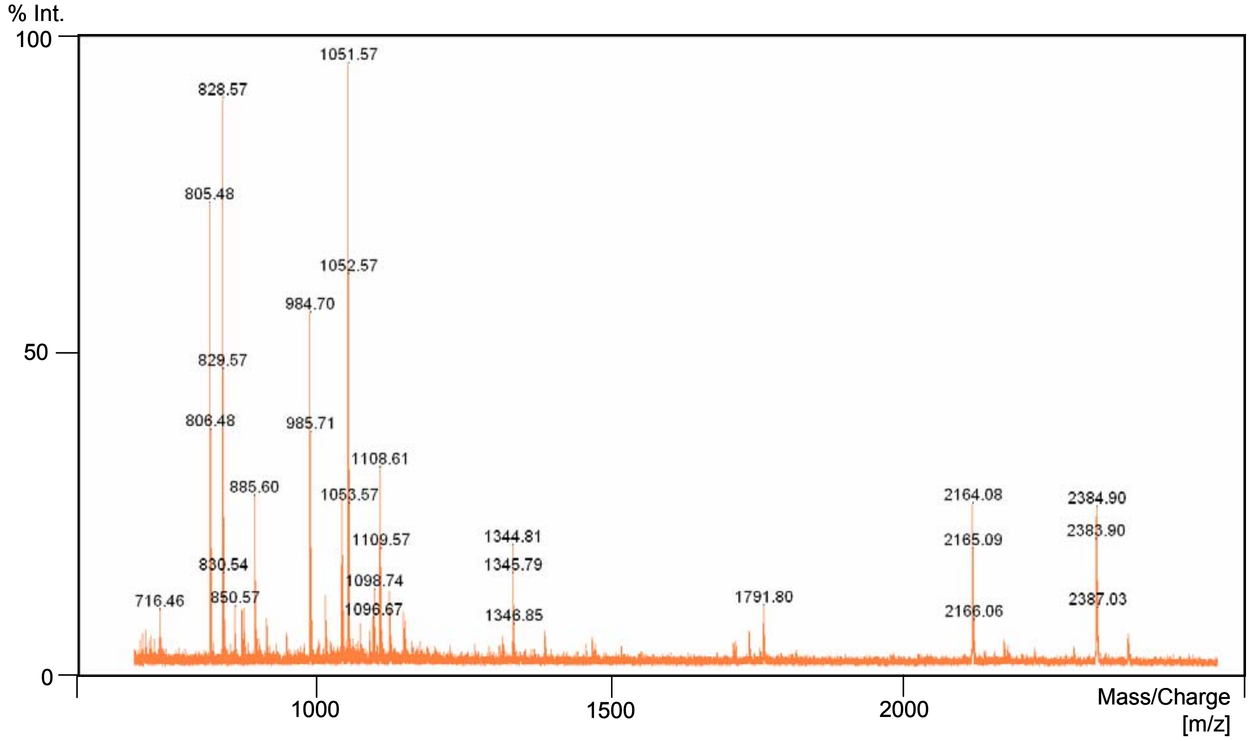

Figure J. Representative peptide mass fingerprint of NDK-A.

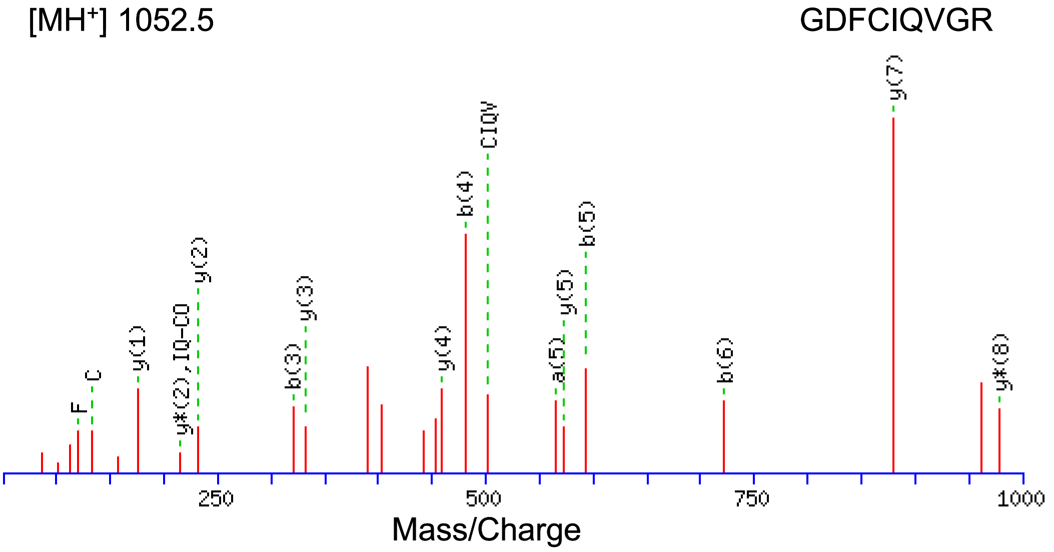

Figure J.a. Mascot result graph of the MALDI-TOF-PSD mass spectrum of the precursor ion m/z = 1052.5 with different ion species indicated.

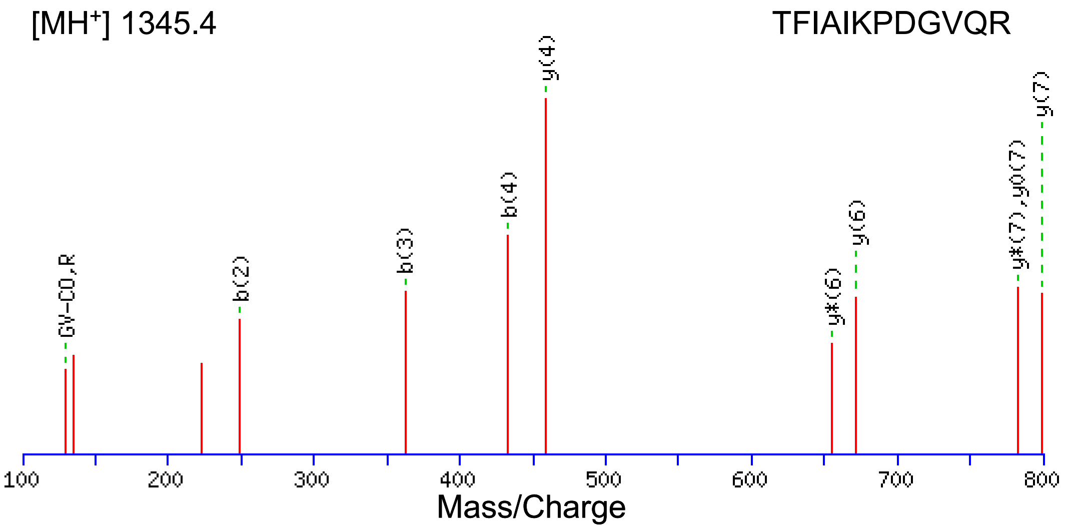

Figure J.b. Mascot result graph of the MALDI-TOF-PSD mass spectrum of the precursor ion m/z = 1345.4 with different ion species indicated.

Protein disulfide-isomerase A6 (PDIA6)

The following monoisotopic m/z values were experimentally obtained: 591.44, 662.41, 676.45, 708.42, 758.50, 1015.68, 1151.72, 1386.85, 1483.84, 1527.93, 1667.89, 2356.22 and 2581.37.

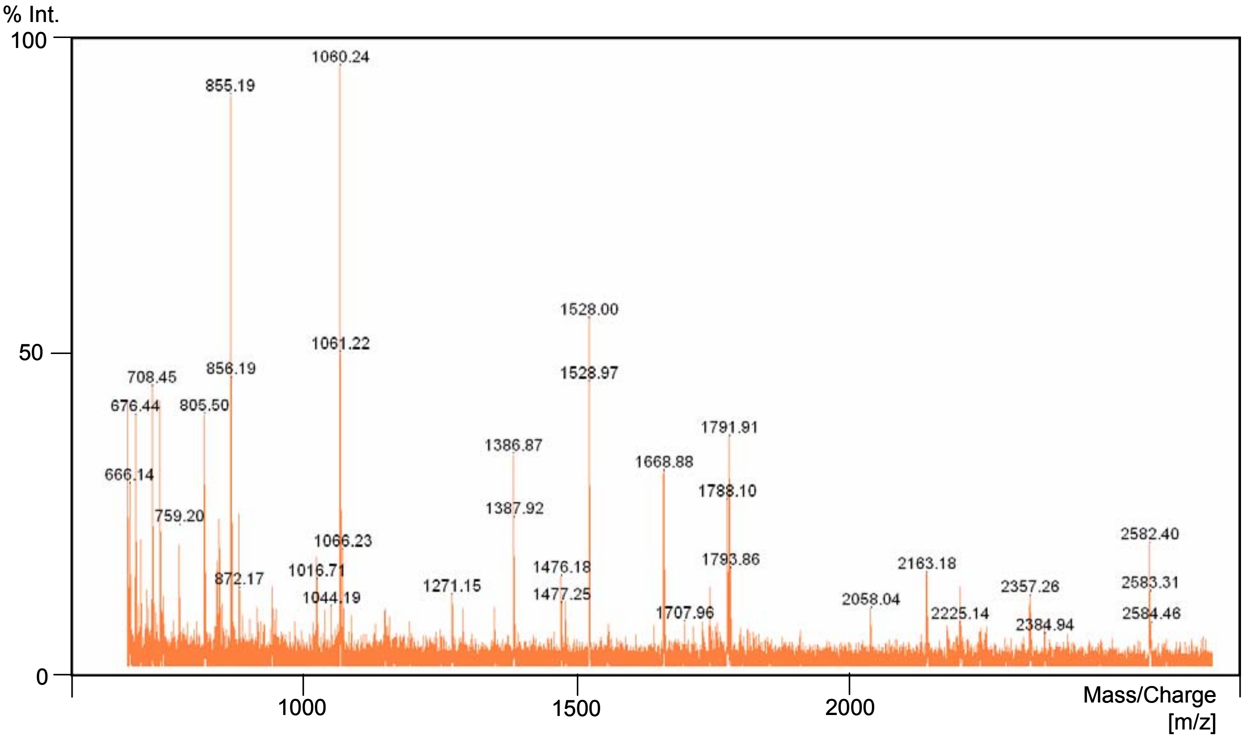

Figure K. Representative peptide mass fingerprint of PDIA6.

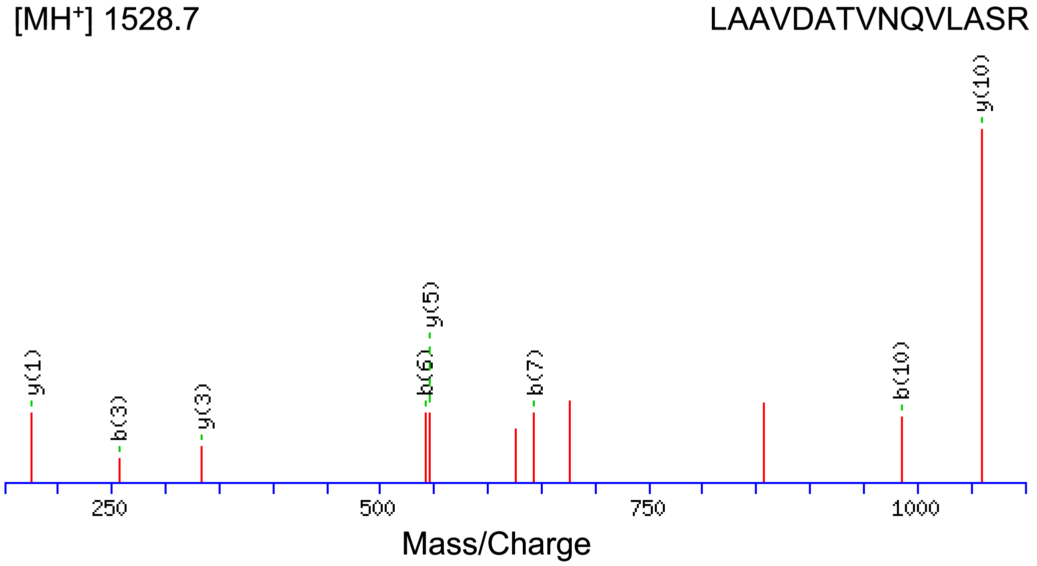

Figure K.a. Mascot result graph of the MALDI-TOF-PSD mass spectrum of the precursor ion m/z = 1528.7 with different ion species indicated.

Lamin A/C (Progerin)

The following monoisotopic m/z values were experimentally obtained: 515.51, 861.36, 919.58, 972.70, 1028.81, 1057.87, 1089.79, 1104.89, 1187.88, 1359.05, 1509.91, 1606.04, 1649.99, 1753.15 and 2384.21.

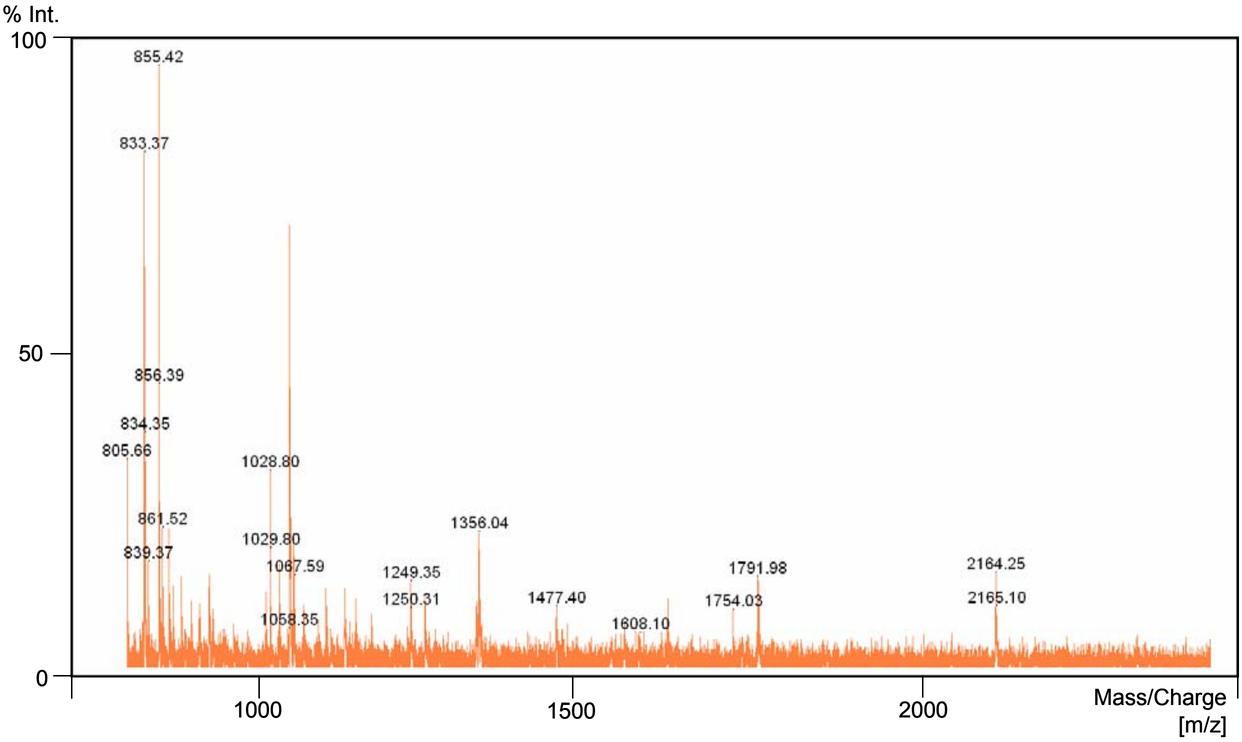

Figure L. Representative peptide mass fingerprint of Progerin.

Proteasome subunit alpha type-3 (PSA-3)

The following monoisotopic m/z values were experimentally obtained: 745.55, 763.52, 1095.68, 1114.69, 1152.73, 1217.80, 1237.77, 1396.91 and 1578.97.

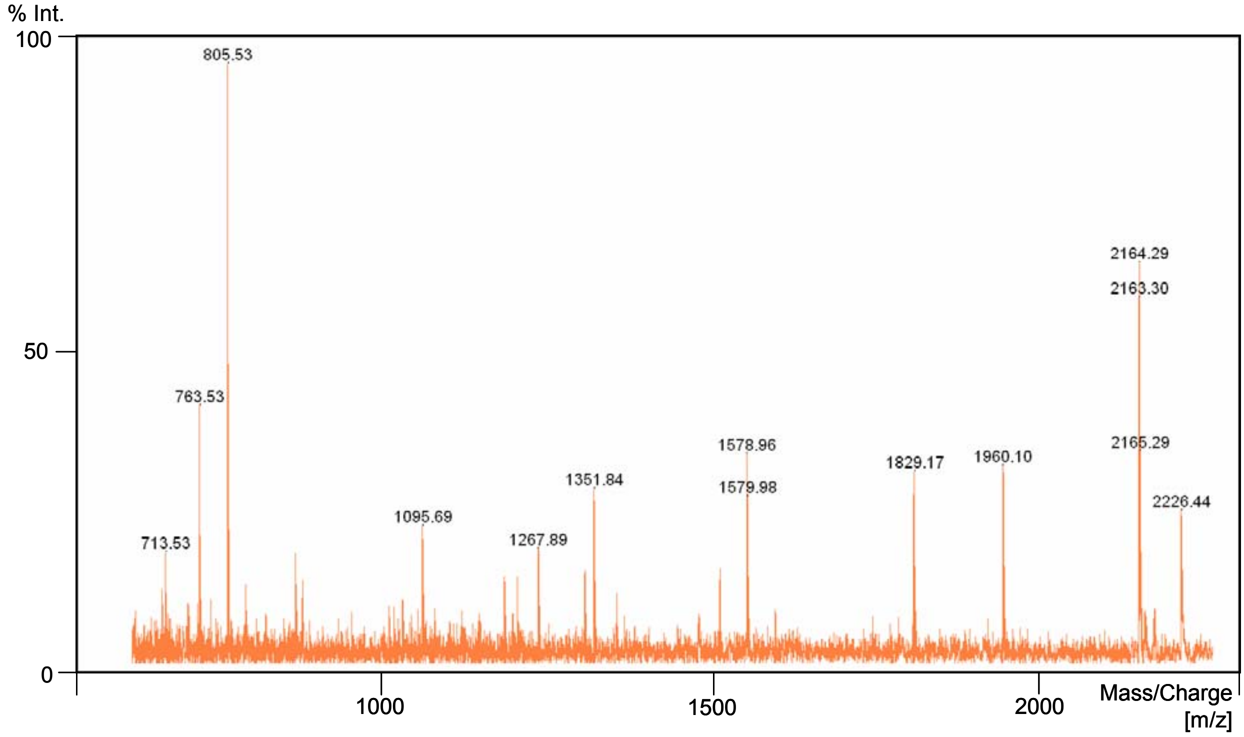

Figure M. Representative peptide mass fingerprint of PSA-3.

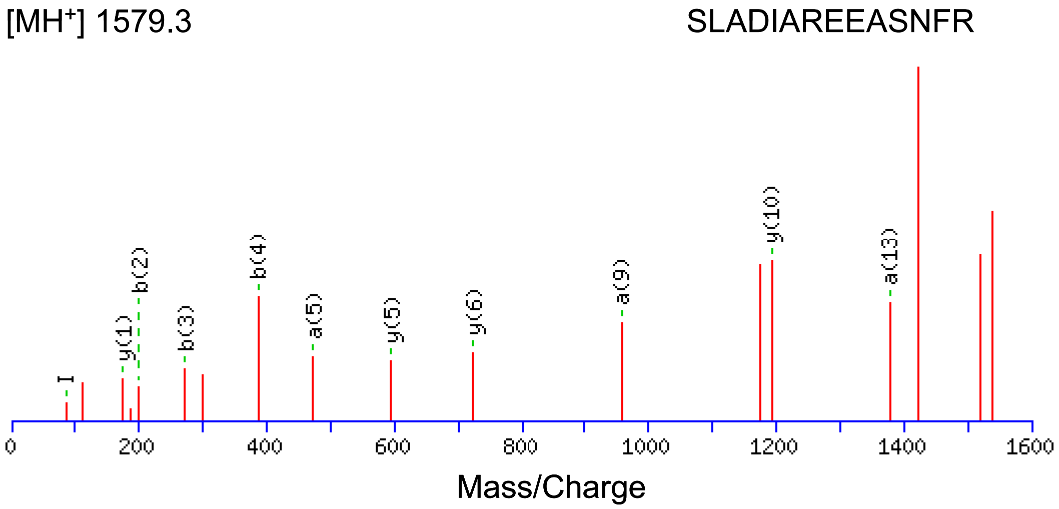

Figure M.a. Mascot result graph of the MALDI-TOF-PSD mass spectrum of the precursor ion m/z = 1579.3 with different ion species indicated.

Bifunctional purine biosynthesis protein PURH

The following monoisotopic m/z values were experimentally obtained: 701.49, 890.66, 1042.79, 1142.71, 1163.78, 1245.74, 1309.85, 1355.99, 1384.87, 1607.94, 1623.93, 2035.21, 2163.29 and 2559.29.

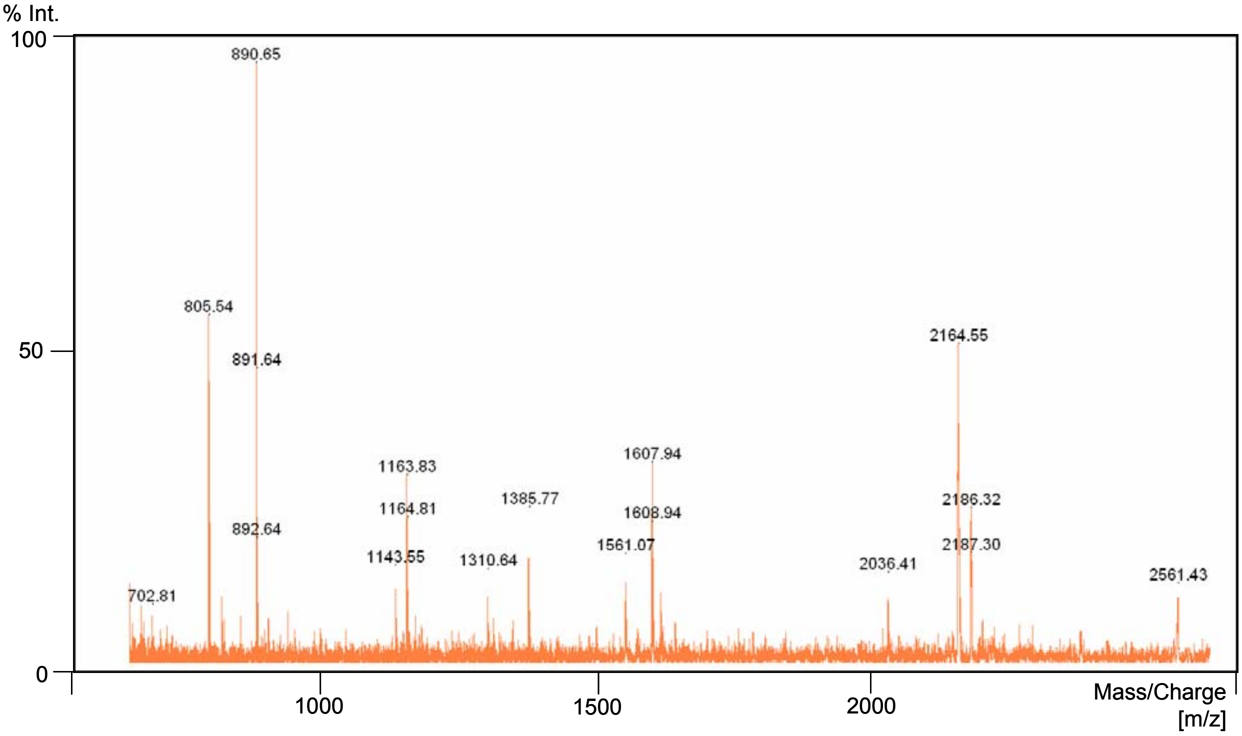

Figure N. Representative peptide mass fingerprint of PURH.

Stress-induced-phosphoprotein 1 (STIP-1)

The following monoisotopic m/z values were experimentally obtained: 616.71, 628.62, 644.62, 652.64, 672.67, 769.57, 800.82, 900.67, 915.65, 1008.88, 1065.71 and 1464.87.

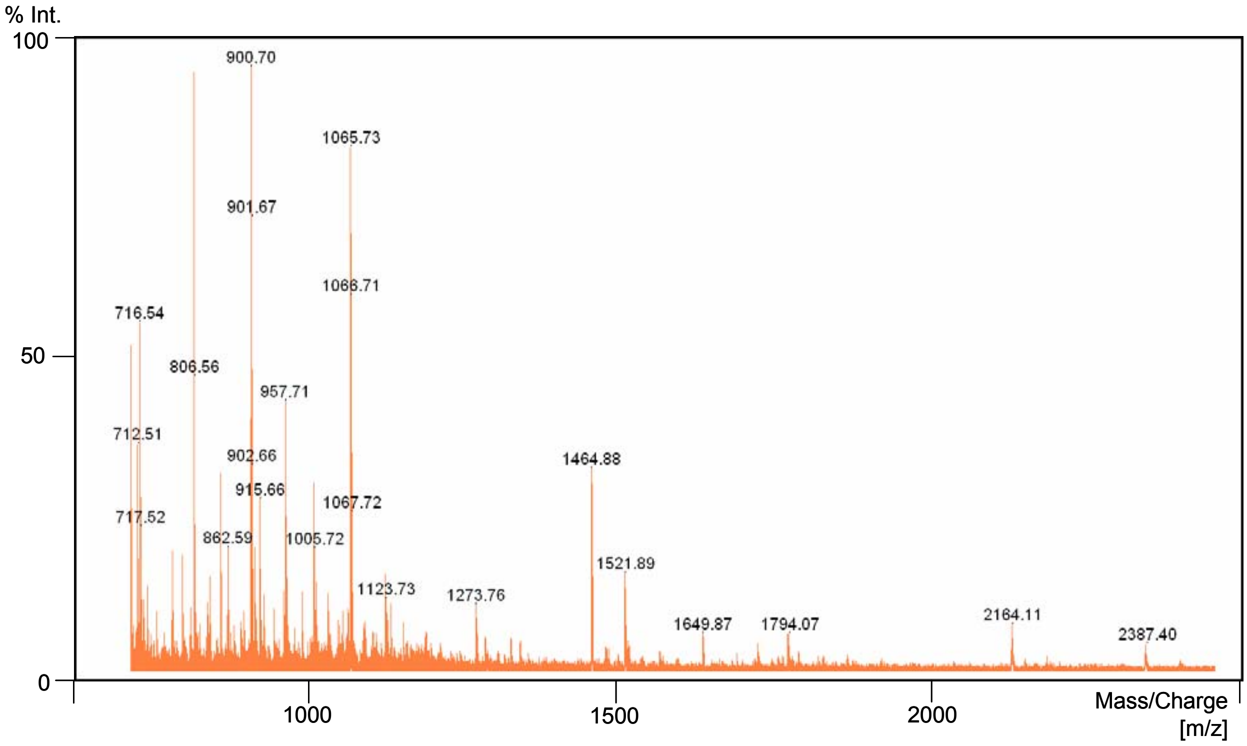

Figure O. Representative peptide mass fingerprint of STIP-1.

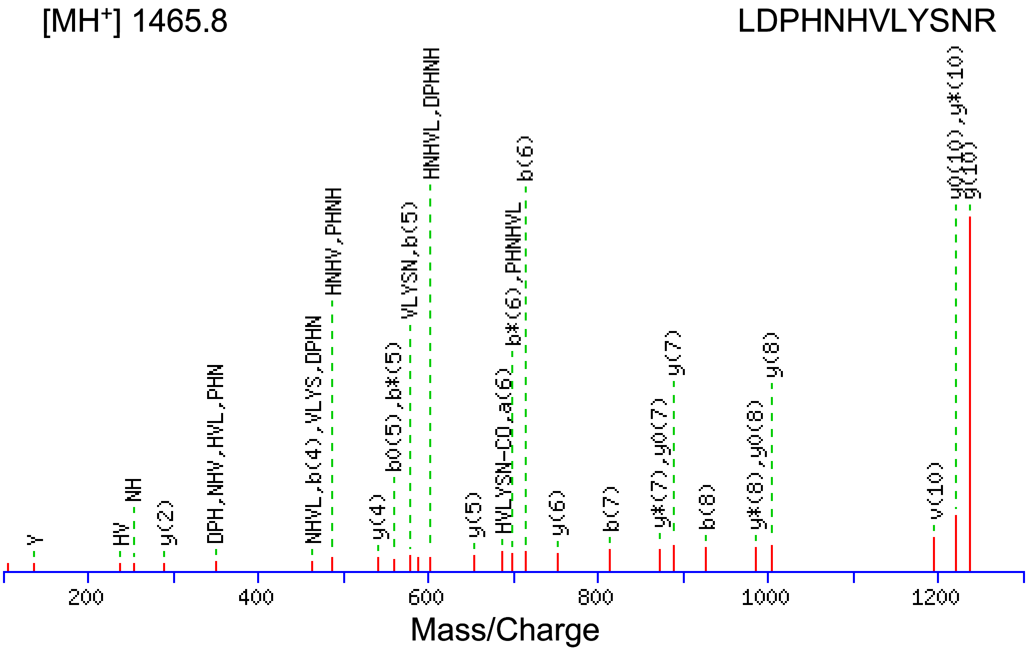

Figure O.a. Mascot result graph of the MALDI-TOF-PSD mass spectrum of the precursor ion m/z = 1465.8 with different ion species indicated.

Tyrosyl-tRNA synthetase, cytoplasmic (SYYC)

The following monoisotopic m/z values were experimentally obtained: 702.54, 706.55, 721.43, 726.59, 744.55, 752.58, 764.53, 790.56, 863.65, 973.68, 985.66, 1011.68, 1205.76, 1235.81, 1256.77 and 1793.86.

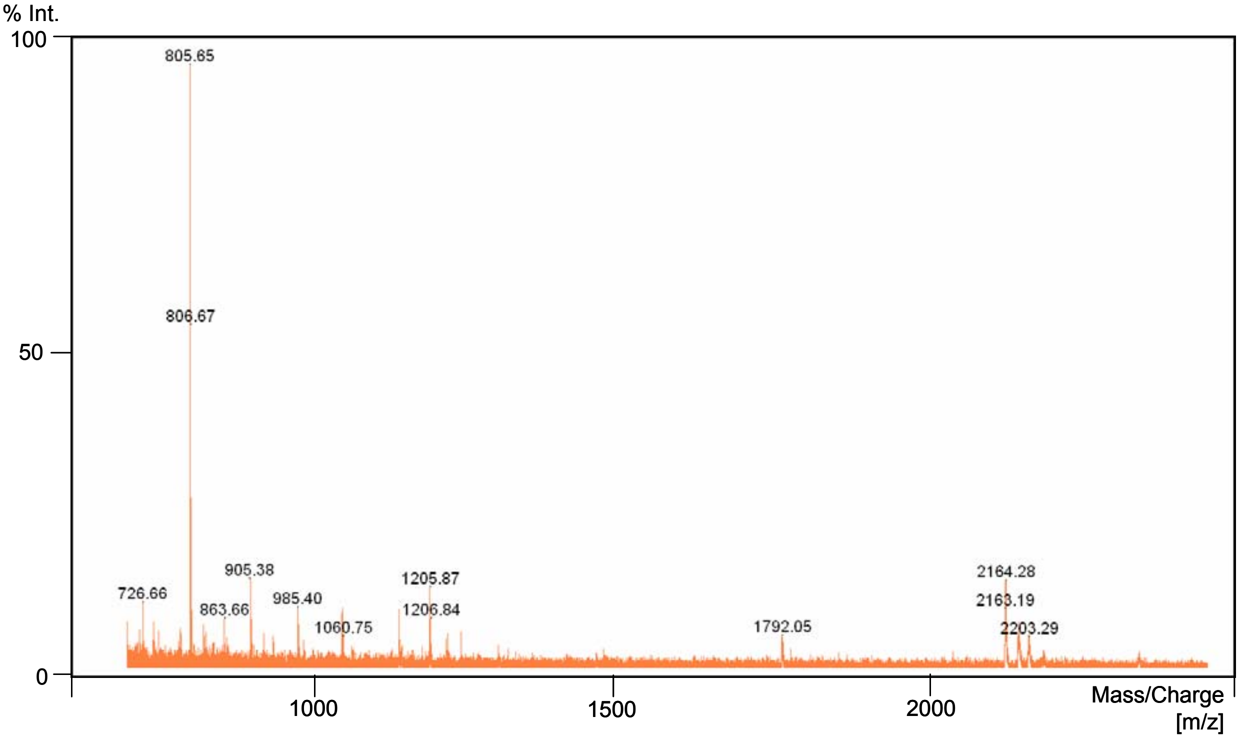

Figure P. Representative peptide mass fingerprint of SYYC.

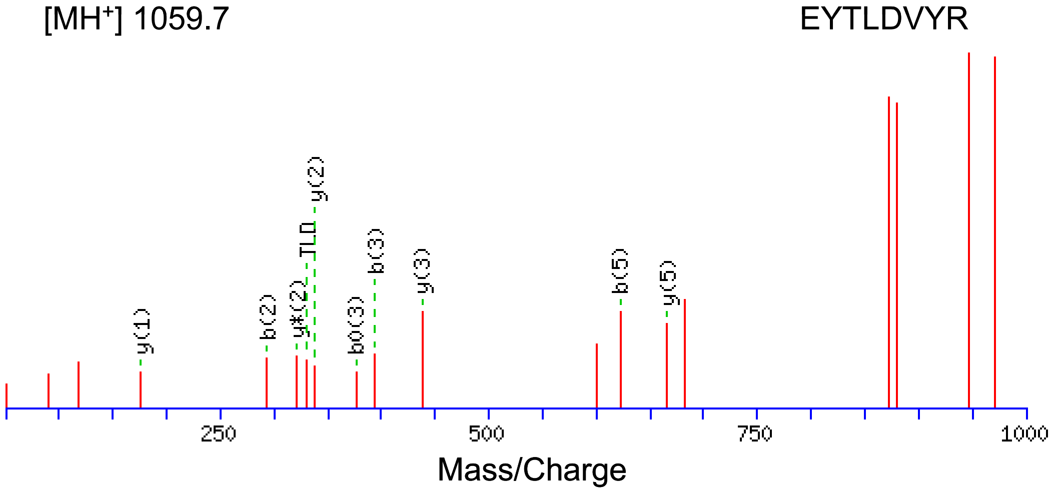

Figure P.a. Mascot result graph of the MALDI-TOF-PSD mass spectrum of the precursor ion m/z = 1059.7 with different ion species indicated.

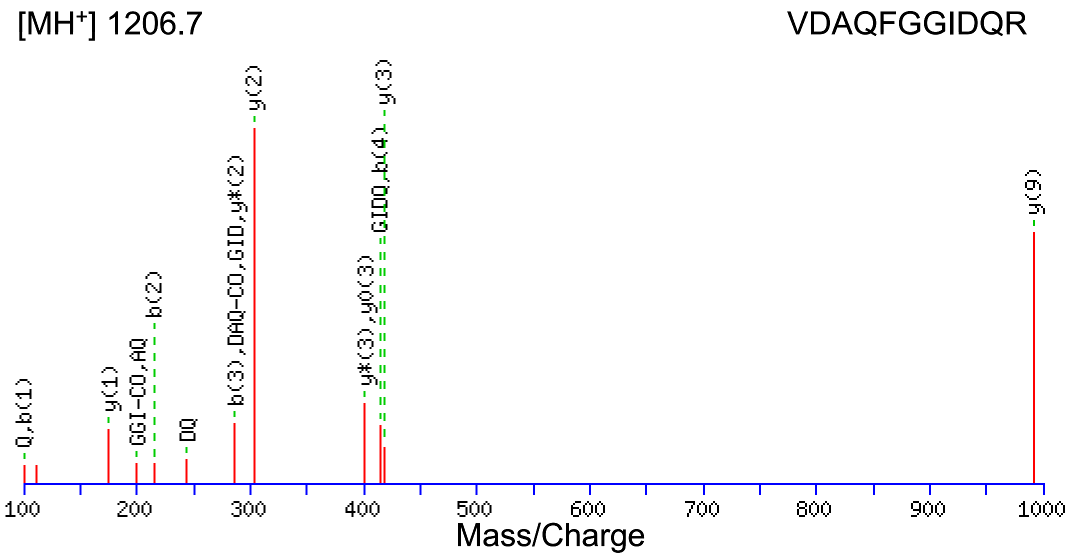

Figure P.b. Mascot result graph of the MALDI-TOF-PSD mass spectrum of the precursor ion m/z = 1206.7 with different ion species indicated.

Tubulin beta chain

The following monoisotopic m/z values were experimentally obtained: 1028.44, 1039.51, 1077.42, 1130.53, 1143.56, 1229.55, 1271.63, 1301.52, 1385.54, 1615.62, 1620.67, 1696.57, 1869.67, 1958.64, 2086.71, 2708.54, 2798.55, 2855.52, 3102.44 and 4593.57.

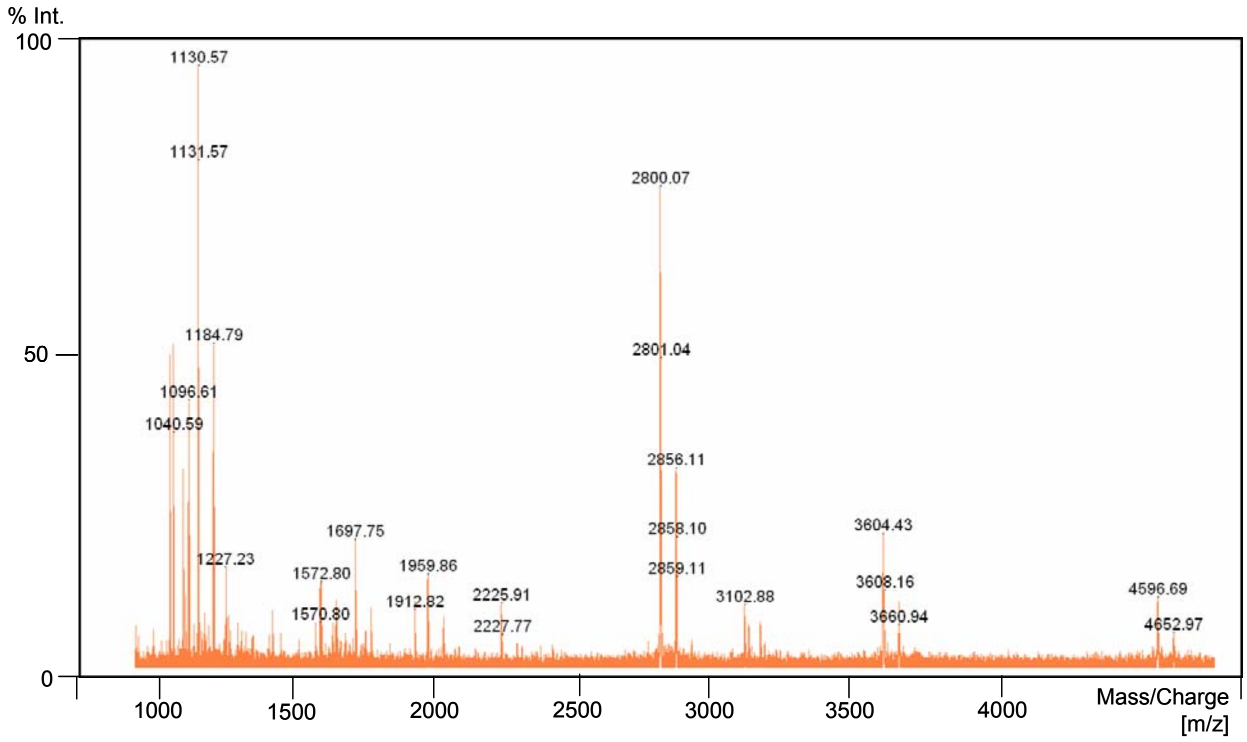

Figure Q. Representative peptide mass fingerprint of Tubulin.

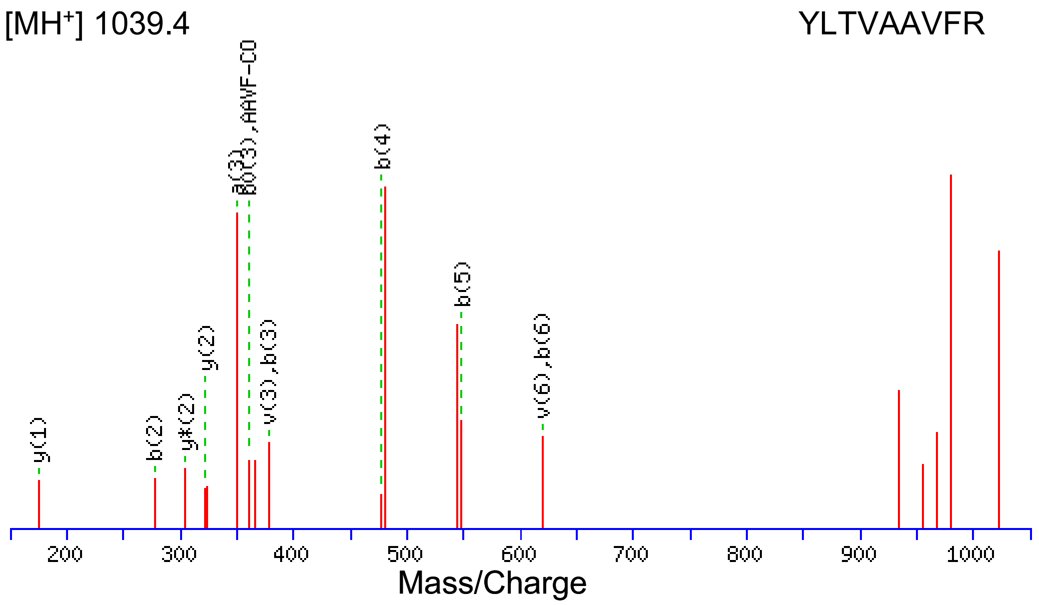

Figure Q.a. Mascot result graph of the MALDI-TOF-PSD mass spectrum of the precursor ion m/z = 1039.4 with different ion species indicated.

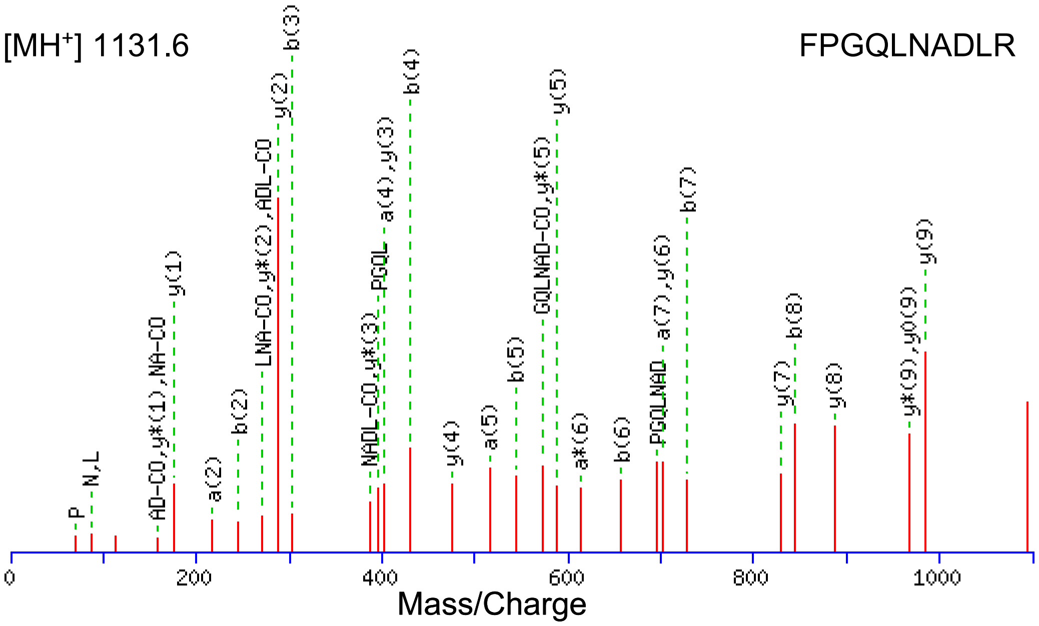

Figure Q.b. Mascot result graph of the MALDI-TOF-PSD mass spectrum of the precursor ion m/z = 1131.6 with different ion species indicated.

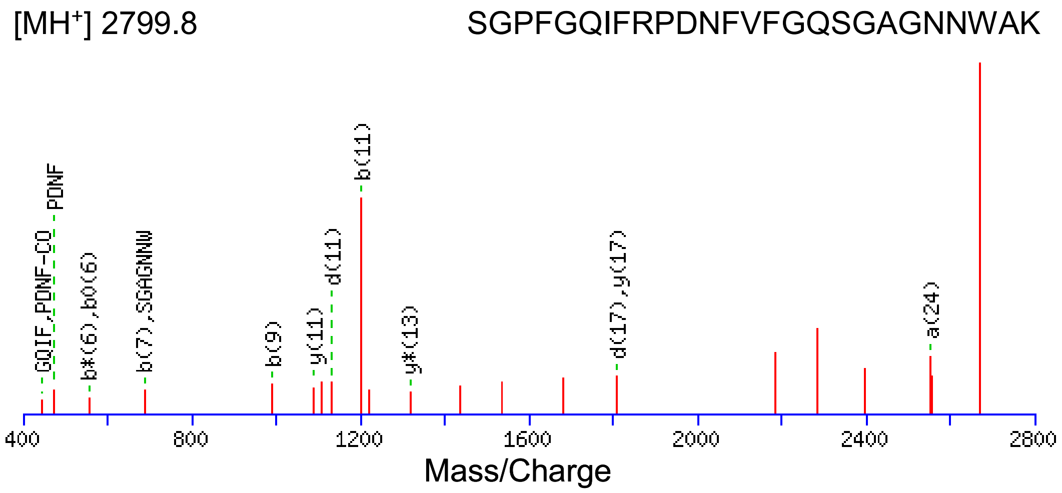

Figure Q.c. Mascot result graph of the MALDI-TOF-PSD mass spectrum of the precursor ion m/z = 2799.8 with different ion species indicated.

Ubiquitin

The following monoisotopic m/z values were experimentally obtained: 648.60, 717.63, 765.67, 1039.84, 1067.90, 1081.79, 1524.03 and 1788.20.

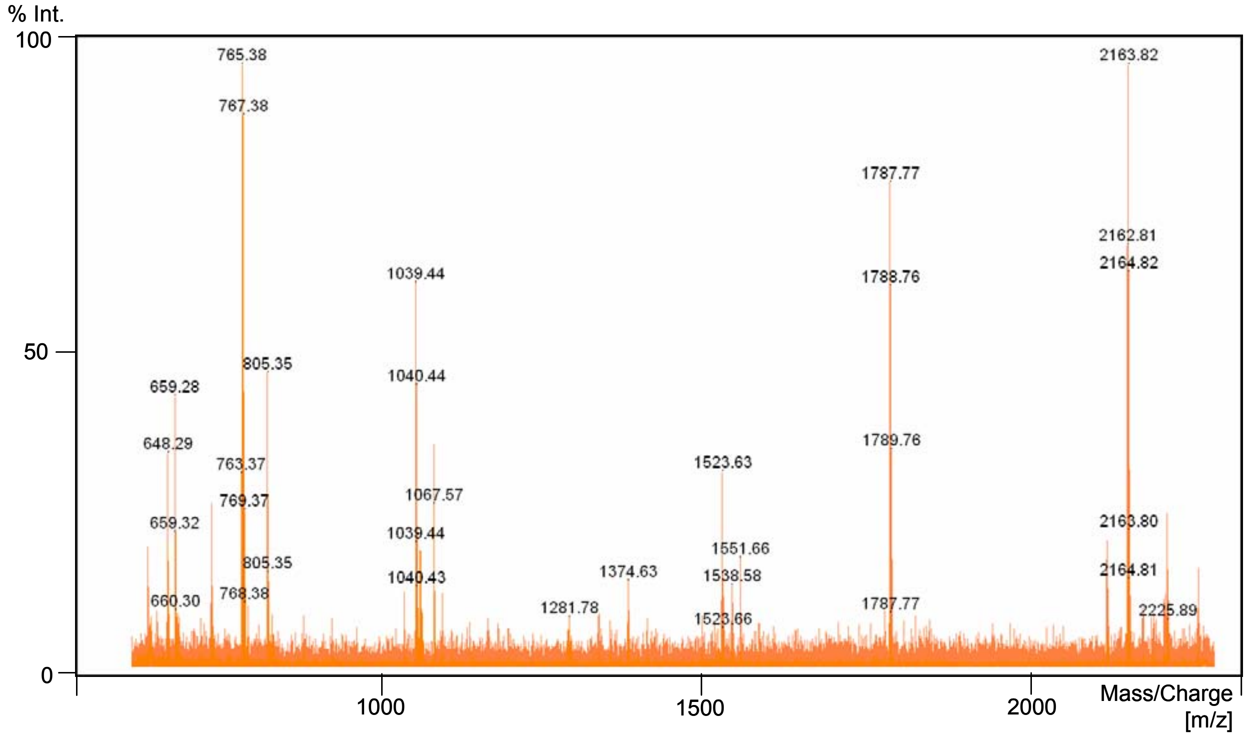

Figure R. Representative peptide mass fingerprint of Ubiquitin.

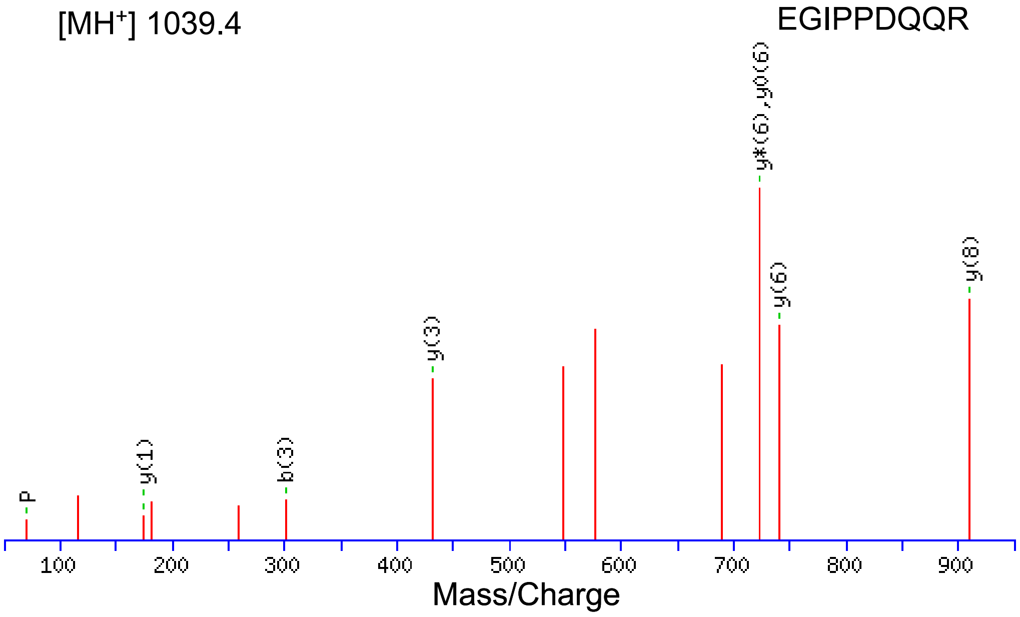

Figure R.a. Mascot result graph of the MALDI-TOF-PSD mass spectrum of the precursor ion m/z = 1039.4 with different ion species indicated.

Vimentin

The following monoisotopic m/z values were experimentally obtained: 519.38, 545.42, 573.41, 587.48, 605.41, 645.42, 701.46, 743.57, 872.50, 914.51, 932.56, 970.66, 1028.55, 1068.55, 1088.58, 1093.58, 1125.63, 1270.54, 1295.64, 1311.65, 1428.67, 1495.74, 1510.71, 1570.87, 1824.84 and 2496.99.

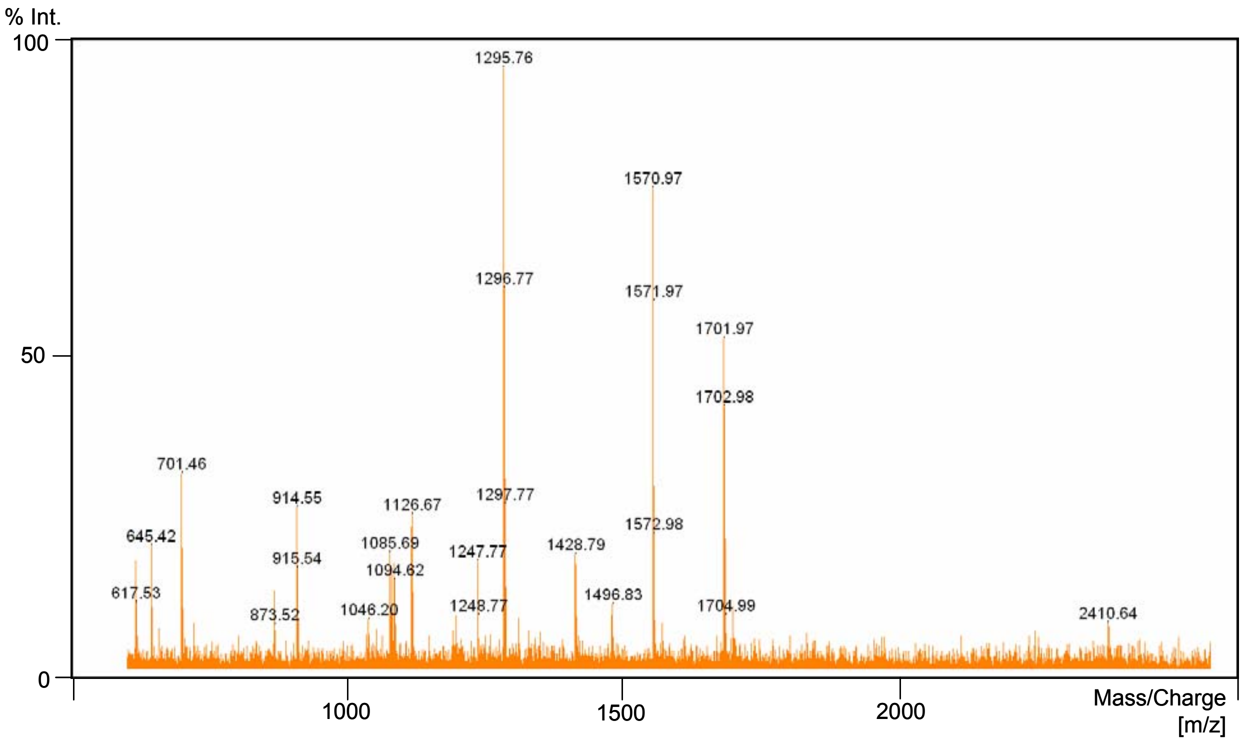

Figure S. Representative peptide mass fingerprint of Vimentin.

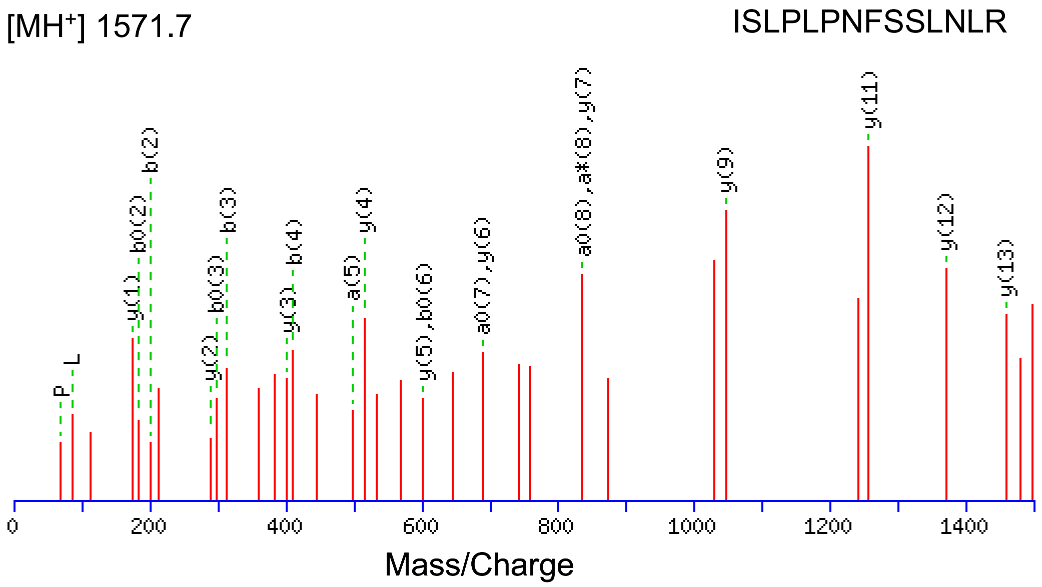

Figure S.a. Mascot result graph of the MALDI-TOF-PSD mass spectrum of the precursor ion m/z = 1571.7 with different ion species indicated.

Supplement B

Mass spectra of differentially expressed proteins

Calumenin (CALU)

The following monoisotopic m/z values were experimentally obtained: 954.63, 1109.70, 1197.97, 1232.86, 1340.81, 1579.88, 1887.92, 1988.17, 2701.47, and 3101.80.

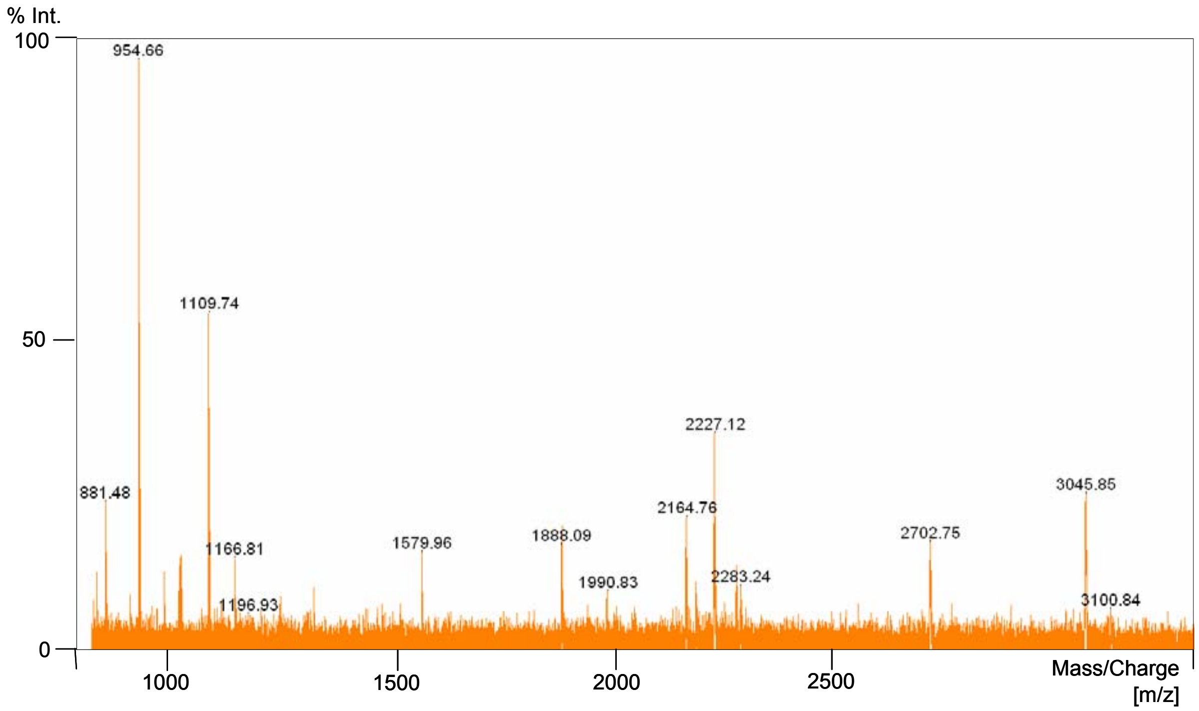

Figure A. Representative peptide mass fingerprint of CALU.

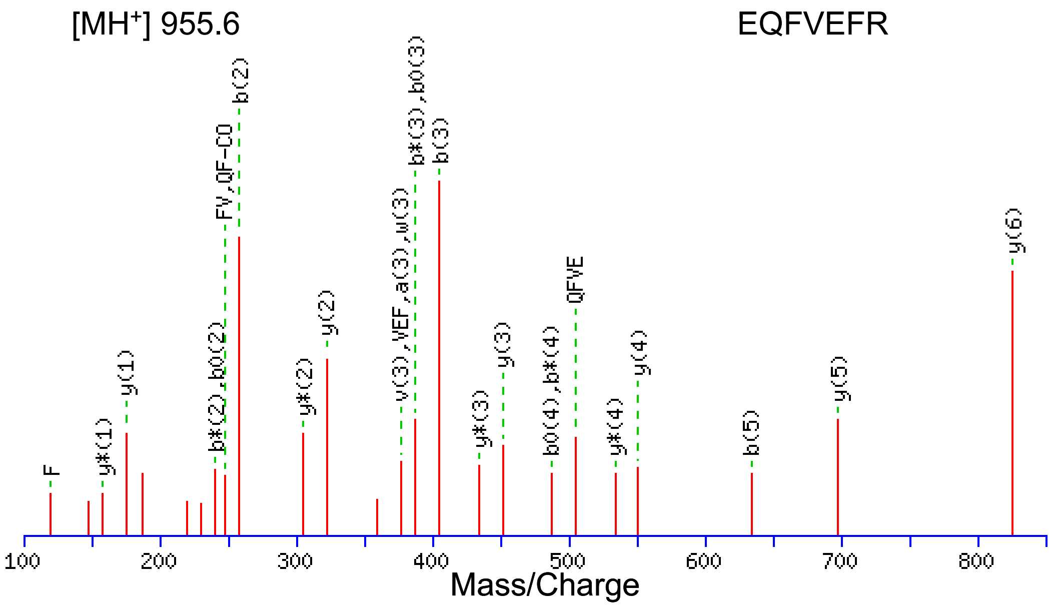

Figure A.a. Mascot result graph of the MALDI-TOF-PSD mass spectrum of the precursor ion m/z = 955.6 with different ion species indicated.

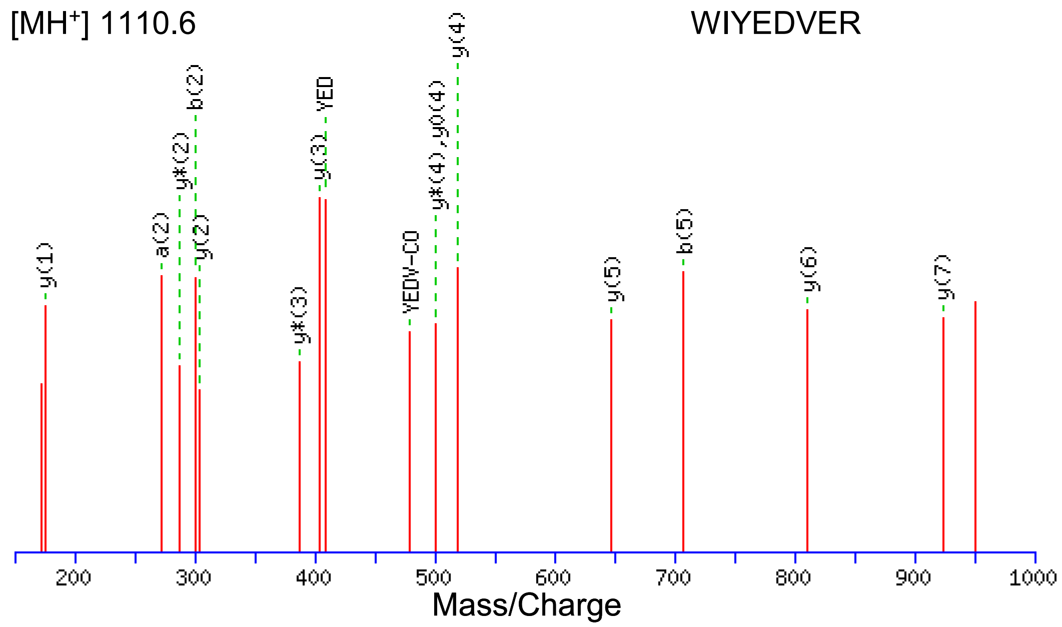

Figure A.b. Mascot result graph of the MALDI-TOF-PSD mass spectrum of the precursor ion m/z = 1110.6 with different ion species indicated.

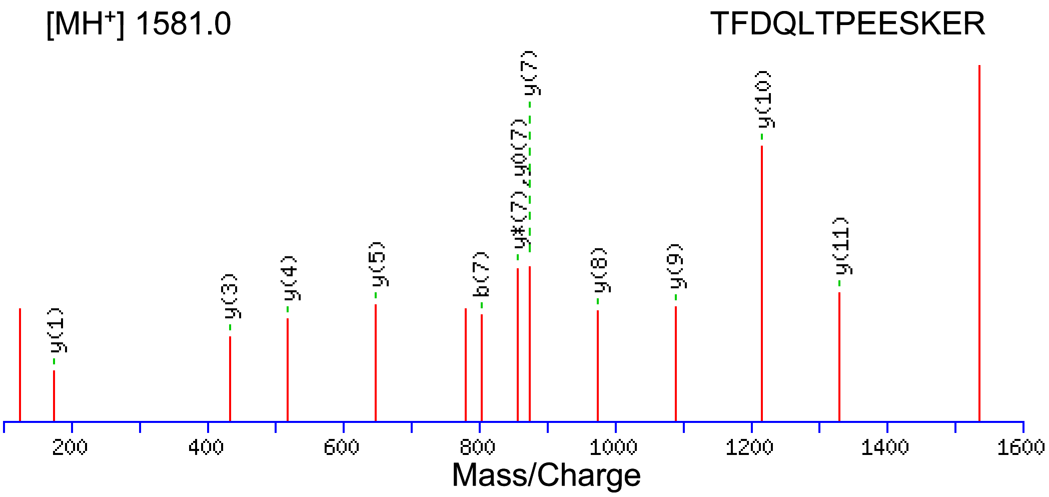

Figure A.c. Mascot result graph of the MALDI-TOF-PSD mass spectrum of the precursor ion m/z = 1581.0 with different ion species indicated.

Galectin-1 (LEG-1)

The following monoisotopic m/z values were experimentally obtained: 533.45, 611.40, 877.68, 968.69, 1041.83, 1076.74, 1482.98, 1486.96, and 1648.03.

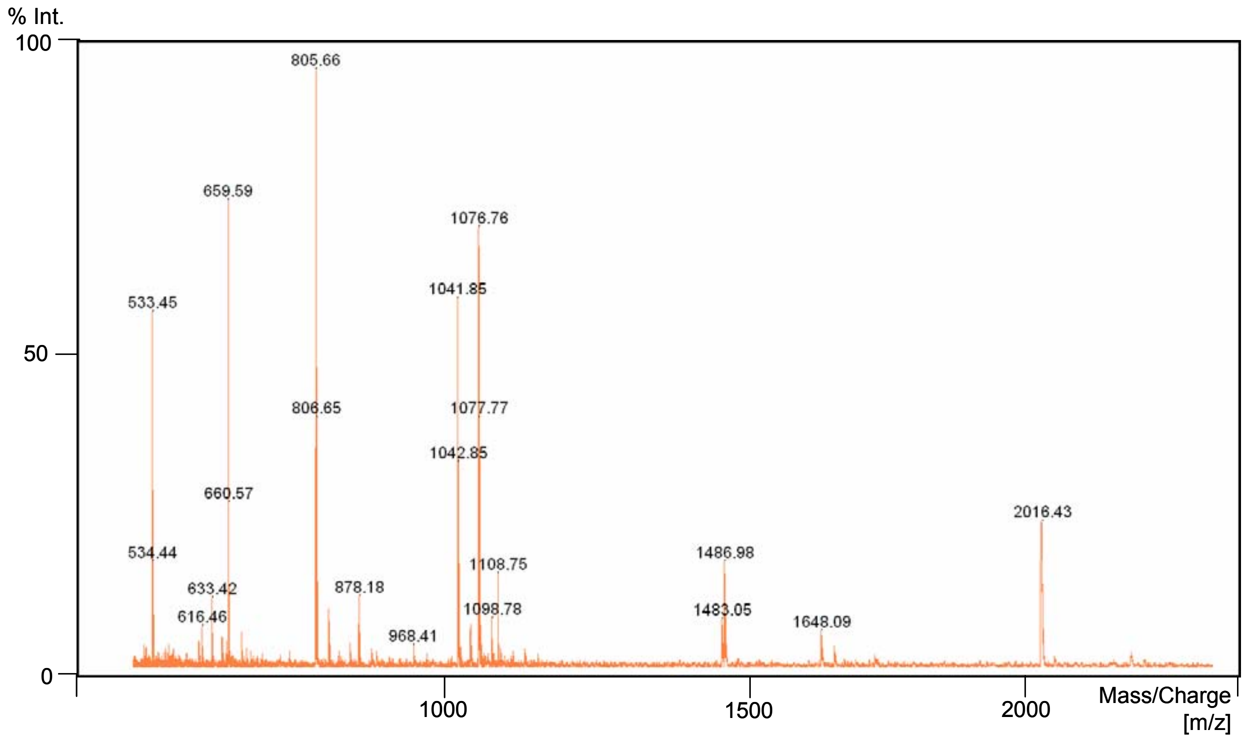

Figure B. Representative peptide mass fingerprint of galectin-1.

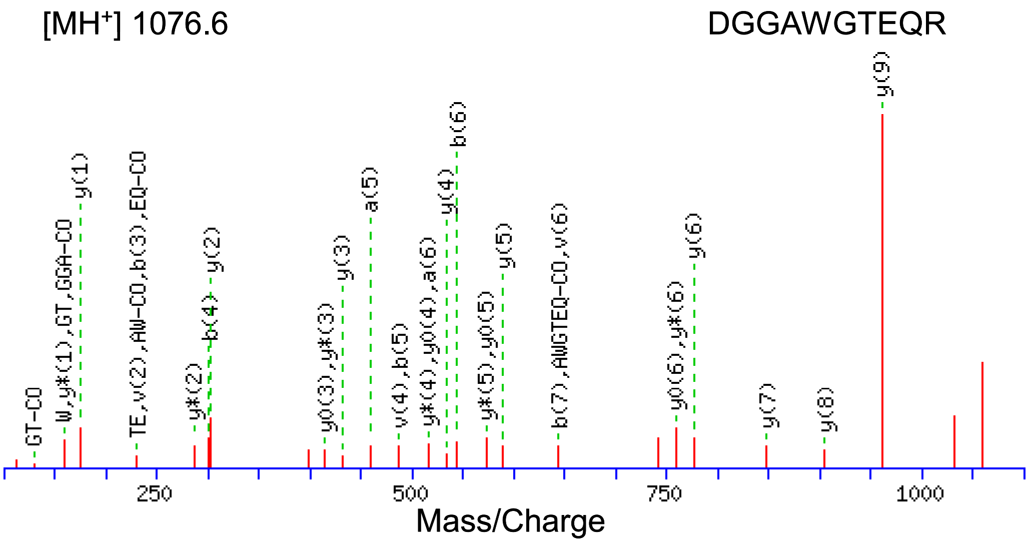

Figure B.a. Mascot result graph of the MALDI-TOF-PSD mass spectrum of the precursor ion m/z = 1076.6 with different ion species indicated.

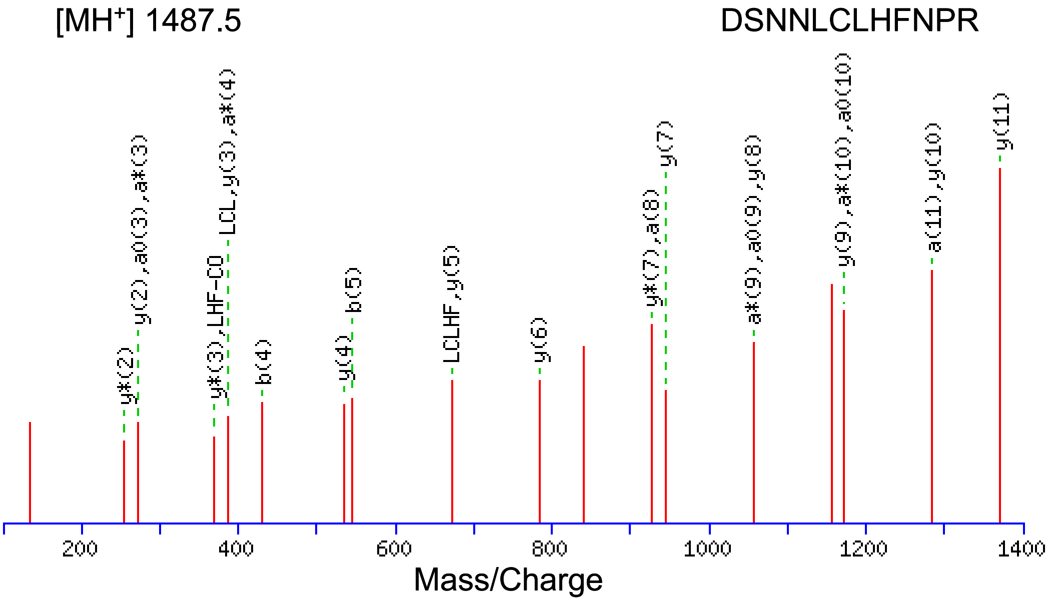

Figure B.b. Mascot result graph of the MALDI-TOF-PSD mass spectrum of the precursor ion m/z = 1487.5 with different ion species indicated.

78kDa glucose-regulated protein (GRP78)

The following monoisotopic m/z values were experimentally obtained: 986.15, 1168.56, 1307.63, 1323.58, 1460.75, 1512.70, 1566.72, 1588.82, 1815.88, 1887.94, 1934.00, and 2164.94.

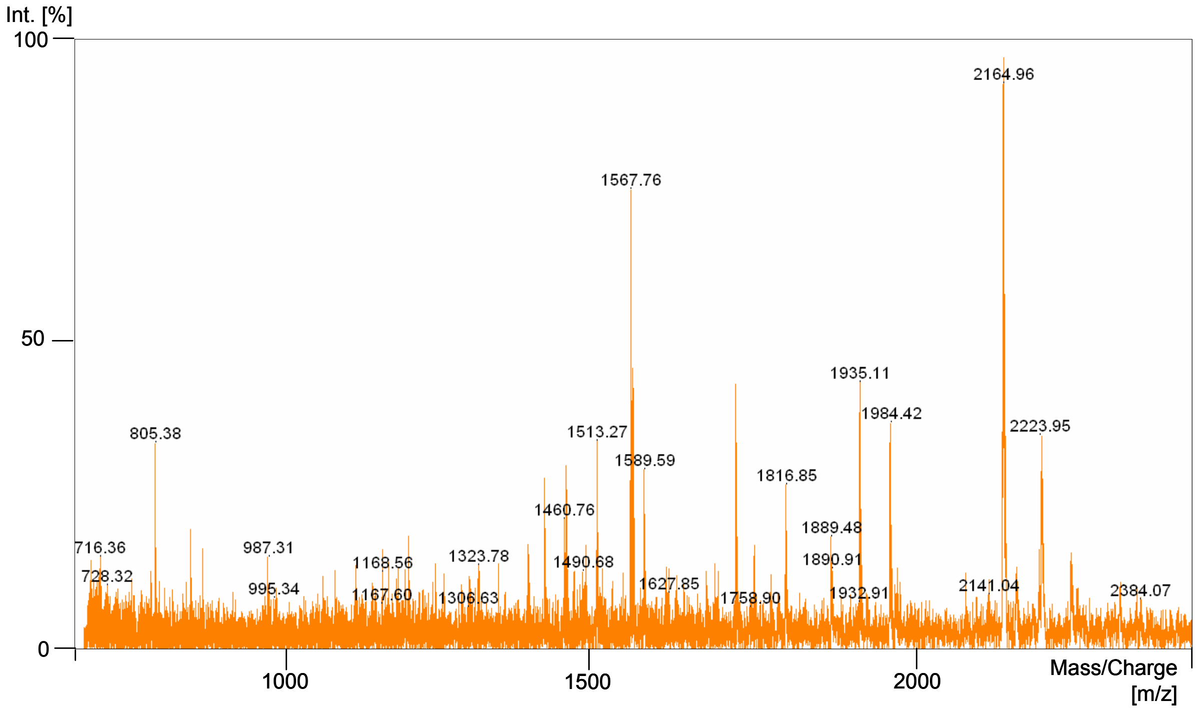

Figure C. Representative peptide mass fingerprint of GRP78.

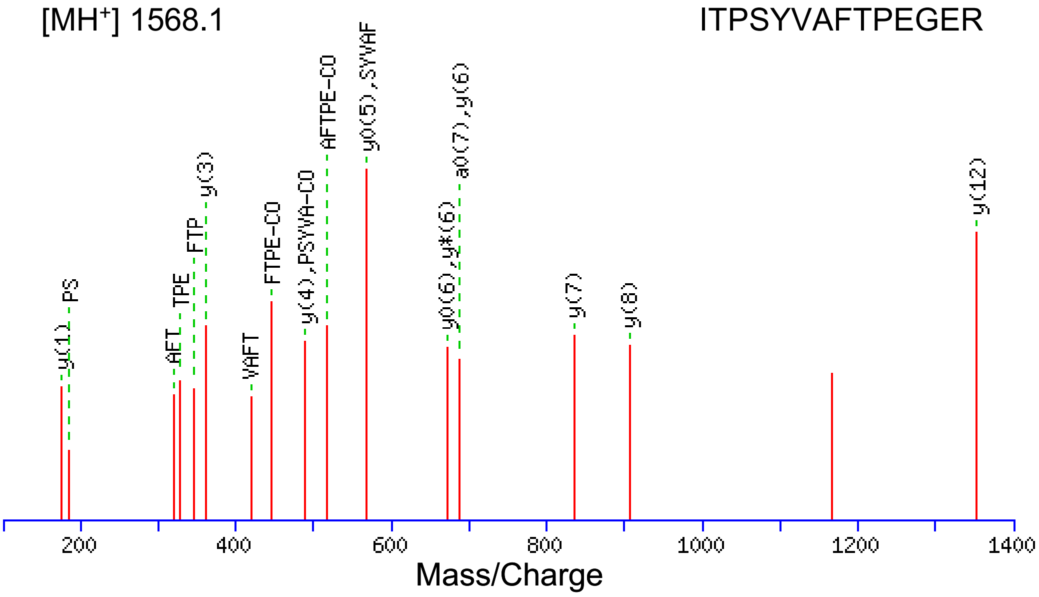

Figure C.a. Mascot result graph of the MALDI-TOF-PSD mass spectrum of the precursor ion m/z = 1568.1 with different ion species indicated.

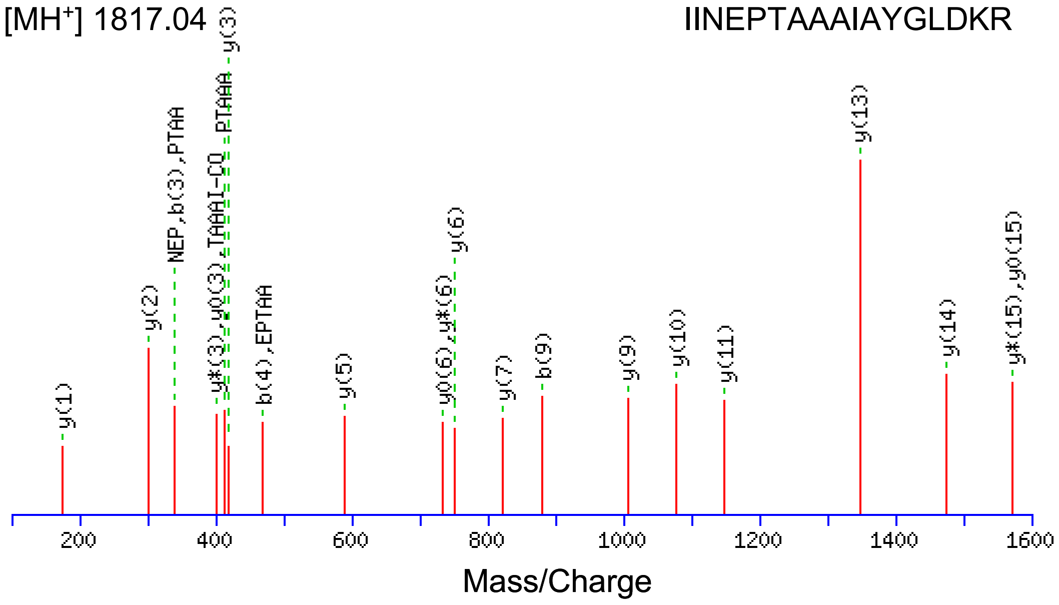

Figure C.b. Mascot result graph of the MALDI-TOF-PSD mass spectrum of the precursor ion m/z = 1817.04 with different ion species indicated.

Heat shock protein 60 (HSP60)

The following monoisotopic m/z values were experimentally obtained: 636.26, 833.35, 855.47, 941.55, 960.44, 1231.55, 1233.58, 1344.57, 1684.70, 1804.76, 1922.80, 2129.50, 2295.65, 2560.45, and 2836.88.

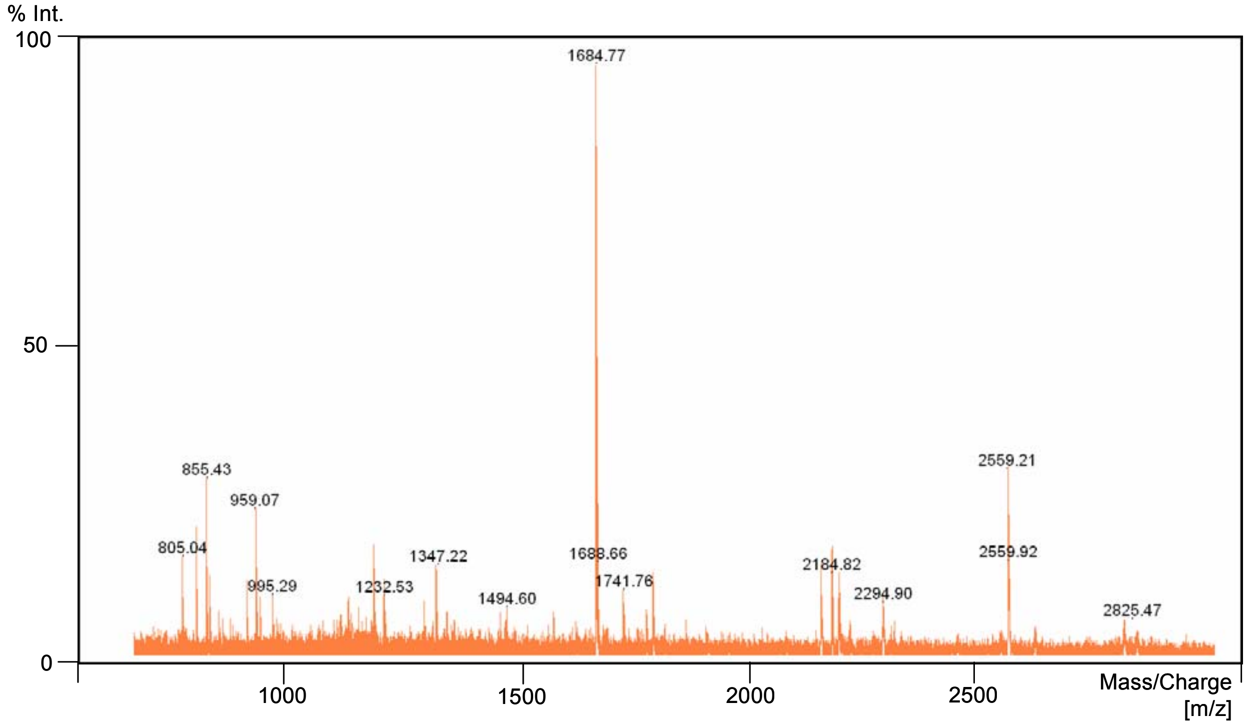

Figure D. Representative peptide mass fingerprint of HSP60.

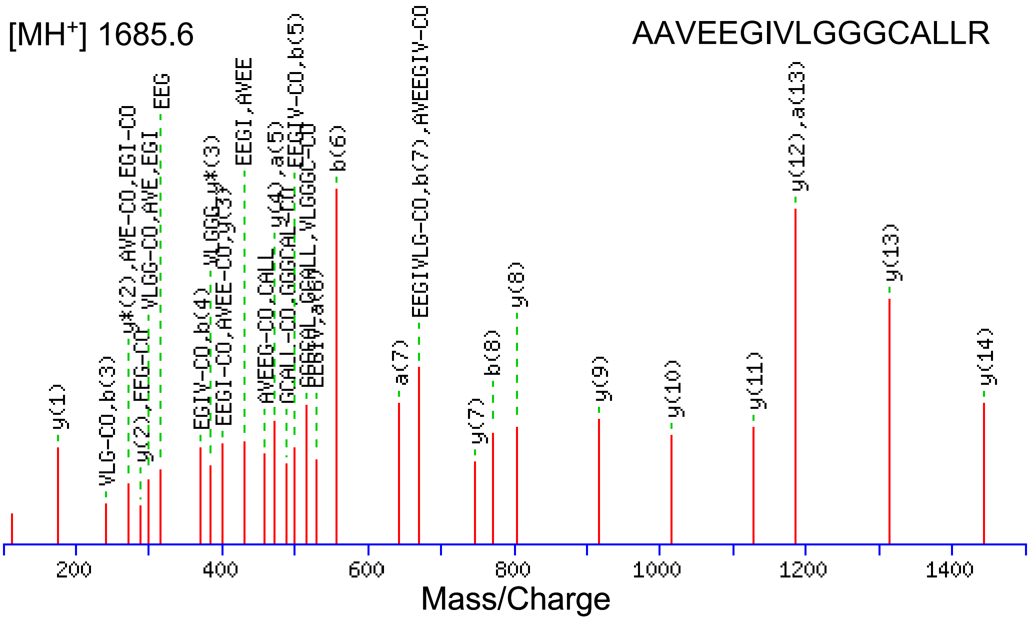

Figure D.a. Mascot result graph of the MALDI-TOF-PSD mass spectrum of the precursor ion m/z = 1685.6 with different ion species indicated.

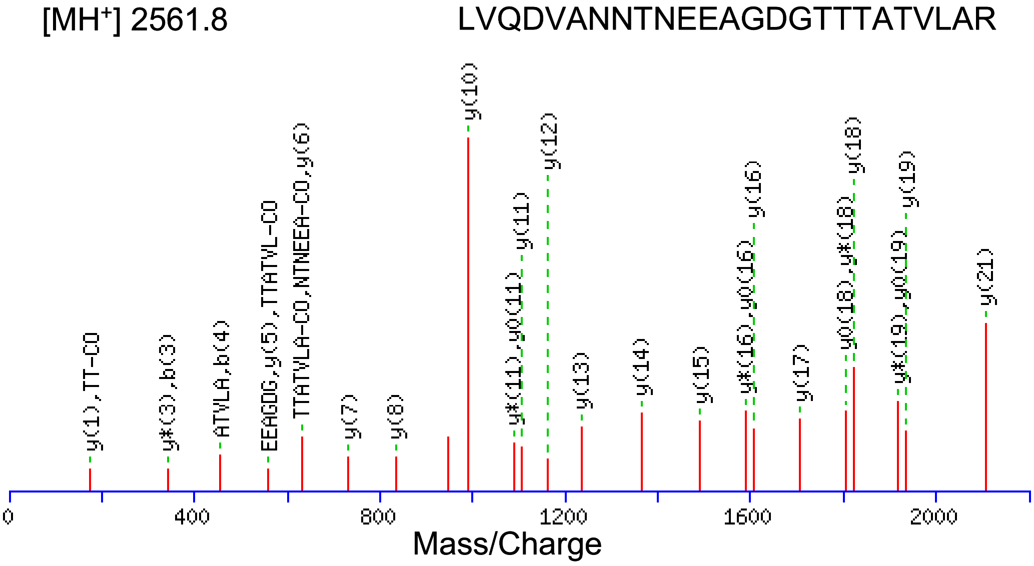

Figure D.b. Mascot result graph of the MALDI-TOF-PSD mass spectrum of the precursor ion m/z = 2561.8 with different ion species indicated.

Nucleophosmin (NPM)

The following monoisotopic m/z values were experimentally obtained: 806.43, 931.45, 974.61, 1568.77, 1819.90, 1835.98, 2227.24, and 2929.71.

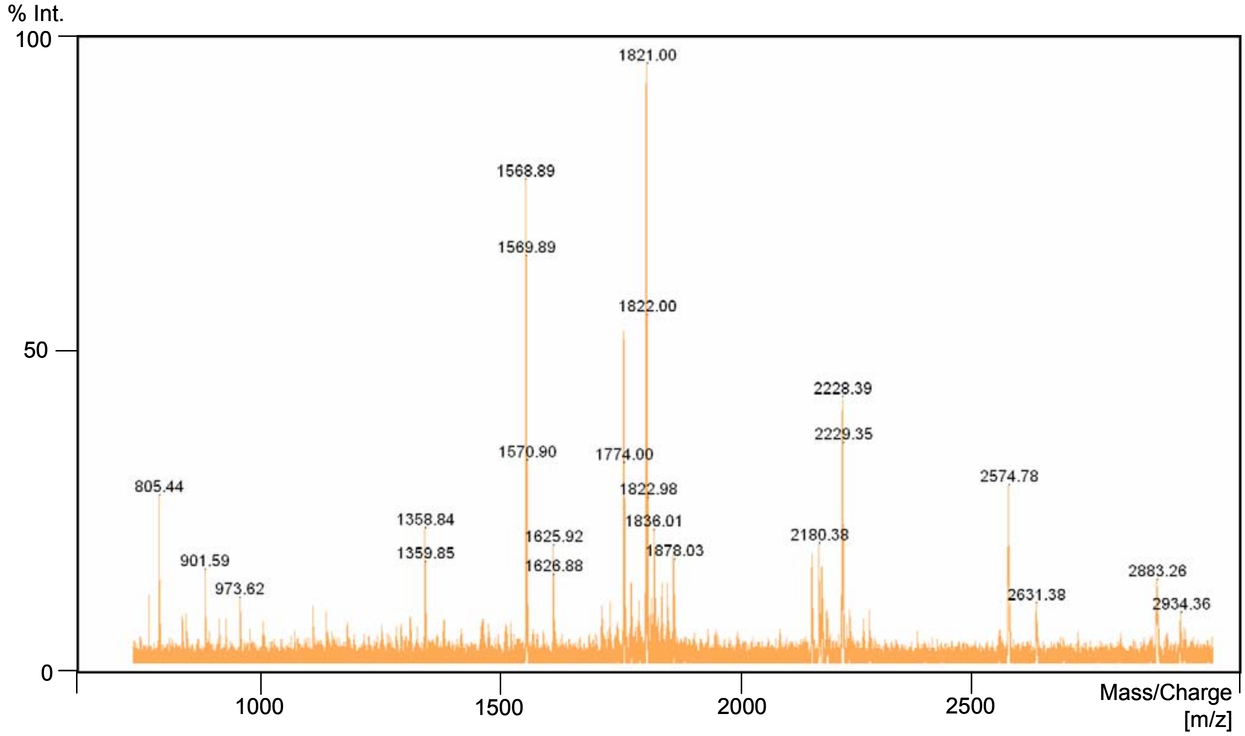

Figure E. Representative peptide mass fingerprint of NPM.

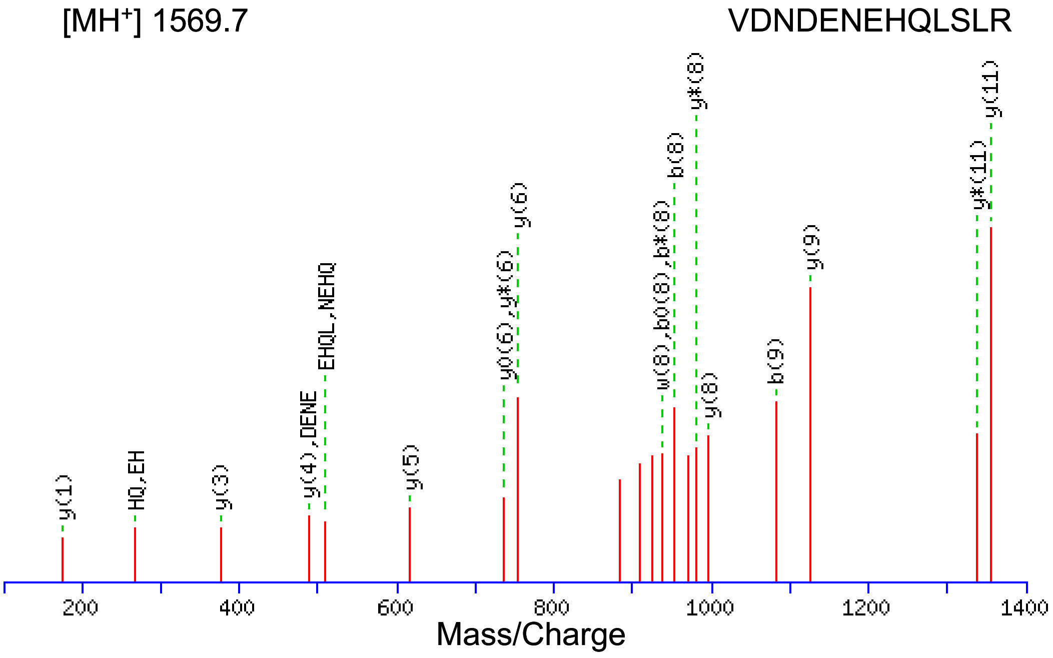

Figure E.a. Mascot result graph of the MALDI-TOF-PSD mass spectrum of the precursor ion m/z = 1569.7 with different ion species indicated.

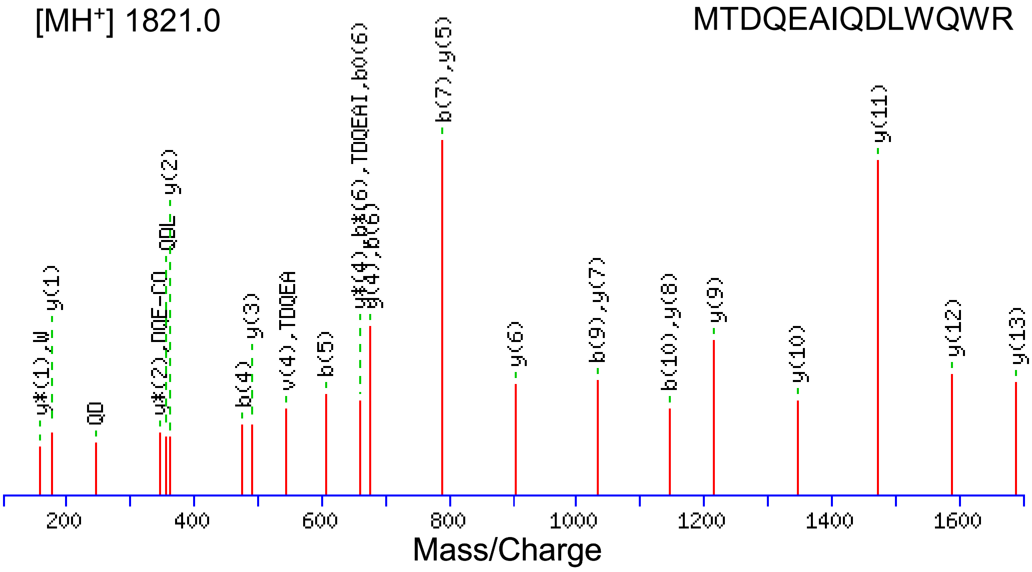

Figure E.b. Mascot result graph of the MALDI-TOF-PSD mass spectrum of the precursor ion m/z = 1821.0 with different ion species indicated.

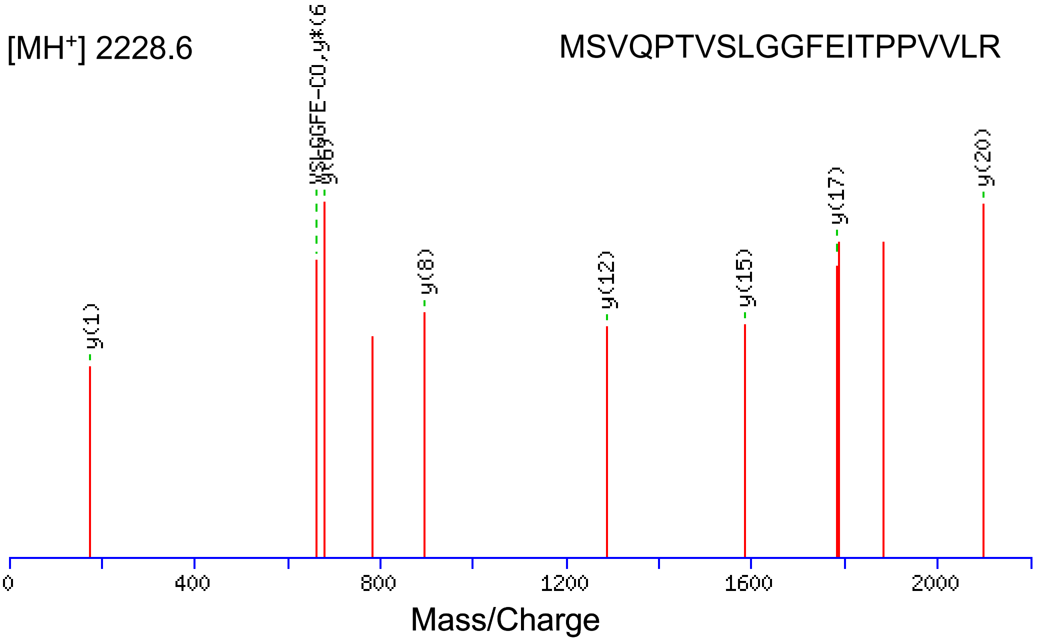

Figure E.c. Mascot result graph of the MALDI-TOF-PSD mass spectrum of the precursor ion m/z = 2228.6 with different ion species indicated.

Peroxiredoxin (PRDX-1)

The following monoisotopic m/z values were experimentally obtained: 819.32, 894.32, 1107.43, 1196.53, 1211.56, 1359.67, and 1982.81.

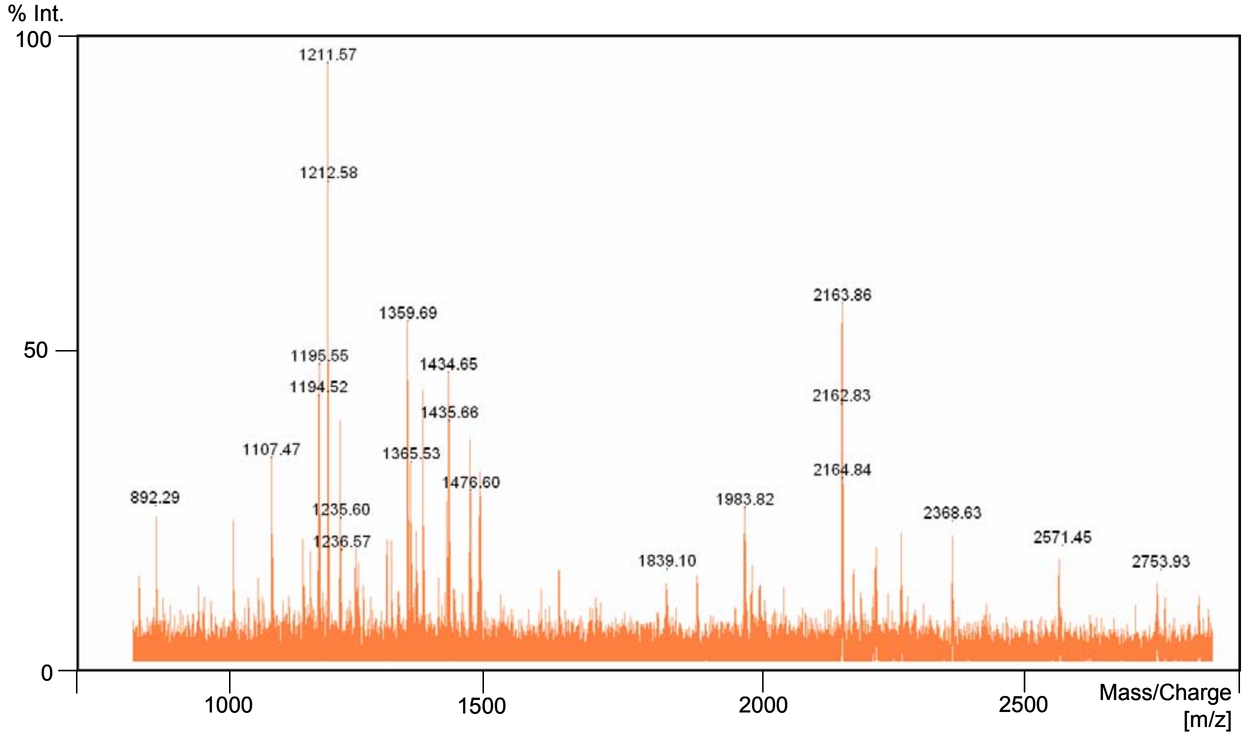

Figure F. Representative peptide mass fingerprint of PRDX-1.

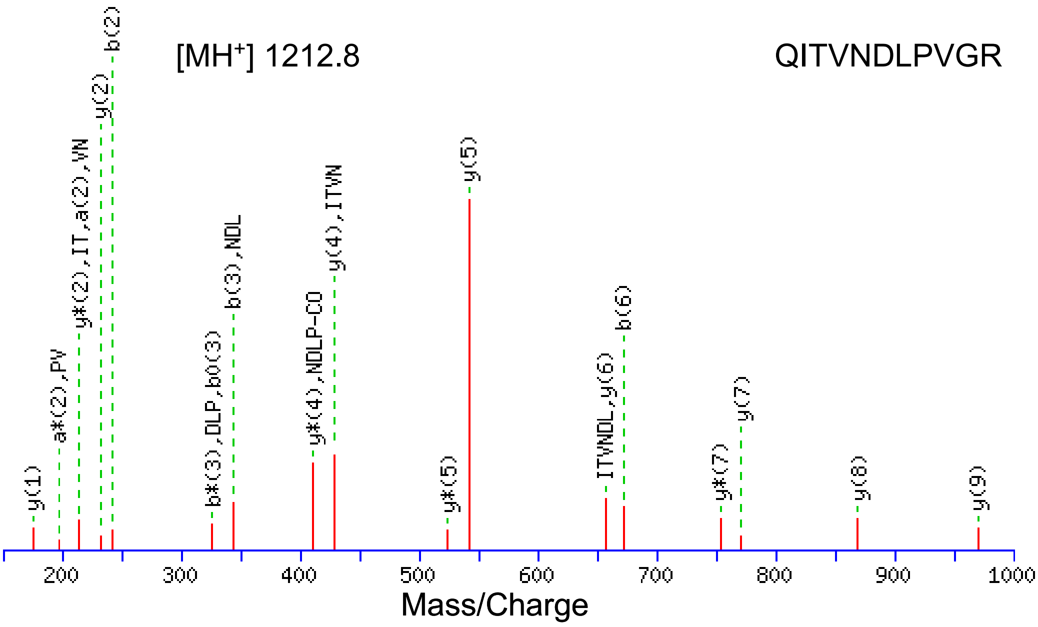

Figure F.a. Mascot result graph of the MALDI-TOF-PSD mass spectrum of the precursor ion m/z = 1212.8 with different ion species indicated.

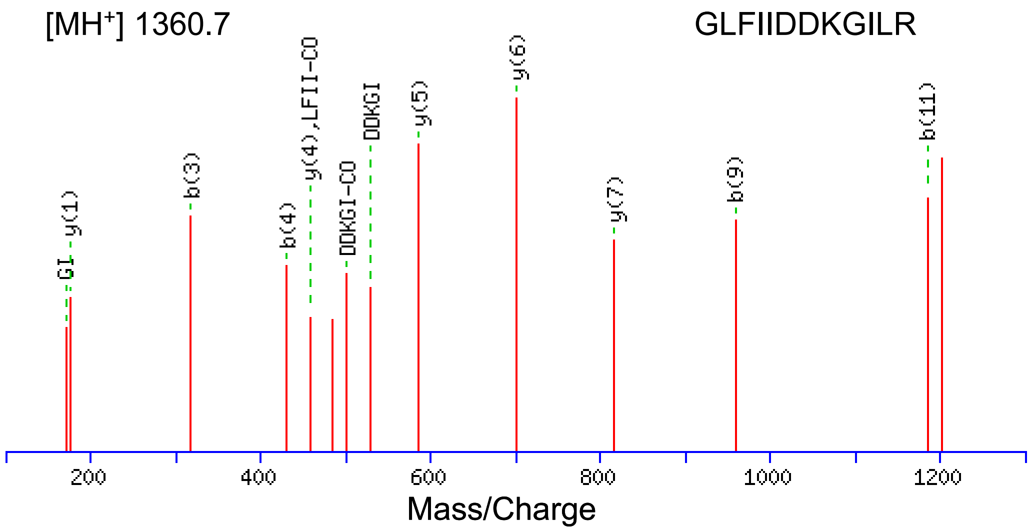

Figure F.b. Mascot result graph of the MALDI-TOF-PSD mass spectrum of the precursor ion m/z = 1360.7 with different ion species indicated.

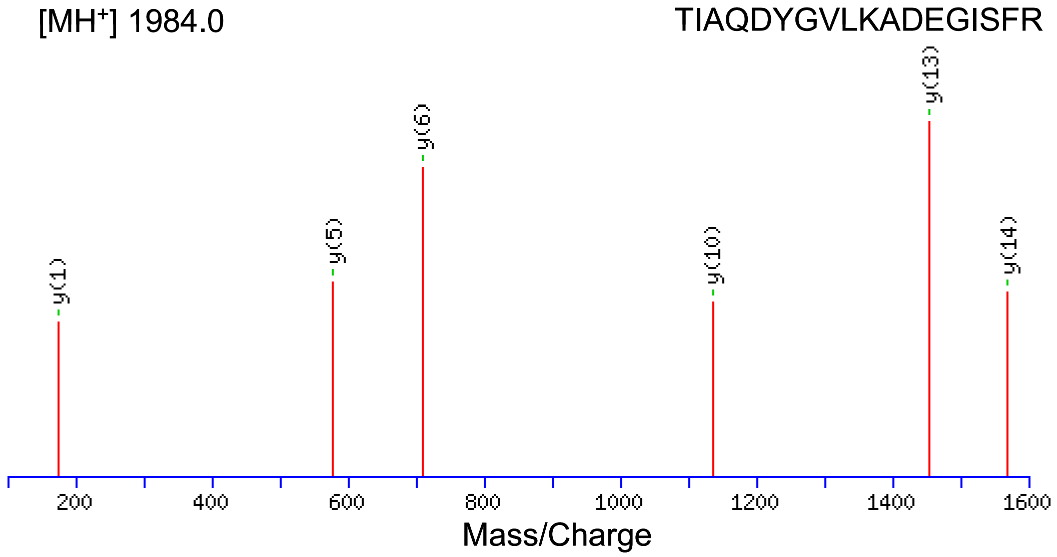

Figure F.c. Mascot result graph of the MALDI-TOF-PSD mass spectrum of the precursor ion m/z = 1984.0 with different ion species indicated.

Peroxiredoxin-6 (PRDX-6)

The following monoisotopic m/z values were experimentally obtained: 906.40, 1085.47, 1191.53, 1356.73, 1395.57, 1512.68, 1884.85, and 2097.84.

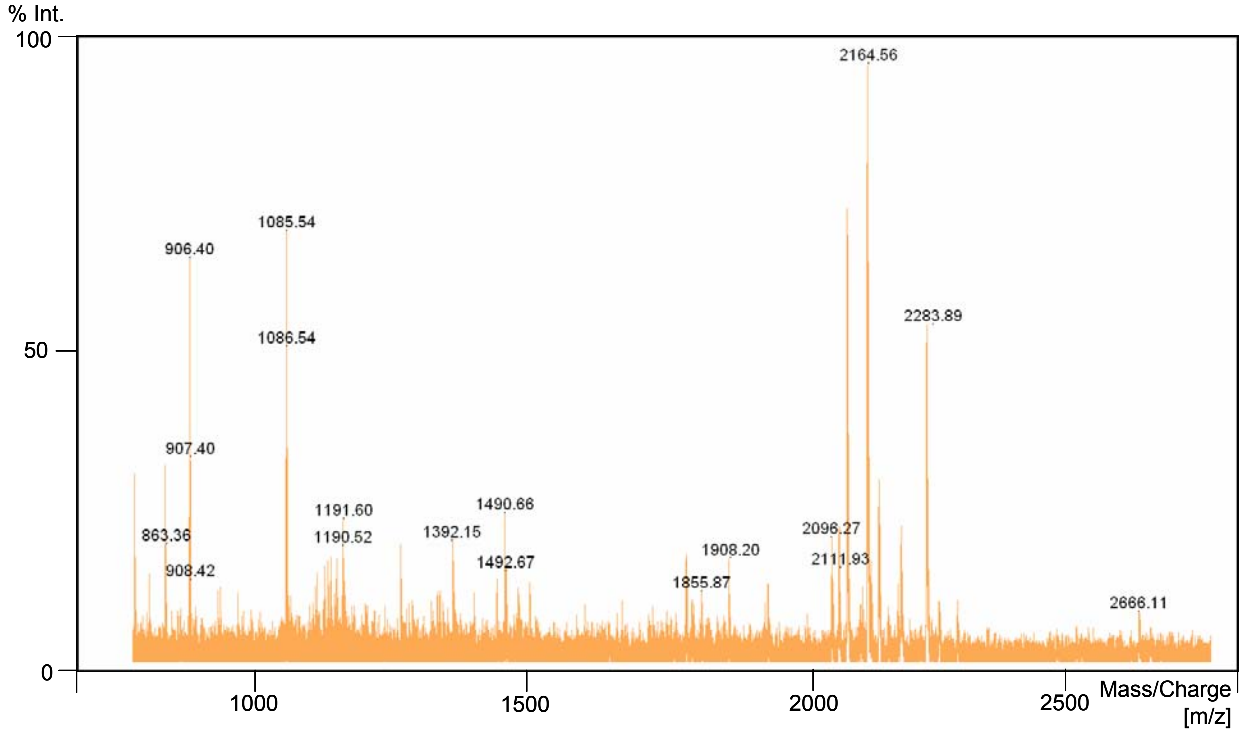

Figure G. Representative peptide mass fingerprint of PRDX-6.

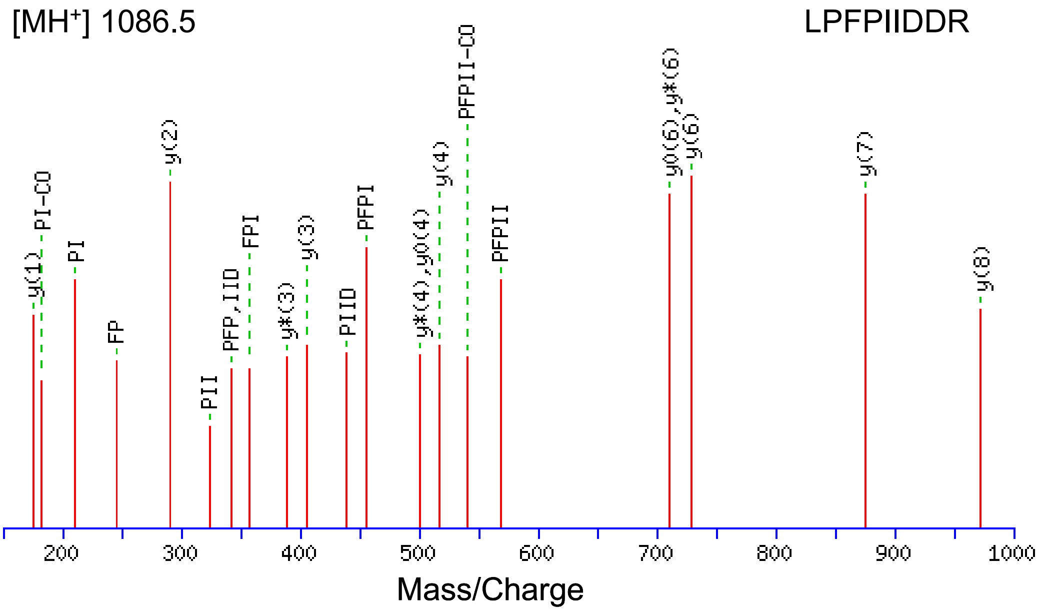

Figure G.a. Mascot result graph of the MALDI-TOF-PSD mass spectrum of the precursor ion m/z = 1086.5 with different ion species indicated.

T-complex protein 1 subunit beta (TCP β)

The following monoisotopic m/z values were experimentally obtained: 745.52, 870.67, 1130.73, 1291.89, 1330.79, 1407.04, 1481.66, 1530.96, 1549.03, 1583.09, 1956.20, and 3209.8.

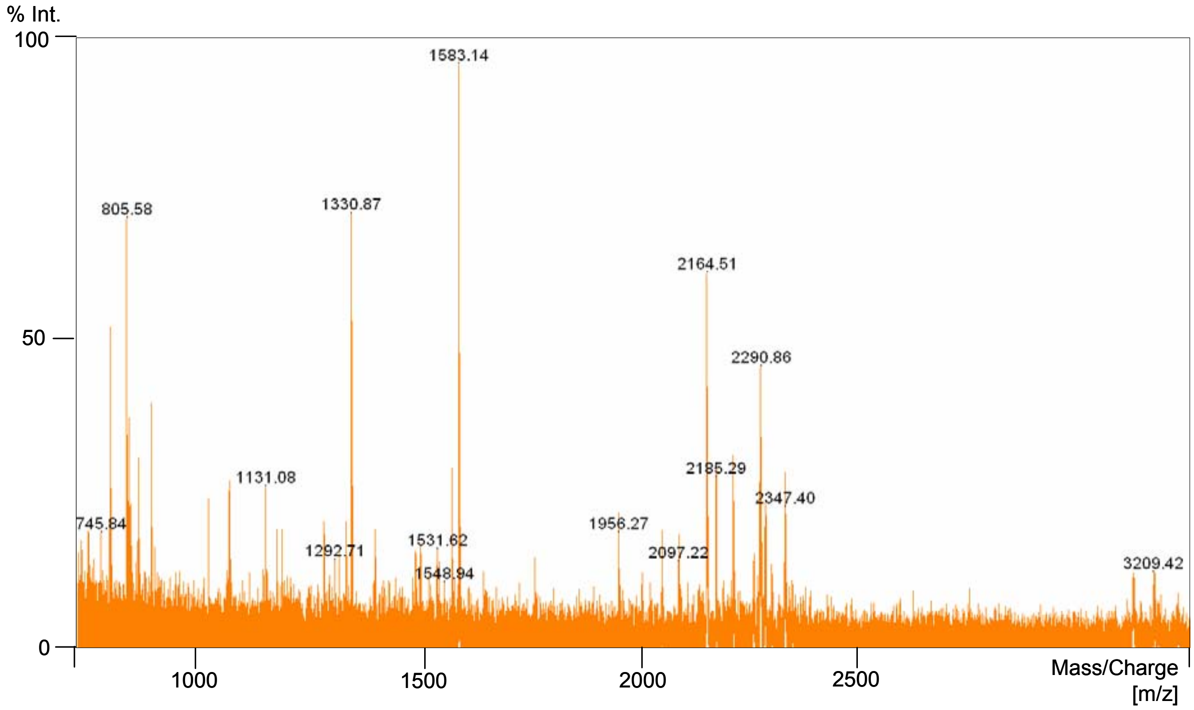

Figure H. Representative peptide mass fingerprint of TCP β.

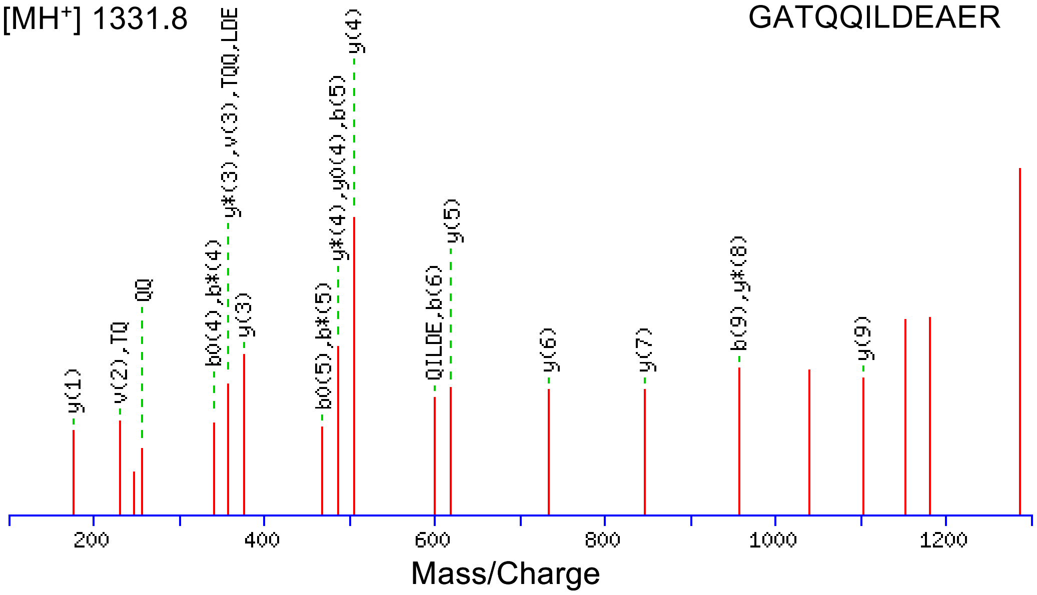

Figure H.a. Mascot result graph of the MALDI-TOF-PSD mass spectrum of the precursor ion m/z = 1331.8 with different ion species indicated.

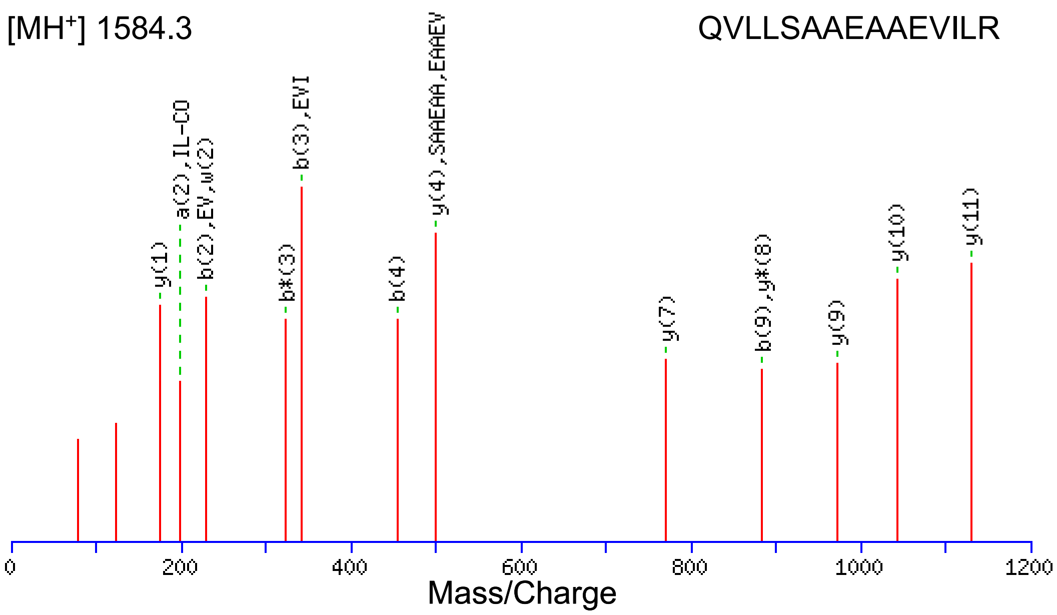

Figure H.b. Mascot result graph of the MALDI-TOF-PSD mass spectrum of the precursor ion m/z = 1584.3 with different ion species indicated.

T-complex protein 1 subunit epsilon (TCP ε)

The following monoisotopic m/z values were experimentally obtained: 692.53, 819.67, 924.58, 1093.66, 1168.74, 1183.80, 1205.87, 1268.91, 1739.11, and 1911.18.

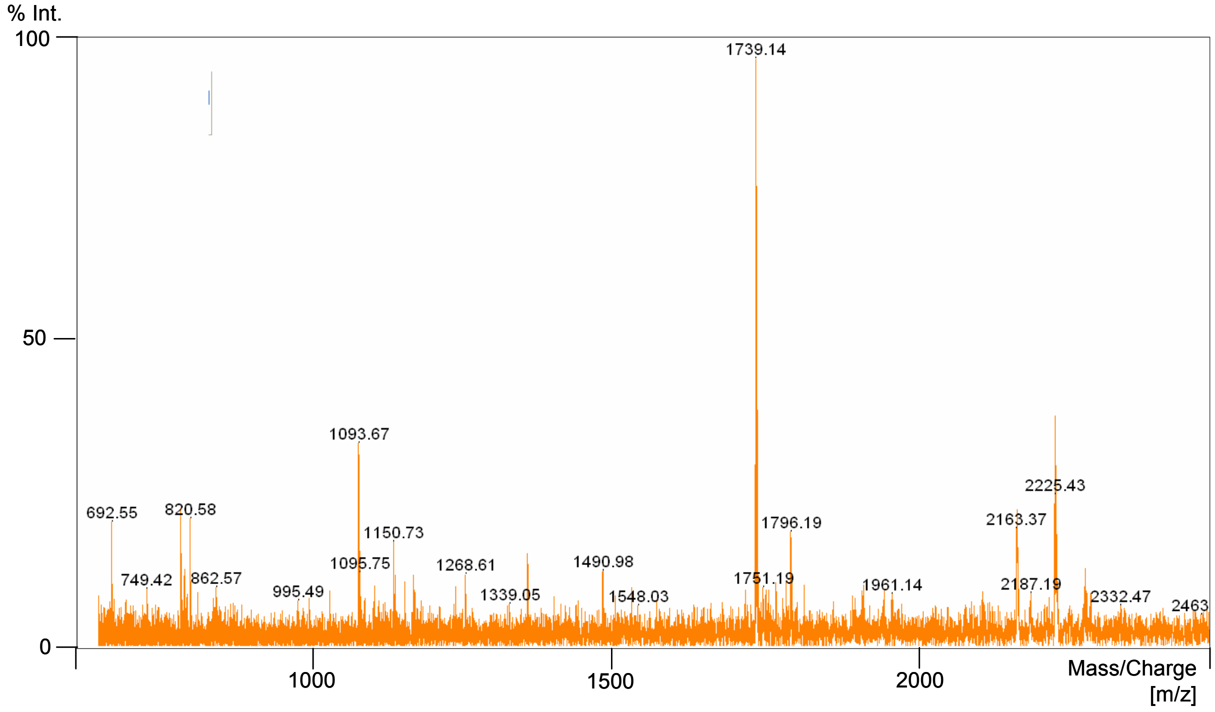

Figure I. Representative peptide mass fingerprint of TCP ε.

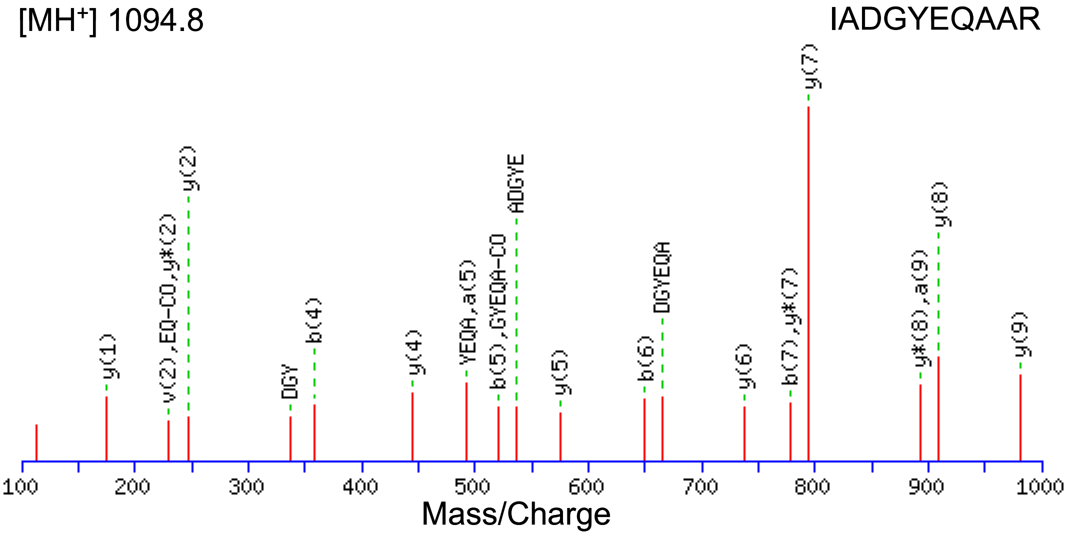

Figure I.a. Mascot result graph of the MALDI-TOF-PSD mass spectrum of the precursor ion m/z = 1094.8 with different ion species indicated.

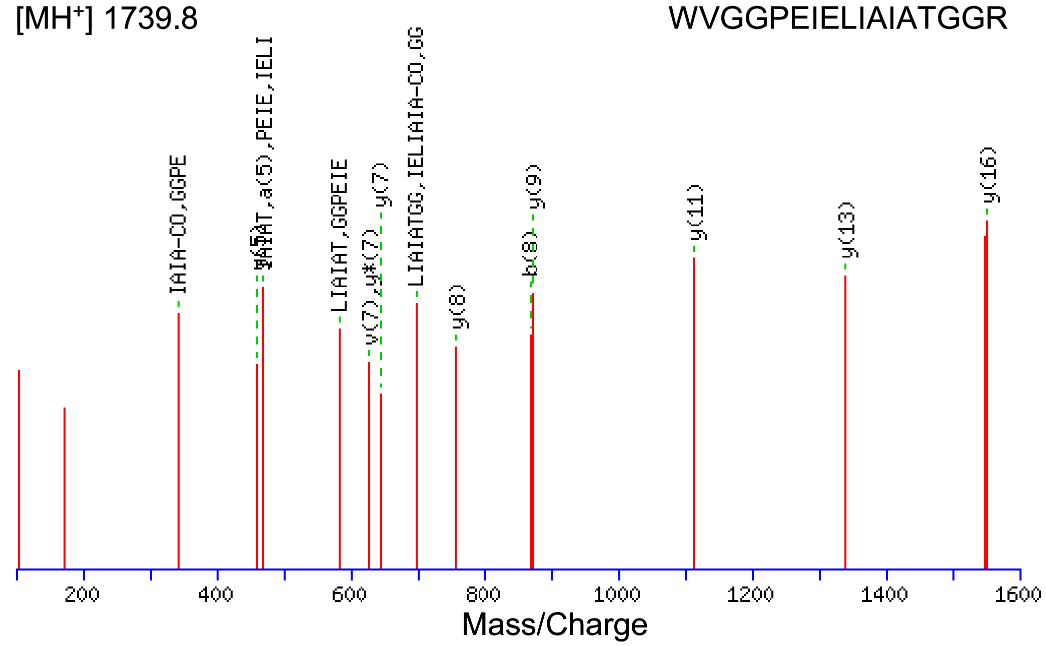

Figure I.b. Mascot result graph of the MALDI-TOF-PSD mass spectrum of the precursor ion m/z = 1739.8 with different ion species indicated.

Actin, cytoplasmatic 1 (ACTB)

The following monoisotopic m/z values were experimentally obtained: 516.36, 631.27, 644.47, 777.51, 795.54, 976.54, 1014.71, 1132.75, 1198.92, 1516.04, 1791.06, and 1954.22.

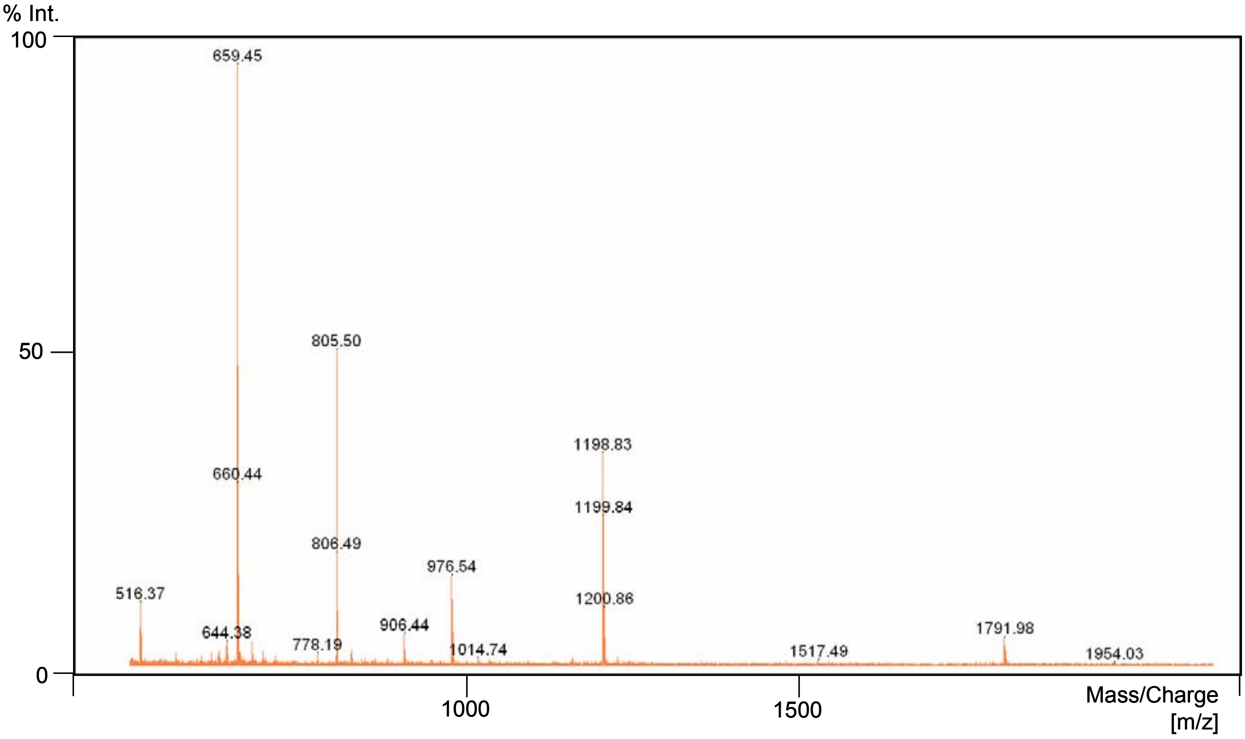

Figure J. Representative peptide mass fingerprint of ACTB.

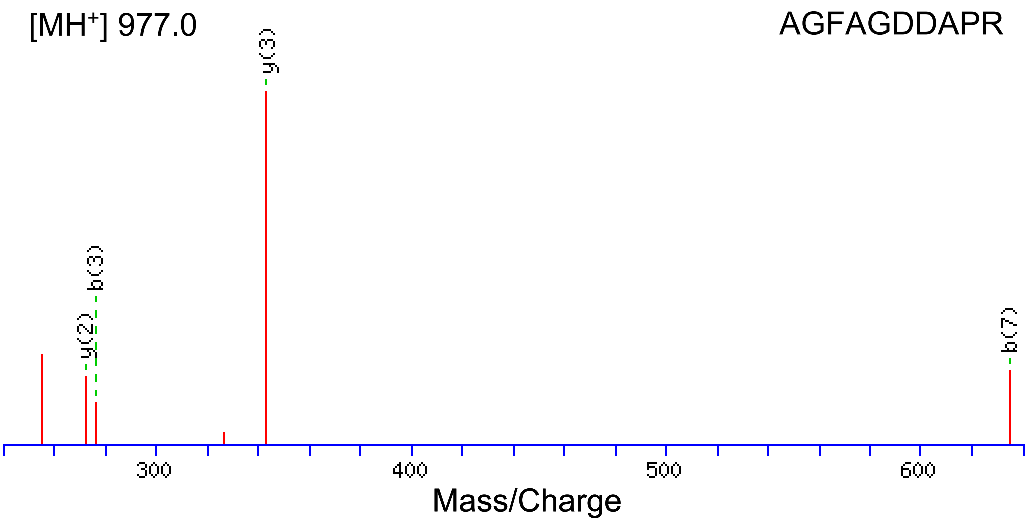

Figure J.a. Mascot result graph of the MALDI-TOF-PSD mass spectrum of the precursor ion m/z = 977.0 with different ion species indicated.

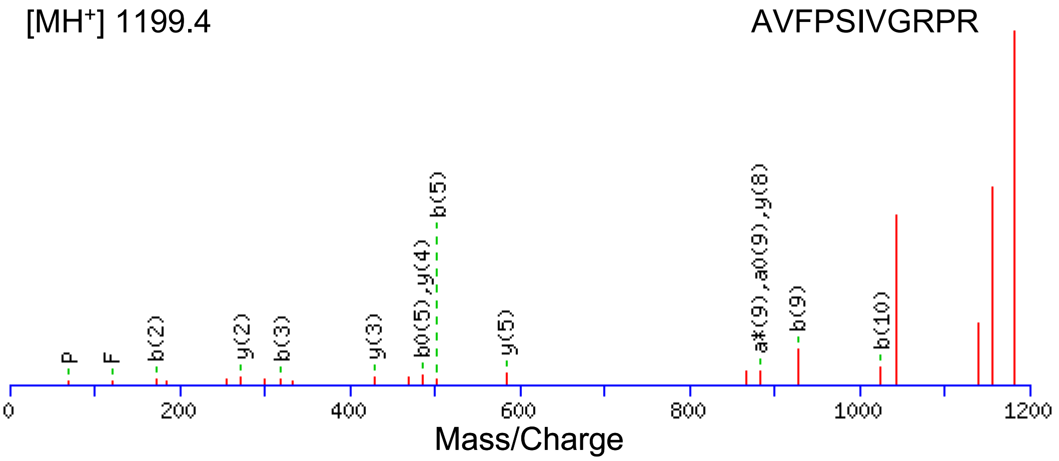

Figure J.b. Mascot result graph of the MALDI-TOF-PSD mass spectrum of the precursor ion m/z = 1199.4 with different ion species indicated.

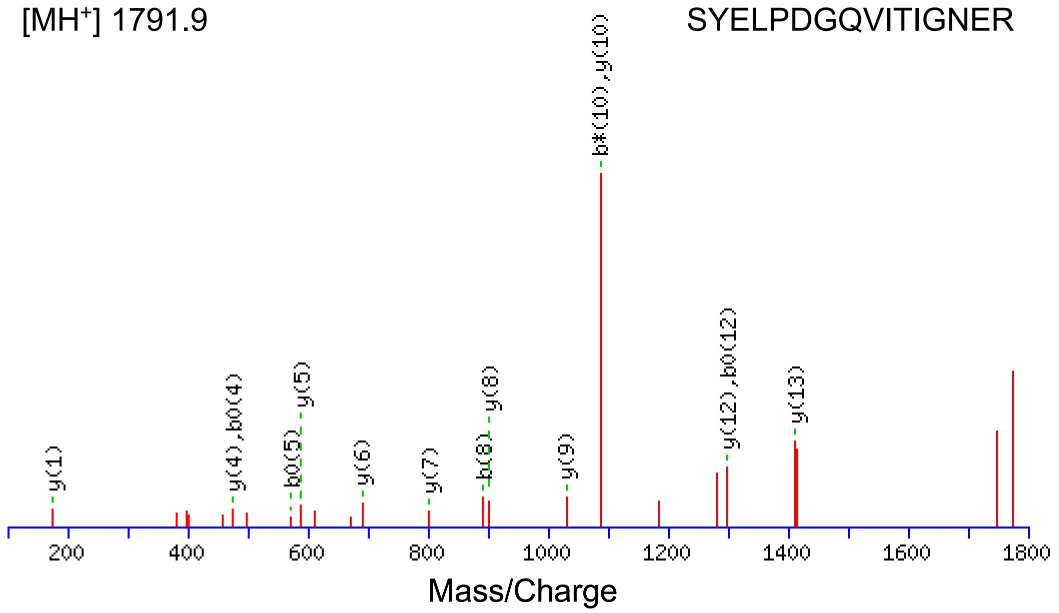

Figure J.c. Mascot result graph of the MALDI-TOF-PSD mass spectrum of the precursor ion m/z = 1791.9 with different ion species indicated.

Cofilin-1 (COF-1)

The following monoisotopic m/z values were experimentally obtained: 721.44, 753.53, 799.55, 915.58, 1034.66, 1309.78, 1337.73, 1340.96, 1790.82, and 1990.10.

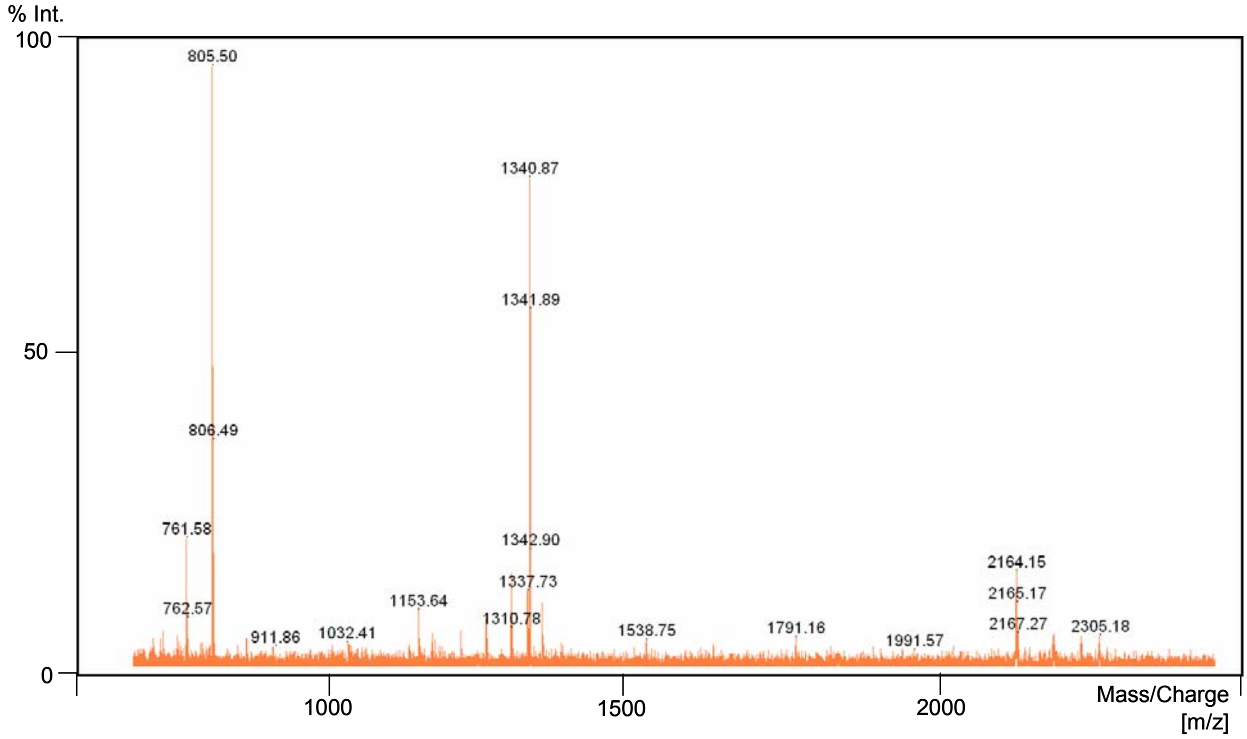

Figure K. Representative peptide mass fingerprint of COF-1.

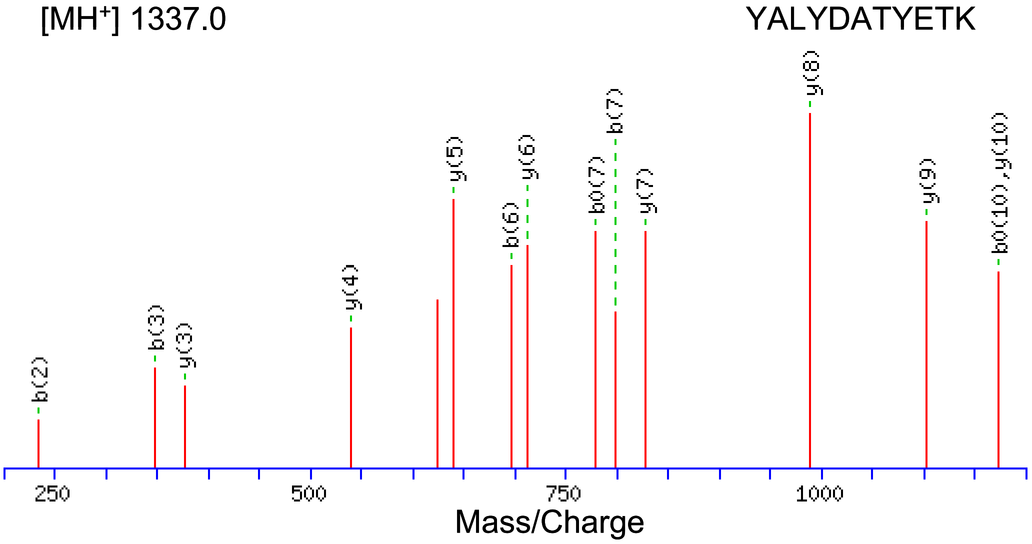

Figure K.a. Mascot result graph of the MALDI-TOF-PSD mass spectrum of the precursor ion m/z = 1337.0 with different ion species indicated.

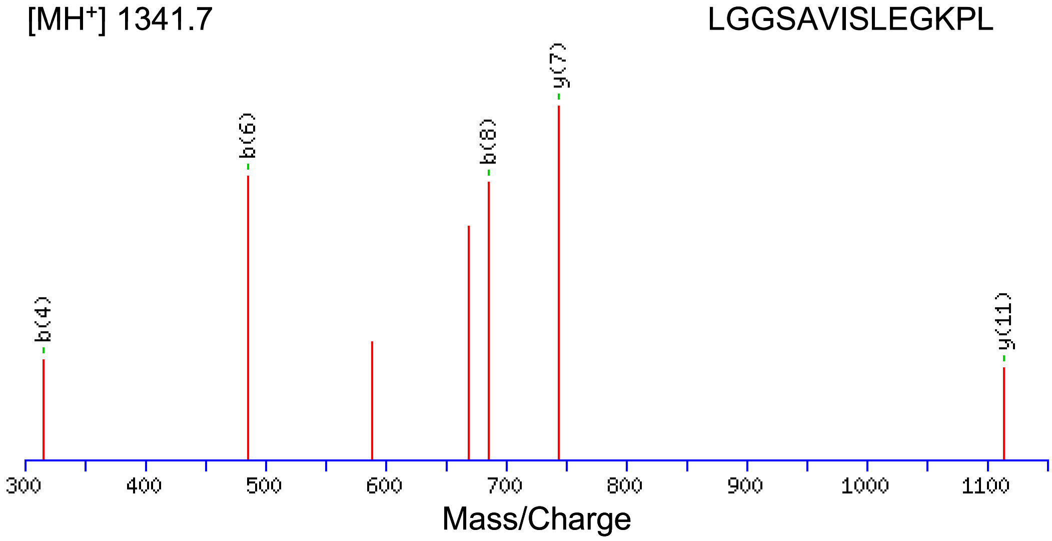

Figure K.b. Mascot result graph of the MALDI-TOF-PSD mass spectrum of the precursor ion m/z = 1341.7 with different ion species indicated.

Tropomyosin α

The following monoisotopic m/z values were experimentally obtained: 894.73, 1228.91, 1243.95, 1285.05, 1316.95, 1400.02, 1544.06, 1672.23, 1728.18, and 1784.23.

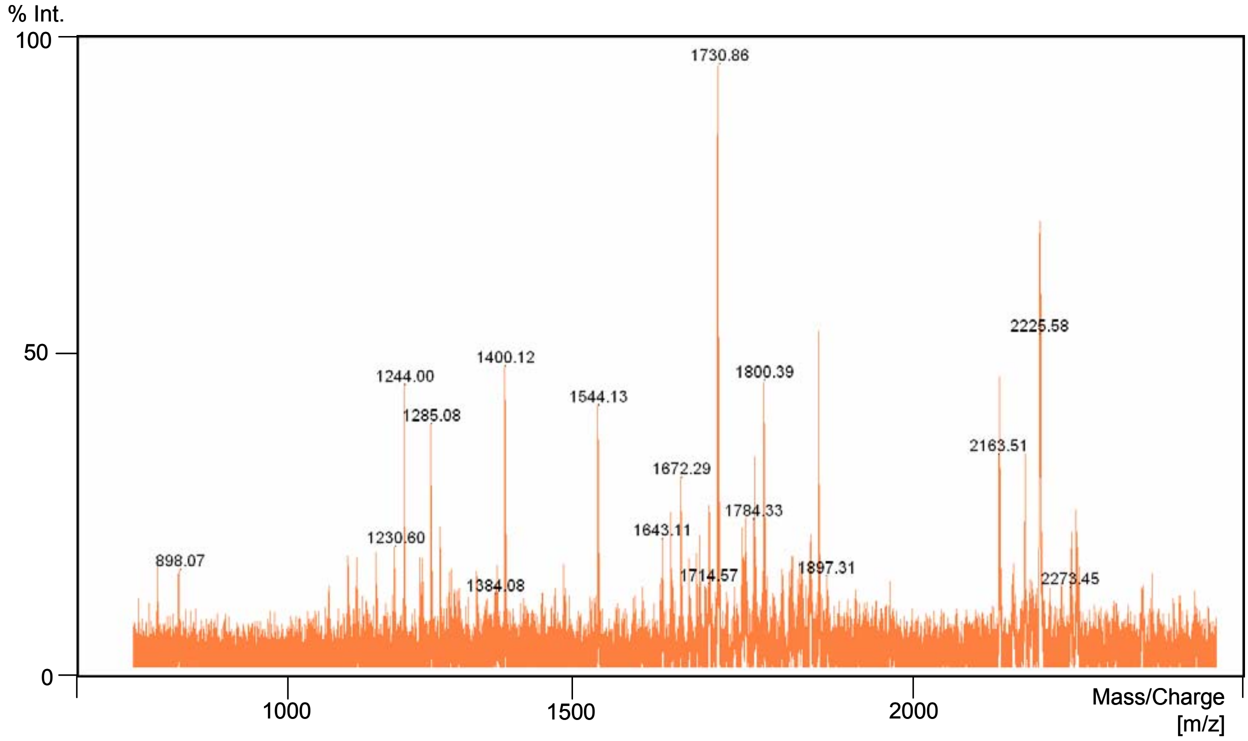

Figure L. Representative peptide mass fingerprint of Tropomyosin alpha.

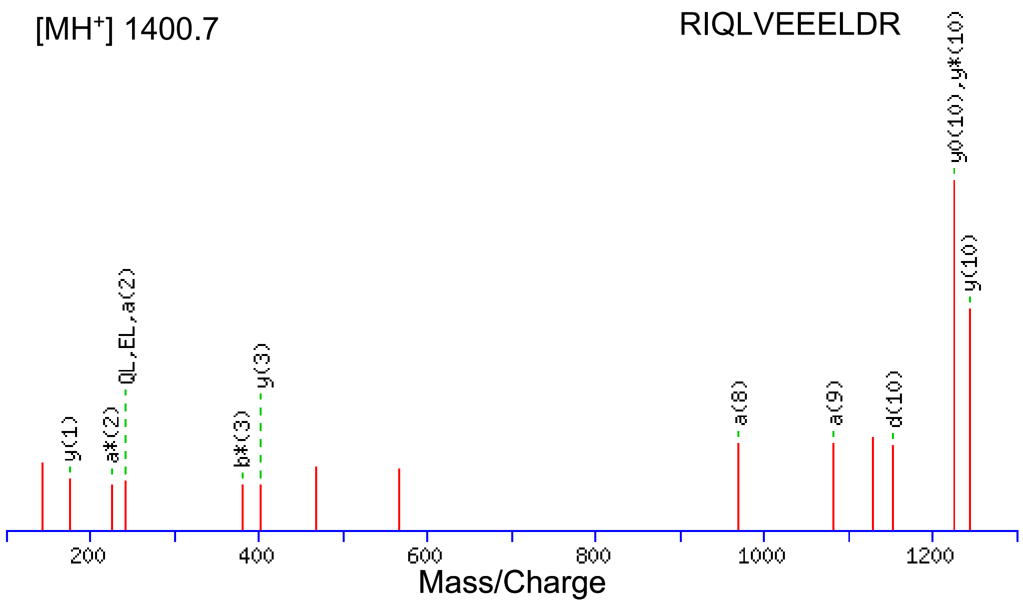

Figure L.a. Mascot result graph of the MALDI-TOF-PSD mass spectrum of the precursor ion m/z = 1400.7 with different ion species indicated.

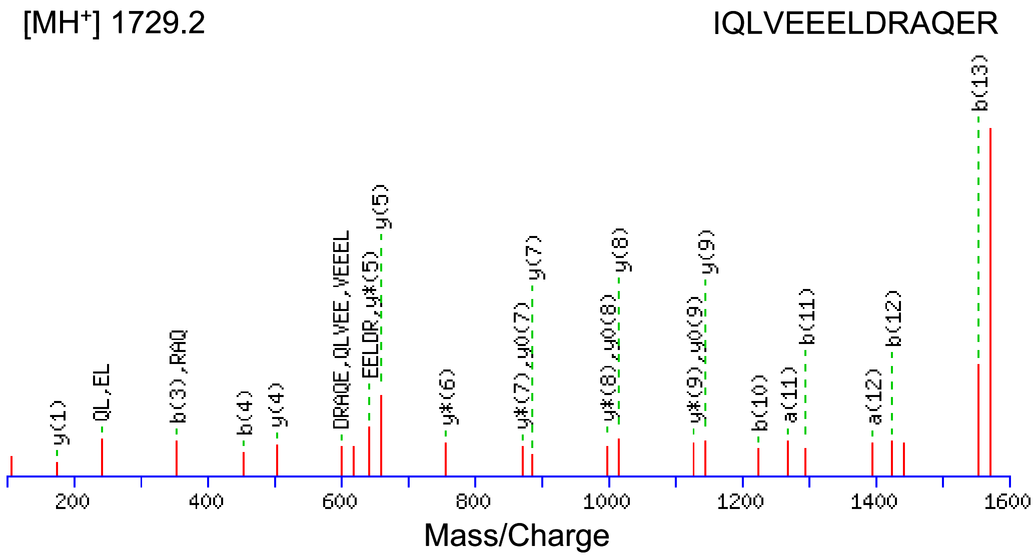

Figure L.b. Mascot result graph of the MALDI-TOF-PSD mass spectrum of the precursor ion m/z = 1729.2 with different ion species indicated.

Tropomyosin β

The following monoisotopic m/z values were experimentally obtained: 1069.64, 1091.62, 1092.70, 1106.67, 1148.70, 1164.71, 1169.74, 1233.71, 1307.70, 1537.90, and 1717.06.

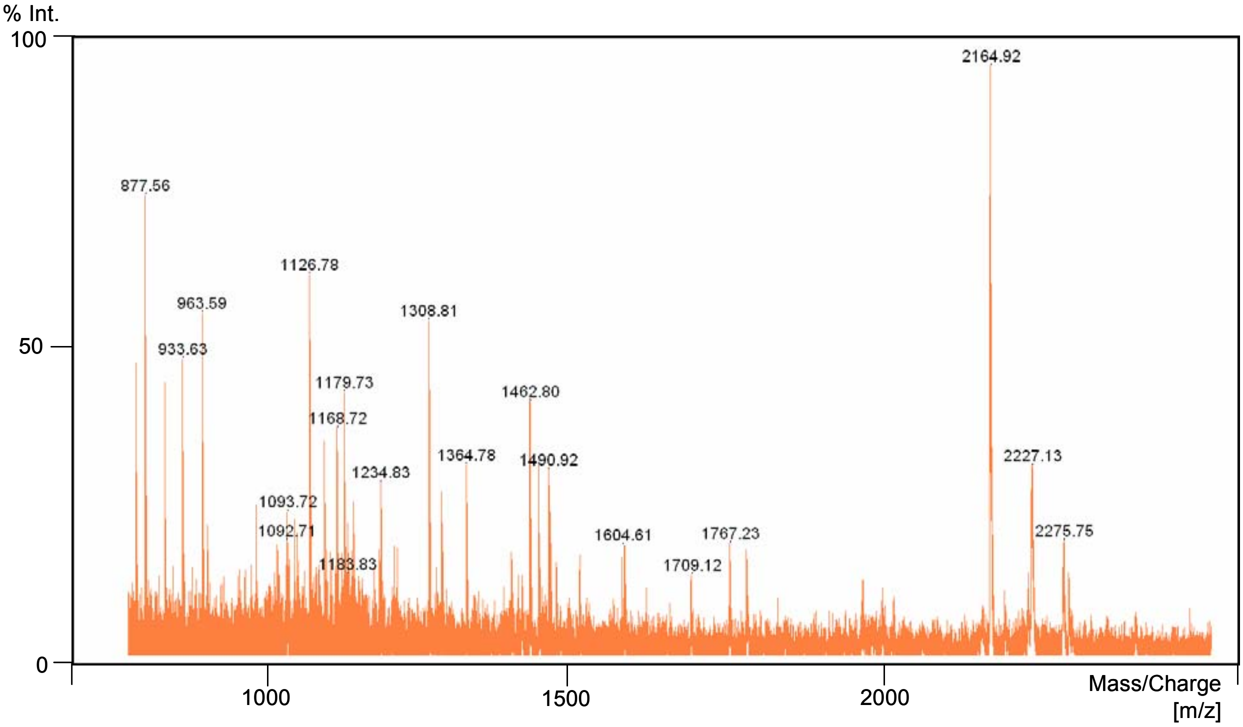

Figure M. Representative peptide mass fingerprint of Tropomyosin beta.

[MH^+] 1539.1 TIDDLEDEVYAQK

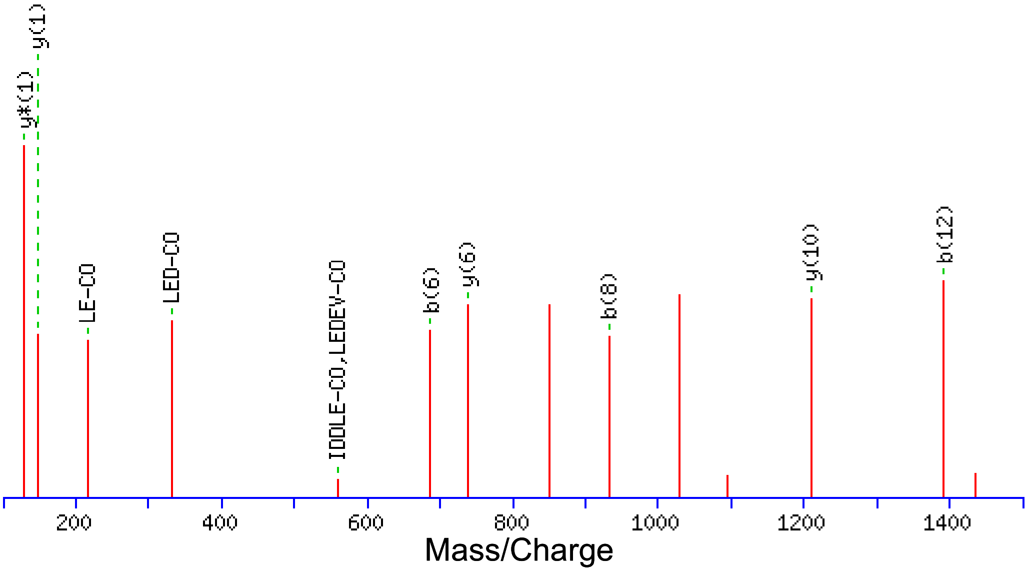

Figure M.a. Mascot result graph of the MALDI-TOF-PSD mass spectrum of the precursor ion m/z = 1539.1 with different ion species indicated.

Alpha-enolase (ENOA-1)

The following monoisotopic m/z values were experimentally obtained: 661.37, 704.49, 766.45, 801.56, 806.53, 1007.6, 1540.92, 1805.10, 1908.13, and 2176.17.

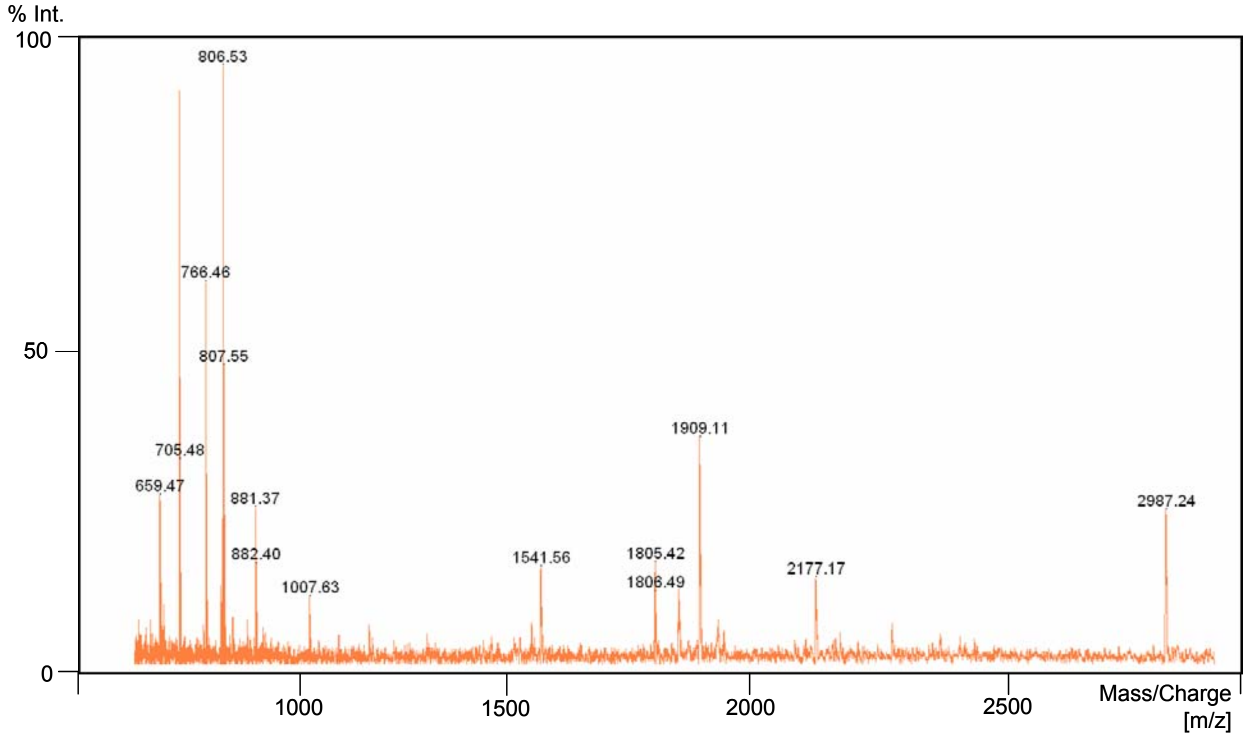

Figure N. Representative peptide mass fingerprint of ENOA-1.

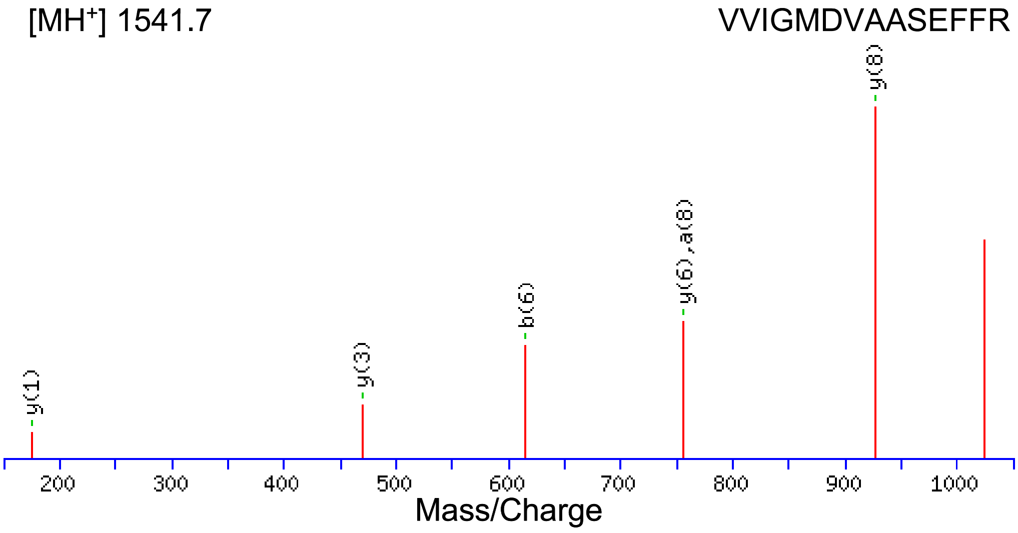

Figure N.a. Mascot result graph of the MALDI-TOF-PSD mass spectrum of the precursor ion m/z = 1541.7 with different ion species indicated.

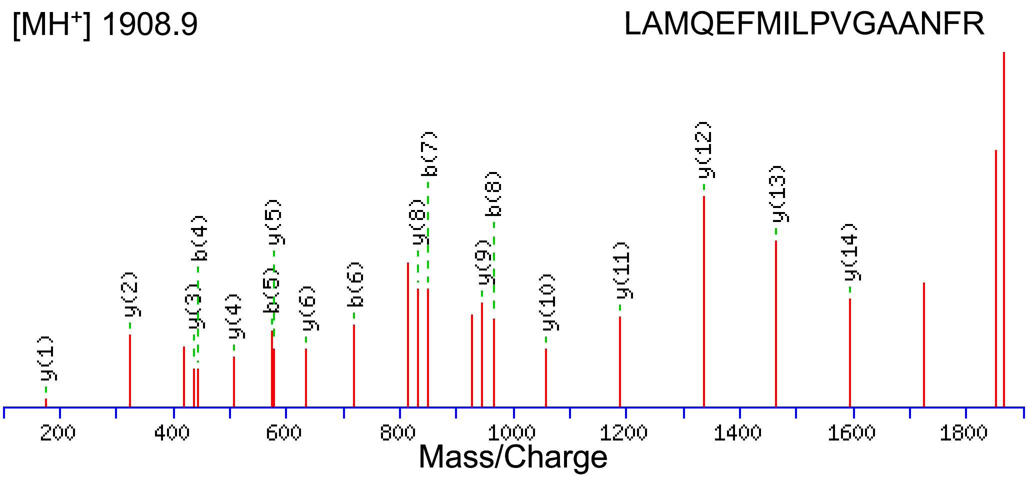

Figure N.b. Mascot result graph of the MALDI-TOF-PSD mass spectrum of the precursor ion m/z = 1908.9 with different ion species indicated.

Phosphoglycerate mutase 1 (PGAM-1)

The following monoisotopic m/z values were experimentally obtained: 601.44, 613.52, 757.56, 768.51, 1059.63, 1150.78, 1174.41, 1312.73, 1684.00, 1935.94, 2136.03, 2156.21, and 2417.12.

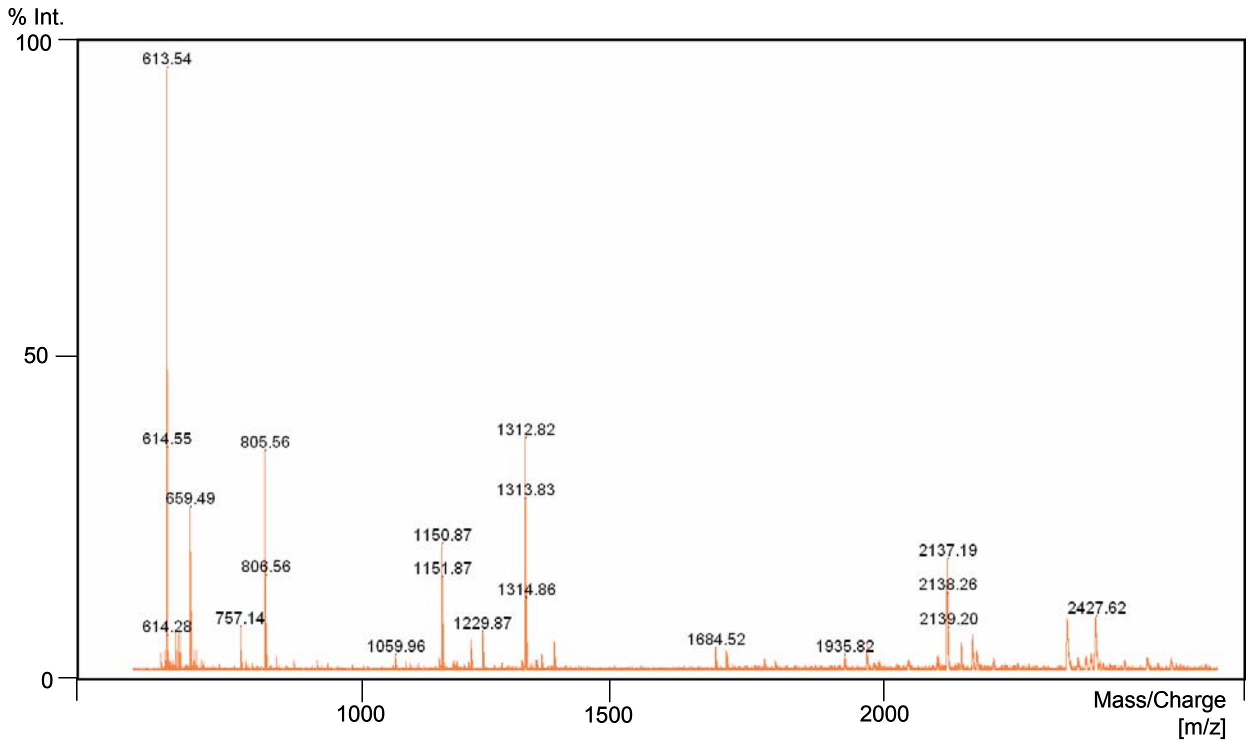

Figure O. Representative peptide mass fingerprint of PGAM-1.

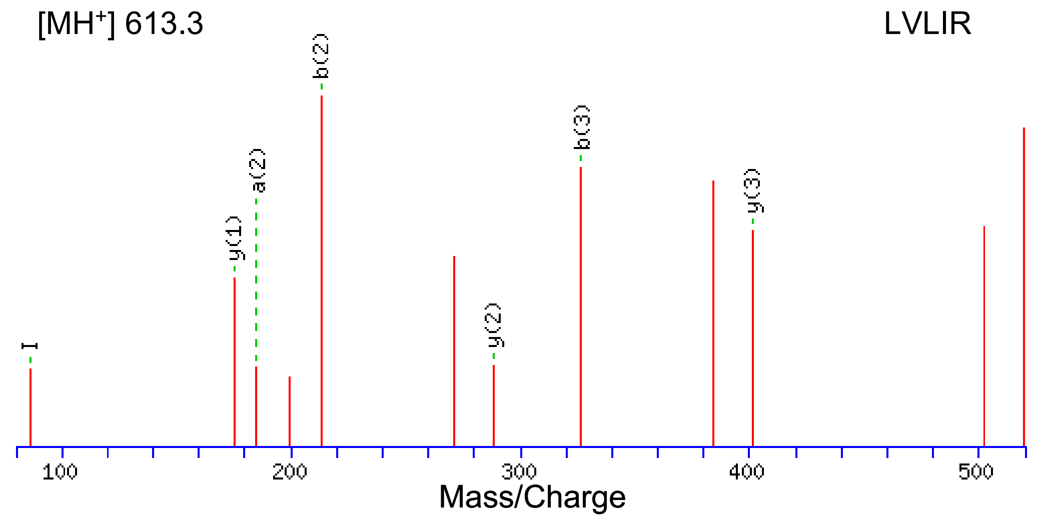

Figure O.a. Mascot result graph of the MALDI-TOF-PSD mass spectrum of the precursor ion m/z = 613.3 with different ion species indicated.

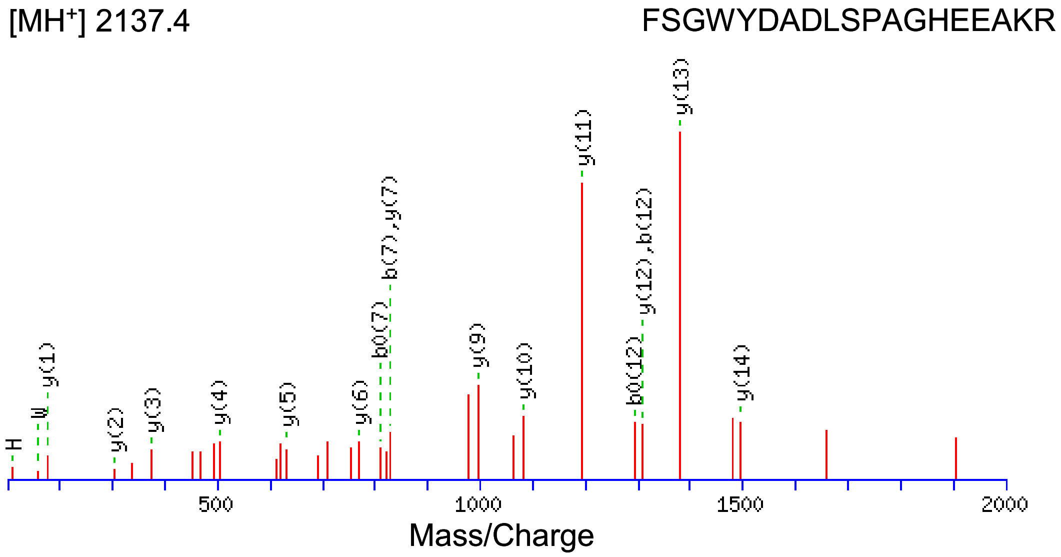

Figure O.b. Mascot result graph of the MALDI-TOF-PSD mass spectrum of the precursor ion m/z = 2137.4 with different ion species indicated.

Phosphoglycerate kinase 1 (PGK-1)

The following monoisotopic m/z values were experimentally obtained: 1101.56, 1159.54, 1190.58, 1217.60, 1434.69, 1634.74, 1768.87, 2022.92, and 2104.88.

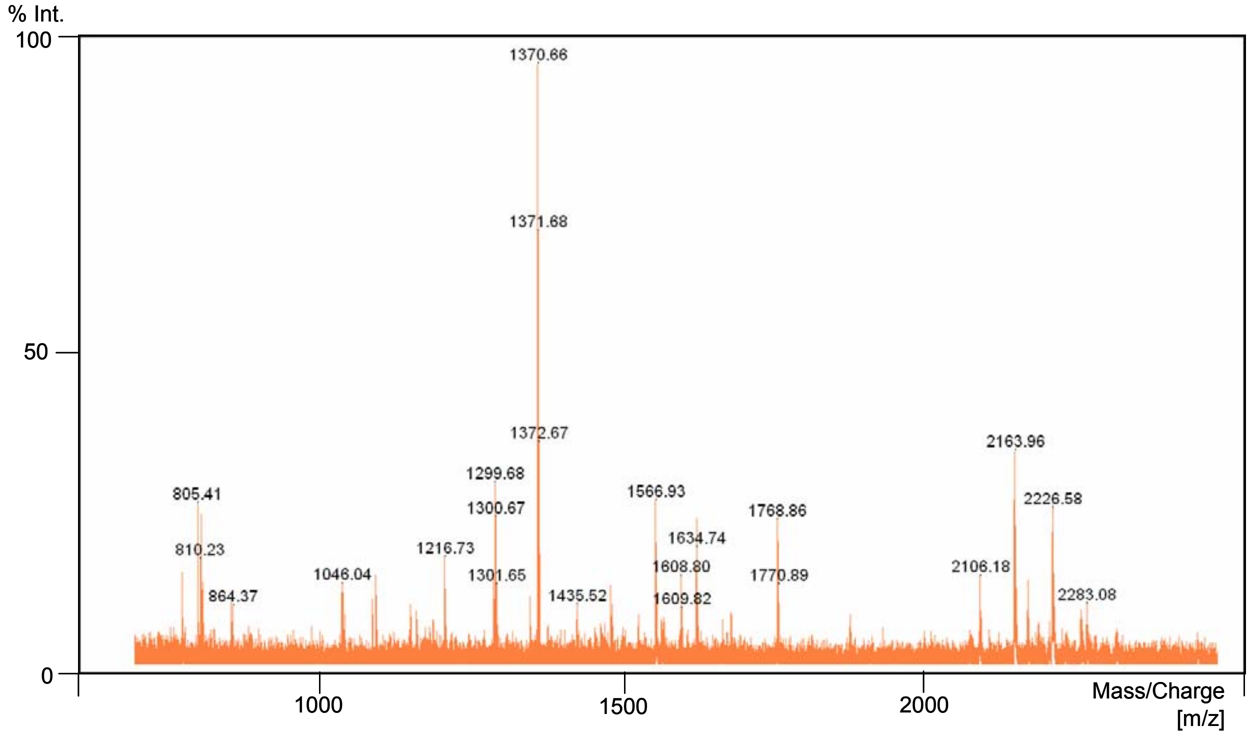

Figure P. Representative peptide mass fingerprint of PGK-1.

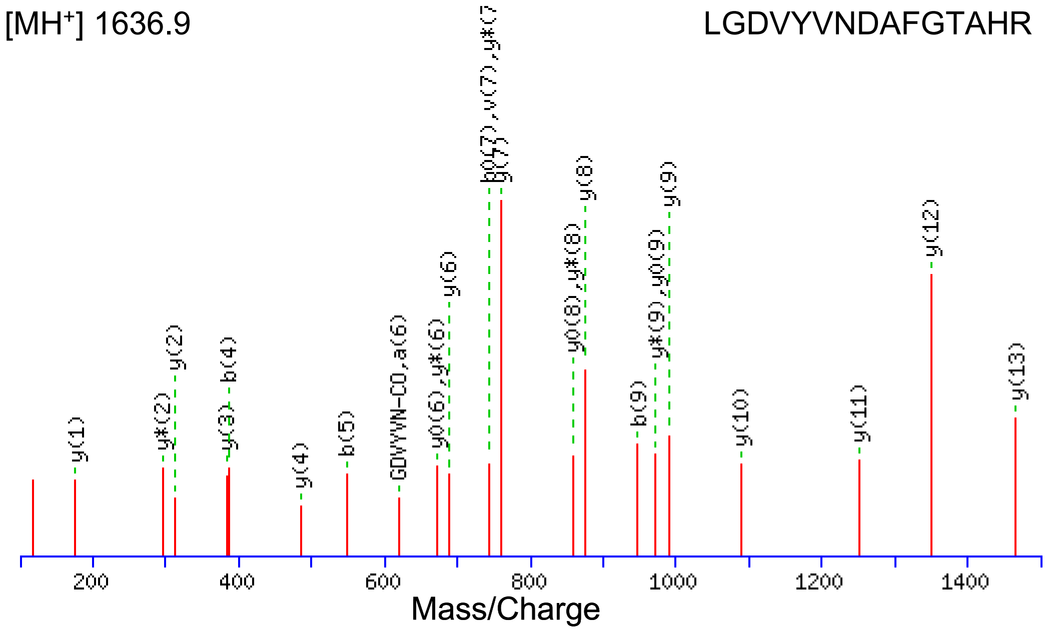

Figure P.a. Mascot result graph of the MALDI-TOF-PSD mass spectrum of the precursor ion m/z = 1636.9 with different ion species indicated.

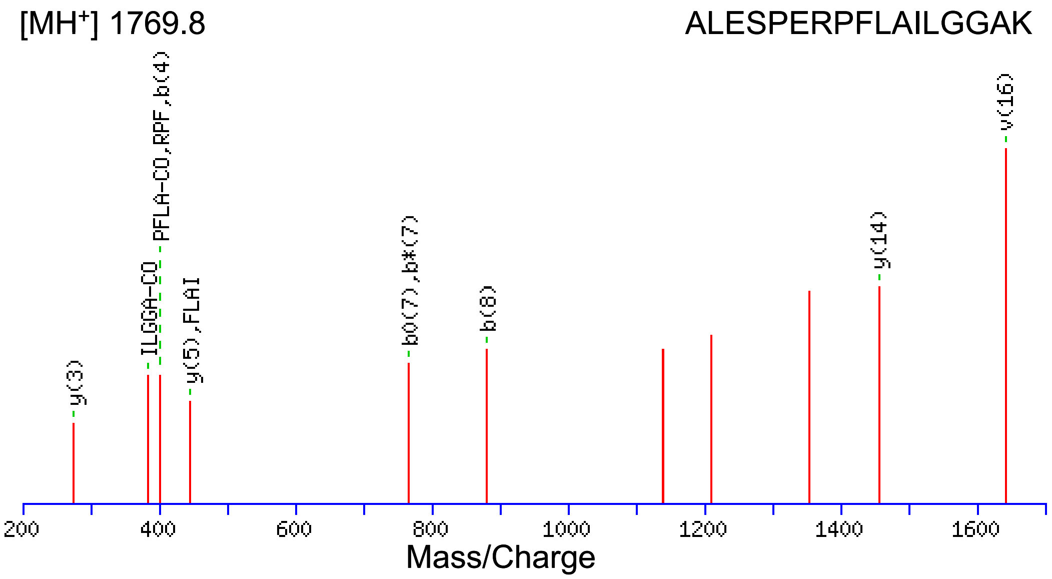

Figure P.b. Mascot result graph of the MALDI-TOF-PSD mass spectrum of the precursor ion m/z = 1769.8 with different ion species indicated.

Triosephosphate isomerase (TPIS)

The following monoisotopic m/z values were experimentally obtained: 621.41, 850.64, 954.67, 1082.79, 1137.80, 1234.86, 1326.90, 1458.98, 1466.97, 1587.05, 1808.34, and 2192.53.

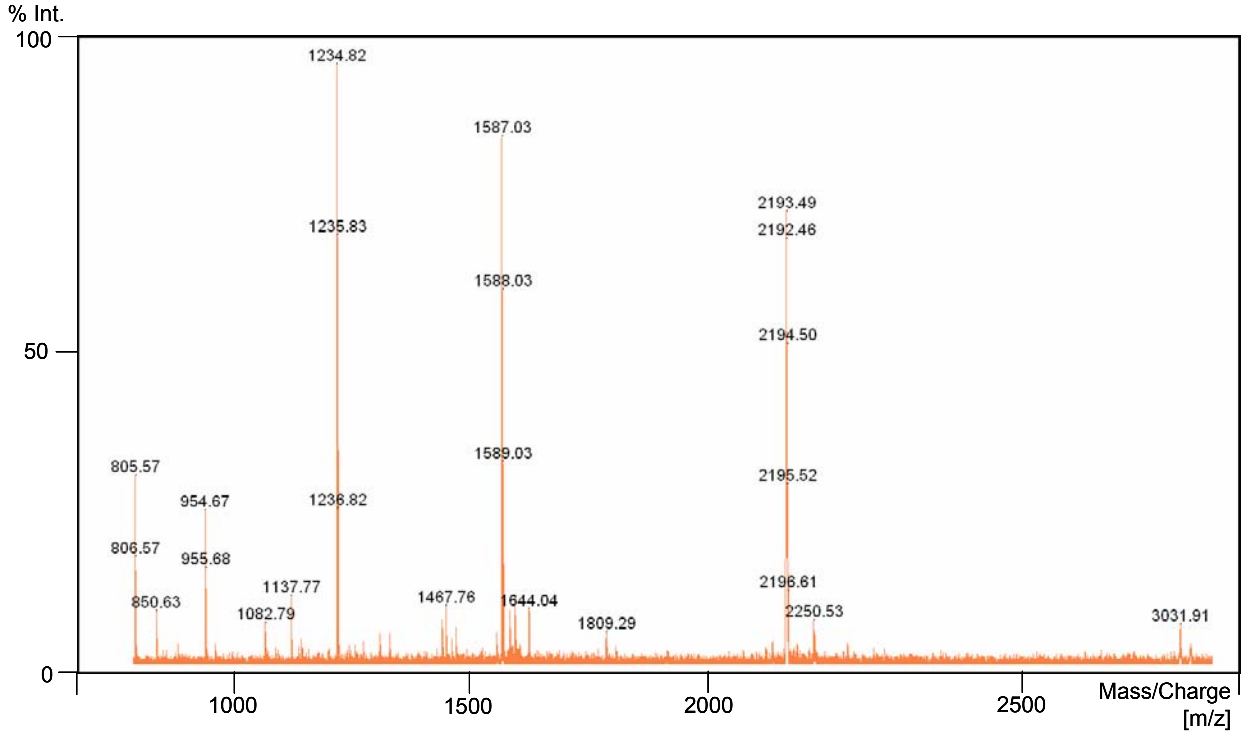

Figure Q. Representative peptide mass fingerprint of TPIS.

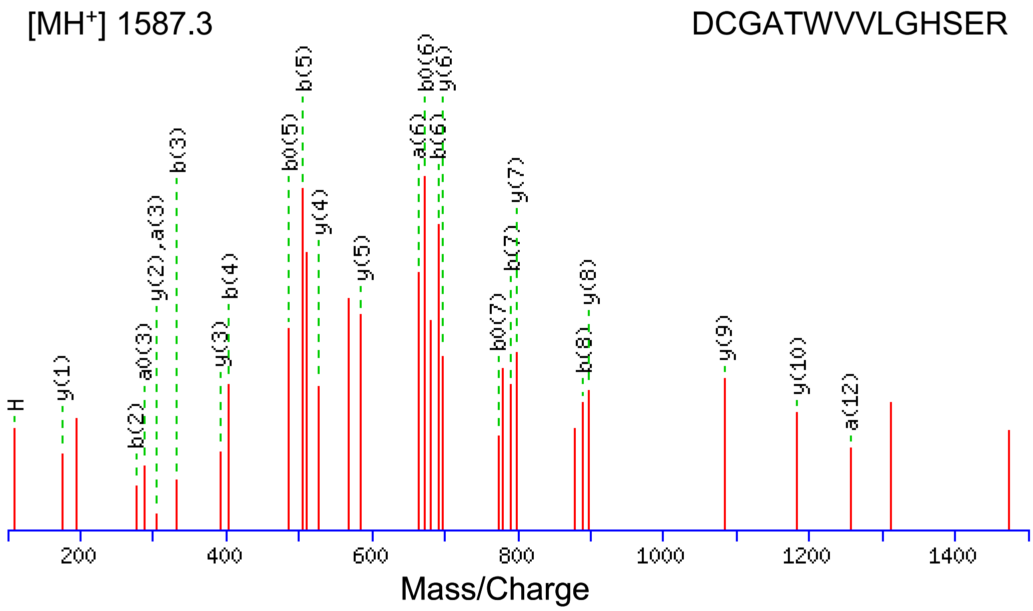

Figure Q.a. Mascot result graph of the MALDI-TOF-PSD mass spectrum of the precursor ion m/z = 1587.3 with different ion species indicated.

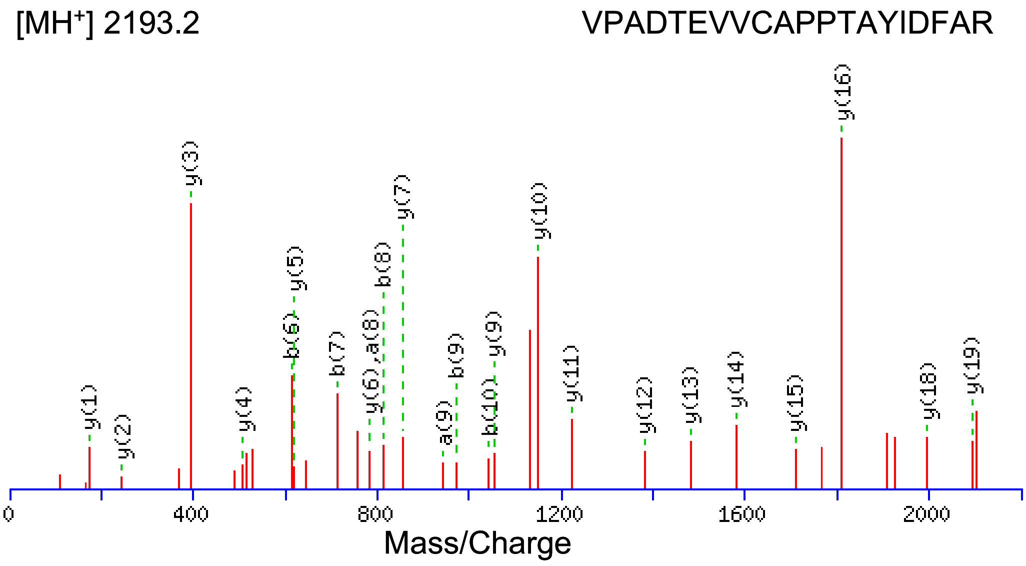

Figure Q.b. Mascot result graph of the MALDI-TOF-PSD mass spectrum of the precursor ion m/z = 2193.2 with different ion species indicated.

Mitotic spindle assembly checkpoint protein MAD2A (MD2L1)

The following monoisotopic m/z values were experimentally obtained: 799.71, 816.76, 844.51, 1299.71, 1326.63, 2348.06, and 2688.36.

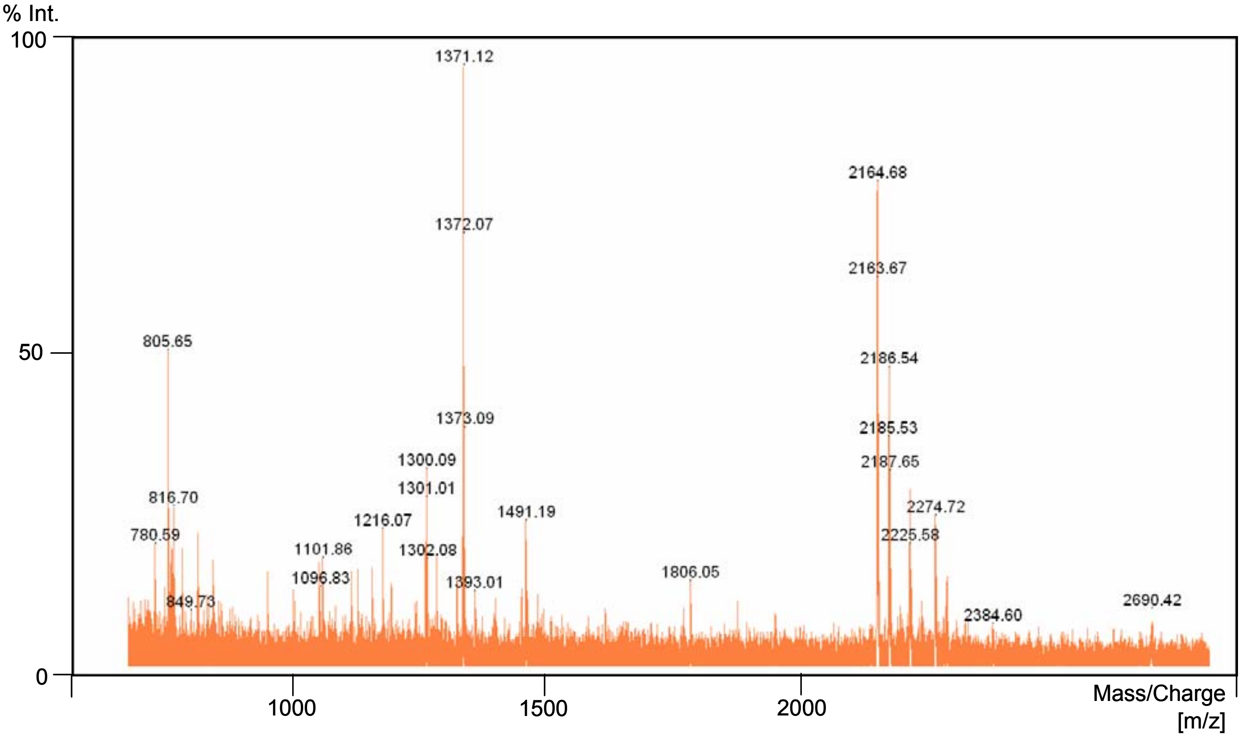

Figure R. Representative peptide mass fingerprint of MD2L1.

Protein disulfide-isomerase A3 (PDIA-3)

The following monoisotopic m/z values were experimentally obtained: 877.52, 995.21, 1172.40, 1188.40, 1191.48, 1359.49, 1370.58, 1515.62, 1652.61, 1664.63, 1758.73, 2703.89, and 2938.49.

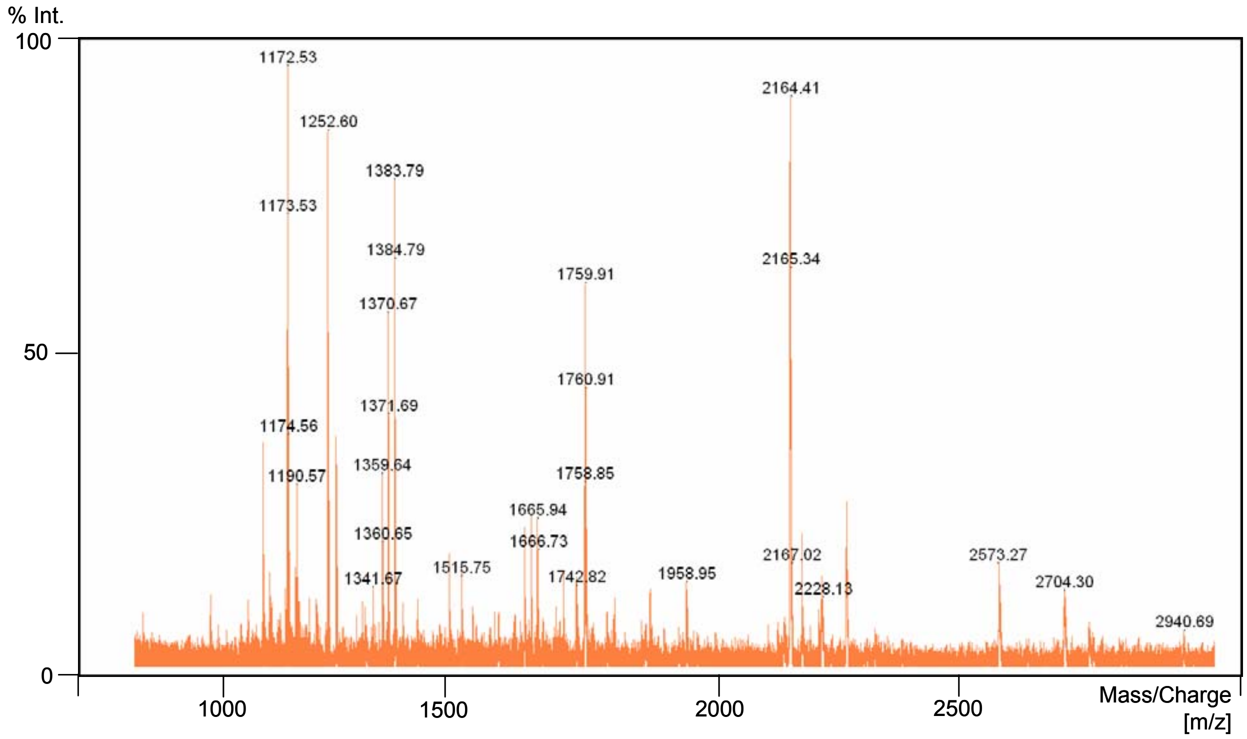

Figure S. Representative peptide mass fingerprint of PDIA-3.

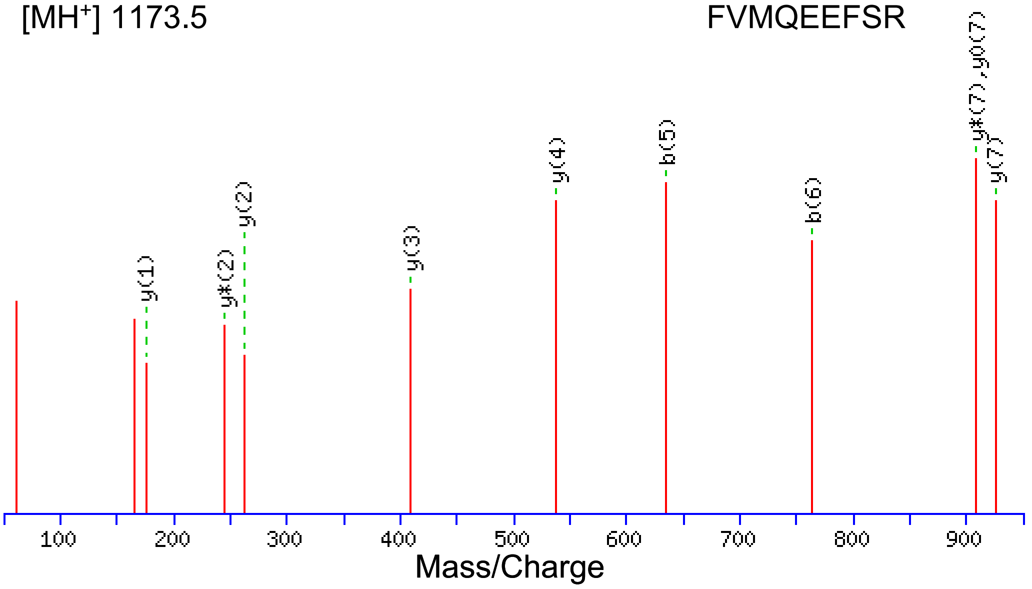

Figure S.a. Mascot result graph of the MALDI-TOF-PSD mass spectrum of the precursor ion m/z = 1173.5 with different ion species indicated.

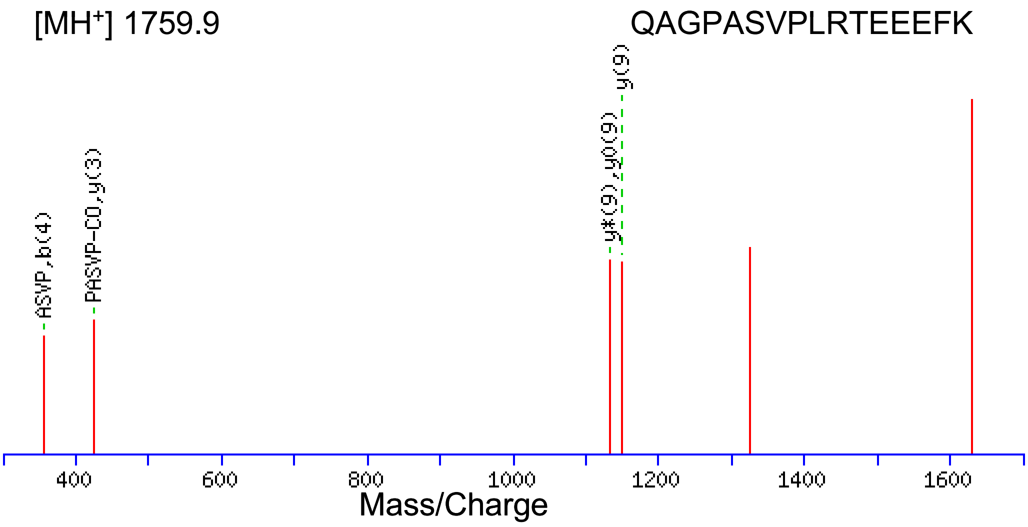

Figure S.b. Mascot result graph of the MALDI-TOF-PSD mass spectrum of the precursor ion m/z = 1759.9 with different ion species indicated.

D-3-phosphoglycerate dehydrogenase (3-PGDH)

The following monoisotopic m/z values were experimentally obtained: 716.42, 718.47, 986.54, 1099.53, 1225.73, 1298.77, 1434.78, 1488.77, 1624.62, 1809.84, 2048.06, 2274.14, 2288.36, and 2488.03.

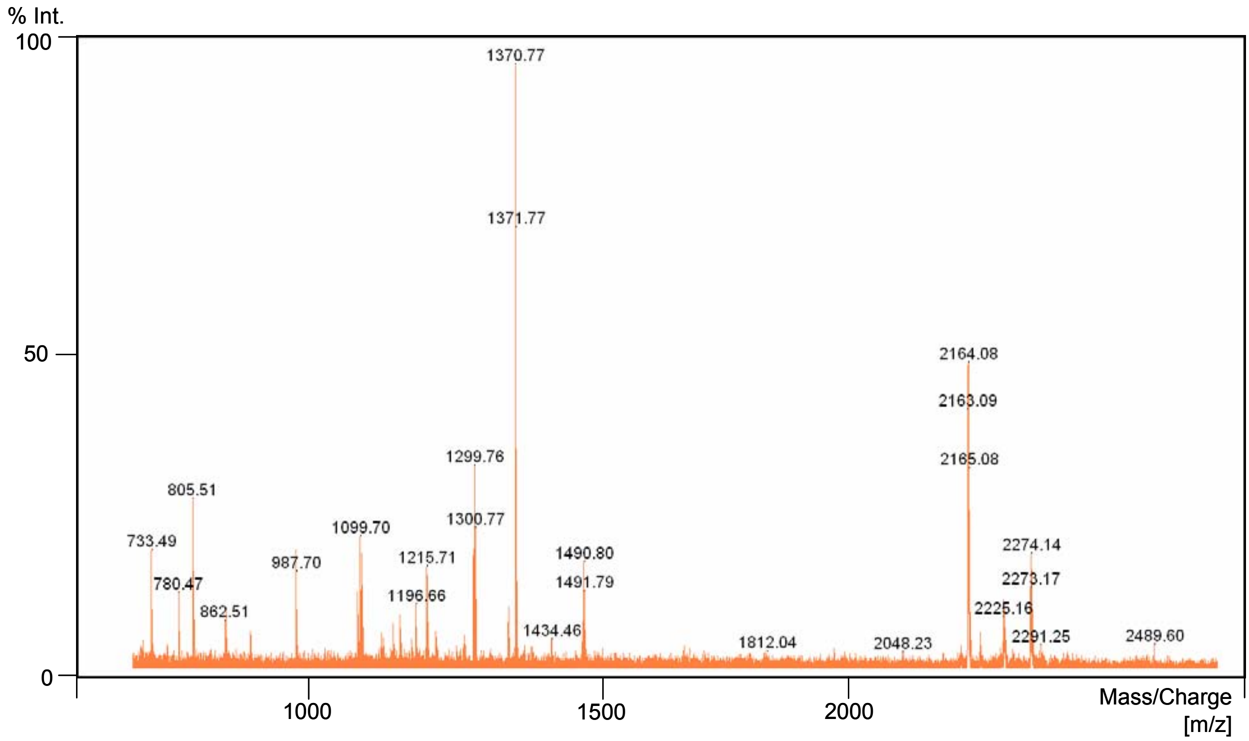

Figure T. Representative peptide mass fingerprint of 3-PGDH.

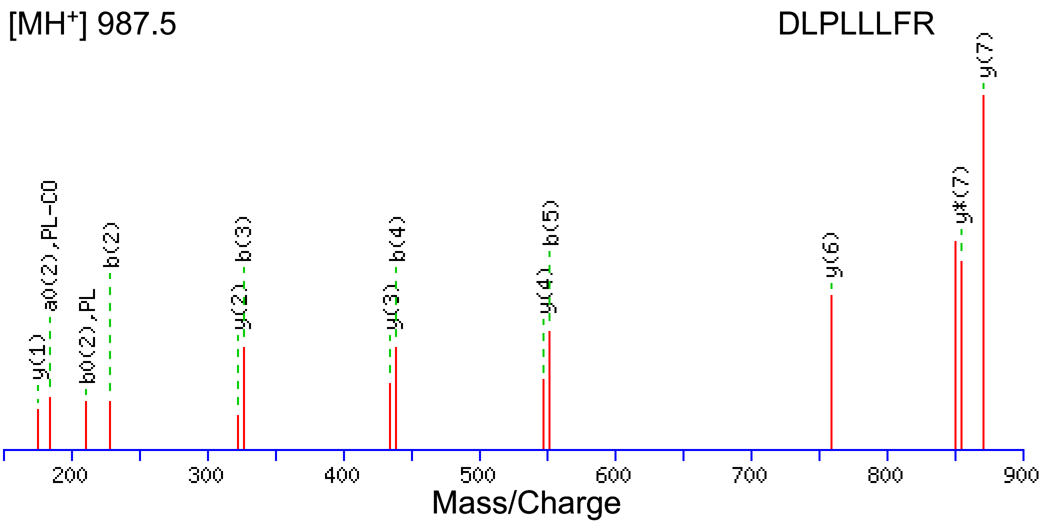

Figure T.a. Mascot result graph of the MALDI-TOF-PSD mass spectrum of the precursor ion m/z = 987.5 with different ion species indicated.

Peptidyl-prolyl cis-trans isomerase A (PPIA)

The following monoisotopic m/z values were experimentally obtained: 686.29, 737.26, 763.22, 765.34, 1154.49, 1379.70, 1598.75, 1831.89, and 1946.01.

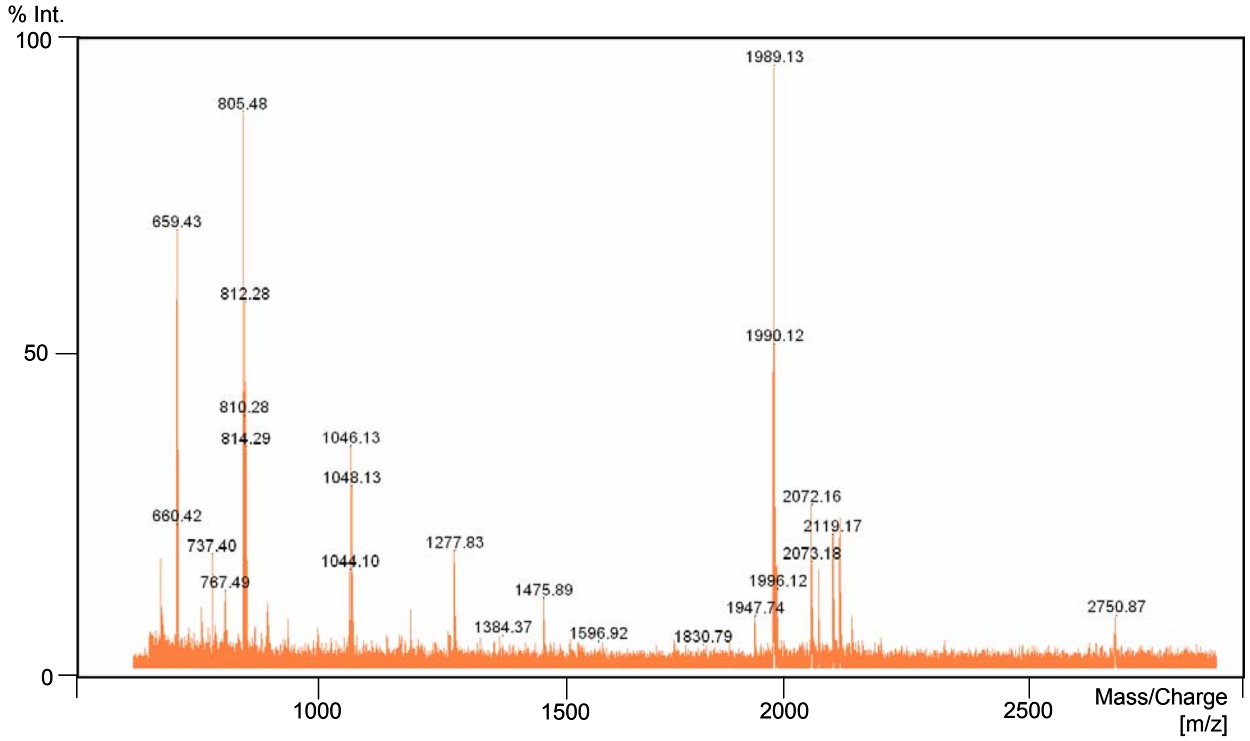

Figure U. Representative peptide mass fingerprint of PPIA.

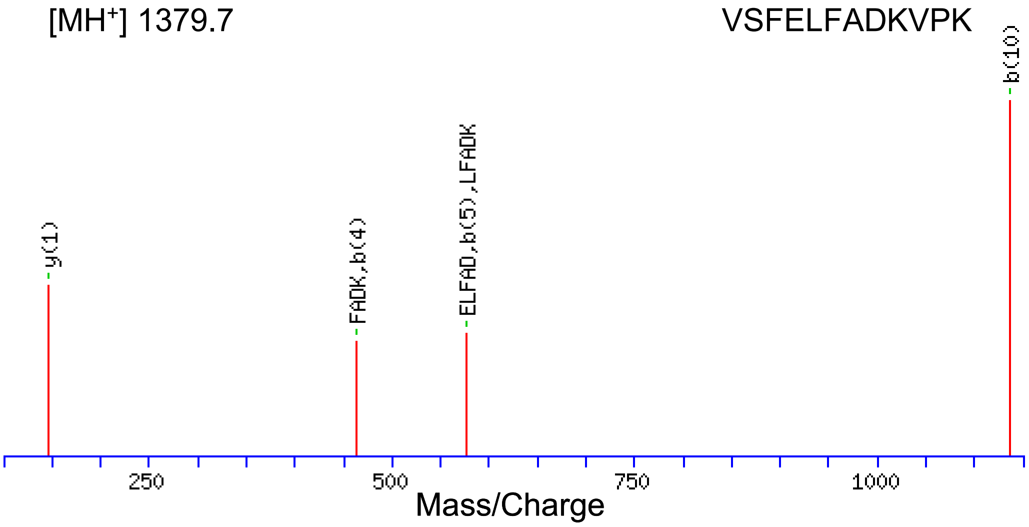

Figure U.a. Mascot result graph of the MALDI-TOF-PSD mass spectrum of the precursor ion m/z = 1379.7 with different ion species indicated.

Ran-specific GTPase-activating protein (RANG)

The following monoisotopic m/z values were experimentally obtained: 969.59, 1034.51, 1309.74, 1335.58, 1381.59, 1620.68, 2739.57, and 3933.83.

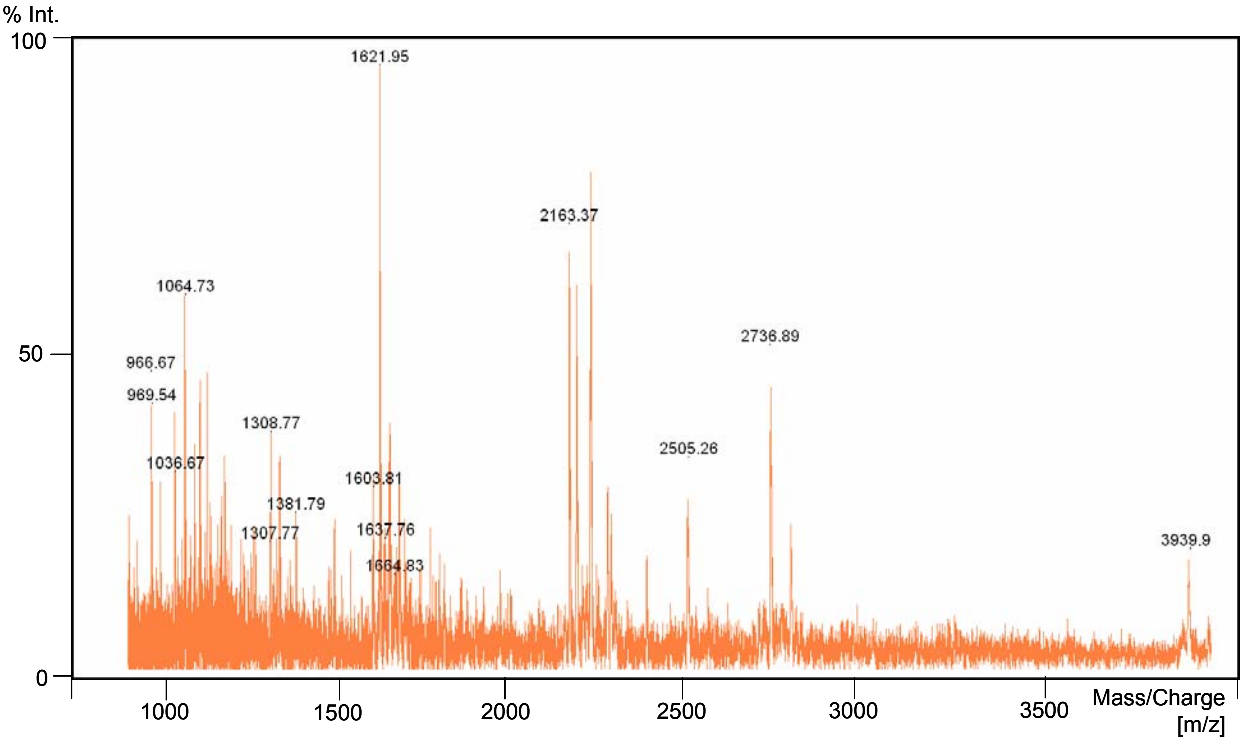

Figure V. Representative peptide mass fingerprint of RANG.

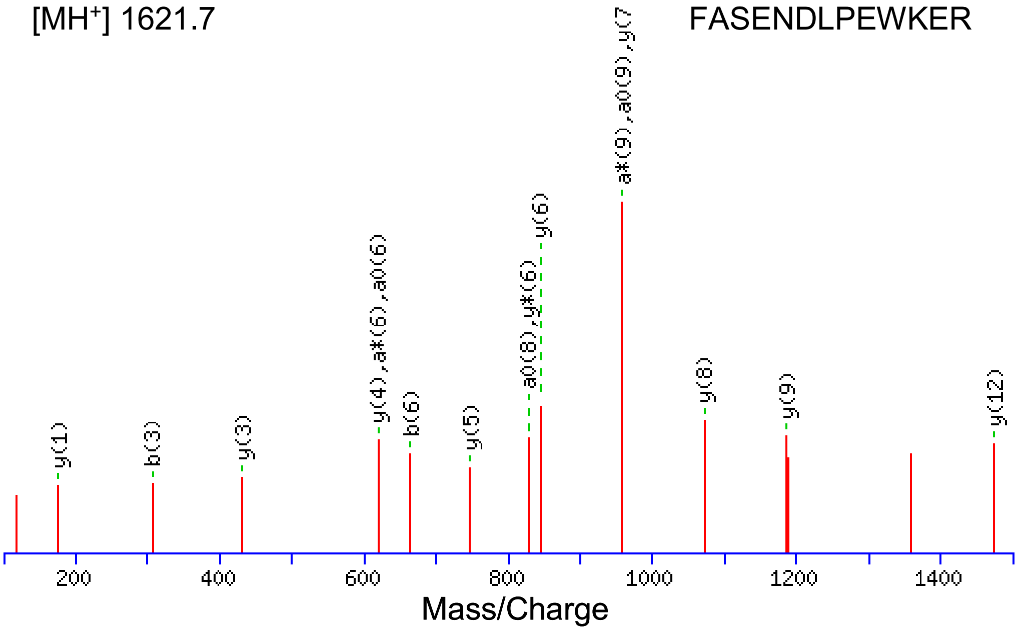

Figure V.a. Mascot result graph of the MALDI-TOF-PSD mass spectrum of the precursor ion m/z = 1621.7 with different ion species indicated.

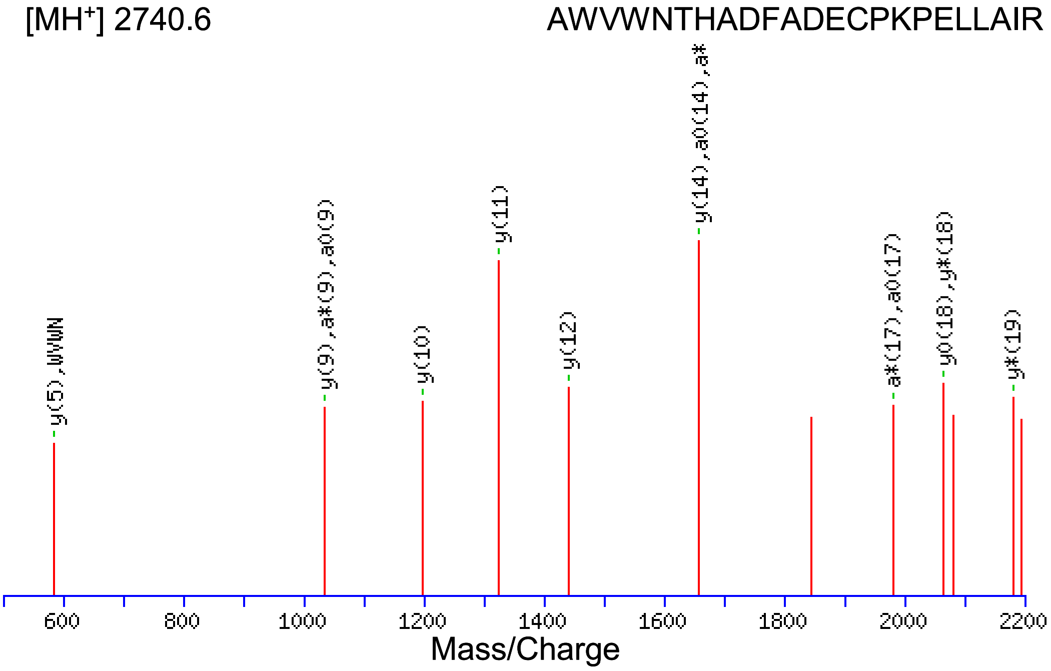

Figure V.b. Mascot result graph of the MALDI-TOF-PSD mass spectrum of the precursor ion m/z = 2740.6 with different ion species indicated.

CURRICULUM VITAE

Mag. Martina Stessl
Kornhäuselstrasse 16/2
2500 Baden bei Wien
Tel: +43-2252-82412 oder +43-650-3973065
Email: martina.stessl@univie.ac.at

Personal Data

Born	May 9, 1981 in Klagenfurt, Austria
Family status	married, 1 son (2008)
Languages	English, Italian, French (basic knowledge)

Education

1987 – 1991	elementary school St. Magdalen/ Villach.
1991 – 1999	grammar school BG/BRG Villach Peraustraße; school leaving examination („Matura“) passed with distinction.
1999 – 2005	academic studies of pharmaceutical sciences at the Karl-Franzens University Graz; graduated with distinction. Diploma thesis at the Swiss Federal Institute of Technology.
from 2005	PhD studies at the Department of Medicinal Chemistry, University of Vienna.

Professional and scientific experience

07/02 – 08/02	Perauapotheke Villach; traineeship.
07/03 – 09/03	Department for Research and Development-Coordination, Boehringer Ingelheim Austria; traineeship.
10/03 – 02/04	Department for Research and Development-Coordination, Boehringer Ingelheim Austria; part-time employment.
03/04 – 08/04	Institute of Pharmaceutical Sciences, Swiss Federal Institute of Technology, Zurich; diploma thesis „Structural Characterisation of Vaccinia Virus Thymidine Kinase“.
10/04 – 06/05	Department of Lead Structure Identification, Boehringer Ingelheim Austria; part-time employment.
11/05 – 11/08	Department of Medicinal Chemistry, University of Vienna. Teaching activities: Courses in quantitative chemical analytics Drug analysis and drug development Supervision of 2 diploma theses.
from 11/08	maternity leave

Publications and presentations

04/07	Stessl M, Winkler J, Marchetti M, Allmaier G, Noe CR “The Influence of Bcl-2 down-regulation by Oblimersen and siRNA using a proteomic approach“, poster-presentation, Pharmaceutical Sciences World Congress, Amsterdam.
06/07	“Current insight in melanoma“, oral presentation, internal research group, Vienna.
09/07	Stessl M, Marchetti M, Allmaier G, Noe CR „Investigation of target specificity of antisense oligonucleotides versus siRNA using a proteomics approach“, oral presentation, 5th Austrian Proteom Research Symposium, Vienna University of Technology.
08/07	Stessl M, Lachmann B, Noe CR „Einfluß von Bild-Bearbeitungssoftware auf Daten der Zweidimensionalen Gel-Elektrophorese“, poster-presentation, Congress of the German Pharmaceutical Society, Erlangen, Germany.
11/07	„2D Fluorescence Difference Gel Electrophoresis (2D-DIGE)”, oral presentation, internal research group, Vienna.

01/08	Winkler J, Gilbert M, Kocourková A, Stessl M, Noe CR. „2'-O-Lysylaminohexyl oligonucleotides: modifications for antisense and siRNA." Published in *ChemMedChem*, **3**(1):102-110.
01/09	Stessl M, Noe CR, Lachmann B. „Influence of image-analysis software on quantitation of two-dimensional gel electrophoresis data." Published in *Electrophoresis*, **30**(2):325-328.
08/09	Stessl M, Marchetti-Deschmann M, Winkler J, Lachmann B, Allmaier G, Noe CR. "A proteomic study reveals unspecific apoptosis induction and reduction of glycolytic enzymes by the phosphorothioate antisense oligonucleotide oblimersen in human melanoma cells." Published in *J Proteomics*, **72**(6):1019-1030.
01/10	Neuhaus W, Stessl M, Strizsik E, Bennani-Baiti B, Wirth M, Toegel S, Modha M, Winkler J, Gabor F, Viernstein H, Noe CR. "Blood-brain barrier cell line PBMEC/C1-2 possesses functionally active P-glycoprotein." Published in *Neurosci Lett*, **469**(2):224-228.
02/10	Winkler J, Stessl M, Amartey J, Noe CR. "Off-target Effects Related to the Phosphorothioate Modification of Nucleic Acids" Submitted to *ChemMedChem.*

Martina Stessl Baden, March 2010